Design and modelling of a fixturing system for an optimal balancing of a part family

Sajid Ullah Butt

2012-ENAM-0022

École doctorale n°432:SMI- Sciences des Métiers de l'Ingénieur

Doctorat ParisTech

T H È S E

pour obtenir le grade de docteur délivré par

l'École Nationale Supérieure d'Arts et Métiers

Spécialité " Génie Mécanique "

présentée et soutenue publiquement par

Sajid Ullah BUTT

Le 5 Juillet 2012

Conception et modélisation d'un montage de fabrication pour le balançage optimisé d'une famille de pièces

Directeur de thèse : **Patrick MARTIN**
Co-encadrement de la thèse : **Jean-François ANTOINE**

Jury

M. Henri PARIS, Professeur, G.SCOP, Université Joseph Fourier, Grenoble, France	Président
M. Cornel Mihai NICOLESCU, Professeur, KTH, Stockholm, Sweden	Rapporteur
M. Jean-François RIGAL, Professeur, LAMCOS, INSA Lyon, France	Rapporteur
M. Jean-François ANTOINE, Maitre de conférences, IUT de Nancy Brabois, France	Examinateur
M. Patrick MARTIN, Professeur, LCFC, Arts et Métiers ParisTech, Metz, France	Examinateur

T H È S E

Arts et Métiers ParisTech - Centre de Metz
Laboratoire de Conception Fabrication Commande EA 4495

Avant Propos

Ce mémoire de thèse représente une synthèse de mes activités de recherche menées depuis Septembre 2008. Ces activités ont été effectuées sous le statut d'allocataire d'une bourse « *Higher Education Commision (HEC) Pakistan* » de Septembre 2008 à Septembre 2011. Cette bourse a été obtenue suite à un concours national, pour le développement des ressources humaines.

Ces travaux s'inscrivent dans la problématique de conception de montage d'usinage. Ils visent plus particulièrement à répondre à la question : « *Quels sont les erreurs de positionnement pendant l'usinage et comment compenser ces erreurs ?* » en développant les modèles associés.

Etant donné l'aspect international de cette thèse et suite à la décision N° DG2009-46 du 1er Octobre 2009, le Directeur Général d'Arts et Métiers ParisTech autorise la rédaction en deux langues : anglaise et française. De ce fait, ce document se divise en deux parties : un résumé étendu en français sans figure et le descriptif des travaux en anglais avec les figures.

Dedicated to my family and fiancé

Acknowledgements

First and foremost, I would like to thank the members of the jury for their time, effort and consideration. I am grateful to Prof. Cornet Mihai NICOLESCU and Prof. Jean-François RIGAL for accepting to be the referees, for their attention and for their detailed review and critique of my thesis. I would also like to thank Prof. Henri PARIS for presiding over the thesis jury and for the comments on the thesis.

I gratefully thank my thesis director, Prof. Patrick MARTIN for his invaluable advice based on his expertise and his continuous help during my thesis writing. His clear, concise and pertinent remarks helped setting the research direction. I am also thankful for his tireless efforts during the review of the French and English thesis manuscripts.

I would also like to acknowledge the support and guidance provided by my PhD supervisor Dr. Jean-François ANTOINE. Although geographically away, he was always available for help with his kind remarks. His patient explanations, continuous support, co-operation and encouragement were the keys to the successful completion of this research work.

I had a wonderful experience at Arts et Métiers thanks to Aamer, Amir, Armaghan, Jawad, Jinna, Liaqat, Marius, Mathieu, Philip, Rafiq, Shirin, Sundar, Xavier and the people at the administration and library.

Apart from institution, I would like to thank my friends Fahd, Mohsin, Muneeb, Sadiq, Shaukat, Wissal and all Pakistani families who were always beside me all the time during my stay in Metz.

I am grateful to thank my mother, father, brother and sisters for their belief and confidence in me. They always supported and provided a motivation to achieve my goals. I would also like to thank my fiancé for her confidence and moral support.

Last but not the least, I am highly indebted to the financial support from the "*Higher Education Commision (HEC) Pakistan*", which enabled me to undertake the PhD program at Arts et Métiers ParisTech, France. I would also like to thank SFERE for their assistance during my stay in France. I am also grateful to the Region Lorraine for their partial financial support during my PhD.

Contents

List of Figures

LIST OF FIGURES

LIST OF FIGURES

List of Tables

LIST OF TABLES

List of Abbreviations

CEA	:	Computer Engineering Analysis
CMM	:	Coordinate Measuring Machine
CNC	:	Computer Numerical Control
CT	:	Computerized Tomography
DDL	:	Degré de Liberté
DOF	:	Degree of Freedom
EGRM	:	Elément Géométrique de Référence Minimum
FEA	:	Finite Element Analysis
FEM	:	Finite Element Modeling/Method
FMS	:	Flexible Manufacturing System
HTM	:	Homogeneous Transformation Matrix
RTL	:	Roulis, Tangage, Lacet Transformation, Tait–Bryan angles
LD	:	Large Displacement
MBS	:	Multi Body System
MMT	:	Machine à Mesurer Tridimensionnelle
MTH	:	Matrice de Transformation Homogène
NC	:	Numerical Control
OMM	:	On Machine Measurement
RMS	:	Root Mean Square
RP	:	Rapid Prototype
SATT	:	Surfaces Associées Technologiquement et Topologiquement
SD	:	Small Displacement
SDT	:	Small Displacement Torsor
TTRS	:	Topological and Technological Related Surfaces
YPR	:	Yaw, Pitch, Roll Transformation, Tait–Bryan angles

Nomenclature for chapter 3

List of symbols

X_i	:	Position vector of reference i
$[P_{ij}]$	:	Matrix transformation form i to j
x'_i, y'_i, z'_i	:	Final position of i^{th} locator in machine coordinate
a'_i, b'_i, c'_i	:	Unit vectors of calculated final planes of baseplate
D'_i	:	Vertical distance of each plane from origin
β_i, β_f	:	Initial and final angle along x-axis
γ_i, γ_f	:	Initial and final angle along y-axis
α_i, α_f	:	Initial and final angle along z-axis
x_P, y_p, z_P	:	Initial position of point P of the workpiece
x_F, y_F, z_F	:	Final position of point P of the workpiece
$d\xi_i$	:	Precision of axial positions of i^{th} locator
δx_P, δy_P, δz_P	:	Precision/uncertainty of workpiece-baseplate position
$\delta\beta$, $\delta\gamma$, $\delta\alpha$	:	Precision/uncertainty of workpiece-baseplate orientation
$\vec{A}.\vec{B}$	:	Dot/scaler product of vectors $\vec{A}$ and $\vec{B}$
$\vec{A} \times \vec{B}$	:	Cross product of vectors $\vec{A}$ and $\vec{B}$. In French it is denoted by $\vec{A} \wedge \vec{B}$

List of arrows

 : Direction of motion of the locator relative to previous position

 : Locator is free to move in both directions unless it make contact with the workpiece surface

 : Locator is fixed or position of locator is same as for earlier workpiece

Nomenclature for chapter 4

List of symbols

U	:	Potential energy, Nm
T	:	Kinetic energy, Nm
W	:	Work done, Nm
$[M]$	:	Mass Matrix of the system, kg
$[K]$	:	Stiffness matrix, N/m
$[I]$	:	Inertial matrix of mass elements kgm^2
$\{F\}$	:	External applied force vector, $\{F_X, F_Y, F_Z\}^T$ N
$\{\mathbb{T}\}$	:	External applied torque vector, $\{\mathbb{T}_X, \mathbb{T}_Y, \mathbb{T}_Z\}^T$ Nm
$\{\Delta X\}$	:	Linear displacement vector, $\{\Delta X, \Delta Y, \Delta Z\}^T$ m
$\{\Delta\Theta\}$	:	Angular displacement vector $\{\Delta\beta, \Delta\gamma, \Delta\alpha\}^T$ rad
α	:	Angle of the baseplate-workpiece along Z-axis, rad
β	:	Angle of the baseplate-workpiece along X-axis, rad
γ	:	Angle of the baseplate-workpiece along Y-axis, rad
Φ	:	Angle between the surface normal and the locator axis, rad
Γ	:	Gamma function
B	:	Beta function
σ	:	Equivalent contact surfaces roughness, m
V	:	Linear velocity of the mass element, m/sec
ω	:	Angular velocity of the mass element, rad/sec
δ	:	Deformation under load, m
k_f	:	Flexure stiffness of the locators, N/m
k_s	:	Shear stiffness of the locators, N/m
E	:	Modulus of elasticity, N/m^2
G	:	Shear modulus of elasticity, N/m^2
A	:	Cross sectional area of the locator, m^2
L	:	Total length of the locator, m
f	:	Point of action of external force
a_i, b_i, c_i	:	X, Y and Z components of the normal vector
a'_L	:	Non-dimensional contact area
P'_O	:	Non-dimensional pressure distribution on the contact
$\Delta X_{\omega,L}$	:	Representation of dynamic to static linear displacement ratio for bode diagram
$\Delta X_{\omega,A}$	:	Representation of dynamic to static angular displacement ratio for bode diagram

List of subscripts

i	:	Number of locator
j	:	Number of clamps
L	:	Locator
C	:	Clamp
B	:	Baseplate
E	:	External applied parameters
F	:	Effect of external force
P	:	Point P, center of mass of the baseplate
f	:	Final position of locator contact after the load
a	:	Axial component
t	:	Radial component
Plu	:	Plucker
Sph	:	Sphere
H	:	Hertz
n	:	Normal to surface
New	:	Calculated value after the iteration
$Stat$	:	static component
Dyn	:	Dynamic component

Glossary

- **Repositioning**
  Repositioning is the placement of the workpiece from initially wrong position to the final required one. In our work, the repositioning is performed through the axial advancement of 6 locators.
- **Optimal position**
  It is the position of the rough part in the fixture so that the volume of the final part is fully included in the volume of the rough part. In addition, the machining allowances are uniformly distributed all around the part at optimal position.
- **Optimal balancing**
  The repositioning of the workpiece at the optimal position is called optimal balancing.
- **Optimal stiffness**
  It is the minimum stiffness of the fixturing elements required to hold the workpiece at the specified position under load with the displacement within the required limit.
- **Small displacement hypothesis**
  Small displacement hypothesis are performed if the displacements are very small as compared to the dimensions of the object. In this hypothesis, it is assumed that the deformed domain is a little different from the un-deformed domain, therefore the approaching values are used; The following assumptions can be made;

$$x^2 \approx 0$$
$$\cos(x) \approx 1$$
$$\sin(x) \approx x$$

- **Fixture stability**
  The ability of the fixture to withstand the machining forces with least possible deformation ({F}=[K].{X}). More stiff fixturing system can hold the workpiece under large machining forces as compared to less stiff.

Première partie

Résumé Étendu En Français

Chapitre 1

Introduction

1.1 Objectif

L'objectif de cette thèse est de proposer un montage d'usinage, ou d'assemblage de pièces complexes qui peut effectuer un repositionnement des 6 DDL dans les coordonnées machine sans l'utilisation de la machine à 4 ou 5-axes ceci à partir de la mesure de la position réelle de la pièce. Ce système de montage de pièce sera capable de ;

- Déterminer l'erreur de positionnement entre la pièce à usiner et l'outil (ou entre les deux pièces en cas d'assemblage)
- Assurer le déplacement axial des 6 appuis de façon à mettre en place de la pièce dans la position optimale

1.2 Contexte

La qualité d'une pièce est influencée par la capacité d'un montage à tenir et à positionner correctement la pièce en tenant compte des différentes conditions fonctionnelles lors de la fabrication. La conception de montage est importante pour tenir la pièce correctement et compenser les erreurs (mise en position, efforts..), que la pièce peut affronter, lors de l'usinage ou assemblage pour assurer la qualité du produit.

La nécessité de la production de haute qualité, à coût compétitif, a accéléré les efforts de recherche dans la conception de montage pour la production de produits rentable sans compromettre la qualité. Pour faire face à la demande actuelle du marché, Ryll *et al.* (2008) insistent sur la nécessité de montages " intelligents" qui seront capables de répondre aux besoins de réduction et de compensation des erreurs dimensionnelles ; assurance de la stabilité et adaptation des forces de bridage pour garantir des performances optimales.

Deux pièces de la même famille peuvent avoir de faibles variations dimensionnelles à l'état brut (avant usinage). Après mise en position de la pièce brute sur des appuis fixes compte tenu des erreurs géométriques, la pièce finie peut ne pas être complètement incluse dans la pièce brute ce qui conduit à un rébus. Afin d'éviter ce problème, une surépaisseur importante est ajoutée à la pièce brute et des passes d'ébauche dont certaines hors matière sont programmées. Afin d'éviter la perte de temps et de matière il est nécessaire de mettre chaque nouvelle pièce en position mais cette opération mobilise la machine. Le système proposé a pour objectif de réaliser cette opération de mise en position d'une façon automatique éventuellement en dehors de la machine pour assurer un pré-positionnement de pièce complexe pour des opérations d'usinage précision.

Le mécanisme étudié doit assurer la transformation cinématique pour mettre la pièce à la position optimale a fin de compenser l'erreur de positionnement entre celle-là et la machine-outil. Ceci peut être réalisé sur une machine avec un grand nombre de degrés de liberté et un nombre élevé de transformations géométriques.

Si une opération (usinage ou d'assemblage) n'a besoin que d'un faible nombre d'axes, ou simplement de petits déplacements, le choix d'une machine 5 axes n'est pas rentable économiquement. Le système étudié peut également être utilisé sur les lignes de fabrication automatisées sur lesquelles le nombre d'axes reste limité par station, il permet de mettre au mieux en position la pièce sur son montage et de limiter les surépaisseurs.

A cet effet, un système de montage ayant la capacité de satisfaire ces besoins ainsi que les modélisations géométriques, cinématiques et mécaniques nécessaires pour son dimensionnement est présenté dans cette thèse.

1.3 Proposition

Ce système est capable de calculer les erreurs de positionnement entre la pièce et l'outil soit après identification des erreurs de position soit en prenant en plus en compte les forces de bridage et d'usinage. Le système de montage est capable d'effectuer la compensation d'erreur suivant les 6 degrés de liberté par l'avancement/rétraction au niveau de chacun des six appuis. Pour la prise en compte des efforts les appuis et les brides sont considérés comme les éléments élastiques dont la rigidité est supposée connue.

Le système étudié est constitué d'un plateau cuboïde[1] sur lequel est fixé la pièce, dont les surfaces sont supposés parfaitement planes et orthogonales, il est posé sur 6 appuis dans une configuration de type 3-2-1r. Chaque appui possède un seul degré de liberté en translation afin de mettre la pièce dans la position souhaitée, il est fixé (liaison rigide parfaite) à un support constitué de trois faces orthogonales qui constitue un montage d'usinage mobile. Le frottement entre le plateau et les appuis est considérer nul.

La thèse se compose de deux parties indépendantes analyse de l'aspect cinématique seul puis prise en compte des aspects mécaniques ; Dans la modélisation cinématique, tous les éléments du système de montage sont supposés rigides. En supposant que la position initiale inconnue de la pièce pourrait impliquer de grands déplacements lors de la phase de correction, le modèle cinématique est construite en utilisant des matrices de transformation homogènes (MTH) avec de grands déplacements. La position initiale de la pièce peut être mesurée en utilisant un MMT, la position finale est connue par le programme pièce. Un algorithme calculant l'avancement unique de chaque appui pour déplacer la pièce à la position souhaitée est développé.

Dans le modèle mécanique, le déplacement de la pièce est calculé en tenant compte des forces d'usinage et de bridage en utilisant la théorie de petit déplacement et les méthodes énergétiques en prenant en compte la rigidité et la masse du système de montage. On considère les appuis comme des éléments élastiques ayant des masses négligeables, la zone de contact du plateau au niveau de l'appui est

[1] Cuboïde : Parallélépipède rectangle avec tous les angles droits et les faces opposées égales

considérée comme élastique, l'ensemble plateau-pièce est considéré comme parfaitement rigide. Le modèle analytique développé permet d'obtenir les matrices de rigidité et de masse rapidement quelle que soit la configuration et la position des appuis et l'orientation du plateau.

L'énergie potentielle de tous les éléments élastiques, l'énergie cinétique des éléments de masse et le travail des l'effort externe sont formalisés, Le déplacement de l'ensemble plateau-pièce en est déduit, il est ensuite transformé compte tenu de la déformation de chacun des appuis selon leurs rigidités. Le déplacement calculé dans le modèle mécanique peut être compensé en utilisant le modèle cinématique développé.

1.4 Plan de la thèse

Ce document de thèse est structuré en 4 chapitres. Après le premier chapitre d'introduction, le chapitre 2 présente une revue de la littérature détaillé à la conception de montage de fabrication, y compris les causes d'erreurs, les forces appliquées sur le montage et la déformation au niveau des contacts des appuis. Le modèle cinématique est présenté dans le chapitre 3, tandis que le modèle mécanique est présenté dans le chapitre 4. Les deux modèles, cinématiques et mécaniques, sont illustrés par des exemples. A la fin du document une synthèse de conclusion est présentée ainsi que des perspectives pour de futures recherches.

Chapitre 2

État de l'Art

Le montage d'usinage est un dispositif permettant de positionner et de maintenir la pièce dans le référentiel de la machine outil en vue de son usinage. Les constituants élémentaires d'un montage d'usinage qui assurent son positionnement, son orientation et le maintien de la pièce sont les appuis et les brides. Le choix de ces éléments à un grand rôle dans la qualité finale du produit. Les fonctions principales de montage d'usinage sont,

- Positionner la pièce précisément dans l'espace de travail
- Maintenir la pièce afin qu'elle ne bouge plus en fonction des forces externes
- Soutenir la pièce pour éviter les déformations et/ou les vibrations indésirables de la pièce durant son usinage

2.1 Les défauts géométriques et dimensionnels

Definition 2.1.1. *La géométrie réelle d'une pièce peut être définie par la surface qui sépare le matériau de son environnement (Bourdet & Mathieu, 1998).*

Une surface peut être mesurée à l'aide d'une MMT[1]. La surface est définie par les "n" points mesurés sur la surface réelle. Pour un élément, plus d'informations peuvent être obtenues en augmentant le nombre "n" de points mesurés.

[1]MMT : Machine à Mesurer Tridimensionnelle

En utilisant les informations des points mesurés, la surface extraite de la surface réelle est appelée surface associée à la surface théorique définissant la pièce. Le nombre de points mesurés doit être au moins égal au nombre de points minimum permettant de définir la surface. Le tableau 2.2 présente le nombre minimum de points à mesurer en fonction de l'entité théorique et les défauts de forme associés.. La référence de l'association mathématique des éléments géométriques est appelé EGRM[1].

Definition 2.1.2. *Un EGRM est composé des trois éléments géométriques simples que sont le point, la droite et le plan. Il est associé à chaque classe de surfaces et il permet le positionnement univoque de la classe de surfaces à laquelle il est rattaché(Lesage, 2002)*

En général tous les éléments mécaniques peuvent être regroupés en sept classes d'invariants en fonction de la forme invariante DDL dans l'espace. Le tableau 2.3 indique ces éléments. Sur la base de ces sept classes, le concept de SATT [2] est développé par Clément *et al.* (1994) pour l'association mathématique des surfaces en particulier dans les logiciels de CAO.

La géométrie idéale, définie par "n" points mesurés, ne passe pas par tous les points, donc il y'aura un écart entre les points mesurés et la surface idéale associée. Ces écarts sont évalués de deux façons différentes : au niveau de chaque point mesuré ou au niveau global de la surface de substitution (Bourdet & Schneider, 2007).

Dans le cas de nombre finis de points mesurés : l'écart de chaque point mesuré est la distance entre ce point et le pied de la normale à la surface idéale passant par le point mesuré (fig. 2.5(a)). La surface idéale est définie en utilisant des critères d'optimisation existants. Par exemple : le critère de moindre carré. Dans le cas de la définition d'une surface de substitution, l'écart est exprimé par un torseur de petit déplacement appelé dans ce cas torseur d'écart (fig. 2.5(b)). Il est encore nécessaire de définir le critère d'ajustement de la surface idéale par rapport à la surface réelle.

[1]EGRM : Elément Géométrique de Référence Minimum
[2]SATT : Surfaces Associées Technologiquement et Topologiquement

Depuis le développement du concept en 1970, le torseur de petit déplacement a été largement utilisé dans le logiciel de MMT et l'analyse de la tolérance. Le torseur de petit déplacement ($T_O = |\overrightarrow{\Omega}, \overrightarrow{D_O}|$) est le torseur obtenu à partir du couple de vecteur de translation et de rotation lorsqu'on suppose que les déplacements sont petits. Le déplacement d'un solide dans un système de coordonnées peut aussi être représenté par MTH[1] contenant un vecteur de translation et une matrice de rotation. Cette dernière peut être exprimée par trois angles (α, β, γ) représentant des rotations successives du solide autour de trois axes $\{\overrightarrow{Z}, \overrightarrow{X}, \overrightarrow{Y}\}$ visibles dans la figure 2.6.

Comme mentionné précédemment, la géométrie idéale associée ne passe pas par tous les points mesurés. Lorsque la pièce est placée sur les appuis dans un état d'équilibre statique, les petites déviations des contacts provoquent la déviation globale (déplacement des corps rigides) de la pièce sur les appuis. Cet écart global peut être représenté en terme de déviation normale à chaque point de contact à l'aide de la matrice de Plucker (Halevi & Weill, 1995). Un exemple est détaillé dans la section 2.2.6 expliquant le calcul de la matrice Plucker pour une configuration spécifique des appuis.

2.2 Conception du montage d'usinage

En général, la conception de montage d'usinage comporte quatre étapes principales, comme indiqué dans la figure 2.14 (Boyle *et al.*, 2011; Kang *et al.*, 2003; Wang *et al.*, 2010). Ces étapes sont :

- Planification de configuration : il s'agit de l'identification des configurations d'usinage sur lequel une combinaison d'opérations d'usinage peut être effectuée

- Planification de montage d'usinage : elle défini le placement des éléments du montage d'usinage pour bloquer 6 degrés de liberté de la pièce pour chaque configuration

[1]MTH : Matrice de Transformation Homogène

- Conception de l'unité : elle porte sur la conception et la sélection des appuis et les brides appropriés pour le montage d'usinage
- Vérification : elle permet de valider si le montage satisfait aux besoins correspondant aux conditions de service (tab. 2.4)

Cette thèse se concentre sur le processus de planification du montage de la pièce à partir d'une configuration d'appuis connue. L'objectif de la planification du montage d'usinage est d'assurer avec précision le placement de la pièce par rapport au référentiel de la machine-outil. Pour cela, toutes les erreurs possibles entre la pièce et la machine-outil doivent être éliminées ou compensées. Les causes principales des erreurs pendant le montage ou l'usinage provoquant un défaut d'alignement de la pièce sont les suivantes :

- Erreur due au placement des appuis
- Défaut de forme de la pièce liée à l'élaboration du brut
- Erreur de déformation du montage d'usinage due aux forces d'usinage et de bridage
- Erreur cinématique ou à la déformation de la machine-outil

Au lieu de chercher à éliminer les erreurs de positionnement, elles peuvent être compensées. La compensation peut être effectuée par un changement de trajectoire de l'outil, le déplacement de l'outil ou le déplacement de la pièce dans les coordonnées machine. Un choix approprié des éléments du montage permet de réduire considérablement les erreurs de positionnement. Ici, nous indiquons une brève revue de la littérature pour déterminer et compenser les causes des erreurs.

2.2.1 Le balançage et le placement optimal des appuis

Selon Marin & Ferreira (2001), la conception du montage d'usinage contient deux étapes. La première étape est le choix de la configuration des appuis. Nous obtenons un placement optimal des appuis dans cette première étape.

La deuxième étape implique le choix des brides qui assurent l'immobilisation complète de la pièce sous l'action des forces extérieures de bridage et de l'usinage. Dans cette sous-section, une brève revue de la littérature est réalisée sur le placement des appuis pour réduire le déplacement de la pièce. La sous-section suivante porte sur la prévision d'erreur de positionnement de la pièce due aux éléments de montage.

Pour le développement de la configuration des appuis, Somashekar R. (2002) a proposé un modèle systématique pour la sélection des surfaces primaires, secondaires et tertiaires ; le numéro des éléments nécessaires pour soutenir, positionner et brider la pièce ; et les faces sur la pièce en contact avec ces éléments basés sur les forces et couples externes.

Roy & Liao (2002) ont déplacé les supports sur un système de montage ayant la configuration 3-2-1r des appuis en tenant compte de la stabilité de la pièce lors de l'application d'un torseur de force virtuel sur le système de montage. Le système est plus stable par une augmentant de la surface du triangle formé par trois appuis sur le plan principal de la pièce (fig. 2.18). Zirmi *et al.* (2009) ont proposé le placement des appuis sur le plan primaire d'un montage à configuration 3-2-1r des appuis qui tient compte des contraintes de qualité, d'accessibilité, de stabilité et de comportement mécanique. Menassa & Devries (1991) ont étudiés le problème de détermination des plans secondaires et tertiaires et les positions respectives des appuis en supposant que la surface principale et les positions des appuis sur cette surface sont connus.

Li & Melkote (1999) ont proposé un modèle d'optimisation de la configuration d'appuis et de brides afin d'améliorer la précision de positionnement de la pièce aux contacts supposés élastiques linéaires. Tandis que, L'effet de la séquence de bridage sur la précision de positionnement de la pièce est démontré expérimentalement par Raghu & Melkote (2004).

2.2.2 Erreur de positionnement de montage d'usinage

La configuration des appuis est choisie et la pièce brute est placée sur ces appuis. La pièce peut avoir l'erreur de positionnement à cause des variations au niveau des contacts entre la pièce et les appuis. De plus, la pièce étant bridée sur ses appuis

se déplace de sa position d'origine sous l'action des forces d'usinage et de bridage. Cette section présente brièvement la revue de la littérature sur la détermination de l'erreur de positionnement de la pièce à cause de défauts géométriques ainsi que les déformations des appuis.

Comme mentionné précédemment, le torseur de petit déplacement est largement utilisé dans l'analyse de la tolérance. La prédiction d'écart géométrique de la surface de la pièce, faite par le torseur de petit déplacement, est réalisée par Villeneuve *et al.* (2001), Zhu *et al.* (2012) and Legoff *et al.* (2004). L'approche analytique du torseur de petit déplacement est lourde, mais elle fournit un modèle détaillé par rapport au modèle numérique de CAO. Asante (2009) a calculé l'erreur global de positionnement de la pièce comme la somme de : l'erreur géométrique de la pièce, l'erreur géométrique des appuis et l'erreur de bridage par la matrice de transformation homogène et l'hypothèse de petit déplacement.

La raideur ou la conformité du montage à une grande importance dans la conception du montage d'usinage, ceci nous aide à déterminer la stabilité du montage sous des charges externes. Jayaram *et al.* (2000) ont établit la relation entre les rigidités de la pièce et celles des appuis. La raideur optimale des appuis est déterminée pour limiter la déformation globale de la pièce.

En considérant que les brides sont en contact élastique avec la pièce, une raideur optimale des appuis est calculée par Hurtado & Melkote (2001) pour une configuration 3-2-1r comme montré sur la figure 2.24. Pour la même configuration des appuis sur le montage, Raghu & Melkote (2005) ont calculé la position finale et l'orientation de la pièce, après serrage mais avant l'usinage, dues à des erreurs géométriques du montage à l'aide du

- Tableau des charges de la pièce présenté par Raghu & Melkote (2004)
- Par linéarisation de la raideur de contact présenté par Li & Melkote (2001).

Asante (2010) a examiné l'effet de la conformité du montage et les conditions de coupe sur la stabilité de la pièce en réponse à toutes les forces externes. Les contacts entre les éléments du montage et la pièce sont considéré élastiques. Il en conclut que la force de coupe a un impact plus important sur la déformation de la pièce que le changement des positions des appuis.

La valeur optimale de la force de bridage est également importante pour limiter le déplacement de la pièce sur le système de montage. La recherche comprend le calcul des forces optimales de bridage en considérant des contacts élastiques en stabilité statique (Li & Melkote, 2001; Li *et al.*, 2000) ainsi que la stabilité dynamique d'une pièce pendant son usinage (Deng & Melkote, 2006).

La détermination de la rigidité de contact du montage d'usinage est l'obstacle principal dans l'analyse de la rigidité du montage en raison de sa nature non-linéaire selon la théorie de contact d'Hertz. Dans la littérature, la FEA/FEM est également utilisé pour déterminer le déplacement de la pièce en prenant en considération le comportement non-linéaire du contact. Zheng *et al.* (2007) ont étudié l'effet de la densité du maillage et le frottement du contact de la pièce et des appuis sur la déformation globale de la pièce. Liao & Hu (2001) ont prédit la qualité de la surface d'usinage en prenant les brides et les appuis comme les éléments élastiques. En raison de leur comportement non-linéaire, les contacts ont été modalisés par les éléments finis.

2.2.3 Erreur de machine-outil

La précision de la pièce usinée est influencée par l'imprécision de la machine-outil qui existe toujours Par conséquent, il est nécessaire de compenser ces erreurs dues aux effets thermiques et mécaniques ainsi qu'au défaut géométrique de construction comme de mouvement de la machine. La compensation de l'erreur la plus facile est effectuée par la prise en compte dans le système de commande des défauts de la machine après une phase d'identification (Ramesh *et al.*, 2000). L'augmentation des axes de la machine provoque la diminution de la rigidité de la machine (Hsu & Wang, 2007). Choi *et al.* (2004) ont utilisé les matrices de transformation homogènes pour évaluer rapidement l'erreur de positionnement d'une machine-outil, par une mesure sur la machine (OMM) à l'aide d'un système de montage appelé "eight cube array artifact ". Jha & Kumar (2003) et Zhu *et al.* (2012) ont calculé l'erreur dans le chaîne cinématique utilisant les matrices de transformation homogènes et la compensation est réalisée en modifiant le programme sur une machines 5-axes. Une compensation complète ne peut être effectuée sur une machine à 3 axes en raison de la limitation d'orientation de l'outil.

Lin & Shen (2000) ont proposé un modèle générique pour l'erreur cinématique d'une machine 3 axes à l'aide des matrices de transformation homogènes. Martin *et al.* (2011) ont simulé l'usinage sur une fraiseuse à trois axes, pendant la phase de conception du produit, pour prédire l'erreur géométrique due aux ;

- Défauts géométriques des mises en position
- Erreurs géométriques de la machine-outil

Les défauts géométriques sont calculés en mesurant l'écart pour chaque mise en position au pire des cas (fig. 2.32), pour la réalisation d'une pièce en plusieurs sous-phases, on obtient finalement la précision globale de la pièce. De plus, l'erreur due à la chaîne cinématique de la machine-outil est calculée en utilisant les matrices de transformation homogènes et les hypothèses de petits déplacements. Raksiri & Parnichkun (2004) ont proposé un modèle pour la compensation d'erreur pour les erreurs géométriques et les erreurs due à la force d'usinage sur une machine de fraisage à 3 axes en utilisant une modélisation par réseaux de neurones.

2.3 Forces sur le système de montage

L'une des tâches principales du montage d'usinage est de soutenir la pièce contre les forces et les couples d'usinage pendant les opérations d'usinage. Le montage doit être capable de supporter les forces maximales d'usinage avec une déformation minimum possible de la pièce, donc l'effet des forces de coupe doit être pris en compte lors de la phase de conception.

La force de coupe, agissant sur l'outil de coupe lors de l'opération de fraisage, peut être caractérisée comme les forces axiales, radiales et tangentielles ou de coupe (fig. 2.34). La mesure directe des forces tangentielles et radiales est difficile parce qu'elles oscillent rapidement pendant la coupe. Un certain nombre de modèles pour les prédictions de force et le calcul de la vitesse de coupe (Araujo & Silveria, 1999; Ber *et al.*, 1988; Kim & Chu, 2004; Mativenga & Hon, 2005) ont été développés pour les outils spécifiques, matériaux de la pièce ou conditions de coupe. Dans notre cas, seule la force maximale agissant n'importe

quel point sur la pièce nous concerne, donc les forces d'usinage sont calculées en utilisant des équations mathématiques classiques obtenues à partir de Sandviken (1997), Sandviken (2011) et Pruvot (1993) détaillées dans la section 2.4 et l'annexe B.

2.4 Mécanique des contacts

Remark 2.4.1. *La capacité de positionner une pièce précisément dans un montage d'usinage est fortement influencée de plus par les déplacements de la pièce due à la déformation de contacts élastique du montage et de la pièce sous charge (Li & Melkote, 1999)*

Il s'agit à la fois des déformations (axiales, cisaillement et flexion) des appuis, et de la surface de contact au niveau de la pièce qui se déforme sous effet des forces externes.

La théorie du contact de Hertz a été établie pour prédire le comportement mécanique des surfaces idéalement lisses en supposant que le contact est parfait. Hertz a utilisé un modèle de contact prenant en compte deux surfaces sphériques élastiques ramené au contact d'un plan ayant une élasticité équivalente $\frac{1}{E'} = \frac{1-\nu_1^2}{E_1} + \frac{1-\nu_2^2}{E_2}$ et d'une sphère rigide ayant un rayon équivalent $\frac{1}{\rho} = \frac{1}{\rho_1} + \frac{1}{\rho_2}$. La formalisation de la théorie du contact de Hertz peut être retrouvée dans Johnson (1987).

Deux surfaces réelles en contact ne sont pas idéalement lisses donc le contact est établi par leurs aspérités qui provoquent une zone de contact plus petite que celle calculée par Hertz. Par similarité à l'hypothèse d'Hertz, le contact de deux surfaces rugueuses se simplifie par le contact d'une surface idéalement lisse et d'une une surface ayant une rugosité équivalente $\sigma = \sqrt{\sigma_1^2 + \sigma_2^2}$ (Johnson, 1987) où, σ est la rugosité moyenne (R_a) de la surface en contact.

La première analyse analytique basée sur la déformation des contacts sphériques rugueux a été effectuée par Greenwood & Tripp (1967) en supposant que la déformation est élastique. Ils ont montré que la zone de contact est directement proportionnelle à la rugosité de contact, tandis que la pression est inversement

proportionnelle à celle-ci. Mikic & Roca (1974) ont proposé une solution alternative numérique qui prend en considération la déformation plastique au contact. Greenwood *et al.* (1984) ont généralisé les résultats des deux modèles précédents en proposant un seul paramètre adimensionnel de rugosité α. Ils ont conclu que la pression de contact est gérée par α, si la valeur de α est inférieure à 0,05, l'effet de la rugosité devient négligeable et la théorie de Hertz peut être appliquée.

Bahrami *et al.* (2005) ont conclu que la distribution de pression maximale est le paramètre principal dans les calculs de contacts rugueux et ils ont proposé une expression généralisée pour la distribution de pression valable pour l'ensemble des contacts rugueux. Leur modèle généralisé donne des résultats analytiques très proches des valeurs expérimentales de (Greenwood *et al.*, 1984; Kagami *et al.*, 1983; Tsukada & Anno, 1979). Comme mentionné précédemment, la raideur de contact a un comportement non-linéaire. Le comportement non linéaire de la raideur de contact, quelque soit le contact « rugueux ou lisse » est montré dans l'équation 2.37.

2.5 Pièce support pour la validation

Pour illustrer et vérifier les modèles développés, un type d pièce complexe qui nécessite un usinage précis , avec des possibilités de variations dimensionnelles d'une pièce à l'autre a été choisi Il s'agit d'une prothèse de hanche fabriquée en une seule pièce, mettant en œuvre un procédé d'usinage et un système de montage précis et rentable.

Pour la plupart des patients, les hanches standards disponibles dans le marché sont utilisables mais, pour certains cas les prothèses personnalisées sont fabriquées pour satisfaire aux besoins. La fabrication d'une prothèse personnalisée donc unique et chère comprend un modèle RP (prototypage rapide) pour la vérification du programme pièce réalisé par dans un matériau standard, puis la pièce est réalisée par fraisage CNC dans un matériau biocompatible par exemple le Titane. la configuration de fabrication est présentée figure 2.40.

Il ya un certain nombre de fabricants de prothèses autour du monde par exemple Johnson & Johnson, Zimmer Holdings, Inc., Implex Corp. etc. (Brewster, 2006). Parmi tous les fabricants, la base de données de la prothèse n'est disponible

que sur le site de Zimmer. Donc, pour la validation du modèle cinématique, le CPT® 12/14 Prothèse de hanche par Zimmer (zimmer, 2011) est choisi.

2.6 Conclusion

Dans ce chapitre, le contexte théorique de la conception du montage a été présenté. Commençant par le concept fondamental d'association des surfaces réelles avec des surfaces théoriques en utilisant MMT (machine à mesurer tridimensionnelle) la conception des montages et leurs effets sur la qualité du produit ont été détaillés. L'erreur de positionnement de la pièce peut être transformée en déformation des appuis par le biais de la matrice de Plucker.

Une revue de la littérature des travaux de recherche existants sur l'erreur de positionnement de la pièce pendant l'usinage est décrite brièvement. Elle comprend les erreurs suivantes : géométrique de la pièce brute, placement des appuis, positionnement du montage, de la machine-outil (géométrie et cinématique). Cette thèse a pour objectif l'erreur de positionnement de la pièce à la fois due à la variation de la géométrie de la pièce brute, et sous l'effet des forces d'usinage et de bridage. Les déformations peuvent être calculées grâce à la rigidité de chaque élément élastique du montage. La déformation de contact est non-linéaire selon la théorie de l'Hertz et donc ne permet pas d'avoir une solution simple. A la fin, une prothèse d'hanche par Zimmer (zimmer, 2011), nécessaire à une opération d'usinage précis, est choisie comme une pièce de démonstration de la méthodologie développée.

Quant au chapitre 3, il présente un modèle analytique cinématique d'un système ayant une configuration 3-2-1r des appuis pour le positionnement précis de la pièce dans les coordonnées machine. Tous les éléments sont considérés rigides et sans frottement au niveau du contact. Un modèle mécanique du système du montage est présenté dans le chapitre 4 en considérant l'ensemble pièce- support-pièce comme les éléments rigides, cet ensemble est placé sur une palette (support) par l'intermédiaire d'appuis considérés comme des éléments élastiques. Le plateau (support-pièce) est aussi considéré comme localement élastique au niveau des contacts. Ce modèle mécanique calcule le vecteur de déplacement de la pièce dans les coordonnées machine. Le déplacement est transformé en une déformation

au niveau de chaque appui en utilisant les équations d'énergie et la matrice de Plucker. La compensation d'erreur peut être effectuée sur la pièce en utilisant le modèle cinématique.

Pour l'illustration et la vérification, le modèle cinématique de repositionnement sera présentée sur un type d pièce complexe dont les dimensions changent d'une pièce à l'autre et qui nécessite l'usinage précis sur un matériel coûteux. A cet effet, une prothèse de hanche est choisie comme une pièce démonstrative.

Chapitre 3

Modèle cinématique de montage d'usinage

Les petites variations dimensionnelles entre deux pièces de la même famille de pièces peuvent causer le mauvais usinage ou assemblage des pièces. Pour un usinage précis, ces variations doivent être compensées par une opération de pré-positionnement. Il est nécessaire d'avoir un mécanisme afin d'effectuer la transformation cinématique pour mettre la pièce à la position requise compensant l'erreur de positionnement entre la pièce et la machine outil. Le nombre d'axes nécessaires sera d'autant plus important que la pièce est complexe. Cette modification de position de la pièce ou de l'outil est habituellement faite en utilisant des machines à quatre ou cinq axes. Si les déplacements restent faibles ou si l'on ne dispose que de machines 3 axes ou bien dans le cas d'une pièce devant subir plusieurs opérations sur différentes machines (ligne de fabrication), il est économiquement intéressant de mettre en œuvre un système de repositionnement de la pièce qui peut être ajouté à n'importe quelle machine ou déplacer entre machines.

3.1 Système de montage d'usinage proposé

Dans ce chapitre, un modèle cinématique d'un système de montage de repositionnement à 6 DDL[1] capable de compenser des erreurs de positionnement de la pièce par la réorientation de la pièce dans la position requise dans les coordonnées machine par l'avancement axial des six appuis est proposé.

Comme il y a une incertitude sur la position des points de contacts des appuis avec la pièce à cause des irrégularités de la pièce brute qui entraine une incertitude sur la position finale de la pièce par rapport à la machine un plateau mobile sur lequel est fixé rigidement la pièce est introduit. Ce plateau cuboïde[2] est fabriqué de telle manière que ses surfaces peuvent supposer parfaitement plane et orthogonales est posé sur 6 appuis possédant un degré de liberté en translation axiale (posage de type 3-2-1r) sur la machine ou sur une palette. Le système de montage d'usinage est proposé montré sur la figure 3.7, où une prothèse de hanche est utilisée comme pièce à usiner.

Pour le modèle cinématique, tous les éléments du système de montage sont supposés être rigides avec un frottement nul au niveau des contacts entre le plateau et les appuis. Les positions et les orientations des appuis sont prédéfinies, l'ensemble pièce, porte-pièce, palette plateau est placé sur les appuis et la position de la pièce est mesurée par la MMT. Un algorithme basé sur les matrices de transformations homogènes avec grands déplacements est développé. Il calcule l'avancement de chaque appui nécessaire au déplacement de la pièce vers la position requise.

3.2 Formalisation du modèle cinématique

Une formalisation mathématique nous permettant de réorienter la pièce par l'avancement axial de six appuis, à partir de la position initiale (mesurée par exemple sur MMT) et jusqu'à la position finale (requise) est développée. Les positions du plateau et de la pièce seront calculées dans les coordonnées machine.

[1] DDL : degrés de liberté

[2] Cuboïde : Parallélépipède rectangle avec tous les angles droits et les faces opposées égales

La position et l'orientation du plateau peut être calculé par les positions de l'ensemble des six appuis. La position du plateau est définie à partir de la cuboïde formé par les centres des sphères des six appuis en contact avec le plateau, avec un offset égal au rayon de sphère comme indiqué dans la figure 3.8. Les avancements des appuis sont la différence entre la position initiale et finale de l'ensemble pièce-plateau. Par conséquent, les centres des sphères en contact peuvent être directement utilisés pour les calculs sans prendre en compte les rayons des sphères (tous identiques). Le plateau est posé sur les appuis suivant une configuration de type 3-2-1r. En ce qui concerne les trois appuis en contact sur le plan principal, les trois centres des ces trois appuis forment deux lignes dans le plan qui donnent un vecteur normal $\vec{N_1}$ au plan principal du plateau. Deux points de contact sur le plan secondaire ainsi que la normale au premier plan forment une normale $\vec{N_2}$ sur le plan secondaire. Comme toutes les surfaces du plateau sont orthogonales, la normale $\vec{N_3}$ au troisième plan peut être directement calculée par le produit vectoriel de $\vec{N_1}$ et $\vec{N_2}$. Les vecteurs unitaires des trois normales sont calculés afin d'obtenir la matrice de transformation homogène (MTH) des coordonnées plateau dans le repère machine. Le calcul des vecteurs unitaires est détaillé dans la section 3.3.1 et la MTH finale de l'origine de la machine (O) à plateau (b) est indiqué dans l'équation 3.13.

Les coordonnées de la pièce sont ainsi définies afin qu'elle puisse subir à RTL[1] transformation. La MTH de la pièce à un point " P" dans les coordonnées de la machine " O" est représentée par $[P_{OP}]$ et écrite dans l'équation 3.15.

La transformation des références du système de montage est indiquée dans la figure 3.10. Les avancements finaux des six appuis peuvent être trouvés comme les fonctions des trois matrices de transformation homogènes,

- La position initiale de la pièce connue et mesurée par le MMT
- La position finale de la pièce considérée comme la position souhaitée de la pièce
- La position initiale du plateau comme fonction des positions des six appuis

[1]RTL :Roulis(α), Tangage(β), Lacet(γ)

Toutes les MTHs ci-dessus sont connues. Par conséquent, le déplacement final des six appuis, calculé par l'algorithme, et qui permettra le repositionnement de l'ensemble pièce-plateau, peut être obtenue comme un MTH et indiquée dans l'équation 3.18. Mais, les appuis ne peuvent avancées que dans leurs directions axiales et ne peuvent pas se déplacer vers les positions calculées par le MTH, un calcul supplémentaire est nécessaire

Ici, nous avons l'avantage de faire l'hypothèse d'un plateau avec les surfaces planes de haute qualité. Les centres des sphères en contact avec le plateau forment un cuboïde avec trois surfaces planes. Les positions finales des appuis forment également un cuboïde. Une formalisation d'avancement des appuis axialement est réalisée de telle manière que leur cuboïde vienne s'aligner avec le cuboïde formé à partir des positions finales des appuis calculés par l'équation 3.18. Le point de contact de chaque appui est calculé à partir des positions latérales identifiées. La méthode est expliquée en figures 3.11 et 3.12.

La matrice de Plucker peut être utilisée pour relier la précision ou l'incertitude des appuis à la précision globale ou l'incertitude de la pièce. La matrice Plucker, pour le système du montage proposé, est calculée dans la section 3.3.5 qui donne la précision du déplacement de la pièce $\{\delta\} = \{\delta x_P, \delta y_P, \delta Z_p, \delta\beta, \delta\gamma, \delta\alpha\}^T$ à la précision de chacun des six appuis $\{\xi\} = \{\xi_1, \xi_2, \xi_3, \xi_4, \xi_5, \xi_6\}^T$. La qualité des appuis et leur précision de positionnement peut être choisie en fonction de la précision de la pièce requise.

3.3 Illustration sur une étude de cas

Une étude de cas a été effectuée afin de simuler et valider le repositionnement d'une prothèse de hanche bridée sur le plateau. L'ensemble pièce-plateau est situé sur les appuis ayant la configuration de type 3-2-1r. Le modèle est créé sous CATIA® en utilisant les données réelles de la prothèse de hanche. Pour simuler l'opération d'usinage, un demi modèle d'empreinte (semblable à un moule) de la pièce (figure 3.15) est créé avec les dimensions d'origine de la prothèse de hanche. Cette empreinte (moule) est placée sur une position fixe par rapport à l'origine de la machine. Le matériau de la pièce, est enlevé en utilisant une opération booléenne pour simulé l'usinage. Après l'usinage de la première moitié,

la pièce est retournée et fixée au plateau pour l'usinage de la deuxième moitié. Deux supports sont également ajoutés de chaque côté de la prothèse pour fixer la pièce et mesurer sa position pendant le positionnement de la deuxième moitié. Une autre empreinte est crée en CATIA® pour simuler l'usinage de la deuxième moitié.

La pièce est placée et fixée sur le plateau avec tous les éléments de bridage sur le plateau. Comme on suppose que la position initiale de la pièce est mesurée par MMT, l'orientation de la pièce et la position d'un point de référence P de la pièce sont mesurées sous CATIA®. Les positions initiales des six appuis sont déjà connues. Elles permettent à l'algorithme de calculer la position du plateau dans le référentiel de la machine. La position finale souhaitée de la pièce et le point de référence P sont également connues. Les avancements de tous les six appuis sont les seuls six paramètres contrôlables dans le modèle CATIA®.

Pour la simulation et la visualisation, une grande erreur initiale est induite dans la position souhaitée de la pièce avant de la fixer sur le plateau. La position initiale du point P et l'orientation de la pièce sont données dans la table 3.1. L'algorithme calcule les positions finales de tous les appuis (tableau 3.4) pour placer la pièce à la position souhaitée en utilisant les avancements axiaux de l'ensemble des six appuis. La même procédure est appliquée pour le repositionnement de la deuxième face de la pièce.

Les positions des appuis sont définies avec deux chiffres significatifs après la virgule en CATIA® donc une erreur de positionnement est constatée entre les positions requises et réelle de la pièce. Comme expliqué précédemment, la précision de repositionnement de la pièce dépend de la précision ou l'incertitude des déplacements axiaux des appuis. Plus la pièce aura une incertitude de position faible plus les appuis devront être précis. Pour des positions données des appuis (tableau 3.2), la précision ou l'incertitude de la pièce est calculé en fonction de l'incertitude axiale en utilisant l'équation 3.36. A fin de mettre en évidence la robustesse de la méthode, l'effet de la précision des appuis sur la précision ou incertitude de la position de pièce est présentée dans le tableau 3.7.

3.4 Conclusion

Ce chapitre présent un modèle cinématique analytique pour le repositionnement de la pièce dans le repère machine par les avancements axiaux des six appuis ayant une configuration de type 3-2-1r. Dans le système de montage proposé, un plateau est introduit entre la pièce brute et les appuis pour éviter des erreurs locales à cause des variations au niveau des contacts entre le plateau et les appuis. Le plateau est réalisé de telle manière que ses surfaces soient planes et orthogonales entre elles. Tous les éléments du système sont considérés rigides. De plus, le frottement au niveau des contacts est considéré comme négligeable et les grands déplacements sont pris en compte.

Pour le repositionnement, les matrices en coordonnées homogènes sont utilisées pour la transformation des coordonnées depuis la machine à la pièce et au plateau. La position initiale de la pièce peut être mesurée sur une MMT. La position du plateau est calculée en termes de normales aux surfaces grâce aux positions des 6-appuis en contact avec le plateau. Les positions finales de tous les appuis, sont calculées en réorientant le cuboïde formé par les six appuis à celui formé par les positions calculées. Le modèle cinématique est illustré et validé par la simulation en CATIA®, effectuée sur une prothèse de hanche. De plus, l'effet de la précision des repères sur la précision de positionnement de la pièce est discuté.

Dans le chapitre suivant, les appuis et les brides seront considérés comme des éléments élastiques et en plus les forces de bridage et d'usinage seront introduites. En prenant en compte les hypothèses de petit déplacement de la pièce, la déformation de chaque appui est calculée La compensation sera effectuée par un repositionnement des appuis en utilisant le modèle cinématique développé dans ce chapitre et en considérant tous les éléments de montage rigides.

Chapitre 4

Déformation des éléments élastiques

Dans le chapitre précédent, un modèle cinématique du système a été présenté en considérant tous les éléments indéformables. Ce modèle est donc capable de corriger l'erreur de positionnement si les positions initiale et requise de la pièce sont connues. En réalité, les appuis peuvent se déformer sous l'effet du poids du plateau, des forces statiques et dynamiques agissant sur la pièce ou sur d'autres pièces du montage. Le plateau, repositionné par modèle cinématique, doit en effet être bridé pour rester dans la position préalablement corrigée et pouvoir supporter les forces d'usinage, par exemple. Ces forces impliquent les déformations du système donc des déplacements de l'ensemble plateau-pièce. Afin que la position précédemment corrigée, soit encore au plus près de la position souhaitée, il est nécessaire de connaitre les déformations engendrées par les efforts, pour en tenir compte dans le calcul de la position corrigée.

Dans ce chapitre, un modèle mécanique du système du montage est donc formalisé pour calculer le déplacement de la pièce sous l'action des forces externes. Pour construire le modèle, on suppose que, de par la conception, l'essentiel des déformations se produisent dans les zones de contact, dans les appuis et dans les brides, l'ensemble pièce-plateau étant réputé indéformable. Du point de vue des masses, on considère que la masse du plateau et de la pièce est très supérieure à celles des appuis sphériques. Par le formalisme de Lagrange, résolu

dans Mathematica®, on obtient la matrice de rigidité qui dépend de tous les paramètres mécaniques (positions des appuis, orientation, dimensions, matériaux). L'hypothèse des petits déplacements peut être appliquée puisque les déformations doivent rester faibles pour la fiabilité et la précision du système.

Ce chapitre se décompose comme suit : D'abord, le modèle mécanique du système du montage proposé est construit en considérant l'assemble pièce-plateau rigide et les appuis élastiques linéaires. Ensuite, l'énergie globale du système composée de l'énergie potentielle contenue dans tous les appuis et les brides, l'énergie cinétique d'éléments de masse et le travail accompli par les forces externes appliquées sont calculés. La formalisation de Lagrange permet de calculer les matrices de rigidité et de masse du système de montage dans une configuration choisie. On peut alors en déduire le déplacement de l'ensemble pièce-plateau sous charge et la déformation de chaque appui. Le frottement de contact appui-plateau est négligé. Puis, pour le contact hertzien, la déformation est calculée pour chaque appui avec la formalisation modifiée qui nous permette d'obtenir la déformation globale de chaque appui et le déplacement d'ensemble pièce-plateau. Enfin on terminera le chapitre par une discussion sur le champ d'application de ce modèle mécanique.

4.1 Représentation et formalisation du modèle mécanique

Le modèle mécanique du système de montage de base, c'est à dire sans brides ni forces externes, est illustré dans la figure 4.1. Dans un premier temps, on considère les appuis comme étant des éléments élastiques linéaires sans masse, représentés chacun par une matrice de rigidité propre. L'essentiel de la masse en mouvement du système se trouvant sur le plateau massif, ce dernier est supposé indéformable et représenté par sa seule matrice de masse. A ce stade, on néglige les déformations des contacts entre les appuis sphériques et les surfaces planes du plateau.

La transformation des repères du système du montage est montrée dans la figure 4.2, où les positions corrigées dans le modèle cinématique sont prises comme

les positions initiales. Les forces d'usinage et de bridage provoquent un déplacement de l'ensemble pièce-plateau sur les appuis élastiques qui peuvent être compensés par une modification de l'avancement des appuis, calculés par le modèle cinématique. On renseigne préalablement les informations sur la configuration du système (positions et orientations des appuis, des brides, matrices de rigidité, matrice de masse du plateau) et sur le cas de chargement (emplacement et amplitudes des forces et des moments appliqués). Le calcul du modèle mécanique du système (rigidité et masse) du montage est effectué en utilisant l'hypothèse des petits déplacements et le formalisme de Lagrange (eq. 4.1).

4.1.1 Formalisation

Pour le système représenté figure 4.1, L'énergie potentielle totale du système est donc la somme des énergies potentielles de chaque appuis, seuls éléments élastiques considérés à ce stade. L'énergie potentielle totale des appuis peut s'écrire comme le suggère l'équation 4.2. Une transformation géométrique est effectuée pour calculer les vecteurs de déformation des appuis en fonction du vecteur de déplacement de l'ensemble pièce-plateau en utilisant l'hypothèse des petits déplacements. L'Énergie cinétique totale, correspondant aux déplacements linéaires et angulaires, de tous les éléments de masse du système du montage est calculée en utilisant la formalisation de Lalanne *et al.* (1986). L'énergie cinétique totale est peut s'écrire sous la forme 4.11.

Le travail effectué par les forces externes est calculé pour résoudre la formalisation Lagrangienne. Le torseur des forces externes comprend le vecteur des forces d'usinage et le vecteur des couples d'usinage. Le travail global sera la somme des travaux des forces et des moments (eq. 4.12). Le vecteur-déplacement du point d'appui de chaque action mécanique est calculée pour en déduire l'ensemble de travail effectué par le torseur de force externe sur le système du montage en fonction du vecteur déplacement de l'ensemble pièce-plateau.

Une fois l'ensemble pièce-plateau positionné sur ses 6 appuis, il est maintenu en position pendant l'opération d'usinage, par le serrage de brides. Cela provoque une déformation des appuis élastiques, et un déplacement additionnel de l'ensemble

pièce-plateau dans le repère machine. Ces brides peuvent être considérées de deux manières ;

- Les brides sont remplacées par des forces statiques constantes et peuvent être considérées comme les forces externes. Le travail des forces de bridage sera calculé en utilisant l'équation 4.14 et le travail total fera la somme des travaux accomplis par les forces externes et les forces de bridage.

- Si les brides sont considérées comme des éléments élastiques, avec une extrémité en contact avec le plateau et une autre déplacée d'une valeur connue (précontrainte) comme illustré dans la figure 4.6, l'énergie potentielle contenue dans chaque bride sera calculée et sera ajoutée à l'énergie potentielle totale du système.

Dans notre cas, nous considérons les brides comme des éléments élastiques dont on connaît les déplacements externes. Le déplacement du point d'appui de la bride sur le plateau est calculé à partir du vecteur-déplacement de l'ensemble pièce-plateau. L'énergie potentielle globale de toutes les brides peuvent être calculées en utilisant l'équation 4.17.

L'énergie potentielle globale des appuis et des brides, l'énergie cinétique du système du montage et le travail effectué par chacune des forces externes sont formulées en fonction du même vecteur- déplacement de la pièce, contenant les coordonnées généralisées de déplacement. Le formalisme de Lagrange permet alors de trouver les équations du mouvement associée à chaque paramètre, puis d'en déduire les matrices de rigidité et de masse. Après application des hypothèses de petits déplacements, certains termes contenant encore des paramètres se simplifient. Le modèle mécanique étant établi, il est alors possible de l'exploiter en étudiant les déformations dues à des forces statiques appliquées (à des fins de compensation) ou la réponse vibratoire à une excitation forcée (schéma de la figure 4.8).

4.1.2 Déformation des appuis sans frottement

La déformation de chaque appui sous les forces de bridage et d'usinage peut être calculée à partir du déplacement de l'ensemble pièce-plateau en utilisant la

matrice pluckérienne du système du montage. La déformation d'un appui sous les forces externes est représenté dans la figure 4.9 où le plan du plateau, en contact avec l'appui est déplacé à partir de la position initiale jusqu'à la position finale sous charge. En l'absence de frottement, l'appui, modélisé par une raideur axiale (direction de réglage) et radiale, ne se déforme pas nécessairement suivant la normale au contact, mais il subit des déformations axiale et radiale dans une proportion correspondant au minimum d'énergie de déformation minimale. La direction de la normale avec l'axe de réglage de l'appui, étant lui aussi déterminant (équation 4.25).

4.1.3 L'énergie potentielle des appuis sans frottement

L'absence de glissement des appuis sur le plateau peut conduire à une surestimation de la rigidité du système, puisque les appuis contribuent à la stabilité du plateau avec une même efficacité quelle que soit leur orientation spatiale.

Les déplacements radial et axial déduit précédemment de l'orientation de l'appui, de ses différentes rigidités en fonction du déplacement normal à l'appui, sont utilisés pour formuler l'énergie potentielle totale via le formalisme de Lagrange.

4.2 Les contacts élastiques non linéaires

Dans la section précédente, la déformation des appuis sous charge est calculée en considérant l'ensemble pièce-plateau comme rigide et les appuis étant élastiques sans déformation au niveau du contact entre les appuis et le plateau. La déformation d'un appui était uniquement dépendante de la matrice de rigidité du volume-matière. En réalité, le contact d'appui-plateau est déformable et subira une déformation locale sous les forces appliquées. La contribution de la déformation de contact au déplacement total devient plus importante, lorsque les appuis sont plus rigides.

Dans cette section, de petites déformations localisées peuvent se produire sur le plateau et sur les sphères d'appuis, en, chacun des points de contact. Le reste du plateau étant toujours considéré comme indéformable. Le contact appui-plateau est montré dans la figure 4.11 en considérant que le contact entre les deux

corps élastiques est assimilable à un contact entre un plateau rigide et une sphère d'élasticité équivalente ; conformément à la théorie de Hertz. Pour le contact entre un plateau plan et l'appui sphérique, la déformation maximale sera localisée au centre de la zone de contact formalisé par Bahrami *et al.* (2005) et détaillé dans la section 2.5.3.

En considérant que les surfaces en contact pourraient présenter des rugosités, contrairement aux hypothèses de Hertz, le modèle de Bahrami *et al.* (2005), essentiellement basé sur une étude adimensionnel à partir de produits sans dimensions, est appliqué, pour calculer, à partir des formules de Hertz, les aires et pressions de contacts, ainsi que les déformations . Pour éviter le recours au calcul numérique et aux tests, proposé par Bahrami *et al.* (2005), les équations de l'aire adimensionnelle a'_L de contact ont été ajustées par le critère des moindres carrés afin de proposé une seule expression analytique (eq. C.1) quelle que soit sur la valeur de P'_0 (eq. 2.34).

L'équation, d'estimation d'aire non-dimensionnelle de contact, proposé est comparée avec celle proposée par Bahrami *et al.* (2005) dans les figures C.1 et C.2. Pour l'estimation de la déformation au centre de l'aire de contact, déterminante pour connaitre la raideur du contact, Bahrami utilise la fonction numérique beta (B), qui n'a pas de formulation analytique (eq. 2.36). La fonction beta (B) est en plus une fonction de la "fonction gamma (Γ) "(eq. C.2). Ces fonctions numériques ont tendance à ralentir les calculs itératifs, d'où la nécessité de trouver des approximations explicites de leurs formules.

Les modèles d'estimation existants pour la fonction de $\Gamma(x)$, l'approximation de Stirling (Abramowitz & Stegun, 1972) et l'approximation de Gergo (Nemes, 2008), entre autres, donnent des erreurs importantes lorsque le paramètre γ est petit, zone qui nous intéresse tout particulièrement dans notre application sur le contact (faible valeurs de γ)

Une expression analytique pour l'estimation de la fonction Γ (eq. C.3) est choisie, et, par l'ajustement de la fonction approchée sur les résultats numériques exacts pour un grand nombre des valeurs de paramètre γ.

Une comparaison des erreurs parmi les estimations existantes de gamma et bêta fonctions et l'estimation proposées est montré dans la figure C.3. L'expres-

sion proposée pour la fonction gamma, donne des meilleurs résultats pour les petites valeurs de γ, intéressants dans le cadre de notre travail.

Une fois la déformation de contact est connue, la raideur de contact peut être calculée. Pour les valeurs réalistes de la rugosité du contact, l'effet de la rugosité du contact sur ses rigidité et déformation sont indiquées dans les figures 4.15 et 4.16. On observe que l'augmentation de la rugosité de surface provoque la diminution de la raideur du contact par rapport à celle donnée par la théorie de Hertz.

La qualité des surfaces en contact doit être choisie en fonction des conditions fonctionnelles ; une surface de très bonne précision n'aura pas nécessairement d'influence sur l'écart géométrique. Si la raideur minimale du contact, dont résulterait une déformation acceptable sous les efforts d'usinage, est connue, une "rugosité économique" peut être définie afin de ne pas réaliser de superfinition inutile fonctionnellement.

4.3 La déformation totale des appuis

Les déformations globales de chaque appui seront la somme des déformations non-linéaires au point de contact et des déformations du corps de l'appui. Le comportement non linéaire des contacts dépend des efforts de contact, qui dépendent du déplacement du plateau, qui est calculé par la matrice de rigidité du système. Cette dernière est, nous l'avons vu, une conséquence de la rigidité des appuis, partiellement liée aux propriétés des contacts. Un calcul itératif est nécessaire afin de déterminer le point de fonctionnement et le déplacement exact à compenser pour positionner le plateau, comme il faut.

Un processus itératif est effectué pour la convergence de la déformation des contacts non-linéaire des six appuis et pour obtenir les déformations finales linéarisées de chaque appui comme montré dans le diagramme de la figure 4.14. La position d'initialisation suppose les contacts indéformables. A chaque itération, on modifie la position du plateau en fonction de la déformation calculée, on en déduit les déplacements imposés aux appuis, la rigidité de chaque appui et enfin la matrice de rigidité.

L'algorithme, stable, présente des oscillations nuisant à la convergence rapide : On applique un gain d'atténuation dans l'équation 4.33 sur la variation de la position, afin de amortir les ondulations.

4.4 Etude de cas

Une étude de cas est réalisée pour présenter le fonctionnement et les résultats du modèle mécanique proposé. La pièce étudiée est une prothèse de hanche en acier M30W. Un système de montage est considéré (fig. 4.17) ayant ; 6-appuis, avec des matrices de raideur $[K]_1, [K]_2, ...[K]_6$, et deux brides élastiques. $\{X_E\}_1$ et $\{X_E\}_2$ sont les vecteurs de déplacement externes, correspondant à la précontraintes des brides de serrage. $\{F\}$ et $\{\mathbb{T}\}$ sont les vecteurs de la force et le couple d'usinage, respectivement.

Les positions initiales des appuis sont choisies arbitrairement (tab. 4.4) pour placer le plateau à une position aléatoire. Les trois angles initiaux d'inclinaison, du plateau suivant la transformation RTL, sont calculés, via les positions initiales des appuis, par calcul des normales aux surfaces du plateau, en utilisant l'équation 4.34. Les positions initiales des appuis et l'inclinaison initiale du plateau nous permettent de calculer la position du point de contact de chaque appuis avec le plateau par rapport au point P du plateau comme indiqué dans le tableau 4.7. La position du point P a été mesurée en utilisant la modélisation volumique sous CATIA®.

La matrice de raideur du premier appui est calculée par ses raideurs axiales, raideur de cisaillement et raideur de flexion. Les matrices de raideurs pour le reste des appuis sont obtenues par leurs avancements et leurs orientations relatives par rapport au premier appui (tab. 4.8). Les matrices de masse et d'inertie du système du montage, au point P, sont mesurées directement à partir du modèle volumique sous CATIA®, la matière choisie étant de l'acier. Les positions des brides sont également mesurées à partir du modèle sous CATIA® et leur positions relative par rapport au point P sont calculées. Les brides sont modélisées comme des ressorts unidirectionnels. Dans l'étude, une opération de fraisage en bout sur une pièce médicale, est choisie et les vecteurs des forces et du moment sur un point de f sont calculés en utilisant les équations dans la section 2.4 et l'annexe B.

Toutes les données sont introduites dans Mathematica® qui calcule l'énergie potentielle totale de tous les brides et les appuis, de l'énergie cinétique des éléments d'inertie et le travail effectué par les forces externes. La formulation de Lagrange calcule la matrice de raideur globale du système de montage, les modes propres et le vecteur de déplacement de l'ensemble pièce-plateau sans tenir compte du contact et également après la convergence du déplacement tenant compte l'effet de la raideur du contact. Les valeurs dans la matrice de rigidité, avec contacts indéformables, est plus grande d'où des déplacements plus grands en final, que ceux utilisés pour la première itération.

Les paramètres de déplacement de l'ensemble pièce-plateau, la déformation de chaque appuis et les modes propres du système de montage sont présentés dans le tableau 4.12, table 4.13 et l'équation 4.39 respectivement. Comme le modèle cinématique peut être utilisé pour compenser les erreurs de positionnement calculées par le modèle mécanique, la compensation peut être effectuée par l'avancement de chaque appui comme indiqué dans le tableau 4.14.

Le système du montage est moins rigide dans la direction X sans tenir compte de la raideur du contact tandis que dans la direction Y après la convergence. Un changement important dans la rigidité globale du système et sur le déplacement calculé pour la pièce sous charge est remarqué. Il souligne l'importance de la raideur de contact sur le calcul d'erreur de la pièce.

La convergence de chaque paramètre du déplacement de la pièce et leurs erreur de convergence sont présentées dans la figure 4.20 et figure 4.21 respectivement, pour le gain de 1. La convergence est atteinte dans 47 itérations pour la limite d'erreur prédéfinie de 0,01%, Pour voir l'impact du gain de la convergence, le paramètre $\Delta\beta$ et ses erreurs sont présentés dans les figures 4.22 et 4.23 respectivement. En effet, ce paramètre est celui qui converge le plus lentement dans l'exemple. Les oscillations des résultats sont bien atténuées par un gain réduit. La vitesse de convergence est peu sensible.

Pour avoir une estimation du comportement dynamique du système, l'analyse dynamique est aussi réalisée utilisant les détails de l'annexe D. Un diagramme de Bode est tracé pour présenter le rapport entre les déformées dynamique et statique en fonction de la vitesse angulaire de la broche pour différentes valeurs de bridage. Il a été remis en évidence que les modes de vibration peuvent être

déplacées vers des valeurs supérieures ou inférieures en serrant ou desserrant les brides.

4.5 Conclusion

Dans ce chapitre, un modèle mécanique du système est construit afin de calculer les petits déplacements de la pièce et son comportement sous charge en fonction de la configuration choisie et de la position initiale avant application des forces. Le calcul de la raideur et la masse de l'ensemble de système du montage est réalisé en tenant compte des appuis élastiques de masse négligeable alors que l'ensemble pièce-plateau est pris comme élément rigide mais pesant. Les contacts sont considérés de type hertzien. Les brides sont considérées comme des éléments élastiques et précontraints.

Mathematica® est utilisée pour résoudre le modèle mécanique en utilisant les équations de Lagrange. La formulation de Lagrange nous permet d'établir les équations des mouvements associés aux 6 DDL du plateau, et d'en déduire les matrice de raideur et de masse du système. L'exploitation permet ensuite d'évaluer le déplacement du plateau sous l'action d'une charge extérieure. L'avantage du formalisme de Lagrange est qu'il est insensible aux variations de configuration du système.

Le comportement non-linéaire de la déformation de contact sous charge est intégré dans le modèle, et permet par un calcul itératif stabilisé de donner les déformations des appuis, avec une précision prédéfinie à l'avance (0,01% ici). Le modèle mécanique proposé peut être appliqué aux problèmes plus complexes avec plusieurs forces externes et des orientations différentes des appuis et des brides. Le problème de la perte de contact sur un appui est traité dans les itérations pour éviter de recherche une convergence sur une pièce déséquilibrée.

Chapitre 5

Conclusion and Perspectives

5.1 Conclusion

Cette thèse est positionnée dans le domaine de la conception et la modélisation d'un montage de fabrication reconfigurable. A partir de la géométrie des pièces du montage, de leur qualité dimensionnelle et de la configuration choisie pour l'assemblage, le travail consistait en l'établissement d'un modèle géométrique, permettant un repositionnement précis de la pièce, puis la construction d'un modèle mécanique permettent de corriger cette position, en tenant compte des efforts appliqués, par le bridage et par le processus de fabrication. Le tout permettant la mise en position de la pièce, avec une précision prévue de 10 μm.

La position de la pièce par rapport au repère machine, ou par rapport à la palette de transport, étant mesurée, le décalage sur les 6 axes par rapport à la valeur demandée par le processus de fabrication est calculé afin d'en déduire les réglages en translation à apporter à chacun des 6 appuis unidirectionnels . Ensuite, en suivant un protocole de bridage, les efforts appliqués étant connus, la déformation imposée au montage est prédite par le modèle mécanique, ce qui permet de déduire les avancements additionnels à apporter aux appuis, pour qu'à l'issue du bridage, la pièce soit placée conformément au contrat de fabrication ou d'assemblage, avec la précision requise.

Pour atteindre cet objectif de modélisation du système de repositionnement, la thèse se décompose comme suit :

- Une étude bibliographique sur les erreurs de positionnements et leur origines rencontrées au cours de la conception du montage est effectuée. Les principales causes des erreurs de positionnement sont : l'écart de la géométrie de la pièce brute par rapport à la géométrie nominale, les erreurs de placement des appuis, les erreurs de posage du montage par rapport à la machine et les erreurs dues à la précision de machines-outils ou les erreurs cinématiques. L'étude se focalise sur les erreurs de positionnement de la pièce dans le repère de fabrication, due aux variations de dimensions, auxquelles s'ajoutent les déformations provoquées par les efforts appliquées à un système déformable. On utilise la théorie de contact de Hertz pour modéliser la comportement non-linéaire des contacts entre appuis et plateau.

- Un modèle analytique cinématique pour le repositionnement de la pièce dans la machine, est proposé. Le modèle cinématique est capable de réorienter la pièce vers la position désirée par le mouvement axial des 6 appuis, disposés suivant un dispositif de type 3-2-1r. Dans cette étude purement cinématique, tous les éléments mécaniques du système proposé sont considérés indéformables et aucun frottement n'est pris en compte au niveau des contacts. La correspondance entre les déplacements des 6 appuis et la transformation géométrique associée est donnée. La transformation nécessaire au bon positionnement de la pièce est calculée à partir de la position initiale de la pièce sur la palette, mesurée par un dispositif de type machine à mesurer tridimensionnelle, et de la position finale, imposée par le processus de fabrication et d'assemblage. De cette transformation, les avancements nécessaires sont déduits en tenant compte de la précision de réglage.

- Afin de corriger les petites déformations dues aux efforts appliqués, un modèle analytique mécanique est proposé en supposant l'ensemble pièce-plateau rigide. Les appuis sont alors des éléments élastiques et l'hypothèse de petits déplacements est appliquée ici. Au niveau des contacts entre appui et plateau, des déformations locales se produisent et le modèle considéré est celui d'un contact hertzien sphère-plan. Pour pouvoir aisément tenir compte des variations dimensionnelles ou du changement de configuration du système, les calculs analytiques réalisés utilisent le formalisme de Lagrange

pour établir les équations du mouvement. Pour tenir compte de la non-linéarité des lois de contact, un calcul itératif est nécessaire. La position qu'aurait le plateau avec des contacts indéformables est prise comme position d'initialisation de l'algorithme. La matrice de rigidité est réactualisée, à chaque itération, au gré des modifications des raideurs de contact puisque les déformations évoluent. De nouveaux déplacements sont calculés pour initier un nouveau cycle de calcul. Compte tenu des couplages et des non-linéarités, la convergence vers le résultat final se fait avec des oscillations. Pour limiter leur amplitude, un gain de calcul a été utilisé. Les résultats obtenus sont satisfaisants, et ont été validés sur deux exemples.

Finalement la position finale de l'ensemble plateau-pièce a été déterminée par la somme des corrections des écarts du aux erreurs géométriques et aux déformations mécaniques (cf figure 4.31).

Le modèle mécanique proposé peut être appliqué aux problèmes plus complexes avec plusieurs forces externes et des orientations différentes des appuis et des brides. Ce modèle résout le problème en utilisant des méthodes énergétiques. Cette méthode est plus flexible par rapport au principe fondamental de la statique, car elle est insensible aux modifications de configuration du système (appuis supplémentaires ou déplacés). De plus, le modèle gère la perte du contact d'un des appuis, provoqué par un déséquilibre des efforts appliquées, afin d'éviter l'absence de convergence du modèle.

Le système du montage proposé permet ainsi un positionnement précis de la pièce sur la machine-outil spécialisée sans la nécessité d'axes supplémentaires de la machine ou sur la ligne de la production sans que celle-ci n'ai besoin de machines multi-axes. La pièce peut être individuellement placée sur les palettes spéciales dédiées et équipées avec le système de positionnement à 6-DDL proposé. Cela assure un positionnement précis de la pièce sur la machine. Le réglage peut facilement être réalisé en ligne ou hors ligne de production.

Le système proposé permet la réduction des surépaisseurs d'usinage en limitant les erreurs dimensionnelles par le balançage optimal de la pièce. Le système contribue à la réduction d'enlèvement de matière, d'usure d'outil et économisant le temps d'usinage. Cela peut être fort appréciable quand la matière transformée

est onéreuse et difficile à usiner. Le positionnement de la pièce devient répétable, rentable et plus fiable.

5.2 Perspectives

Le système mécanique doit être réalisé, dans un premier temps, avec un actionnement manuel, afin de valider les modèles. Par la suite, un processus de reconfiguration automatique du système pourra être développé pour effectuer le repositionnement de la pièce après la mesure par MMT et le calcul des corrections nécessaires.

Une autre application du système est le positionnement optimal des grandes pièces, complexes ou flexibles lors d'opération d'assemblage, où la précision de présentation d'une pièce par rapport à l'autre est cruciale (ajustements, déformabilité ou pièces fragiles ou friables). Ces pièces peuvent être réorientés ou repositionnés dans une position optimale pour une opération d'assemblage automatique.

Le processus de mesure sur MMT a souvent besoin d'un pré-positionnement pour placer la pièce à mesurer sur un endroit convenable sur le marbre de mesure, avant le palpage. Le système proposé permet le positionnement de la pièce, augmenter la précision de mesure en utilisant le principe de Abbe, ou d'obtenir une meilleure orientation de la pièce pour assurer au mieux l'accessibilité des capteurs de mesure.

Une compensation dynamique des vibrations, se produisant pendant opération d'usinage, peut être effectuée en utilisant des actionneurs rapides comme les actionneurs piézoélectriques et capteurs de position. Cette compensation serait consacrée à des opérations de superfinition avec les conditions de coupe peu variées, des efforts de coupe limités, des volumes de copeau faibles où la prévision des modes vibratoires ne seraient pas trop influencés par la modification de forme de la pièce usinée.

Part II

English Version

Chapter 1

Introduction

1.1 Objectives

The objective of this thesis is to propose a fixturing system, for complex parts, which is capable of performing a 6-DOF repositioning in the machine coordinates without the use of 4 or 5-axis machine. The proposed fixturing system will be capable of :

- Determining the relative positioning error (due to geometrical defects or due to deformation of elastic elements under load) between the workpiece and the machine-tool before and during machining or between the two parts during assembly process,
- Insuring the error compensation by reorientation of the workpiece at an optimal position through the axial displacement of 6-locators.

1.2 Context

There is a competition in the manufacturing industry to design and deliver a variety of high quality products to their customers in shorter time. Due to rapid change in production technology and customer demand, the manufacturers need to develop flexible manufacturing practices to achieve a rapid turnaround in product development (Boyle *et al.*, 2011).

Among other factors, the use of feasible fixtures is one of the factors influencing the final part quality. Fixtures are devices used to support, locate and hold a workpiece at a desired position and orientation in machine space during manufacturing. This positioning and orientation is achieved by the locators and the clamps. The quality of a part is influenced by the capability of a fixture to precisely hold and locate it on the machine considering different functional conditions during fabrication. According to an estimate, about 10-20% of total manufacturing cost is associated with the fixtures in traditional FMS systems (Zhang, 2001). The design of fixtures is important to precisely hold the workpiece and compensate the errors that the workpiece can encounter during machining or assembling operation to ensure high quality of the product.

The need of high quality production, at low cost, accelerated the research efforts in fixture design for production of cost effective products without compromising on quality. To cope with current market demand, Ryll *et al.* (2008) emphasize on the need of "intelligent" fixtures which should be capable of self-configuring; reducing and compensating dimensional errors; providing stability and adapting clamping forces to guarantee optimum performance. The "intelligent" fixture should be generic and should be able to adopt to different workpiece configurations. Besides locators and clamps, "intelligent" fixturing system have micro-actuators for repositioning of mechanical elements and a computer support which manages the repositioning of the workpiece at each stage through actuators. The rough workpiece, placed on the locators, may not be completely included in the required position of the workpiece due to these geometrical variations, which cause the workpiece to be waste. To avoid this problem, allowances are added to the part body and its supports which needs the programming of tool path other than the part body. To avoid the loss of time and the material, it is necessary to place each new part precisely but this operation needs the mobilisation of machine.

The machine mechanism should assure the kinematic transformation to place the workpiece at an optimal position by compensating the positioning error between the workpiece and the machine-tool. This compensation is possible on a machine having a large number of degrees of freedom and high number of geometric transformations. If a processing operation (machining or assembling) only

needs a low number of axes or simply the small displacements, the choice of a 5-axis machine is not an economically feasible choice. The proposed system aims to realize that workpiece repositioning operation automatically without the mobilization of the machine tool avoiding the need of high DOF machines. It insures a prepositioning of complex parts for precise machining operations.

The studied system can also be used on the existing automatic production lines on which the number of axis are limited for each station. The proposed fixturing system gives high product quality at low cost due to its flexibility to be added to any existing machine unit of production/assembly line. The proposed system allows better positioning of the workpiece on the fixture and hence limiting the allowances. The necessary geometric, kinematic and mechanical modelling of the proposed fixturing system are presented in this thesis.

1.3 Proposition

The proposed fixturing system consists of a set of six axially controllable locators placed on the machine table or pallet, a cuboid[1] baseplate controlled through six locators and a workpiece (hip prosthesis) fixed rigidly on the baseplate as shown in figure 1.1. Friction at the contact between the baseplate and the locators is negligible. The 6-locators are assumed to be in a 3-2-1 locating configuration and their positions are defined through locating holes. The locators possess only one axial DOF to position the workpiece at desired place. The position of each locator is chosen by considering the constraints of accessibility, stability of the workpiece and manufacturing knowledge. It is also assumed that the workpiece is mounted rigidly on the baseplate and no additional deformation occurs between workpiece and baseplate except those caused during clamping the workpiece. The system to rigidly mount the workpiece on the baseplate depends upon the complexity of the workpiece.

In case of rough contacting surfaces, it is impossible to attain the precise positioning of the baseplate/workpiece through the axial displacement of 6 locators due to uncertainty of the contacting points caused by the local geometrical defect

[1]Cuboid: Rectangular box, rectangular hexahedron, right rectangular prism, or rectangular parallelepiped

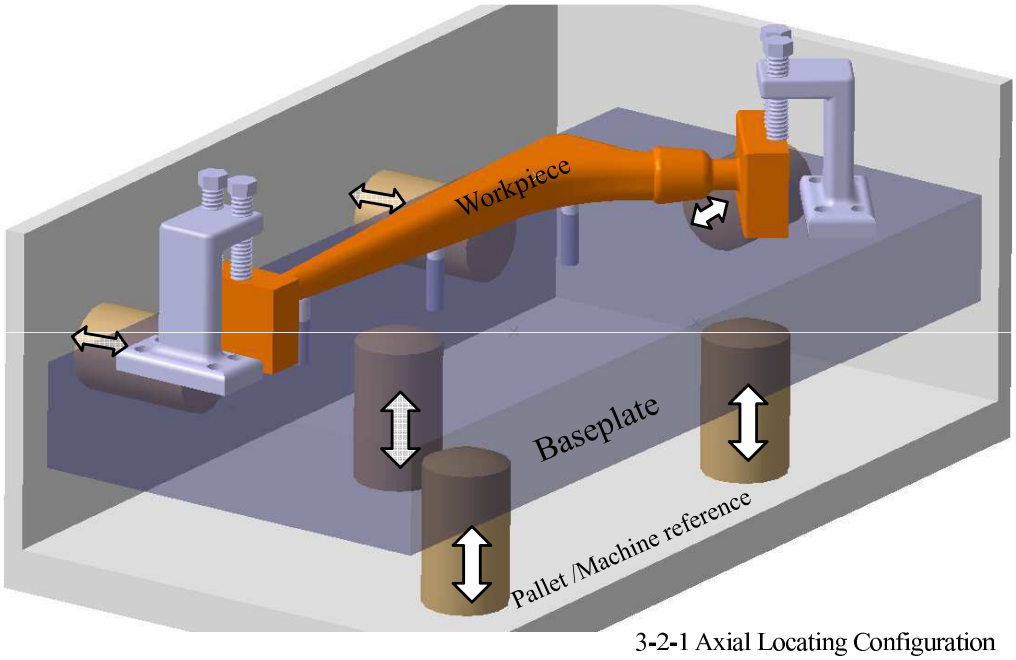

Figure 1.1: Proposed fixturing system

at the rough contact between the locators and the rough fixtured part (or baseplate in our case). To avoid this positioning uncertainty, a baseplate is added in between the locators and the rough workpiece. The positioning surfaces of the baseplate are considered to be perfectly plane and orthogonal. Because of this assumption, the surface normals always remain parallel to the contacts' normals enabling us to predict the exact location of the workpiece by the locators' positions.

The proposed system is capable of identifying and calculating the relative positioning errors between the workpiece and the machine-tool. This positioning error can be due to geometrical defects of the workpiece or the errors caused by the elastic deformation of the fixturing elements under machining and clamping forces. The proposed system is also capable of performing the 6-DOF error compensation by the advancement/retraction of six axial locators. All the elements are considered rigid for workpiece repositioning calculations or error compensation. To calculate the error due to deformation of fixturing elements under external applied forces, the locators and clamps are considered as elastic elements with known stiffness.

The thesis consists of two independent parts; analysis of only kinematic aspects and then also considering the mechanical aspects. In kinematic modeling, all the elements of the fixturing system are assumed to be rigid. Assuming that unknown initial position of the workpiece could imply large displacements (LD) during correction phase, the kinematic model is built using homogeneous transformation matrices (HTM) and LD formulation. Using the geometrical properties of the baseplate, exact position of the baseplate can be calculated from the six positioning locators. The initial position of the workpiece can be measured using a CMM which can be compared to the final required position of the workpiece. If the difference is more than the allowed tolerance, the algorithm calculates the unique relative position of each locator to relocate the workpiece at the required position. The precision of the workpiece placement depends upon the precision of locator which will be detailed under the robustness of the kinematic model.

In the mechanical model, the displacement of the workpiece is calculated due to the deformation of elastic fixturing elements under machining and clamping forces. This is performed by calculating the stiffness and mass matrices of the whole fixturing system considering the locators being elastic elements with negligible masses, the baseplate is also considered elastic at the contacts with the locators while the workpiece-baseplate assembly is considered to be perfectly rigid. Friction at the contacts between the locators and the baseplate is also taken as negligible. The clamps also assumed to be elastic and their one ends are fixed to the baseplate, with no slippage, while their other ends are displaced externally at a known displacement. As the deformation must remain small for the system reliability, therefore, small displacement (SD) hypothesis may be used. A computational tool is necessary to obtain the quick results of the developed analytical mechanical model, for that purpose, Mathematic® has been chosen. This developed analytical mechanical model allows obtaining the mass and stiffness matrices quickly for any configuration and position of locators as well as for any orientation of the baseplate.

As compared to the static equilibrium conditions method, widely used in literature, the mechanical model is developed using energy method. Potential energy of all the elastic elements, kinetic energy of inertial elements and the work done by the external load are formalized. The rigid body displacement of the

workpiece-baseplate assembly is obtained using Lagrangian formalization. This rigid body displacement is then transformed to the deformation of each of the locator depending upon the stiffness of each locator. In parallel, the mechanical behavior of the fixturing system is also obtained. The stiffness of the fixturing system can be changed using the controllable external displacement of the clamps.

The displacement of the workpiece, calculated under the machining and clamping forces, will be the workpiece positioning error due to deformation of elastic fixturing elements under machining and clamping forces. This error has to be compensated in order to place the workpiece at the desired position under load. This compensation can be performed by the axial advancements of the six locators using the proposed kinematic model. As the kinematic model is developed assuming all the elements to be rigid, the positioning errors can again be verified with the new axial positions of the locators using the mechanical model.

1.4 Thesis organization

This thesis document is structured in 4 chapters and conclusion. Following the first introductory chapter, chapter 2 details the basic concepts of geometrical and dimensional defects of the part and reviews the existing research in the field of the fixture design. A brief literature review on the locators placement errors, fixture positioning error and machine tool error followed by the machining force calculation is presented. The existing work on the deformation of the elastic contact is also detailed. The chapter concludes with the demonstration of a sample hip prosthesis used for the model validation.

Chapter 3 presents an analytical kinematic model of a 3-2-1 fixturing system for precise positioning of the workpiece in machine coordinate system with the hypothesis of all the elements being rigid and having no friction at contacts. The formalization includes HTM from machine to different parts of the fixturing system giving the advancement of each of six locators to reposition the workpiece to the required position. The formalization is followed by a case study performed on a hip prosthesis workpiece and verified in CATIA®.

A mechanical model of the fixturing system is presented in chapter 4 by taking the workpiece-baseplate assembly as rigid and the locators being elastic elements.

The baseplate is assumed to be elastic at the contacts. The model calculates the displacement of the workpiece in machine coordinate system using energy equations. The workpiece displacement is then transformed into the deformation of each locator though the plucker matrix of the fixturing system. The error compensation can be performed on the workpiece through the kinematic model.

Chapter 5 is the last chapter of the document. It presents a general discourse on the research work carried out with discussion on the capability and limitations of the proposed approach as well as future avenues of development and improvement in the work presented.

Chapter 2

State of the Art

This chapter provides the literature review in the field of fixture design, fixture positioning error, workpiece defects etc.. First the basic concept of associating real surfaces with theoretical surfaces using scanning machine in metrology for manufacturing is discussed, then the design of fixtures and its effects on the product quality is presented. Different constraints and requirements of fixture design are characterized and the existing solutions are presented. The main sources of workpiece machining errors are placement error of fixturing elements, geometrical or form defect errors, error due to deformation of elastic elements under load, machine tool kinematic error and errors due to temperature and tool wear. Machining forces cause rigid body motion of the workpiece and induce the deformation at workpiece-locator contact. Therefore, contact deformation under load is detailed before introducing a demonstrative workpiece which will be used in this thesis for model validation. The chapter concludes with a discussion on the pertinence of the existing tools and methods to the research objectives of this work.

2.1 Fixtures

Fixtures are devices used to support, locate and hold a workpiece at a desired position and orientation in machine space during manufacturing. The fixturing elements, assuring the positioning and orientation of a workpiece and hold it, are the locators and the clamps. The quality of the final product in machining

and assembly is highly dependent upon fixture's location accuracy and choice of clamps. About 10-20% of total manufacturing cost is associated with the fixtures in traditional FMS[1] systems (Zhang, 2001). The main functions of the fixture are detailed in the following subsections,

2.1.1 Locating a workpiece

A workpiece has a total of 12 linear and rotational movements along x,y and z axes(Trappey & Liu, 1990) as shown in figure 2.1. These 12 movements are also referred to as 6 degrees of freedom. Usually, nine movements are restricted by locators while the remaining three are constrained by clamps.

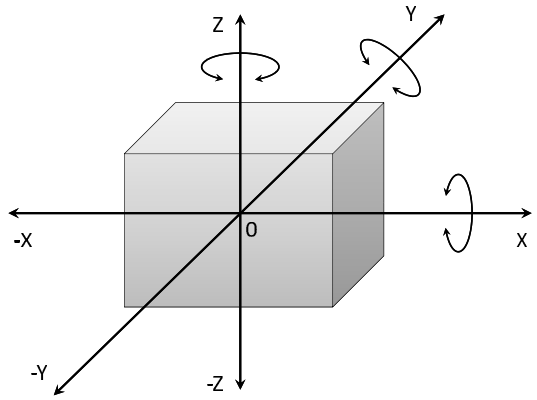

Figure 2.1: Possible movements of a workpiece in machine coordinate system (Trappey & Liu, 1990)

Locators enable the precise positioning and stability of the workpiece in machine coordinate system. Paris (1995) defined three possibilities of locating principles (3-2-1c, 3-2-1r & 4-1-1) depending upon the type of workpiece which are shown in figure 2.2. The technological representation of locators and clamps (Halevi & Weill, 1995; Trotignon *et al.*, 1996) is shown in table 2.1 (French Standard NF 04-013, 8.85), where black arrows represent the exact positioning while white arrows represent the element opposing against the vibration or deformation.

[1]FMS: Flexible Manufacturing System

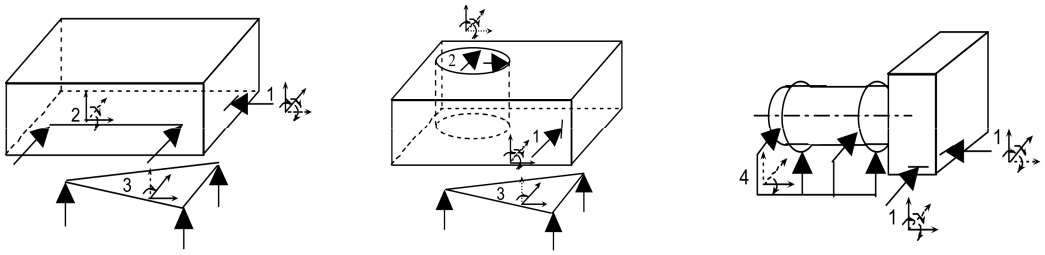

(a) 3-2-1r (b) 3-2-1c (c) 4-1-1

Figure 2.2: Different locating principles (Paris, 1995)

Table 2.1: Symbolization of technological elements (Halevi & Weill, 1995)

Technological type	Symbols	
Fixed support		
Fixed centering		
System with clamping		
System with concentric clamping		
Irreversible fixed support		
Reversible support		
Sliding positioning		

Nature of contact	flat	curved	serrated	free	pan	swing bar	vee	fixed center	turning center
Symbol									

2.1.2 Holding a workpiece

During machining operation, the workpiece has to be held precisely on the locators so that it does not move due to machining forces, weight of the workpiece or inertial forces. This can be done by adding appropriate clamps to the workpiece. Paris (1995) proposed three clamping principles depending upon the direction and type of clamps.

2.1.3 Supporting a workpiece

The fixture should be able to support the workpiece during the machining operation. A fixed or adjustable support can be used to support the workpiece when

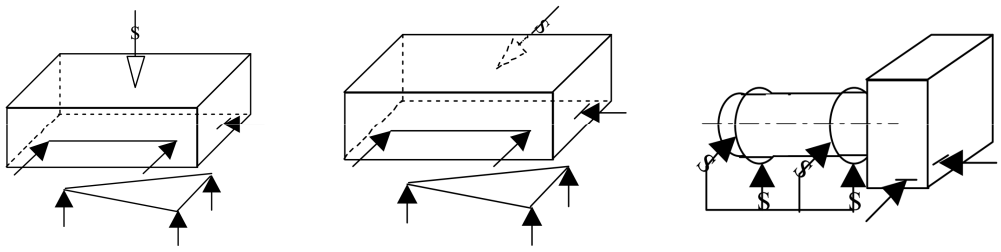

(a) Clamp type (b) Vice type (c) Chuck type

Figure 2.3: Clamping principles (Paris, 1995)

the workpiece is expected to deform or displace significantly under the clamping or processing forces (Nee *et al.*, 2004).

2.2 Geometrical and dimensional defects

The objective of this section is to introduce the theoretical basis of surface representation during fabrication. A real workpiece geometry has to be associated to an ideal geometry by certain optimization criteria. The kinematic model proposed in chapter 3 includes,

- Measuring the positioning errors of the workpiece on fixture
- Calculating the locators' advancements for compensation
- Relocates the workpiece in machine reference frame

where, the real surface may be measured using a CMM[1], which gives a theoretical surface associated with the real one. Before going in to the details of the surface association, different types of surfaces are detailed.

2.2.1 Types of surfaces

Definition 2.2.1. *The real geometry of a workpiece can be defined by the surface which separates the material from its environment (Bourdet & Mathieu, 1998).*

[1]CMM: Coordinate Measuring Machine

A surface is the separation between the material and its surrounding. Measurement of an object is performed on its limiting surfaces, so it is necessary to have an understanding of the surfaces used in metrology. In measurement by a CMM, the following surfaces can be defined (Dursapt, 2009);

2.2.1.1 Theoretical surface

For practical reasons, the designer will determine the form of surface which would represent the actual surface theoretically, so that its behavior gives satisfaction to the end user. The theoretical forms might be simple (plane, sphere, cylinder), complex mathematical form functions (conic, torus, surface of revolution), profiles defined by complex mathematical functions using physics (vane blade profile realized considering the fluid and heat transfer effect, propeller profile etc.) or aesthetic surfaces with indifferent profiles (car body, objects of art, etc.). In addition to these, a theoretical surface can always be defined by a continuous function.

2.2.1.2 Real surface

The manufacturer will do the best to achieve the required theoretical surface using appropriate means of fabrication depending upon the quality and dimensions of the surface to be obtained, materials used, availability of the industrial equipments and economic situation. Despite of all the care taken by the manufacturer, the real surface would have an indifferent form which would be very close to the theoretical surface. The real surface would always have irregularities at any scale.

2.2.1.3 Extracted surface

Extracted surface is obtained by tracing the scatter points on the real surface. Practically, the extracted surface can be defined by "n" measuring points (Mr_i) of real surface by any scanning equipment e.g. CMM machine. For an element, more information can be gathered by increasing the number of measuring points (fig. 2.4(a)).

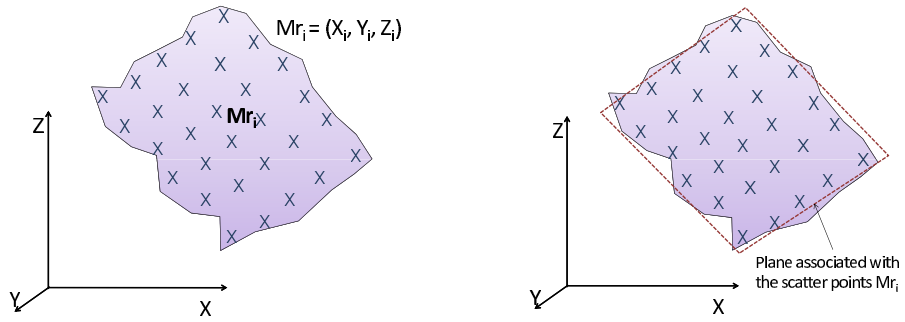

(a) Extraction of theoretical surface (b) Plane associated with extracted element

Figure 2.4: Extracted and Associated Surface (Dursapt, 2009)

2.2.1.4 Associated surface

The associated surface is a theoretical surface which is associated with a real surface and is placed in a manner that it defines the real surface in the best possible way. The associated surface is acquired from "n" measured points followed by a given mathematical algorithm. The surface extracted in figure 2.4(a) can be associated with an ideal surface as in figure 2.4(b).

2.2.2 Association of geometrical elements

Real surfaces are never perfect. Mathematical optimization is performed under certain constraints to obtain an associated ideal geometry from "n" measured points. For the definition of a real element, the measured points should be equal to or more than the points necessary for defining the mathematical geometry (tab. 2.2). Bourdet (1999) and Coorevits & David (1991) presented the ISO standards of real geometrical elements associated with the ideal geometries in Coordinate Measuring Machine (CMM). Table 2.2 also presents vector representation and the form defects that might be encountered during association of geometrical elements. The reference of the mathematical association of geometrical elements is referred to as DATUM or EGRM [1] (in French) and it is defined as,

[1]EGRM: Elément Géométrique de Référence Minimum

Table 2.2: Association criteria (Bourdet, 1999; Coorevits & David, 1991)

Geometric Element	Min. Points Measured | Suggested	Vector Representation	Form Defect
Point	1 | 1	Point	----
Line	2 | 3	Point + Vector 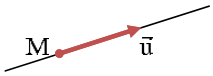	Distance between two lines 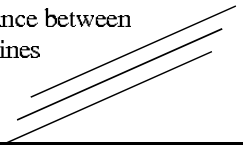
Plane	3 | 4	Point + Vector 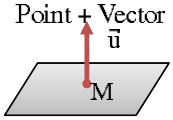	Distance between two planes 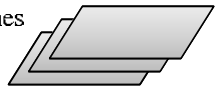
Circle	3 | 4	Point + Vector + Radius 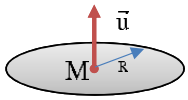	Distance between two circles 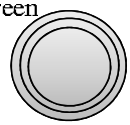
Sphere	4 | 9	Point + Radius 	Distance between two spheres 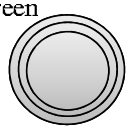
Cylinder	5 | 8	Point + Vector + Radius 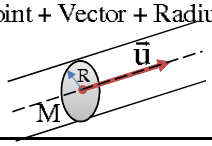	Distance between two concentric cylinders 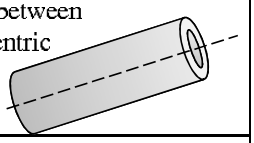
Cone	6 | 8	Point + Vector + ½ angle 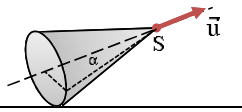	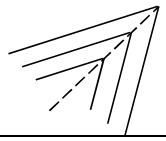

Definition 2.2.2. *DATUM or EGRM is a mathematical element composed of three simple geometric elements; point, line and plane. It is associated with each invariant class and enables an univalent positioning of the surface of the class it is attached (Lesage, 2002)*

Generally, all the mechanical elements, depending upon the form invariant

DOF in the space, can be regrouped in to seven classes as shown in table 2.3. These classes are called "Invariant Classes" (Bourdet & Mathieu, 1998). On the basis of these seven classes, TTRS[1] (SATT[2] in French) model is developed by Clément *et al.* (1994) for mathematical association of surfaces specially in CAD software.

Definition 2.2.3. *It is a pair of surfaces or TTRS, or a pair composed of a surface or a TTRS belonging to same solid and associated for the functional reasons (Clément* et al.*, 1994)*

The union of two classes gives one class, depending upon the degree of invariance and EGRM. For the union of two classes, the reference of one class should be defined in the other one. This constraint gives a total of 28 possible combinations of SATT. All the possible combinations are detailed in Clément *et al.* (1994).

2.2.3 Association with real surface or points

The ideal geometry, defined from "n" measured points, does not pass through all points and hence the measured points will have deviation from the ideal associated surface. There could be two cases of deviations: deviation of each measured point and global deviation of substitute surface (Bourdet & Schneider, 2007), which are discussed further:

2.2.3.1 Case 1: Finite measured points

In case of finite measured points, the deviation of point "i" is the distance between measured point M_i and point P_i on the ideal surface corresponding the normal passing through the measured point (fig. 2.5(a)). The deviation of each measured point depends upon the position of the ideal surface, and it changes with the position of the surface. It is therefore necessary to define the ideal surface precisely to minimize the surface deviation using existing optimization criteria for example root mean square criterion.

[1]TTRS: Topological and Technological Related Surfaces
[2]SATT: Surfaces Associées Technologiquement et Topologiquement

Table 2.3: Invariance Classes (Bourdet & Mathieu, 1998; Bourdet & Schneider, 2007; Clément *et al.*, 1994)

Class	Illustration	Dim	EGRM	Examples	SDT
Complex	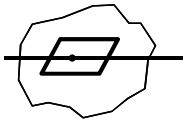	0	Plane Point Line	- Ellipse - Surface with reference to poles	$T_o \begin{vmatrix} \beta & x \\ \gamma & y \\ \alpha & z \end{vmatrix}$
Prismatic	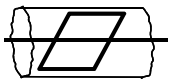	1	Plane Line	- Prism with elliptic base - Prism with	$T_o \begin{vmatrix} \beta & x \\ \gamma & y \\ \alpha & ind \; z \end{vmatrix}$
Revolution	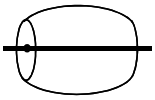	1	Line Point	- Circle - Cone - Tore	$T_o \begin{vmatrix} \beta & x \\ \gamma & y \\ ind \; \alpha & z \end{vmatrix}$
Helicoids	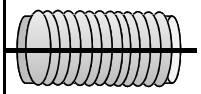	1	Oriented line	-Helix -Helicoids from development of circle	$T_o \begin{vmatrix} \beta & x \\ \gamma & y \\ \alpha & p.\gamma \end{vmatrix}$
Cylindrical	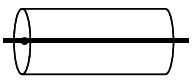	2	Line	-Line - Cylinder from revolution of surface	$T_o \begin{vmatrix} \beta & x \\ \gamma & y \\ ind \; \alpha & ind \; z \end{vmatrix}$
Plane	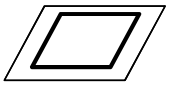	2	Plane	- Plane	$T_o \begin{vmatrix} \beta & ind \; x \\ \gamma & ind \; y \\ ind \; \alpha & z \end{vmatrix}$
Spherical	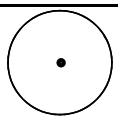	3	Point	- Point - Sphere	$T_o \begin{vmatrix} ind \; \beta & x \\ ind \; \gamma & y \\ ind \; \alpha & z \end{vmatrix}$

2.2.3.2 Case 2: Substitute surface

In case of deviation of substitute surface, the deviation between each substituted and ideal surface is expressed by a SDT[1] or deviation torsor as shown in figure 2.5(b). In the figure, the surface is invariant in x, y and γ directions while the remaining components are small displacements or small rotations for the

[1]SDT: Small Displacement Torsor

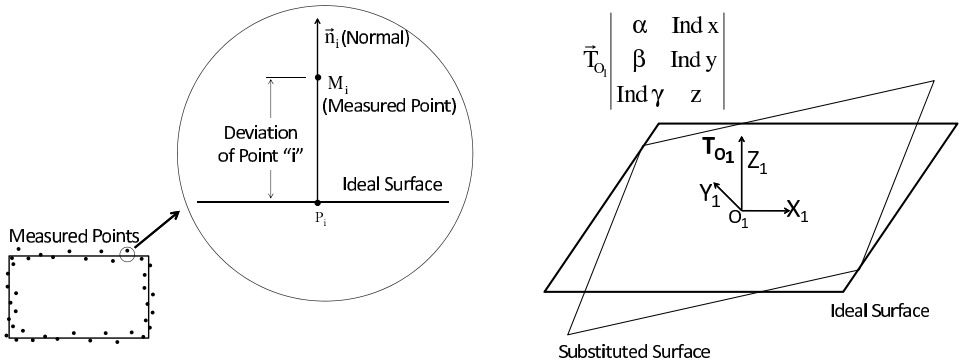

(a) Association of measured points (b) Association of substituted surface

Figure 2.5: Association of real surface (Bourdet & Schneider, 2007)

transformation from substitute to ideal surface.

Like in the first case, it is necessary to precisely define the criteria to adjust ideal surface with respect to real surface. Before explaining the optimization criteria, It is important to detail SDT concept.

2.2.4 Small Displacement Torsor (SDT) and Homogeneous Transfer Matrix (HTM)

Since the development of the concept in 1970, SDT has widely been used in the CMM[1] softwares and tolerance analysis. Generally, the displacement torsor can be defined as,

Definition 2.2.4. *When a solid is displaced in a coordinate system "$\{O'|X', Y', Z'\}$", the displacement can be characterized in original coordinate system "$\{O|X, Y, Z\}$" by a translation vector $\overrightarrow{D_O}$ and a rotation matrix $\bar{\bar{R}}$. This rotation can be expressed by three angles (α, β, γ) representing successive rotations of the solid around three axes $\{\overrightarrow{Z_0}, \overrightarrow{X_1}, \overrightarrow{Y'}\}$*

Using the YPR[2] transformation, from figure 2.6, the displacement $\overrightarrow{D_M}$ is expressed in equation 2.1 (Bourdet & Schneider, 2007) while its HTM[3] form is

[1]CMM: Coordinate Measuring Machine
[2]YPR: Yaw (α), Pitch (β), Roll (γ)
[3]HTM: Homogeneous Transformation Matrix

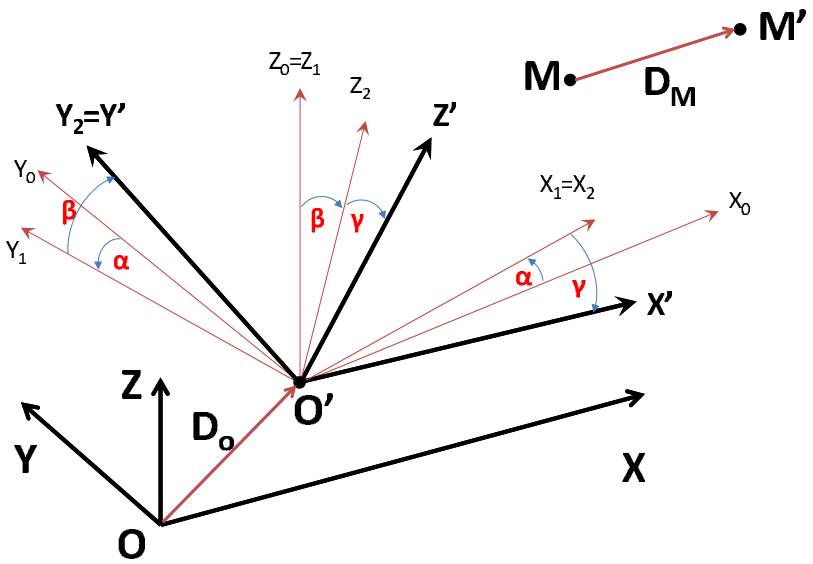

Figure 2.6: Displacement of a solid

shown in equation 2.2.

$$\overrightarrow{D_M} = \overrightarrow{D_O} + (\bar{\bar{R}} - \bar{\bar{1}})\overrightarrow{OM} \tag{2.1}$$

$$\left\{ \begin{array}{c} \overrightarrow{D_M} \\ 1 \end{array} \right\} = \left\{ \begin{array}{c} \overrightarrow{OM'} - \overrightarrow{OM} \\ 1 \end{array} \right\} = \left[\begin{array}{ccc|c} & \bar{\bar{R}} - \bar{\bar{1}} & & \begin{array}{c} O_X \\ O_Y \\ O_Z \end{array} \\ \hline 0 & 0 & 0 & 1 \end{array} \right] \left\{ \begin{array}{c} OM_X \\ OM_Y \\ OM_Z \\ 1 \end{array} \right\} \tag{2.2}$$

where, $\bar{\bar{R}}$ is the rotation matrix obtained after YPR transformation.

$$\bar{\bar{R}} = \left[\begin{array}{ccc} cos\alpha cos\gamma - sin\alpha sin\beta sin\gamma & -sin\alpha cos\beta & cos\alpha sin\gamma + sin\alpha sin\beta cos\gamma \\ sin\alpha cos\gamma + cos\alpha sin\beta sin\gamma & cos\alpha cos\beta & sin\alpha sin\gamma - cos\alpha sin\beta cos\gamma \\ -cos\beta sin\gamma & sin\beta & cos\beta cos\gamma \end{array} \right] \tag{2.3}$$

In case of small rotations, the matrix $\bar{\bar{R}}$ from equation 2.3 can be written in reduced order form as in equation 2.4,

$$\bar{\bar{R}} = \begin{bmatrix} 1 & -\alpha & \gamma \\ \alpha & 1 & -\beta \\ -\gamma & \beta & 1 \end{bmatrix} \tag{2.4}$$

The vectorial representation of displacement of any point on solid can be obtained from equations 2.1 and 2.2,

$$\overrightarrow{D_M} = \overrightarrow{D_O} + \overrightarrow{MO} \times \overrightarrow{\Omega} \tag{2.5}$$

where, $\overrightarrow{D_O}(u, v, w)$ is the translation vector and $\overrightarrow{\Omega}(\beta, \gamma, \alpha)$ is the rotation vector. SDT is the torsor obtained from the couple of translation and rotation vectors. SDT ($T_O = |\overrightarrow{\Omega}, \overrightarrow{D_O}|$) can be defined for each invariant class as shown in table 2.3, where, *ind* represents indeterminate or invariant of the surface class.

2.2.5 Optimization criteria

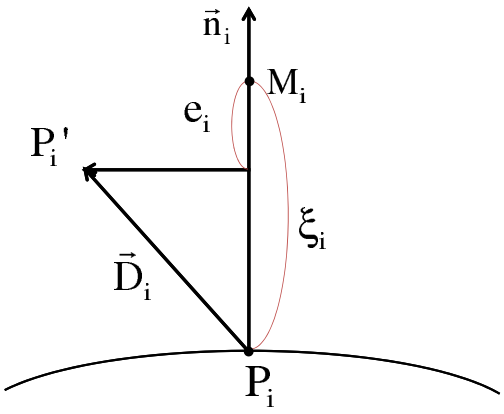

Figure 2.7: SD deviation of i^{th} measured point (Bourdet & Schneider, 2007)

Real surface can be described by all the measured deviations ξ_i on normal from the point P_i of the ideal surface which is initially placed close to measured points. For a majority of surfaces, P_i can be found from the measured point M_i if the surface form is known (Bourdet & Schneider, 2007).

Classically, the position of M_i can be defined by $\overrightarrow{OM_i} = \overrightarrow{OP_i} + \xi_i.\overrightarrow{n_i}$, where $\overrightarrow{n_i}$ is the unit vector normal to the surface and ζ_i is the deviation in the normal

direction. In case of small displacement with the SDT, $T_O = |\overrightarrow{\Omega}, \overrightarrow{D_O}|$, the point P_i will move to point P_i' due to small displacement $\overrightarrow{D_i}$. The optimized deviation e_i at a point P_i, projected on the normal to the surface $\overrightarrow{n_i}$, can be written by the equation 2.6 (Bourdet & Schneider, 2007; Dursapt, 2009);

$$e_i = \xi_i + \overrightarrow{D_i}.\overrightarrow{n_i} \tag{2.6}$$

where, $\overrightarrow{D_i}$ can be calculated from equation 2.5. If n is the number of measured points defining surface and p is the number of unknown parameters. In case when $n = p$, the small displacements obtained by solution of equations give the surface which passes through all the n points and deviation becomes zero. In the other case when $n > p$, all the deviation cannot be equal to zero and it is necessary to satisfy the constraints by the optimization criteria. For this purpose, two types of criteria are mostly used: Root Mean Square(RMS) criterion and Chebyshev criterion (Bourdet & Schneider, 2007).

2.2.5.1 Association by Gauss criterion (Root Mean Square(RMS) criterion)

The objective of RMS[1] criterion is to minimize the sum of squares of errors or deviations i.e. $W = \sum_{i=1}^{n} {e_i}^2$. For W to be minimum, derivatives of W with respect to each component of SDT is equated to zero and the solution is obtained by resultant linear equations.

$$\frac{\partial W}{\partial \alpha} = 0;\ \frac{\partial W}{\partial \beta} = 0;\ \frac{\partial W}{\partial \gamma} = 0;\ \frac{\partial W}{\partial u} = 0;\ \frac{\partial W}{\partial v} = 0;\ \frac{\partial W}{\partial w} = 0; etc.$$

Here the optimized surface will pass inside all the points and the distribution is not necessarily Gaussian but depends on the surface texture. RMS method can be explained by a 2D example (fig. 2.8).

In figure 2.8, a surface is measured along X-axis through a CMM, the height of the point is along Y-axis. For the ease of calculation, the first point is taken as the reference point. Straight line D_0 associated with measured points M_i is calculated from equation $y = a.x + b$, where,

[1]RMS: Root mean square

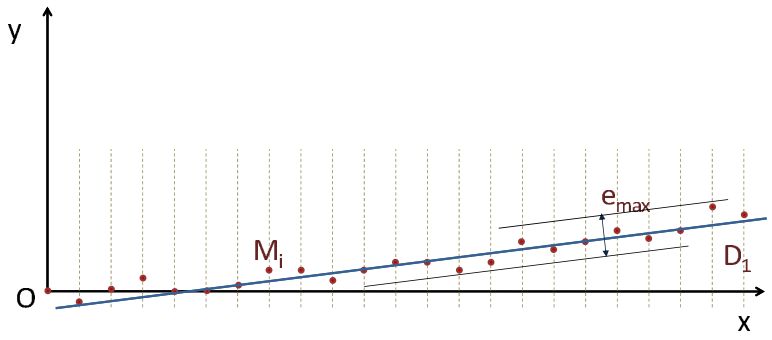

Figure 2.8: Association of measured points by RMS criteria (Dursapt, 2009)

$$a = \frac{\Sigma x_i.\Sigma y_i - n.\Sigma x_i.y_i}{(\Sigma x_i)^2 - n.\Sigma {x_i}^2}$$
$$b = \frac{\Sigma x_i.\Sigma x_i.y_i - \Sigma y_i \Sigma {x_i}^2}{(\Sigma x_i)^2 - n.\Sigma {x_i}^2}$$

Hence here, there is no need to calculate the deviation of each measured point.

2.2.5.2 Chebyshev criterion

Chebyshev criterion minimizes or maximizes the relation between two unknowns of the problem. In the case of optimization, the aim of Chebyshev criterion is to minimize the deviation of two unknowns e_{max} and e_{min}, which are the maximum and minimum optimized deviations respectively, and the magnitude of these deviations should never be less than any of the optimized deviation ξ_i.

Besides RMS criterion and Chebyshev criterion, the surfaces can be optimized by imposing constraints on SDT and/or intrinsic parameters for example by imposing diameter of cylinder, cone angle, orientation/position of two surfaces etc.

For the same measured points, in figure 2.9, the aim of Chebyshev criterion is to find two parallel lines so that all the measured points come in between these two lines and the lines are apart at the least possible distance.

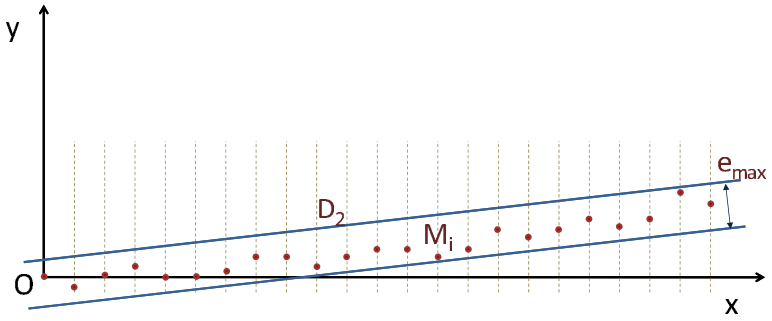

Figure 2.9: Association of measured points by Tchebytchev criteria (Dursapt, 2009)

2.2.6 Positioning error due to locators' geometric errors

When the workpiece is positioned on the fixture locators, due to geometrical error of workpiece and locators, the real position of the workpiece can deviate from theoretical one. The locator's position error is very small but still it has the influence on the overall positioning error of the workpiece. Therefore the precision of the workpiece is limited due to inaccuracy or precision limit of the locators. In figure 2.10, the theoretical workpiece and locator are shown with dashed lines and their contact point is M_i. Due to small displacement ξ_i of the locator in normal direction, the workpiece moves on the locator and the contacting point M_i is moved to M_i'.

Here the displacement of the workpiece can be described by SDT. The total motion of the solid is composed of a translation vector $\vec{V} = \{X, Y, Z\}^T$ and a rotation vector $\vec{\Omega} = \{\beta, \gamma, \alpha\}^T$. The displacement of point M_i of the workpiece can be written as in section 2.2.4 which is given below,

$$\overrightarrow{M_iM_i'} = \overrightarrow{V} + \overrightarrow{\Omega} \times \overrightarrow{OM_i} \tag{2.7}$$

Here the projection of M_iM_i' is estimated on the normal $\vec{n}$, which is equal to ξ_i, the positioning error of the locator:

$$\xi_i = \overrightarrow{V}.\overrightarrow{n_i} + (\overrightarrow{\Omega} \times \overrightarrow{OM_i}).\overrightarrow{n_i} = \overrightarrow{V}.\overrightarrow{n_i} + (\overrightarrow{OM_i} \times \overrightarrow{n_i}).\overrightarrow{\Omega} \tag{2.8}$$

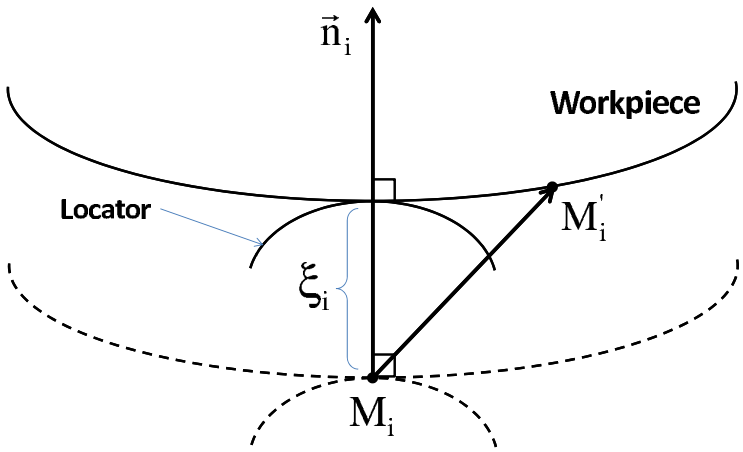

Figure 2.10: Position error due to locator deviation (Halevi & Weill, 1995)

The displacement ξ_i is a function of six parameters (Three translation and three rotation), therefore six locators are necessary to completely define the rigid body motion of the workpiece as the function of locators' error. A given workpiece which is positioned through six locators is shown in figure 2.11.

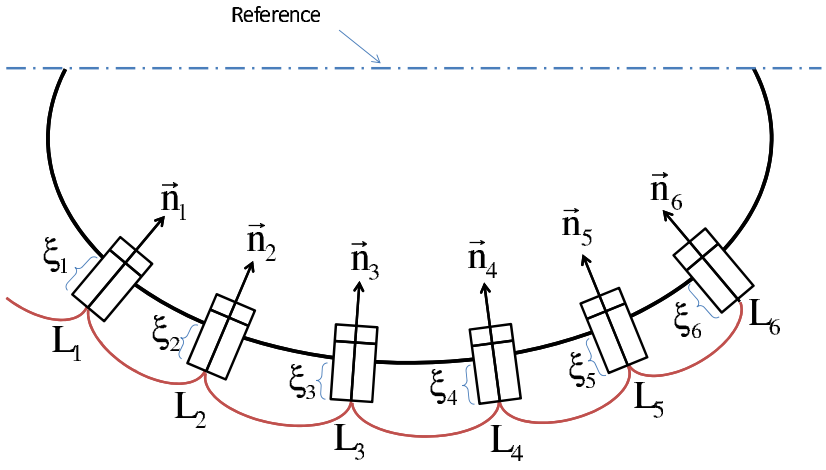

Figure 2.11: Error of a workpiece on a isostatic fixture (Halevi & Weill, 1995)

The position error of each of six locators will be the function of six parameters called twist and Plucker coordinates for normals $\vec{n_i}$, where $i = 1, 2, ...6$. Here six

locators form six linear equations, which can be written in matrix form as;

$$\begin{Bmatrix} \xi_1 \\ \xi_2 \\ \xi_3 \\ \xi_4 \\ \xi_5 \\ \xi_6 \end{Bmatrix} = \begin{bmatrix} a_1 & b_1 & c_1 & k_1 & l_1 & m_1 \\ a_2 & b_2 & c_2 & k_2 & l_2 & m_2 \\ a_3 & b_3 & c_3 & k_3 & l_3 & m_3 \\ a_4 & b_4 & c_4 & k_4 & l_4 & m_4 \\ a_5 & b_5 & c_5 & k_5 & l_5 & m_5 \\ a_6 & b_6 & c_6 & k_6 & l_6 & m_6 \end{bmatrix} \begin{Bmatrix} \delta X_P \\ \delta Y_P \\ \delta Z_P \\ \delta\beta \\ \delta\gamma \\ \delta\alpha \end{Bmatrix} \tag{2.9}$$

where, a_i, b_i and c_i are the X, Y and Z components of the i^{th} unit vector n_i with $a_i^2 + b_i^2 + c_i^2 = 1$, while k_i, l_i and m_i are the components of vector $\overrightarrow{OM_i} \times \overrightarrow{n_i}$. For the displacement to be statically determinate, the plucker matrix has to be a non-zero matrix. If $[Plu]$ is the Plucker matrix of normals $\vec{n_i}$ and δ is the small twist of the workpiece, the equation 2.9 can be written as;

$$\{\xi_i\} = [Plu]\{\delta\} \tag{2.10}$$

The above equation 2.10 gives the positioning error of locators if the Plucker matrix and the twist of the workpiece is known. In other case, if the precision of the locators is known, we can find the uncertainty in the position of the workpiece using equation 2.11.

$$\{\delta\} = [Plu]^{-1}\{\xi_i\} \tag{2.11}$$

The calculation of Plucker matrix for a configuration of locators and the effect of positioning error of locators on the precision of the workpiece is explained through an example found in Méry (1997). The workpiece of figure 2.12 is located through six locators (M1-M6). Locators M1, M2 and M3 are in vertical direction along z-axis, M4 is along y-axis while M5 and M6 are inclined to angles θ_5 and θ_6 with the y-axis (fig. 2.13). The contact normals (n_1 to n_6) of all the six locators are shown in equation 2.12.

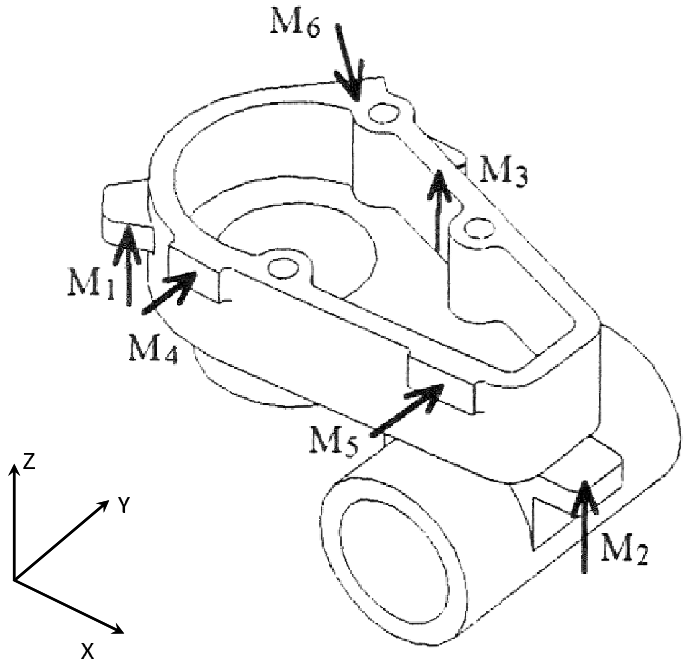

Figure 2.12: Locating a workpiece by six axial locators (Méry, 1997)

$$n_1 = n_2 = n_3 = \begin{Bmatrix} 0 \\ 0 \\ 1 \end{Bmatrix}, \quad n_4 = \begin{Bmatrix} 0 \\ 1 \\ 0 \end{Bmatrix}, \quad n_5 = \begin{Bmatrix} -\sin\theta_5 \\ \cos\theta_5 \\ 0 \end{Bmatrix}, \quad n_6 = \begin{Bmatrix} \sin\theta_6 \\ -\cos\theta_6 \\ 0 \end{Bmatrix} \tag{2.12}$$

The rigid body displacement of the workpiece causes the contacting points to move away from the locators' contacts. The projection of displacement of contacting points on the contact normals (n_1 to n_6) can be calculated using equation 2.8 which can be written as equation 2.13 for this example considering that $\delta\alpha$, $\delta\beta$ and $\delta\gamma$ are the small angles of rotations along z, x and y directions respectively.

$$\xi_i = \begin{Bmatrix} \delta X_P \\ \delta Y_P \\ \delta Z_P \end{Bmatrix} . \begin{Bmatrix} a_i \\ b_i \\ c_i \end{Bmatrix} + \left[\begin{Bmatrix} x_i \\ y_i \\ z_i \end{Bmatrix} \times \begin{Bmatrix} a_i \\ b_i \\ c_i \end{Bmatrix} \right] . \begin{Bmatrix} \delta\beta \\ \delta\gamma \\ \delta\alpha \end{Bmatrix} \tag{2.13}$$

where, $\{\delta X_P, \delta Y_P, \delta Z_P\}^T$ and $\{\delta\beta, \delta\gamma, \delta\alpha\}^T$ are the small linear and angular dis-

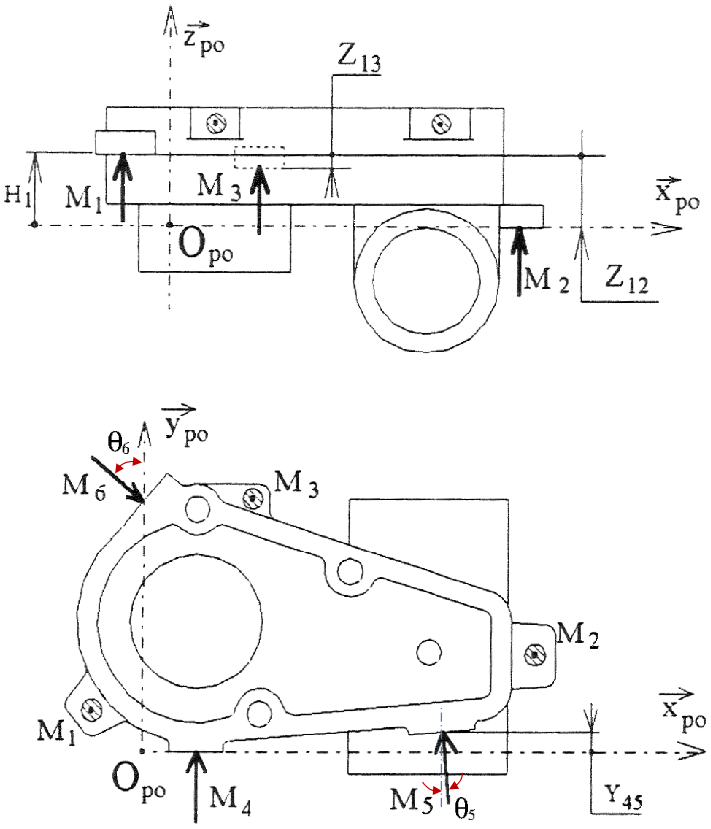

Figure 2.13: Isometric views of workpiece locating (Méry, 1997)

placement vectors of the workpiece, while $\{x_i, y_i, z_i\}^T$ is the position of initial contacting point of the workpiece with i^{it} locator ($\overrightarrow{OM_i}$). The calculated error of 6 contacting points along the direction of their normals which are functions of the axial advancements of locators is shown in equation 2.14.

$$\begin{aligned}
\xi_1 &= \delta Z_P + \delta\beta y_1 - \delta\gamma x_1 \\
\xi_2 &= \delta Z_P + \delta\beta y_2 - \delta\gamma x_2 \\
\xi_3 &= \delta Z_P + \delta\beta y_3 - \delta\gamma x_3 \\
\xi_4 &= \delta Y_P - \delta\beta z_4 + \delta\alpha x_4 \\
\xi_5 &= -\delta X_P \sin\theta_5 + \delta Y_P \cos\theta_5 - \delta\beta z_5 \cos\theta_5 - \delta\gamma z_5 \sin\theta_5 + \delta\alpha(x_5 \cos\theta_5 + y_5 \sin\theta_5) \\
\xi_6 &= \delta X_P \sin\theta_6 - \delta Y_P \cos\theta_6 + \delta\beta z_6 \cos\theta_6 + \delta\gamma z_6 \sin\theta_6 - \delta\alpha(x_6 \cos\theta_6 + \delta y_6 \sin\theta_6)
\end{aligned} \tag{2.14}$$

Here, equation 2.11 can be used to calculate the uncertainty in the position of the workpiece as the function of small displacement precision of the locators with the Plucker matrix for this locating configuration is given in equation 2.15.

$$[Plu] = \begin{bmatrix} 0 & 0 & 1 & y_1 & -x_1 & 0 \\ 0 & 0 & 1 & y_2 & -x_2 & 0 \\ 0 & 0 & 1 & y_3 & -x_3 & 0 \\ 0 & 1 & 0 & -z_4 & 0 & x_4 \\ -\sin\theta_5 & \cos\theta_5 & 0 & -z_5\cos\theta_5 & -z_5\sin\theta_5 & x_5\cos\theta_5 + y_5\sin\theta_5 \\ \sin\theta_6 & -\cos\theta_6 & 0 & z_6\cos\theta_6 & z_6\sin\theta_6 & -x_6\cos\theta_6 - y_6\sin\theta_6 \end{bmatrix}. \tag{2.15}$$

As mentioned earlier, this plucker matrix has to be a non-zero matrix in order to remain statically determinate. Plucker matrix is unchanged for a specific configuration of locators. If the position of any locator changes, plucker matrix changes which further changes the overall 6-DOF displacement of the workpiece. For two different configurations of locators, the configuration with least displacement of the workpiece will be preferred, therefore it can be concluded that Plucker matrix can be used to choose the best possible configuration of the locators for the same workpiece. It is to be noted that for stability of the workpiece-baseplate assembly, the locators have to be placed as far as possible from the central axis of the baseplate.

2.3 Fixture design

Precision of fabricated parts is one of the primary concerns of manufacturing industry. Quality of the fabricated part is influenced by the capability of a fixture to precisely hold and locate the workpiece on the machine considering different functional conditions during fabrication. Physically, a fixture consists of locators and clamps which further consist of supporting units to fix them on the machine table.

Recent developments in technology increased the need of producing diverse products with high quality at low cost. This need accelerated the research efforts in fixture design for production of cost effective products without compromising on quality. To cope with current market demand, Ryll *et al.* (2008) emphasis on the need of "intelligent" fixtures which should be capable of self-configuring, reducing and compensating dimensional errors, providing stability and adapting

clamping forces to guarantee optimum performance. The "intelligent" fixture should be generic and should adapt to different workpiece configurations. Besides locators and clamps, "intelligent" fixturing system have micro-actuators for repositioning of mechanical elements and a computer support which manages the repositioning of the workpiece at each stage through actuators. Most of the research is oriented towards the automation of fixtures, which turned the recent research towards repositioning of the workpiece, machine tool and managing the machining errors for quick adjustment of the operation. The adjustment can be performed by measuring the position of the workpiece in machine space, comparing it with the required position or tool path and adjusting the workpiece position or machine tool configuration to compensate positioning errors.

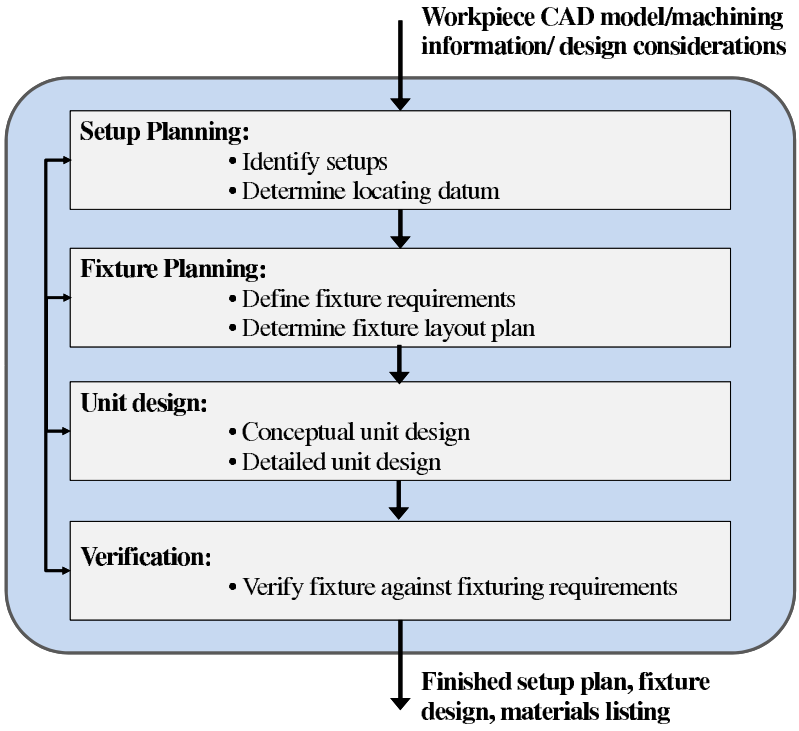

Figure 2.14: Fixture design process (Boyle *et al.*, 2011)

Generally, the fixture design involves four main steps which are shown in figure 2.14 (Boyle *et al.*, 2011; Kang *et al.*, 2003; Wang *et al.*, 2010);

1. **Setup planning**
   This step deals with the identification of machining setups where each setup

is a combination of operations performed on the workpiece without changing its orientation. The remaining three steps are performed for each setup.

2. **Fixture planning**
   Once setups are defined, the fixturing layout is generated while respecting the fixturing requirements (tab. 2.4). This layout details the configurations of locators and clamps to block all six degrees of freedom of the workpiece for each setup e.g. 3-2-1r locating principle.

3. **Unit design**
   This step involves the design or selection of suitable locators and clamps for the fixture.

4. **Verification**
   The verification is necessary to validate if the fixture satisfies the fixturing requirements (tab. 2.4) under operating conditions, it can also be performed before the unit design.

This thesis deals with the deformation of elastic elements of the fixturing system caused by the external forces. The comparison of possible locating configurations and locators positions can be performed and the configuration giving the best stability of the workpiece can be chosen. The setup surfaces of the workpiece are known initially, so the work of this thesis remains in the domain of the fixture planning process for the setup with known locating datum of the workpiece. Fixture planning deals with the generation of the fixture layout plan respecting the fixturing requirements. The fixturing requirements can be grouped into six classes by Boyle *et al.* (2011) as detailed in table 2.4. Usually, fixture planning is also followed by verification.

Besides the requirements listed in table 2.4, quality of the contacting surface, contact friction and clamping forces are fixture design parameters which can be changed from one workpiece to another. Clamps can be considered as active fixturing elements because workpiece holding forces are exerted through them while locators are passive elements. Location of clamps, minimum/maximum force by clamps and clamping sequence also effect the positioning of the workpiece in

Table 2.4: Fixturing requirements (Boyle *et al.*, 2011)

Fixturing Requirement	Examples
Physical	- Fixture must be physically capable of accommodating the workpiece geometry and weight. - Fixture must allow access to the workpiece features to be machined.
Tolerance	- Fixture locating tolerances should be sufficient to satisfy part design tolerances.
Constraining	- Fixture shall ensure workpiece stability - The fixture shall ensure that the fixture/workpiece stiffness is sufficient to prevent deformation.
Affordability	- Fixture cost shall not exceed desired levels. - Fixture assembly/disassembly times shall not exceed desired levels. - Fixture operation time shall not exceed desired levels.
Collision prevention	- Fixture shall not cause toolpath–fixture collisions - Fixture shall cause workpiece–fixture collisions to occur (other than at the designated locating and clamping positions).
Usability	- Fixture weight shall not exceed desired levels. - Fixture shall not cause surface damage at the workpiece-fixture interface. - Fixture shall provide tool guidance to designated workpiece features. - Fixture shall ensure error-proofing (i.e., the fixture should prevent incorrect insertion of the workpiece into the fixture). - The fixture shall facilitate chip shedding.

machining fixture. Research carried out for workpiece positioning error determination considering different criteria will be discussed in the following sections.

The final product quality is influenced by the machine tool error, fixture error and datum error[1] (Wan *et al.*, 2008). Fixture planning can be performed by concentrating on the fixturing requirements. The aim of fixture planning is

[1]datum error: Error induced due to contact of locators on imperfect datum surfaces of the workpiece

to assure the precise placement of the workpiece with respect to machine tool reference. To do so, all possible errors should be eliminated or compensated. The main causes of machining errors, which in turn cause misalignment of the workpiece, are the following:

1. Error due to placement of locators
2. Error due to geometrical/form defects of workpiece
3. Error due to clamping and machining forces
4. Machine tool error or machine kinematic error, error due to temperature, tool wear and mechanical error

Instead of finding and eliminating, the positioning errors can be compensated. The compensation can be performed either by changing tool path, moving the cutting tool or moving the workpiece in the machine coordinate system. An appropriate choice of fixturing elements enables us to significantly reduce the positioning errors. Here we state a detailed literature review of the following causes of errors and compensating techniques.

2.3.1 Optimal placement of locators

According to Marin & Ferreira (2001), the design of machining fixture is divided into two stages. First stage is the development of the locating scheme which gives an optimal placement of locators. In this section, the work performed on the placement of locators for reducing the rigid body motion of the workpiece, is reviewed. Second stage involves the choice of set of clamps to insure the immobilization of the workpiece under external clamping and machining forces. Section 2.3.2 deals with the work performed on the prediction of workpiece positioning error due to fixturing elements i.e. locators and clamps.

Cecil (2001) presented a brief literature review on CAFD[1] and proposed recommendations for works to be performed in future. This review focuses mainly

[1]CAFD: Computer-Aided Fixture Design

on the development of the fixture setup planning including locating surface determination, locating and clamping position selection and stability analysis using algorithmic, mathematical and expert system based approaches.

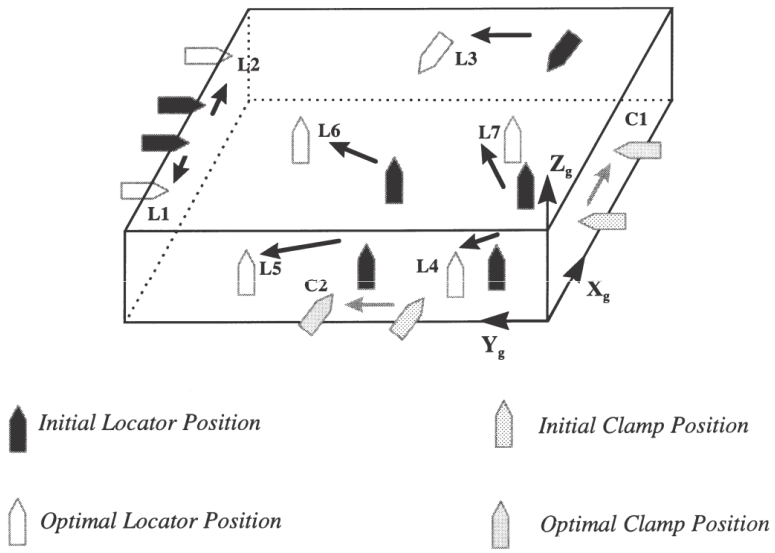

Figure 2.15: Fixture layout optimization (Li & Melkote, 1999)

Li & Melkote (1999) presented a model to improve workpiece location accuracy by fixture layout optimization taking fixture-workpiece contact deformation into account. The fixture is considered to be rigid as compared to workpiece which is further considered to be linear elastic at contact and rigid elsewhere. The optimization model is tested on a system of locators which were intentionally placed on positions differed from the required positions. The model gave optimal orientation of all the locators and clamps (fig. 2.15) which enabled the author to reduce the rigid body motion of the workpiece, forces on the locators and increased the accuracy.

Somashekar R. (2002) proposed a model to select the primary, secondary and tertiary planes of the workpiece, number of supporting, locating and clamping features and their faces on the workpiece based on the moment and force acting on the workpiece. The model is explained for drilling and milling operation, and the choice of workpiece surfaces is performed as follows: (a) Tool direction is

identified (b) Candidate faces for support are selected from the tool axis direction (c) Primary locating plane is selected farthest from the tool direction (d) Maximum force is determined and the surface experiencing the maximum force is chosen as secondary face (e) The surface experiencing the maximum moment is chosen as tertiary face. The clamping features can be determined either by direct opposition or by resisting frictional forces.

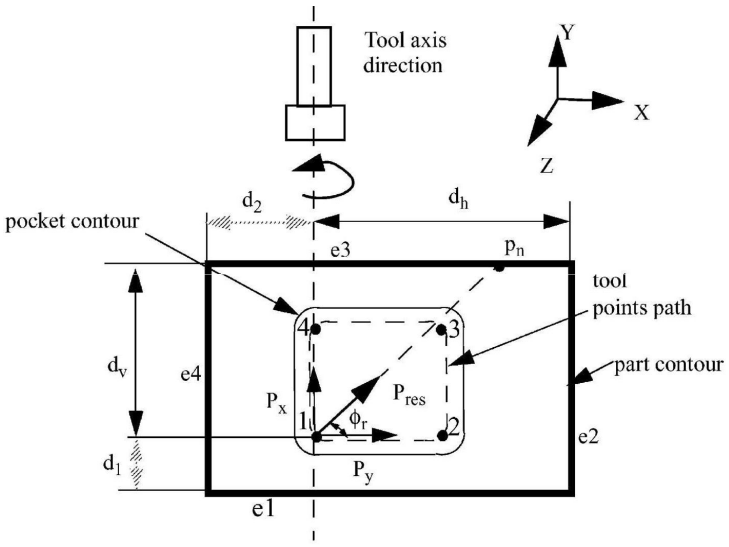

Figure 2.16: Force and moment in pocket milling (Somashekar R., 2002)

Roy & Liao (2002) relocated the supports on a 3-2-1r fixturing system considering the stability of the workpiece which they calculate by applying a virtual wrench on the fixturing system and by calculating the work done by this virtual wrench. Negative coefficient of work done by the virtual wrench gives a more stable system which is obtained by increasing the area of the triangle formed by three supports on the primary plane (see fig. 2.18). They also calculated minimum clamping force required for the workpiece stability during the machining using static equilibrium conditions.

Zirmi *et al.* (2009) demonstrated an algorithm of choosing the fixturing elements according to the application and depending on the surface and quality of the workpiece by a flow chart (fig. 2.17). Later, they proposed a strategy to place the locators on the primary contact plane in a 3-2-1r fixturing system,

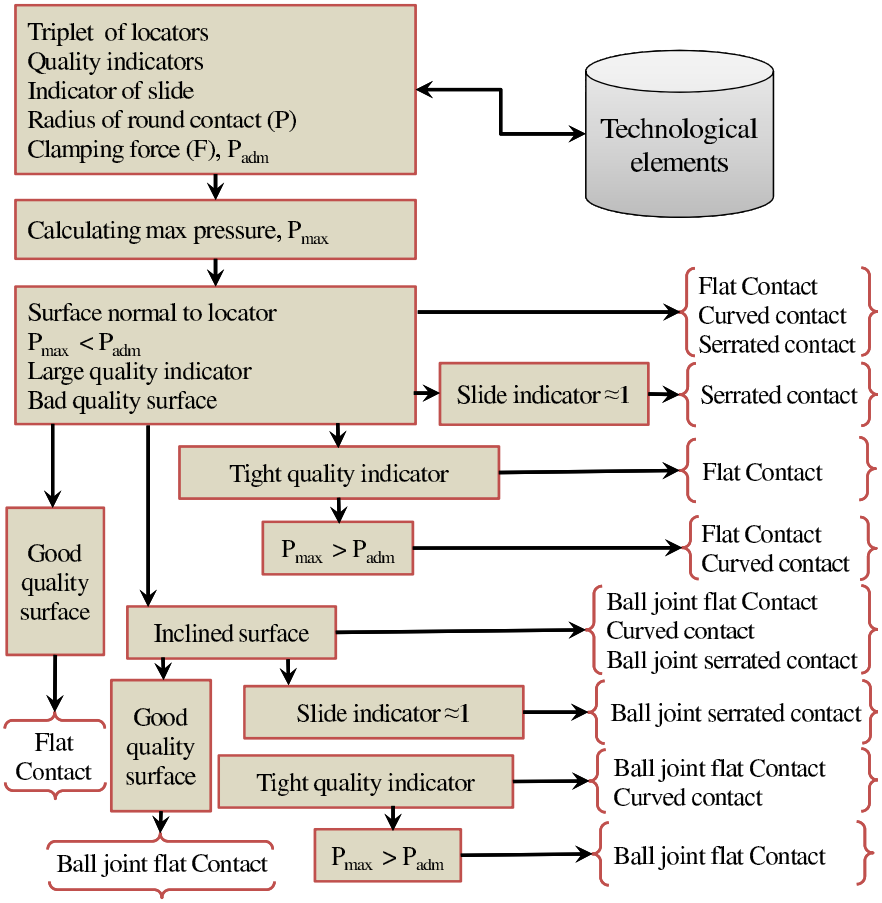

Figure 2.17: Algorithm of choosing technological elements to be in contact with the workpiece (Zirmi *et al.*, 2009)

considering the constraints of quality, accessibility, stability and mechanical behavior. According to them, the three locators should be placed as far as possible or they should make the biggest possible triangle of placement for the stability constraint(fig. 2.18). Menassa & Devries (1991) assumed the primary locating surface and its related locator positions as given. They determined the secondary and tertiary planes with their respective locator positions.

Raghu & Melkote (2004) analysed the effect of clamping sequence on the location error of a workpiece through an analytical model on a 3-2-1r locating fixture. The analytical model is based on the following assumptions:

- The workpiece is in contact with all the locators

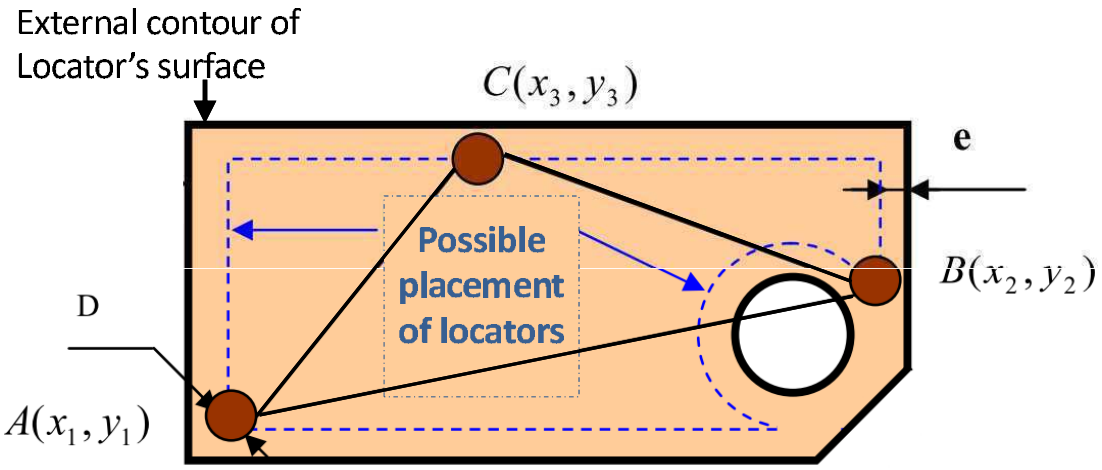

Figure 2.18: Possible placement of locators on primary plane forming biggest possible triangle (Zirmi *et al.*, 2009)

- Clamps are applied simultaneously
- Workpiece is rigid and its new position will be given by rigid body motion
- Normal reactions at the fixture elements opposite to applied clamps are fixed

A two step clamping process is performed for a fixture in figure 2.19, where clamp C1 is applied which caused reactions R_4 and R_5. In second step, clamp C2 is applied which causes reaction R_6 at L6. The analytical solution of this problem involves the calculation of rigid body motion of workpiece through the initial deflection and geometric errors of the locators. Jacobian vectors are used to calculate final positions of locators and workpiece. Locators and clamps are assumed to be elastic elements having contact(non-linear), tangential and shear stiffness. Principle of minimum potential energy is used to calculate the deflection at the each point of workpiece. The same problem is revised for C2 followed by C1. Experimental result shows that the sequence of clamps have a huge impact on the locating errors. This model is important for the designer because it gives an initial idea to designer about the clamping sequence to be followed in order to reduce the location error to the minimum possible value.

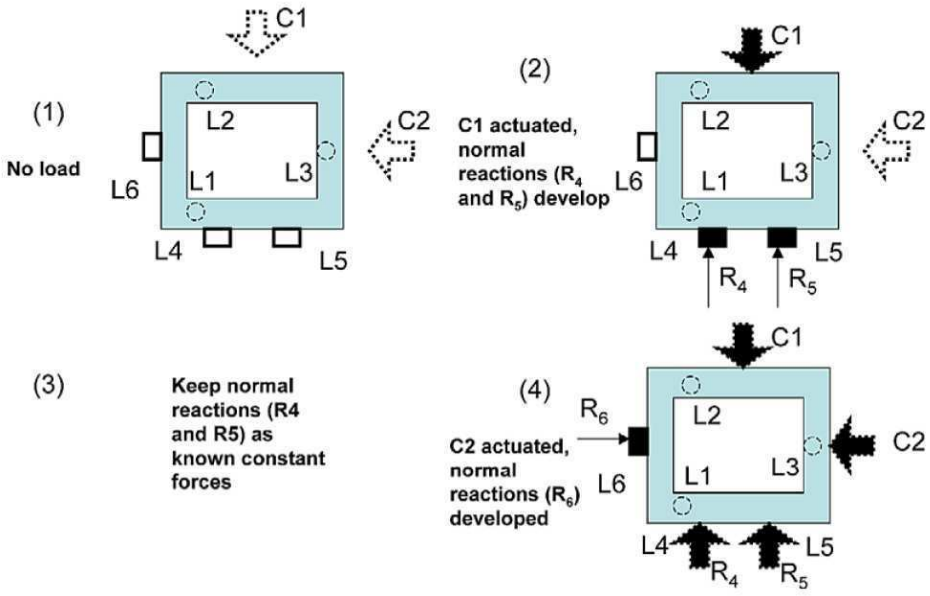

Figure 2.19: Clamping sequence model: Clamp C1 is followed by C2 (Raghu & Melkote, 2004)

The misalignment between the workpiece and machine tool is called localization error, one of the reason of localization error is error of the contacting point of the locator with the workpiece. Wang (2002) calls this point as fixel and its error as fixel error. Main sources of fixel error are: locator position, locator's shape and geometric variation of the workpiece (fig. 2.20). He shows the relationship of manufacturing errors with fixel errors and provides the basis of locators layout scheme. He verifies that each locator does not contribute equally on the manufacturing errors, but the position of locator is also crucial for error.

2.3.2 Positioning error of fixture

The positioning error of the workpiece on the fixture is further composed of geometrical errors of the workpiece and the error due to the deformation of locators under clamping and machining forces. This section details the literature review on the positioning error determination of the workpiece due to the local geometrical defects as well as the deformation of the locators under load.

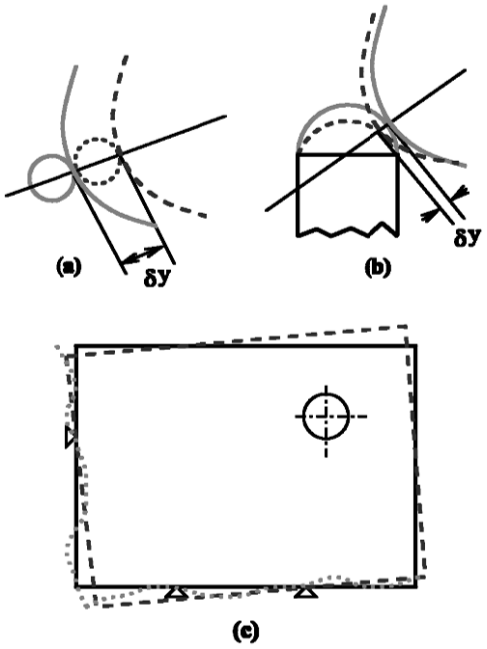

Figure 2.20: Fixel errors (a) Position error (b) Profile error (c) datum error (Wang, 2002)

2.3.2.1 Error due to workpiece geometrical defects

The locators are placed at their optimal positions to balance the workpiece with minimum displacement. The rough workpiece is then placed on these locators. Local geometrical defects of rough workpiece cause the dislocation of the workpiece from the desired position.

To locate a prismatic part, 3-2-1r locating configuration (Kang & Peng, 2008; Paris, 1995) is widely used. In contrast, to hold thin or soft workpieces with reduced deformation, Aoyama & Kakinuma (2005) used a bed of nails type fixture in which the locators are adopted to contact surfaces of a workpiece but this fixture must be reset for a different part family. Bed of nails type fixture provides a stable location of a workpiece but is inefficient to ensure a repeatable positioning.

Small Displacement Torsor (SDT)(Bourdet, 1999; Clement & Bourdet, 1988) approach is used to find the localization error of the workpiece. In CMM, SDT is used to associate the measured points with the ideal geometries. Using the same approach, Villeneuve *et al.* (2001) presented the geometrical deviation of

machining surface relative to its nominal position of the part. This deviation depends upon SDT of the workpiece in the setup, and deviation torsor of the machined surface relative to its nominal position in the setup. Zhu *et al.* (2012) also identified the geometrical error using SDT and the compensation is performed by modifying the NC code of a 5-axis machining tool. Legoff *et al.* (2004) presented two approaches of a manufacturing simulation; one through a mathematical model based on SDT while the other is based on virtually manufactured part through CAD/CAM system. The mathematical approach is bulky but it provides a detailed model as compared to CAD/CAM model.

Asante (2009) proposed a model using HTM[1] to calculate the positioning errors of the workpiece located and clamped in a 3-2-1r fixture using the hypothesis that all the elements are rigid and displacements are small so SDT can be applied. Overall positioning error of the workpiece is the sum of workpiece geometric error, locator geometric error and clamping error.

- Workpiece geometric error
  Workpiece geometric error is the error in workpiece dimension or surface roughness caused by machining, forging or casting processes. This dimensional error makes the successive workpiece to be in contact with the locator at varied points and causes error. The author used HTM with SDT to formalize the workpiece geometric error.

- Locator geometric error
  In a 3-2-1r locating system, the locators define three mutually perpendicular planes that are used as a reference for workpiece reference. Any geometric error of locators causes the planes to rotate or translate which in result causes the workpiece not to be placed correctly. The author defined three perpendicular normal planes and then used HTM and SDT to formalize the locators' geometric error.

- Clamping error
  Workpiece is located on the locators and clamps are introduced. Clamping error is the shift of workpiece surface due to the clamping force (fig.

[1]HTM: Homogeneous Transformation Matrix

2.21). The author used the formalization of Faux & Pratt (1979) to calculate clamping errors.

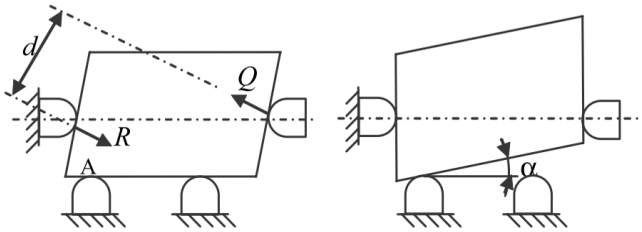

Figure 2.21: Clamping error (Asante, 2009)

The author calculated all the errors separately and summed them up later. The final equation gives the final position of any point on the workpiece surface with respect to its theoretical position. Result obtained from the model had an average of 3.7% deviation from the experimental values for a drilled hole. It is concluded that the orientation errors have more effect on the workpiece than the translational errors.

2.3.2.2 Error due to deformation of locators

After locating the workpiece on the locators, it is then clamped and the machining forces are applied. The workpiece displaces from its original position under these clamping and machining forces due to the deformation of the locators. The deformation of each locator is the sum of its body deformation and the local deformation at the contact. This section briefly presents a literature review on the deformation of locators and positioning error of the workpiece under load.

Fixturing stiffness is of great importance in fixture designing. If the fixture stiffness and the machining forces are known, the fixture stability can easily be determined. The effect of the force applied on the workpiece, clamped on the fixture with 3-2-1r configuration, is detailed in Jayaram *et al.* (2000). The workpiece is taken to be 10 times more rigid than the locators so that most of the deformation takes place at locators. Six locators are assumed to be springs having stiffness k_i. The author solves the problem in two ways: forward and backward. In forward problem, the stiffness of the part at the machined surface is determined

based on the stiffness of locators, i.e. unit force is applied on the workpiece and the deflection at that point is determined through the wrench and the stiffness of each locator is calculated which gives the stiffness of the machined surface. In the inverse problem, the equations are given to calculate the smallest values of the stiffness of each locator to withstand the applied forces on the workpiece. The maximum of the minimum stiffness is the optimum stiffness of that locator.

Raghu & Melkote (2005) presents a model that predicts the final position and orientation of the workpiece due to fixture geometric errors and fixture workpiece compliance. They used a rectangular workpiece with three orthogonal planes on a 3-2-1r fixturing system. For the fixture geometric errors, it is assumed that the deflection and geometric error at all the locators are known. Rigid body transformation of the workpiece is calculated using the part loading chart same as Raghu & Melkote (2004) which is shown in figure 2.22. While calculating the compliance of the fixturing system, contact stiffness is linearized by the proposition of Li & Melkote (2001) and the workpiece-fixture bulk compliance is calculated by the help of ANSYS®. The authors determined the final position of the part after clamping but prior to the machining. The results are compared with the experimental values and they found a maximum of 35% of deviation of experimental and proposed position of the part.

Hurtado & Melkote (2001) proposed a model for fixture stiffness optimization considering a 3-2-1r fixturing configuration as shown in figure 2.23. Pin array locators are used which are replaced by equivalent point reaction forces while the locators and clamps are considered as elastic elements. Workpiece is considered to be elastic at the contacting points and rigid elsewhere. The positions of locators and clamps are considered to be known initially. They calculated optimal stiffness of each locator and clamp to limit the maximum rigid body displacement of the workpiece as shown in the flowchart in figure 2.24. Stiffness higher than the optimum value would also keep the workpiece rigid body motion below the desired value but would result in an over-designed fixture. The model is demonstrated on two examples and for each example, optimum stiffness and clamping load/reaction forces for each clamp and locator is calculated along with the actual maximum rigid body displacement.

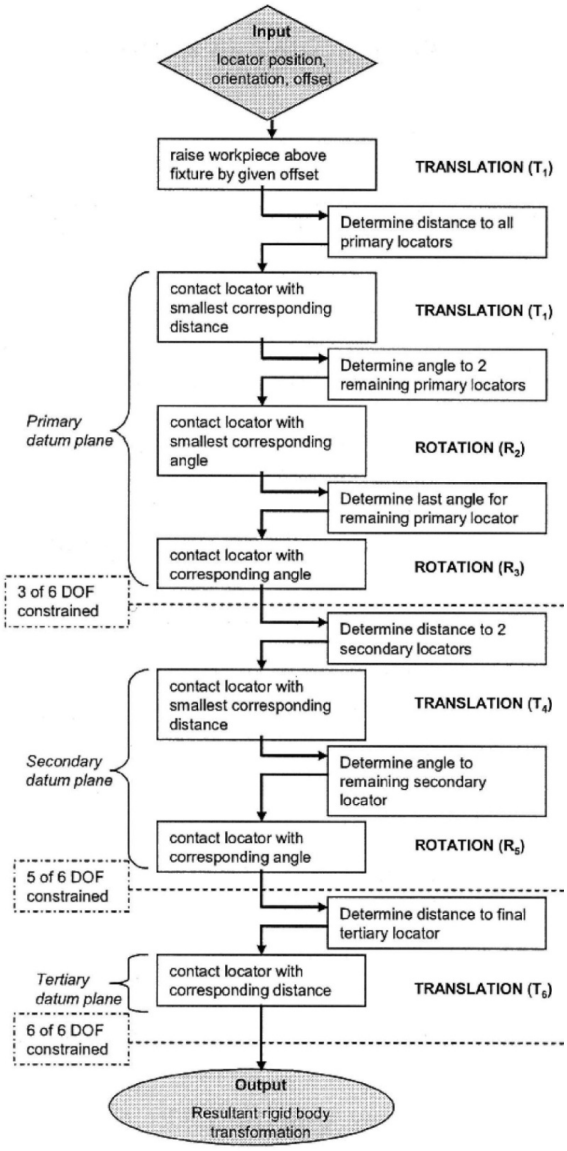

Figure 2.22: Part loading flow chart for rigid body transformation calculation (Raghu & Melkote, 2005, 2004)

Asante (2010) examined the effect of fixture compliance and cutting conditions on workpiece stability, which is determined by the minimum eigenvalue of the fixture stiffness matrix in response to all external forces. If any of the eigen values are zero or negative, the workpiece is not stable. The author calculated the Internal (contact force) and external (gravity and machining) force wrench

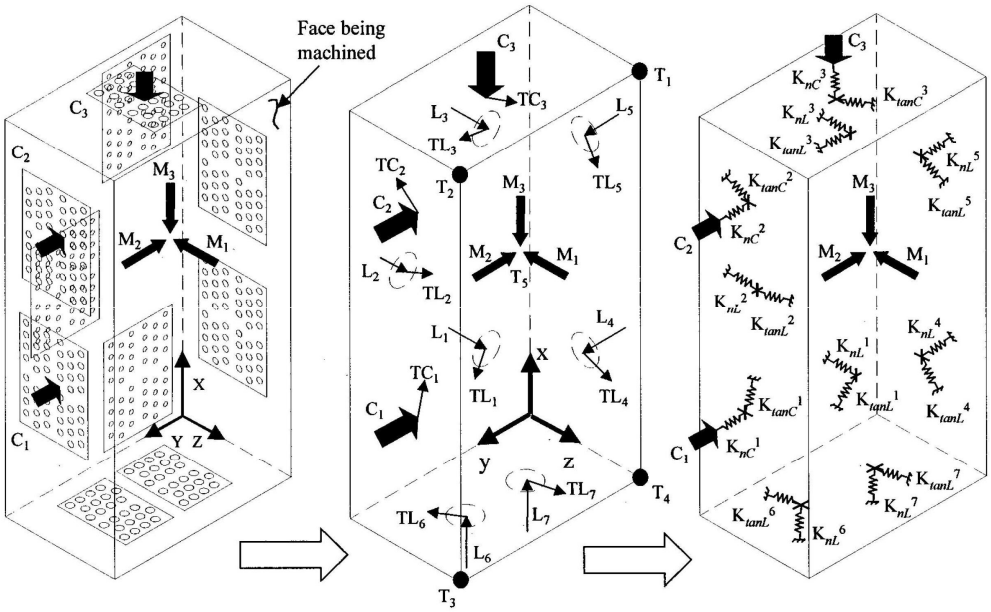

Figure 2.23: (a)Pin array type locators and clamps (b) equivalent locators and reaction forces (c) fixture stiffness model (Hurtado & Melkote, 2001)

using static equilibrium conditions and calculated the fixture compliance matrix. The workpiece and fixturing elements are taken to be deformable only at contacts, so linear 3D stiffness is used on each contact of the workpiece (w) with fixturing elements (f) as shown in figure 2.25 where k represents the stiffness, superscript i is used for i^{th} fixturing element, subscripts f and w are used for the axial direction while subscripts a and b are used for two radial directions.

In the presence of machining forces, fixture restoring force tends to bring the workpiece in the equilibrium position depending upon the stiffness of the fixture. Therefore a fixture with higher value or less machining force is more stable and experiences lesser workpiece deformation under load. The overall workpiece deformation and stability are verified for different workpiece materials, cutting conditions and location of fixturing elements through an example. It is concluded that all of these parameters have effects on the fixture stability. A 68% reduction of workpiece deformation is noticed by changing only cutting conditions

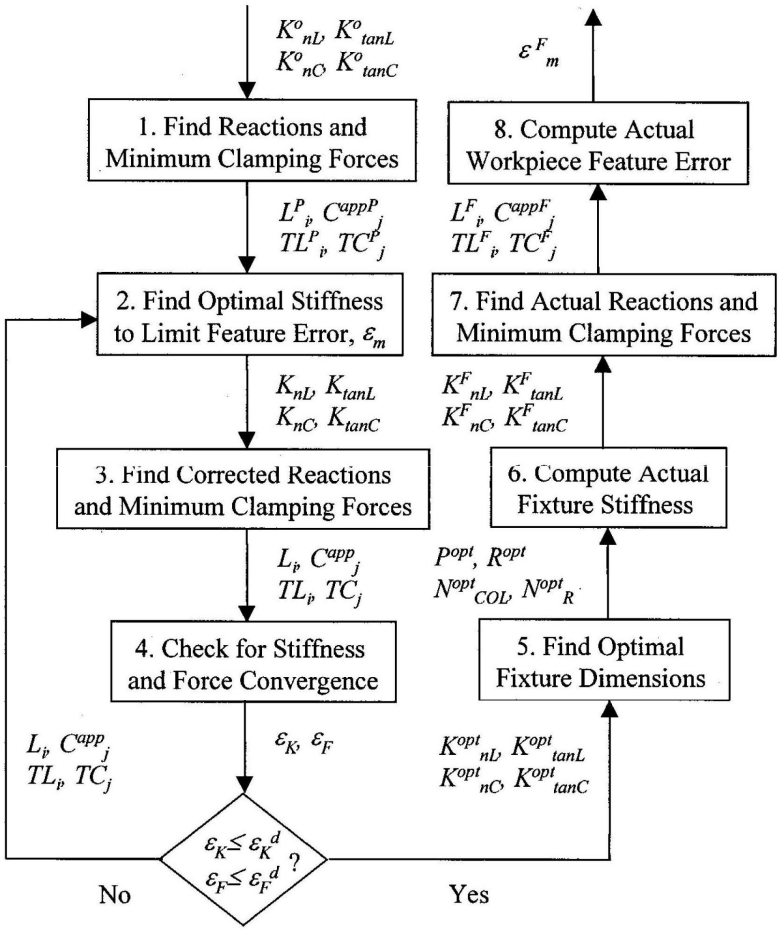

Figure 2.24: Stiffness optimization flowchart (Hurtado & Melkote, 2001)

e.g. force magnitude.

Marin & Ferreira (2003) transformed inaccuracies and tolerance of the locators in displacement of the workpiece to see if the entity is within the tolerance zone using Jacobian matrix, the author calls it sensitivity matrix. The same problem is then performed in inverse direction in which the tolerances are allocated to the locators so that the workpiece entity remains within the tolerance zone.

Li & Melkote (2001) proposed an algorithm to determine the optimum clamping forces on a multi clamp system considering the contact to be elastic. The optimization problem is solved as a multi-objective constrained optimization problem. Li *et al.* (2000) calculated minimum clamping forces required to keep the workpiece in static equilibrium condition on the large contact area fixtures (e.g.

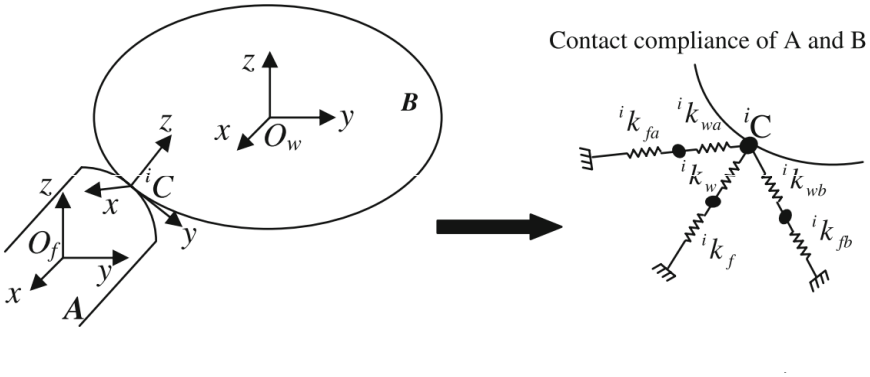

Figure 2.25: Locator/clamp in contact with workpiece (Asante, 2010)

mechanical vice) assuming the workpiece to be elastic at contact and the fixturing elements to be rigid. The multiple contact problem is solved using the minimum energy principle.

Deng & Melkote (2006) also presented a model to determine the minimum clamping force required to ensure the dynamic stability of a workpiece during machining. A geometric model captures the geometry change and inertia of the workpiece and the dynamic model simulates the vibratory behavior of the workpiece during machining. A static model calculates the static deformation at the fixture-workpiece contact due to clamping using three virtual springs at each contacting point. The model searches for the minimum clamping force needed to stabilize the workpiece during machining, the flow chart is show in figure 2.26. They concluded that the minimum required clamping force is decreased with the material removal and the authors suggested the need for implementing dynamically varying clamping force during machining to achieve better fixture performance.

Zheng *et al.* (2007) mentioned that the determination of fixture contact stiffness is the key barrier in the analysis of the fixture stiffness due to its non linear nature. They developed a FEM model to predict the stiffness of fixturing unit by introducing non linear contact elements on the contact between fixture components. They took the contact as three unidirectional springs, one in normal while two in radial directions. An iterative calculation is used to calculate the final

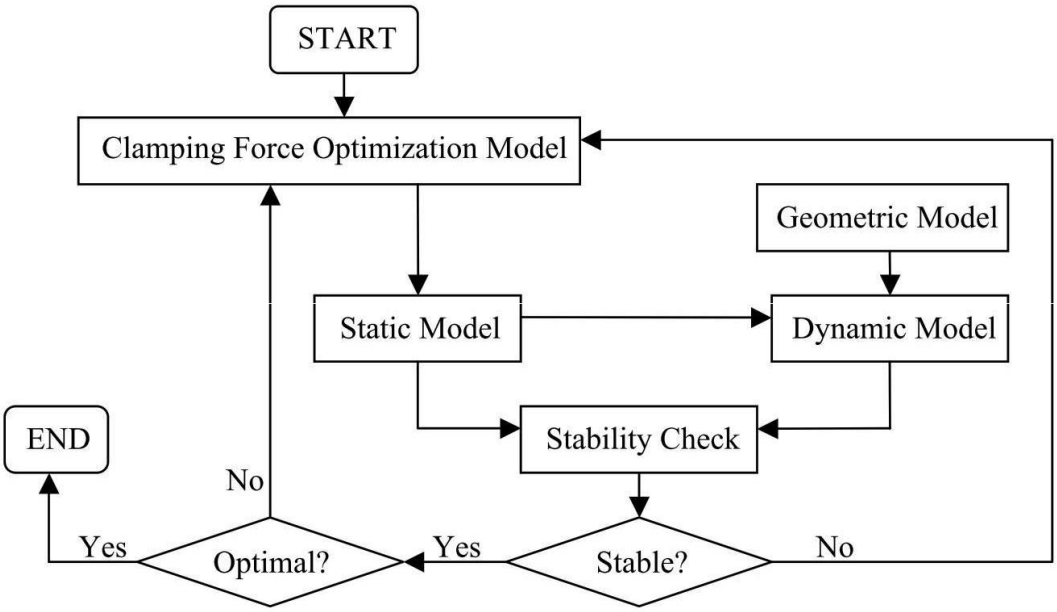

Figure 2.26: Clamping force optimization flow chart (Deng & Melkote, 2006)

stiffness of the fixturing element. Penalty function method is used in each iteration to calculate the updated stiffness matrix until the convergence is attained. The procedure is shown in the flow chart in figure 2.27.

Siebenaler & Melkote (2006) investigates the effect of mesh density and friction of the locator workpiece contact on the overall deformation of the workpiece through FEM[1] analysis on a 3-2-1r located workpiece. In addition, the effect of compliance of locators and clamps are also considered. Overall compliance of the supports does not have a significant effect on the workpiece deformation while analyzing through FEM. This model covers the deformation at the contact tip which is 98.1% of overall deformation.

Liao & Hu (2001) developed a FEA model to predict the machined surface quality of a clamped workpiece taking into account;

- external clamping preload
- machining forces

[1]FEM: Finite element method

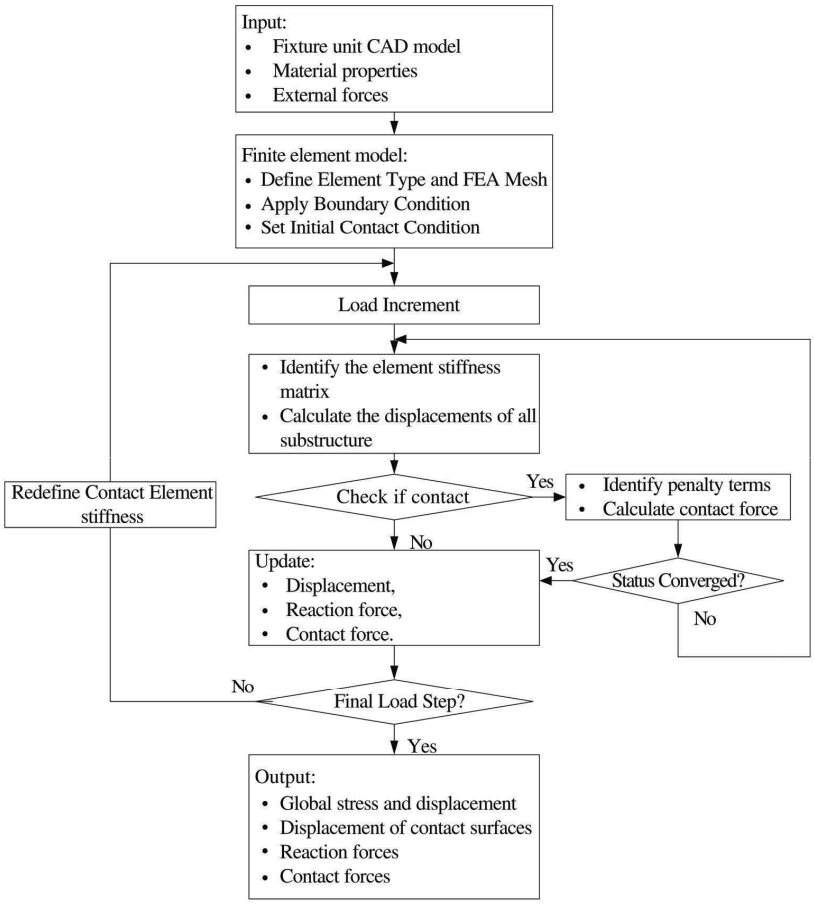

Figure 2.27: Flow chart to calculate the stiffness of fixturing element (Zheng *et al.*, 2007)

- fixture compliance
- workpiece and locators/clamps contact interaction
- fixture base stiffness and dynamic stiffness of the fixture-workpiece system

Locators and clamps are supposed to be elastic elements with constant body stiffness so they are modeled as springs while locator contact tip is not taken as spring (fig. 2.28) due to non linear behavior of the contact according to Hertz contact theory (eq. 2.37). Deflection of a part is found with and without machining force and they concluded that the machining forces have great impact on the surface quality as compared to the clamping preloads.

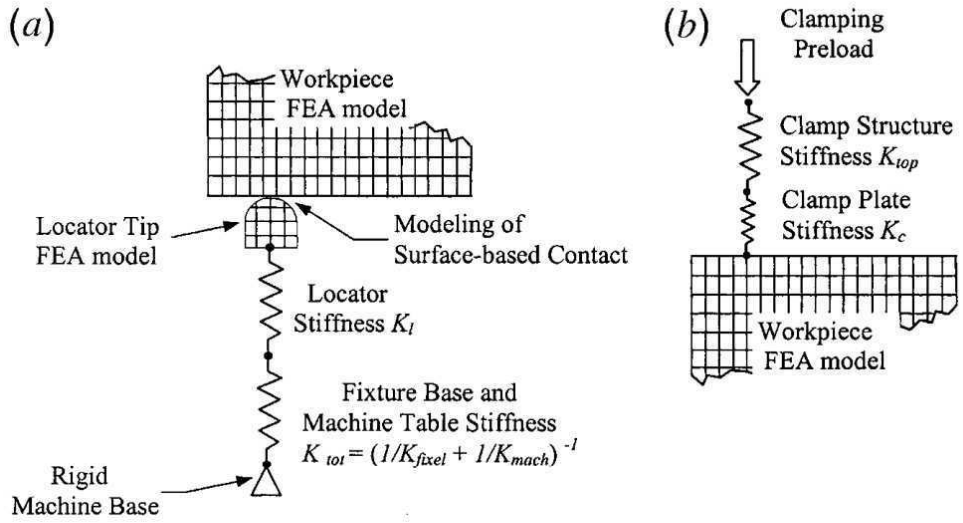

Figure 2.28: FEA modeling (a) Workpiece and locator contact (b) workpiece and clamp contact (Liao & Hu, 2001)

2.3.3 Machine tool error

Remark 2.3.1. *The accuracy of the machine tool is primarily affected by the geometric errors caused by mechanical-geometric imperfections, misalignments and wear of the linkages and elements of the machine tool structure, by the non-uniform thermal expansion of the machine structure and static/dynamic load induced errors. As a result a volumetric error which is the relative error between the cutting tool and the workpiece is created (Okafor & Ertekin, 2000)*

There is also the error due to NC code limitations or due to the backlash of the tool, but these errors cannot be compensated through the workpiece repositioning. Therefore, these errors are not discussed here. Precision of machined workpiece is influenced by the inaccuracy of the machine tool. In machine tool, there are three major sources of errors, which are geometric errors, thermal induced errors and load induced errors (Okafor & Ertekin, 2000; Ramesh *et al.*, 2000).

It is impossible to eliminate machine tool error due to structural and production limitations therefore, it is necessary to compensate them. Hsu & Wang (2007) simplified error compensation in three steps:

- measuring errors

- developing an error model
- compensating errors

Their research is focused on the structural error compensation in 5-axis machine tool using HTM. According to Hsu & Wang (2007), five-axis machining is not suitable for heavy-duty and high speed machining as machine tool has poor machining stiffness.

Lin & Shen (2000) proposed a generic kinematic error model for 3-axis machine tool using homogeneous coordinate transformation. Ahn & Cho (2000) concentrated on the stochastic error in a three axis machine tool to predict the uncertainties in the tool positioning. They focused on the use of beta distribution of errors instead of widely used normal distribution, as beta distribution is defined by four parameters compared to two parameters of normal distribution. For three axis machine tool, 21 error model is used to formalize error distribution and it is concluded that the stochastic error depends upon the direction of approach of a tool/workpiece.

Choi *et al.* (2004) suggests a new error model to quickly assess the positioning error of a machine tool by an on machine measurement (OMM) using an eight cube array artifact as shown in figure 2.29. Here, HTM are used to determine the positioning error within the workspace and 21 error components are measured to predict the tool positioning. The iterative compensation is performed until the required accuracy is obtained. The author obtained an accuracy of less than 5μm.

Jha & Kumar (2003) develops a generalized error model to calculate the positioning error due to the components of kinematic chain of a five-axis machine using HTM. The error compensation is performed by NC[1] part program for the generation of a CAM profile. The compensation produced a vivid improvement in the CAM profile.

Zhu *et al.* (2012) proposed a small displacement geometric error model for a five-axis machine tool based on the kinematics of MBS[2] and HTM. The workpiece geometrical and orientation error is calculated using 12-line method. The

[1]NC: Numerical Control
[2]MBS: Multi-Body System

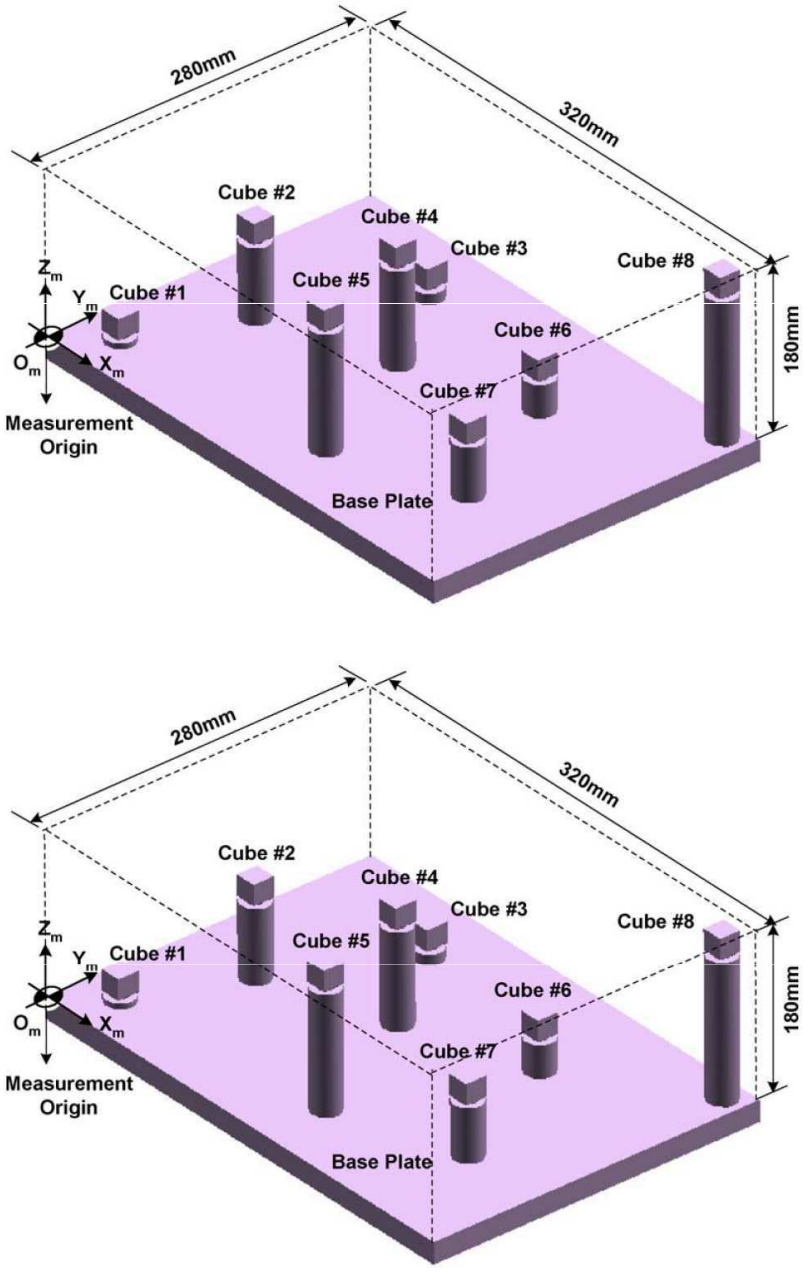

Figure 2.29: Cube array artefact

compensation is performed by modifying NC code of the machine tool as shown in figure 2.30 where the error E is compensated by changing the tool path by a value E in opposite direction (-E). The experimental study shows an evident

error reduction after compensation.

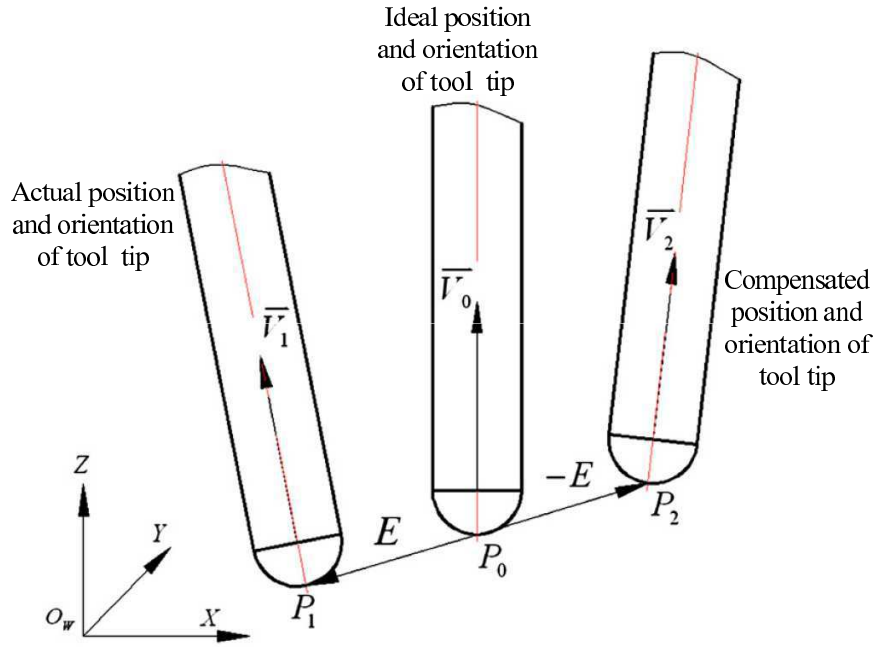

Figure 2.30: Basic idea of error compensation (Zhu *et al.*, 2012)

Ramesh *et al.* (2000) mentioned that the easiest error compensation can be obtained by measuring the inaccuracy and compensate it by changing the CNC tool path through commands. A complete NC compensation cannot be performed on 3-axis machines because of tool orientation limitation and the machine tool must have at-least 4-axis in order to completely compensate the workpiece error.

Wan *et al.* (2008) calculated the deviation of tool with respect to the workpiece (fig. 2.31) taking into account machine tool error, fixture error and datum error. The unified model is verified by three cases of workpiece locating:

- **Under deterministic**, when the locators are less than required to block 6 DOF motion e.g. 3 locators in z-direction
- **Deterministic**, when the locators are just enough to block 6 DOF motion e.g. 3-2-1r locating principle
- **Over deterministic**, when the locators are more than required to block 6 DOF motion e.g. N-2-1 locating principle, where n>3

The compensation of this unified model is performed by controlling the advancements of locators. Locators' advancements are calculated through Plücker coordinates of the system.

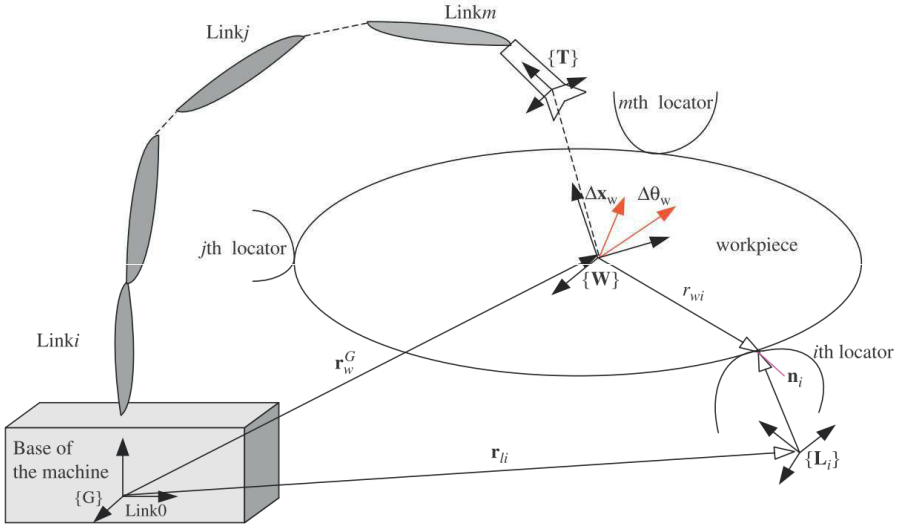

Figure 2.31: A generic machining system (Wan *et al.*, 2008)

Martin *et al.* (2011) simulated the machining on a three axis milling, during the product design stage, to predict the geometric error that the workpiece could encounter during real machining process. They focused on the errors due to geometrical defects of the workpiece positioning and the machine tool geometric error.

The workpiece setup is composed of sub-setups. The final global geometrical defect and precision of the workpiece are calculated by considering the worst position of each sub-setup (fig. 2.32(a)). Furthermore, the error due to the kinematic chain of machine tool is calculated using HTM and small displacement hypothesis (fig. 2.32(b)).

Martin *et al.* (2011) used HTM to predict the machine tool positioning error by taking into account the error present in each of the element of the kinematic chain using SD[1](fig. 2.33).

The simulation is performed in DELMIA® considering both the setup and machine tool errors. The errors are included in the simulations as mathematical

[1]SD: Small Displacement

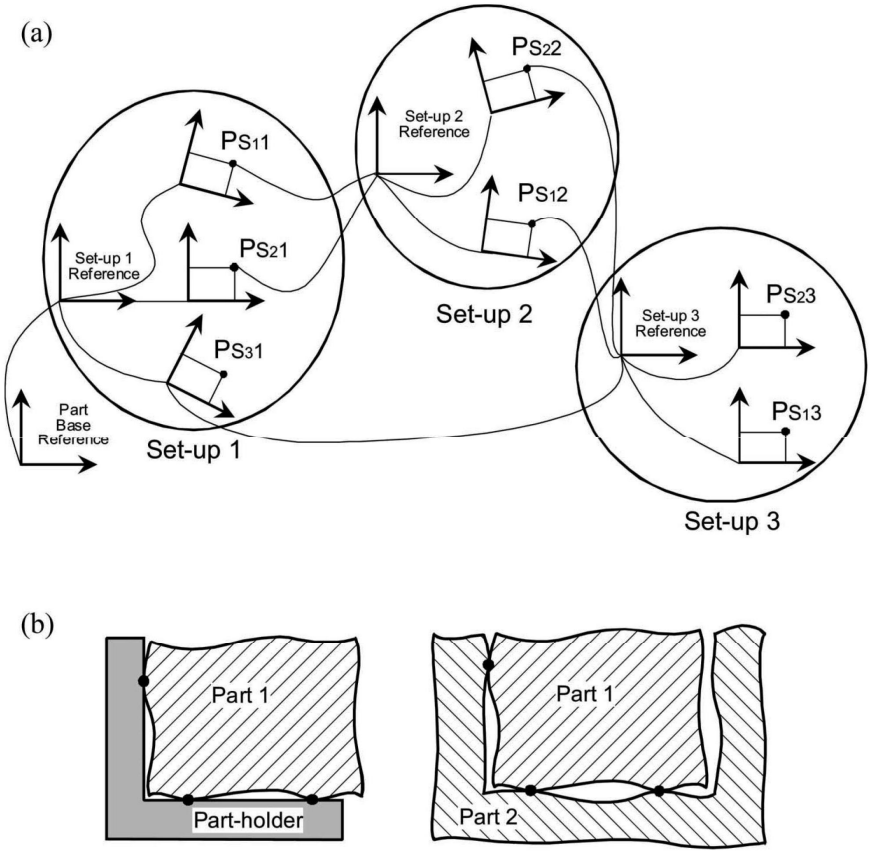

Figure 2.32: Geometrical defects due to set-ups. (a) Arborescence structure of the manufacturing set-up process plan (b) Contact schema (Martin *et al.*, 2011)

functions and simulations are performed for five different types of defects; orientation, straightness, rotation, part position and total defect, and their effect on the final machined product is analyzed. It is concluded that the workpiece position defect is predominant in the orientation and form error while the orientation and rotation defects have dominant effect on the positioning accuracy of the workpiece.

Raksiri & Parnichkun (2004) proposed an error compensation model for geometrical and cutting force induced errors on a 3-axis CNC milling machine using neural network. Geometrical error was modeled using 21 error components while the cutting tool deflection is calculated as the result of cutting force. Both the

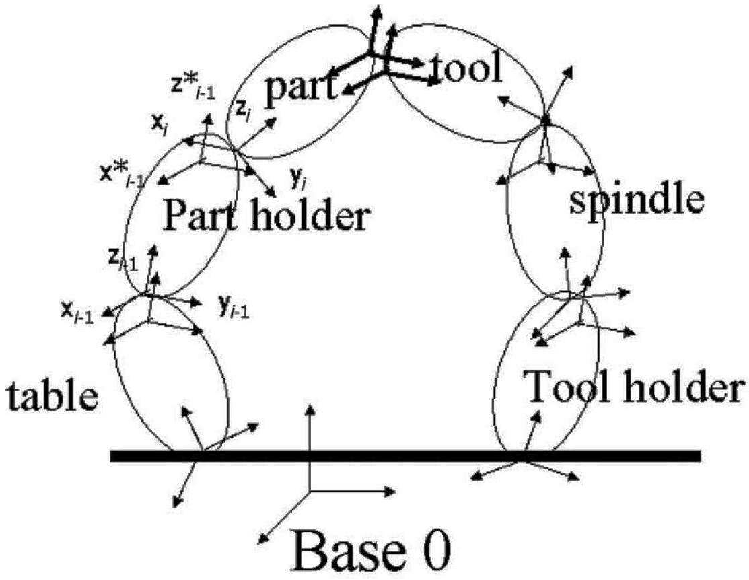

Figure 2.33: Machine tool architecture (Martin *et al.*, 2011)

errors are compensated by modifying the cutting tool position in CNC command module. The model showed a significant error reduction after error compensation.

2.3.4 Synthesis

Two different parts of a batch cannot have the same geometry. The geometrical and form defects of the workpiece can cause large positioning errors if the locators are directly in contact with the workpiece. In this thesis, a high quality baseplate is added in between the workpiece and the locators in order to achieve high positioning accuracy. The rough workpiece is placed and clamped rigidly on the baseplate instead of locators and it is assumed that no deformation is possible between the workpiece and the baseplate. The workpiece repositioning is performed through baseplate mobilization using 6-locators. Because the baseplate surfaces are considered to be perfectly plane, the positioning uncertainty is eliminated and the workpiece can precisely be positioned on the machine.

The work performed to calculate the deformation of the elastic fixturing elements under clamping, external static and machining forces is summarized in table 2.5. The existing models use static equilibrium conditions, rule based flow chart method or FEA analysis which are used for specific system configuration.

Our proposed model is reconfigurable/generic and it uses energy methods to calculate quickly the displacement vector of the workpiece and stiffness matrix of the fixturing system for any configuration of locators, baseplate and clamps. Our proposed model calculates the deformation of each locator under clamping and machining forces. The baseplate is assumed to be elastic at contact with the locators and rigid elsewhere. The locators and clamps are designed to be elastic. Analytical formulation is performed using Lagrangian, to calculate the deformation of elastic elements and as the result the rigid body displacement of the workpiece-baseplate assembly. The proposed kinematic model again enables us to compensate these errors due to locators deformations through the advancement of 6 locators.

Table 2.5: Existing work for the deformations of elastic elements under external load

Reference	**Analysis**	**Elastic elements**	$F_{Applied}$	**S/D**	**Objective /Result**
Jayaram *et al.* (2000)	Analytical	L	F_S	S	K_{op}
Raghu & Melkote (2005)	FC+FEA	L+C	F_{CL}	S	RBD and K
Li & Melkote (2001)	Analytical	C	F_{CL}	S	$F_{CL,op}$
Hurtado & Melkote (2001)	Analytical	L+CL	F_{CL}	S	$K_{CL,op}K_{L,op}$
Asante (2010)	Analytical	C	F_M	S	X
Li & Melkote (2001)	Analytical	C	F_M	S	$F_{CL,min}$
Deng & Melkote (2006)	Analytical	CL	F_M	D	$F_{CL,min}$
Zheng *et al.* (2007)	FEA	C	F_S	S	K
Siebenaler & Melkote (2006)	FEA	C	F_{CL}	S	δ_P
Liao & Hu (2001)	FEA	C+CL+P	$F_{M,CL}$	D	Surface quality
Current work	Analytical	L+C+CL	$F_{M,CL}$	S	RBD, [K],[M],$\{\delta_L\}$, $[K_L]$,ω

L	Locator	C	Contact
CL	Clamp	S	Static aspect
D	Dynamic aspect	M, [M]	machining forces and mass matrix
K,[K]	Stiffness and stiffness matrix	F	Force
P	Part	δ	Deformation of elastic elements
X,RBD	Workpiece ridig body displacement	FC	Rule based flow chart

The proposed model does not calculate the optimal positions of the locators and clamps to hold the workpiece during machining. Instead, if we know a few possible locating configurations and locators and clamps placements, the proposed analytical mechanical model enables us to choose the best possible configuration by calculating the displacement of the workpiece under machining and clamping forces. The configuration having minimum displacement will be more stable and will be the suitable locating choice.

Similarly, our model does not calculate the kinematic, thermal, NC system errors or the error due to tool wear. But if these errors are known, our system is capable of performing the compensating of these errors as well.

2.4 Forces on the fixturing system

One of the main tasks of the fixture is to support the workpiece against the machining forces and torques during machining operation. The fixture should be able to support the maximum machining forces with least possible deformation of the workpiece; therefore the effect of cutting forces should be taken into account at the design stage.

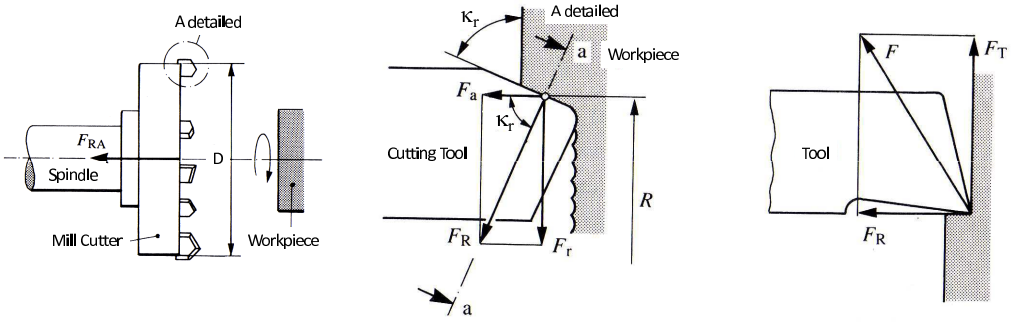

(a) Milling of the workpiece (b) Tooth A detailed (c) Section a-a detailed

Figure 2.34: Forces on the cutting tool during milling operation Pruvot (1993)

The cutting force, acting on the cutting tool during the milling operation, can be characterized as axial (F_a), radial (F_r) and tangential (F_T) cutting forces as shown in figure 2.34, where F_R is the repulsion force. The axial force acts parallel to the axis of the cutting tool, tangential force is regarded as the cutting force (F_c) while the radial force is regarded as the rubbing force between the workpiece and the cutting tooth. Direct measurement of tangential and radial forces is difficult because they are oscillating rapidly during the cutting; a suitable dynamometer is capable of recording the fluctuations on a time base (Black *et al.*, 1996). A number of cutting force and cutting speed prediction models (Araujo & Silveria, 1999; Ber *et al.*, 1988; Kim & Chu, 2004; Mativenga & Hon, 2005) were developed for specific cutting tool, workpiece material or cutting conditions. In our case, we are

concerned with the maximum force acting anywhere on the workpiece, so we are using classical mathematical equations for the cutting force calculations obtained from Black *et al.* (1996), Sandviken (1997) and Sandviken (2011).

The mathematical equation for cutting force per tooth can be written as (Sandviken, 2011),

$$F_c = k_c * a_p * f_z \tag{2.16}$$

Where,

F_c : cutting force, N
k_c : specific cutting force, N/mm^2
a_p : depth of cut, mm
f_z : feed per tooth (it is usually given and is unction of number of teeth), $f_z = \frac{v_f}{n*Z_c}$ mm
v_f : Advancement of table, mm/min
n : Spindle speed, rpm

The specific cutting force depends upon the workpiece material, and can be written as;

$$k_c = k_{c1} * h_m^{-m_c} \tag{2.17}$$

where,

k_{c1} : Material dependent specific cutting force, N/mm^2
m_c : Workpiece material constant
h_m : Average chip thickness, mm

m_c and k_{c1} depend upon the material of the workpiece and can be found in Sandviken (2011) while for the face milling operation, h_m can be written as;

$$h_m = \frac{a_e * f_z * \sin\kappa_r}{D_{cap} * \sin^{-1}\left(\frac{a_e}{D_{cap}}\right)} \tag{2.18}$$

Where,

a_e : Working engagement, mm
D_{cap} : Cutting tool diameter at actual depth of cut, mm
Ψ_r : Lead angle, degree
κ_r : Entering angle, degree , $\kappa_r = 90 - \Psi_r$

D_{cap} depends upon the cutting depth and the geometry of mill cutter. Mill cutters having straight cutting edge, round cutting edge and ball nose end mills are shown in figures 2.35, 2.36 and 2.37 while their D_{cap} are shown in equations

2.19, 2.20 and 2.21 respectively. In all of the three cases, the case of maximum a_e ($a_e > D_{cap}$) is taken to get the maximum cutting force.

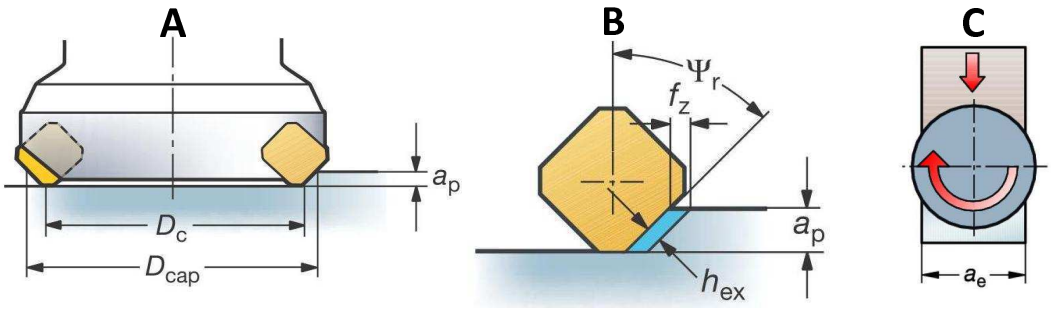

Figure 2.35: Straight cutting edge cutter (Sandviken, 2011)

$$D_{cap} = D_c + \frac{2 * a_p}{\tan \kappa_r} \tag{2.19}$$

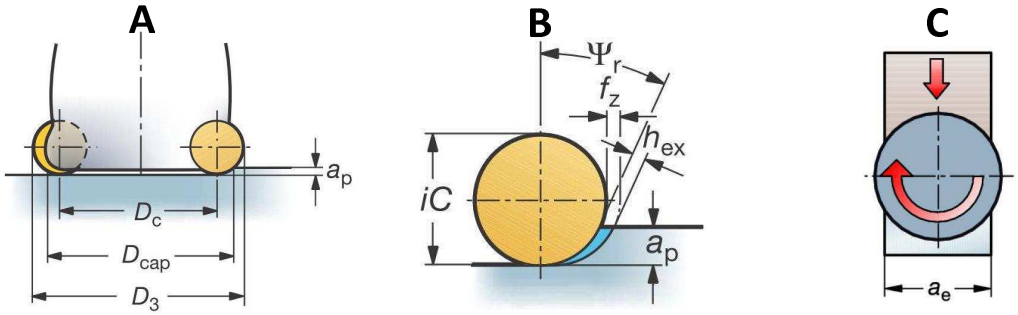

Figure 2.36: Round cutting edge cutter(Sandviken, 2011)

$$D_{cap} = D_c + \sqrt{ic^2 - (ic - 2 * a_p)^2} \tag{2.20}$$

$$D_{cap} = \sqrt{D_3^2 - (D_3 - 2 * a_p)^2} \tag{2.21}$$

where,

D_3 : Diameter of cutting tool, mm

D_c : Diameter of tool cutting edges

The cutting speed of V_c and cutting torque M_c for the engagement of a single tooth can be calculated using;

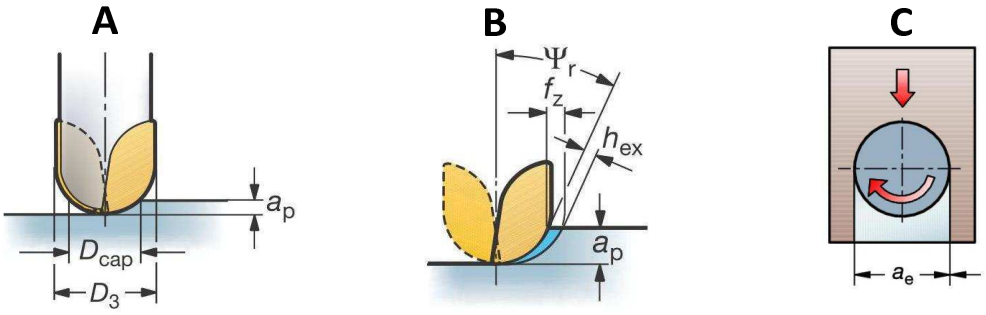

Figure 2.37: Ball nose end mill cutter (Sandviken, 2011)

$$V_c = D_{cap} * \pi * n$$
$$M_c = F_c * D_3/2 \tag{2.22}$$

The formalization of calculating the radial, axial and tangential cutting forces can be found in Pruvot (1993) and Pruvot (1995). This formalization can be used for the machining force calculation for simulation and it gives the values of the cutting force which are probable and near to the real values. These values change correctly with the change of different parameters. These equations do not have any physical interpretation and they are constructed experimentally (Pruvot, 1993). The tangential of cutting force is calculated from equation 2.16 while the repulsion force can be obtained from equation 2.23 whose formulation is detailed in Appendix B.

$$F_R = \frac{K_R}{K_T} * F_T \tag{2.23}$$

where, K_R and K_T are the radial and tangential specific force coefficients and the ratio $\frac{K_R}{K_T}$ depends upon the cutting material strength and cutting angle. The equations for K_R and K_T are valid for the materials having the stress range from 40 daN/mm^2 to 180 daN/mm^2. At the end, the radial and axial force components (fig. 2.34(b)) can be obtained by using,

$$F_r = F_R \sin \kappa_r$$
$$F_a = F_R \cos \kappa_r \tag{2.24}$$

Forces, following x, y and z directions, for the proposed fixturing (fig. 4.6) system can be obtained from equation 2.25 which can be found in Ber *et al.* (1988) with θ_t being the tool rotation angle. These forces will be used during the case study of chapter 4.

$$\begin{Bmatrix} F_x \\ F_y \\ F_z \end{Bmatrix} = \begin{bmatrix} \cos\theta_t & -\sin\theta_t & 0 \\ \sin\theta_t & \cos\theta_t & 0 \\ 0 & 0 & 1 \end{bmatrix} \begin{Bmatrix} F_r \\ F_T \\ F_a \end{Bmatrix} \tag{2.25}$$

The force vector depends upon the cutting tool rotation angle and the values of F_X and F_Y interchange after $\theta_t = \pi/2$. As F_T is the largest force, the max value of F_X and F_y is F_T which is attained at $\theta_t = 0$ for F_x and at $\theta_t = \pi/2$ for F_y.

2.5 Contact mechanics

Remark 2.5.1. *The ability to accurately locate a workpiece in a machining fixture is strongly influenced by rigid body displacements of the workpiece caused by elastic deformation of loaded fixture-workpiece contacts (Li & Melkote, 1999).*

In the previous sections, workpiece positioning error is discussed which involves the deformation induced in the locating and clamping elements due to clamping or machining forces. Besides axial, shear and bending deformations of locators, contacting surface would also deform under load which induces displacement to the workpiece position. In this section the deformation of contact for different surface condition under load are discussed, in order to study the effect of deformation at the locator-workpiece contact surface.

2.5.1 Hertz contact theory

Hertz contact theory was established to predict mechanical behavior of ideally smooth surfaces assuming the contact to be perfect. However, real surfaces are not smooth and their asperities make contact, which cause the real contact area to be smaller than the one calculated thanks to Hertzian contact theory. Hertz replaced contacting spherical surfaces with paraboloids, so that the contact between two spheres (fig. 2.38(a)) is simplified to sphere-plane contact and an equivalent sphere-plane geometry could be defined with an equivalent sphere radius given by $\frac{1}{\rho} = \frac{1}{\rho_1} + \frac{1}{\rho_2}$. For the calculation, the sphere is assumed to be rigid with only the half-space supporting deformations (fig. 2.38(b)). An effective modulus of elasticity is defined for this half-space, which is $\frac{1}{E'} = \frac{1-\nu_1^2}{E_1} + \frac{1-\nu_2^2}{E_2}$.

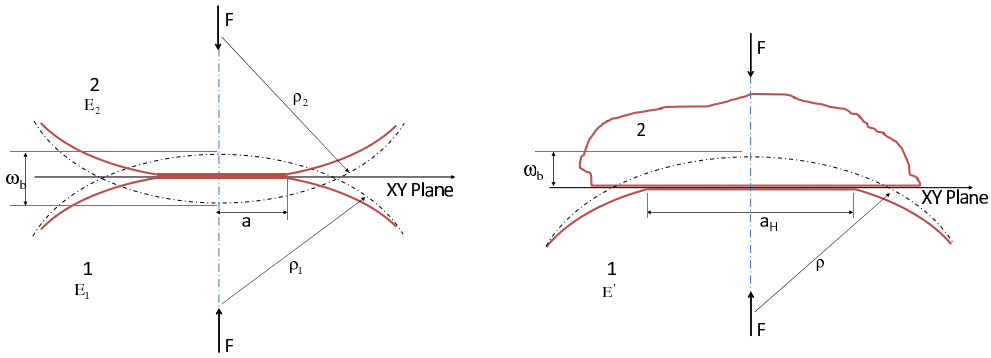

(a) Contact of two spheres

(b) Contact of a plane and sphere with equivalent sphere properties

Figure 2.38: Hertz contact theory of two spheres

The Hertz pressure distribution $P_H(r/a_H)$, max Hertz pressure at center $P_{O,H}$, Hertz contact area a_H and deformation at the center of the contact δ_C can be written as in Johnson (1987),

$$P_H(r/a_H) = P_{0,H}\sqrt{1-(r/a_H^2)} \tag{2.26}$$

$$P_{O,H} = \frac{3F}{2\pi a^2} = \left(\frac{6FE'^2}{16\pi^3\rho^2}\right)^{1/3} \tag{2.27}$$

$$a_H = \left(\frac{3F\rho}{4E'}\right)^{1/3} \tag{2.28}$$

$$\delta_H = \frac{{a_H}^2}{\rho} = \left(\frac{9F^2}{16\rho E'^2}\right)^{1/3} \tag{2.29}$$

Analytical models defining $A = 1/\rho_1$ and $B = 1/\rho_2$ as principal curvature radii, to calculate the contact area for the Hertzian elliptical contacts, can be found in Greenwood (1985), Brewe & Hamrock (1977) and Hamrock & Brewe (1981). Greenwood (1997) performed a comparison of all the three models for principle curvature range of $1 \leq B/A \leq 25$. The model of Houpert (2001) is valid for $B/A \leq 13,576$. Antoine *et al.* (2006) proposed an analytical formulation dedicated to rolling bearings and whose single formula fits the Hertzian theoretical values for a large range of B/A ratio with the precision of 0.006%.

2.5.2 Contact of rough surfaces

The problem of asperities can be considered similar to the contact of two spheres. The contact of two rough surfaces is dealt as the contact of ideally smooth surface and a surface with the equivalent roughness $\sigma = \sqrt{\sigma_1^2 + \sigma_2^2}$ in (Johnson, 1987) as shown in figure 2.39(a), where σ is the average deviation of the profile from a mean line which is also called as average roughness[1] of contacting surface.

The first analytical study based on the deformation of the spherical rough contacts was performed by Greenwood & Tripp (1967), who presented the deformation produced by an arbitrary pressure over the circular half space assuming the deformation to be elastic. The model was based on two non dimensional parameters T and μ. They showed that the contact area was directly proportional while the pressure was inversely proportional to the contact roughness. This

[1] σ: Average roughness, Represented as R_a

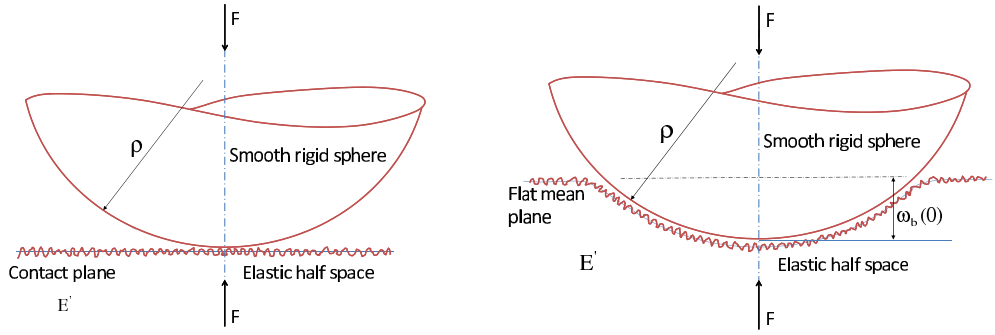

(a) Equivalent contact geometry of two spherical rough surfaces

(b) Deformation of rough spherical contact

Figure 2.39: Contact of rough spheres (Bahrami *et al.*, 2005)

model is complex and requires extensive numerical calculations. Also the parameters β and η cannot be measured directly and should be estimated through statistical calculations. Additionally, these parameters are sensitive to surface measurements Bahrami *et al.* (2005); Greenwood & Wu (2001); Johnson (1987).

Mikic & Roca (1974) proposed an alternate numerical solution considering plastic deformation of asperities but they did not report a generalized relation to calculate the contact parameters. Greenwood *et al.* (1984) generalize the results of both previous models by proposing a single non-dimensional roughness parameter α. They conclude that the contact pressure is governed by α and if the value of α is less than 0.05, the effect of roughness becomes negligible and Hertzian theory can be applied.

Bahrami *et al.* (2005) concluded that the maximum pressure distribution is the key parameter in rough contact calculations and proposed a generalized pressure distribution, which is valid for the whole range of rough contacts. Their proposed generalized model gives analytical results very close to the experimental values of Greenwood *et al.* (1984); Kagami *et al.* (1983); Tsukada & Anno (1979).

2.5.3 Model of Bahrami

The model of Bahrami is based on the following hypothesis

- Deformation mode of asperities is plastic

- Bulk deformation of the contact is elastic and all the bulk deformations occur at elastic half space with effective modulus of elasticity E'
- Pressure at micro-contacts is the micro-hardness of the softer of the two materials
- Surface roughness acts like plastic layer in the sense that the pressure distribution can be considered as continuous, P(r)
- The external pressure P(r) is the summation of pressures at micro-contacts
- Effective micro-hardness is constant throughout the contact area

Proposed non-dimensional pressure distribution equation of rough contacts is found to be the function of non-dimensional radial position (ξ).

$$P(\xi) = P_0(1 - \xi^2)^\gamma \tag{2.30}$$

where, γ can be calculated from equation 2.31,

$$\gamma = 1.5\frac{P_0}{P_{0,H}}\left(\frac{a_L}{a_H}\right)^2 - 1 \tag{2.31}$$

The maximum pressure is related to the applied force by the relation,

$$P_0 = (1 + \gamma)\frac{F}{\pi a_L^2} \tag{2.32}$$

When contact roughness approaches to zero, equations 2.30, 2.31 and 2.32 give Hertzian pressure distribution. Bahrami *et al.* (2005) generalized the model interms of two non-dimensional parameters: first parameter is α as in Greenwood *et al.* (1984) while the second is $\tau = \frac{E'}{H_{mic}}\sqrt{\frac{\rho}{\sigma}}$. The equations for non-dimensional pressure (eq. 2.33) and non-dimensional contact area(eq. 2.34) are calculated by curve fitting.

$$P_0' = \frac{1}{1 + 1.22\ \alpha\ \tau^{-0.16}} \tag{2.33}$$

$$a'_L = \begin{cases} 1.605/\sqrt{P'_0} & 0.01 \leq P'_0 \leq 0.47 \\ 3.51 - 2.51P'_0 & 0.47 \leq P'_0 \leq 1 \end{cases} \tag{2.34}$$

Maximum deviation of equations 2.33 and 2.34 from the real model is claimed to be less than 4.5%. As calculation of a'_L in equation 2.34 involves test for each value of pressure, Bahrami (2004) proposed a single equation(eq. 2.35) to approximate a'_L.

$$a'_L = \frac{a_L}{a_H} = 1.80\frac{\sqrt{\alpha + 0.31\ \tau^{0.056}}}{\tau^{0.028}} \tag{2.35}$$

Elastic deformation of the half space is calculated by substituting the values in the deformation equations from Greenwood & Tripp (1967). Numerical results of Bahrami *et al.* (2005) are valid over full range of contact area but, in this thesis, the contact of a spherical locator with the workpiece on the machine fixturing system will be focused. In this kind of contact, maximum deformation occurs at the center of the contact, i.e. $\xi = r/a_L = 0$.

This deformation as shown in figure 2.39(b) is given by Bahrami *et al.* (2005):

$$\delta_C(0) = \frac{P_0 a_L}{E'}\ B(0.5, \gamma + 1) \tag{2.36}$$

where, B is beta function giving the maximum deformation value numerically.

2.5.4 Contact stiffness

Estimating the influence of contact stiffness on the global stiffness is primordial for precise modeling of the mechanical behavior. The force acting on the contact of a sphere and a surface is non-linear in behavior as shown here (Yeh & Liou, 1999).

$$F = \kappa\ {\delta_C}^{3/2} \tag{2.37}$$

where, $\kappa = \sqrt{\frac{16RE'^2}{9}}$. Differential of the above equation, with respect to displacement, furnishes the stiffness on the contact which is,

$$K = \frac{3}{2}\,\kappa\sqrt{\delta_C} \tag{2.38}$$

The stiffness is the function of applied force and also roughness (σ) of the contact in case of rough contact. δ_C can be found from equation 2.29 for smooth (Hertz) contact and from equation 2.36 if contact is rough. Stiffness calculated from equation 2.29 can be referred to as Hertz stiffness and would be used as benchmark or maximum possible stiffness of the contact.

2.6 Demonstrative sample workpiece

For illustration and verification of the purposed models, a workpiece which requires precise repetitive machining on expensive material and whose dimensions change from one part to another is chosen. This workpiece is a hip prosthesis which is fabricated as a single part, by employing machining process on a precise cost effective fixturing system.

2.6.1 Hip prosthesis

Prosthesis replacement of large human joints is one of the most promising methods in treating joint diseases. In 2004, annual number of such operations performed all over the world were within 8 and 12 lacs (Dietrich & Skalski, 2004). In 2006, the annual number of prosthesis replacements of only hip joints were 300,000 in the USA, 60,000 thousands in Germany and 20,000 in Russia (Rosenberg *et al.*, 2006).

Depending on the body structure and weight of a patient, prosthesis are available in a wide range of standard sizes. In a single word, modern implants guarantee 15 to 20 years of normal operation. The basic hip-joint prosthesis element is loaded in its head therefore, the rubbing hinged pair, i.e. the head and the cup, must have the greatest wear resistance . The average wear of heads made of zirconium dioxide is 0.09 nm per year (Rosenberg *et al.*, 2006).

A wide range of materials are used for manufacturing of the hip-joint prosthesis head, including titanium and cobalt alloys, aluminum and zirconium ceramics. The basic materials used in medicine and their biocompatibility are

Table 2.6: Biocompatibility of some metals (Rosenberg *et al.*, 2006)

Element	Response to the implant in soft tissue	Organic culture growth	
		Response to the implant	Level of toxicity
Mn	-	-	-
V	Toxic	No influence	2×10^{-5}
Mo	*	No influence	-
Co	Toxic	Suppression	2×10^{-4}
Ni	Toxic	Suppression	2×10^{-4}
Fe	*	Suppression	-
Cr	-	-	-
Al	*	-	-
Sn	-	-	-
Zr	Inert**	No influence	-
Ti	Inert**	No influence	-
Ta	Inert**	No influence	-
Ni	Inert**	No influence	-

* Formation of a conjunctive tissue layer around the implant
** Minimum response in the cell

classified in Table 2.6. Extensive research is underway regarding optimal ceramic compositions and the technology of their manufacturing in order to improve the production characteristics of hip-joint prostheses. For the manufacturing of hip prosthesis stem and head, high precision has to be guaranteed. For example for the fabrication of the head, spherical shape should approach to a perfect sphere as much as possible (within the limits of 0.1 to 0.15 μm). The diameter tolerance is $28 \pm 1\mu$m and the roughness must lie within 0.02 and 0.03 μm.

Once machined, the endoprosthesis has to be turned over on the milling machine to perform machining on the other face (fig. 2.41).

2.6.2 Manufacturing of hip prosthesis

For most of the patients, standard hip joint endoprosthesis available in the market are used but, for some special cases custom made endoprosthesis are produced satisfying their individual needs. The fabrication of custom (unique and expensive) endoprosthesis involves the following main steps (Dietrich & Skalski, 2004; Werner *et al.*, 2000). CT (Computerized tomography) scanning is performed to

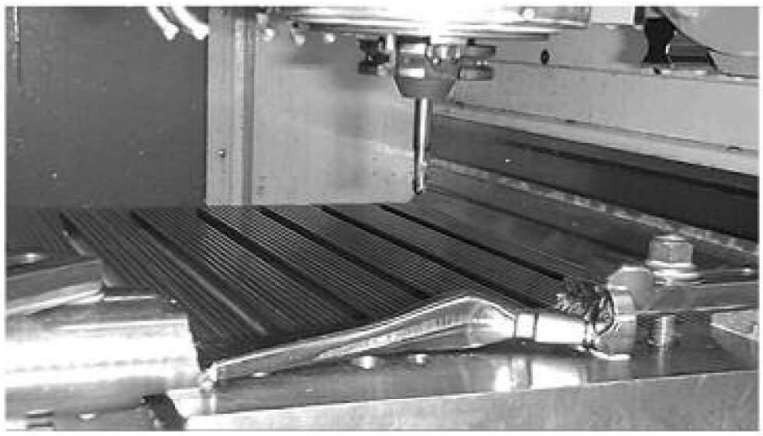

Figure 2.40: Machining of the endoprosthesis using a CNC milling (Dietrich & Skalski, 2004)

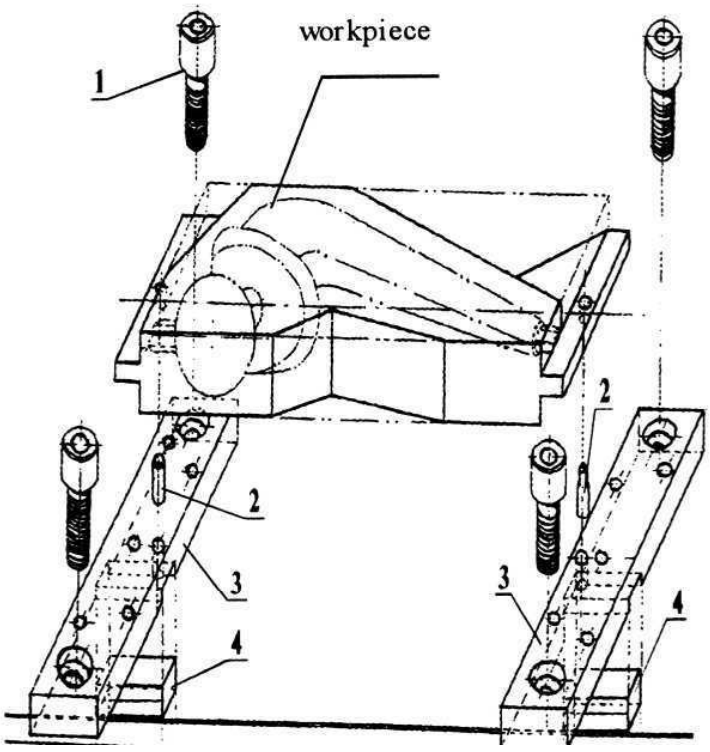

Figure 2.41: Fixturing system used for endoprosthesis machining (1) fixing screws (2) locating pins; (3) bearing strip;(4) block for bearing strip(Werner *et al.*, 2000)

obtain the medical image of the bone, the data is transfer to a CAD system for implant design and engineering analysis (CEA). Once the model is finalized, a

rapid prototype (RP) model is constructed for the part program verification on a standard material. The RP is performed on an inexpensive material but it is an expensive process by itself. The last step is the fabrication of implant with a biomaterial like titanium.

The fabrication of an orthopedic hip implant is also an expensive process. Its manufacturing involves five basic steps (News, 1992):

1. Manufacturing of alloy and raw materials
2. Casting or forging
3. Machining and finishing
4. Coating
5. Packaging

Four main alloys are used in the production oh hip stem their price ranged from $7/lb to $41/lb in 1992. To produce the intermediate forms of the stems, forging or casting processes are applied depending upon the type of material used for fabrication. The average cost of primary hip stem ranged from $30/piece to $150/piece. The machining is one of the most expensive process in the production of hip stem. According to News (1992), about 20 hours of direct labour was involved in the machining and finishing of the one hip stem in 1992. Coating ranged from $30/piece to $150 /piece depending upon the type of material and process. At the end, the packaging costed an average of $1-20/piece. These were the costs of a hip stem production in 1992. The costs are much higher today due to inflation. Due to the nature of custom design process, the reasonable method for manufacturing, which can be employed is the CNC milling the manufacturing setup is shown in figure 2.40.

2.6.3 Demonstrative hip stem

There are a number of prosthesis manufacturers around the world e.g. Johnson & Johnson, Zimmer Holdings, Inc., Implex Corp. etc. (Brewster, 2006). Among all the manufacturers, a data base of the prosthesis has been published on the

website by Zimmer. Therefore, for the validation of the kinematic model the CPT® 12/14 Hip Prosthesis by Zimmer (zimmer, 2011) is illustrated. Sketch of the workpiece is shown in figure 2.42 and its product data is shown in table 2.7.

Table 2.7: CPT® 12/14 product data(zimmer, 2011)

		A	B					C					D	E
Prod. No.	Stem Size	Stem Length	Offset (mm) When Head/Neck Component Selected Is:					Neck Length (mm) When Head/ Neck Component Selected Is:					A/P	M/L
Standard Offset	(mm)	(mm)	-3.5	0	+3.5	+7	+10.5	-3.5	0	+3.5	+7	+10.5	Width	Width
00-8114-000-00	0-STD	105	29	32	35	37	40	24	26	28	30	32	7.5	9.0
00-8114-001-00	1-STD	130	31	34	37	39	42	24	26	28	30	32	9.0	10.5
00-8114-002-00	2-STD	130	33	36	38	41	44	24	26	28	30	32	9.0	13.0
00-8114-003-00	3-STD	130	35	37	40	43	46	24	26	28	30	32	9.0	15.5
00-8114-004-00	4-STD	130	35	38	41	44	46	24	26	28	30	32	10.0	17.5
00-8114-005-00	5-STD	130	37	40	43	45	48	24	26	28	30	32	10.0	20.0

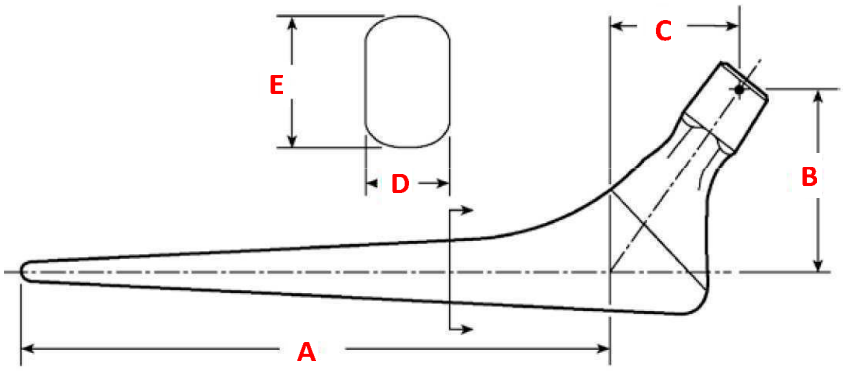

Figure 2.42: Zimmer CPT® 12/14 Hip Prosthesis (zimmer, 2011)

2.7 Synthesis

In this chapter, the theoretical background of fixture design was presented. Starting with the basic concept of associating real surfaces with theoretical surfaces using metrological scanning machine for manufacturing, the design of fixtures and its effects on the product quality are detailed. The positioning error of the

workpiece can be transformed into the deformation of the locators using Plucker matrix.

A brief literature review of the existing research on the positioning error of the workpiece during locating and machining is detailed which include the error due to locators placement, fixture positioning error and machine tool or kinematic errors. This thesis is focused on the prepositioning of the rough part and calculation and compensation of the positioning error of the workpiece under machining and clamping forces. External forces cause the elastic deformation of locator bodies and locator-workpiece contact. These deformations can be obtained by calculating the stiffness of each elastic element of the fixturing system. Contact deformation cannot be obtained directly due to its non linear behavior according to Hertz contact theory. At the end a hip prosthesis by Zimmer (zimmer, 2011) is chosen as a workpiece for the demonstration of the developed methodology. The hip prosthesis requires precise machining operation.

Further chapter 3 presents an analytical kinematic model of a 3-2-1r fixturing system for precise positioning of a misplaced workpiece (due to geometrical error) in machine coordinate system with the hypothesis of all the elements being rigid and having no friction at contacts. A mechanical model of the fixturing system is presented in chapter 4 by considering the workpiece-baseplate assembly as rigid and the whole assembly is placed on a support by intermediate locators which are considered to be elastic elements. The baseplate is taken as locally elastic at the contacts. The mechanical model calculates the displacement of the workpiece in machine coordinates system which is transformed into the deformation of each locator using energy equations. The error compensation can be performed on the workpiece through the kinematic model.

For illustration and verification, the kinematic repositioning model will be demonstrated on the complex workpiece whose dimensions change from one part to the other and which requires a precise machining on an expensive material. For this purpose, a hip prosthesis is chosen as a demonstrative workpiece.

Chapter 3

Workpiece Repositioning through rigid fixture kinematics

During manufacturing (machining or assembling), two parts in the same part family can have small dimensional variations. These small dimensional variations can cause the part not to be machined or assembled correctly. Fabrication process, carried out on expensive or hardly machinable materials must include a precise prepositioning operation to reduce the material removing and this operation is called optimal balancing. Optimal position is the position of the workpiece in machine's coordinate system to center final part geometry into first volume. At optimal position, allowances variations concerning further processing surfaces are minimal according to chosen calculation criteria. The definition of optimal position of workpiece, in the machine coordinate system, allows the manufacturers to reach part quality requirements. During assembling, optimal balancing helps to avoid the wear due to non-uniform surface contact which could be the result of positioning error of the part to be assembled.

Even if this optimal balancing is important for material and tool wear sparring reduction, the processing system must include a mechanism to attain the calculated optimum position of the workpiece with reference to previously measured one. This mechanism should be able to perform the necessary kinematic transformation to put the workpiece at the chosen optimal position. Number of machine axis becomes more and more important for more complex workpieces.

Therefore, the position modification of the workpiece or cutting tool is usually performed by using high DOF machines.

If the workpiece displacements are small, we have only 3-axis machines or we are in the case where the workpiece has to go through different operations on different machines (production line), it is economically feasible to place a workpiece repositioning system which can be added to any machine or can easily be moved between them. Therefore, a model for 6-DOF repositioning of fixturing system called "kinematic model" is proposed in this chapter. The model is developed considering a given reconfigurable configuration of the 6 locators (spatial positioning) and in addition the initial position of the workpiece is assumed to be measured by CMM as demonstrated in Appendix A.

While measuring the initial position of a fixed workpiece through CMM, the lateral motion of the sensor causes a small measuring error called Abbé error. To avoid Abbé error, the axis of the sensor should always be in line with the measuring system i.e. the sensor has zero Abbé error if it moves only in its axial direction in-line with the measuring system. By having large displacement movable locators, the workpiece can be displaced so that the measuring point comes in the axis of the sensor. The workpiece displacement on the locators can easily be calculated, and also it eliminates the Abbé uncertainty of the CMM measurement. The development of the CMM architecture for very precise measurement was performed by Lahousse *et al.* (2005).

The kinematic model developed in this chapter, is capable of calculating the error present in the workpiece and compensating this repositioning error by the locators' axial advancements. For this kinematic model, all the components of the fixturing system are assumed rigid with no deformation under load. This chapter is divided as follows: Initially, the principle of the fixturing system is explained followed by the proposed fixturing system. The formalization includes HTM from machine to different parts of the fixturing system giving the advancement of each of six locators to reposition the workpiece to the required position. The formalization is followed by a case study performed on a hip prosthesis workpiece. The chapter concludes with the discussion on the scope and use of this kinematic model on the further development of the fixturing system.

3.1 Principle of proposed fixturing system

The principle of proposed fixturing system is explained by a simple two-dimensional example. A workpiece in figure 3.1 is located by locators and clamped (clamps are not shown). The locators are assumed to be movable only in their axial directions. The rectangle shows the part's material removal by cutting tool. After machining operation, the first workpiece moves forward and the next workpiece with dimensional error is located and clamped on the fixture as shown in figure 3.2.

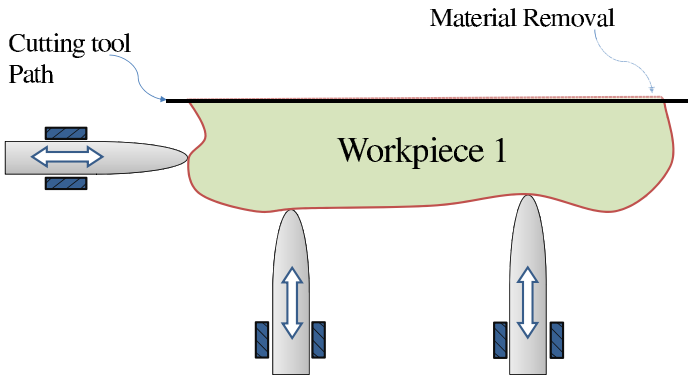

Figure 3.1: Workpiece held for machining

The workpiece in figure 3.2 is same as in figure 3.1 but only the surface in contact with the locators is assumed to be having extra material. The locators are kept on the same place as in figure 3.1 and the second workpiece is clamped. Due to surface irregularity at the contacting points, the machining surface is disorientated which causes the removal of extra material of the workpiece. Similarly, if the workpiece is a bit smaller in dimension, less material would be removed but in both the cases, the workpiece would not be in accordance with the production requirements.

This error can be eliminated by moving locators axially, for that reason an analytical model is necessary to measure the orientation of the workpiece, calculate the positioning error and then calculate the axial movement of the locators in order to achieve the final required position of the workpiece. Assuming that unknown initial position could imply large displacements (LD) of workpiece during

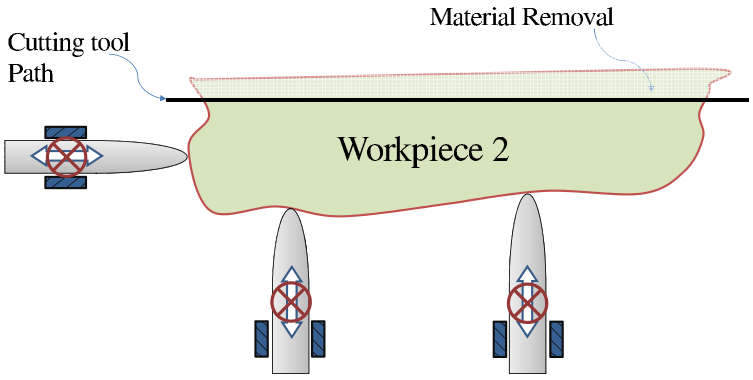

Figure 3.2: Workpiece held for machine but having dimensional error

correction phase, precise control of workpiece position becomes impossible because the real contact point would highly depend upon local geometrical defects (fig. 3.3). In contrast, the normal of the flat contacting surface in figure 3.4 always remains parallel to the contacts' normals. So, it is more realistic to relocate a flat surface in contact with the positioning locators than irregular surfaces.

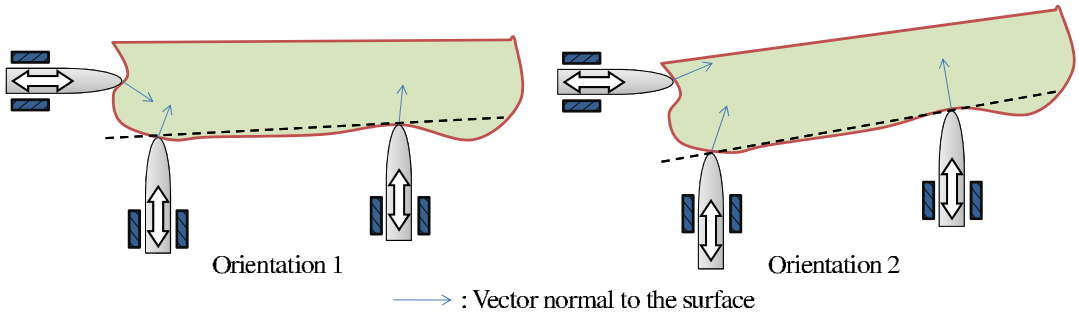

Figure 3.3: Changes in contact normals due to surface waviness

Considering the geometrical defects to vary from one part to another, it becomes necessary to introduce a high quality interfacing part whose geometry allows kinematic laws to be defined once and assumed to be true under all conditions. For this purpose, a rectangular (cuboid in three dimensional case) baseplate is used in between the locators and the workpiece. The baseplate is fabricated in such a way that its surfaces can be assumed perfectly plane and orthogonal. The workpiece of figure 3.1 is supposed to be fixed on the baseplate rigidly and the baseplate is located on the locators (fig. 3.5).

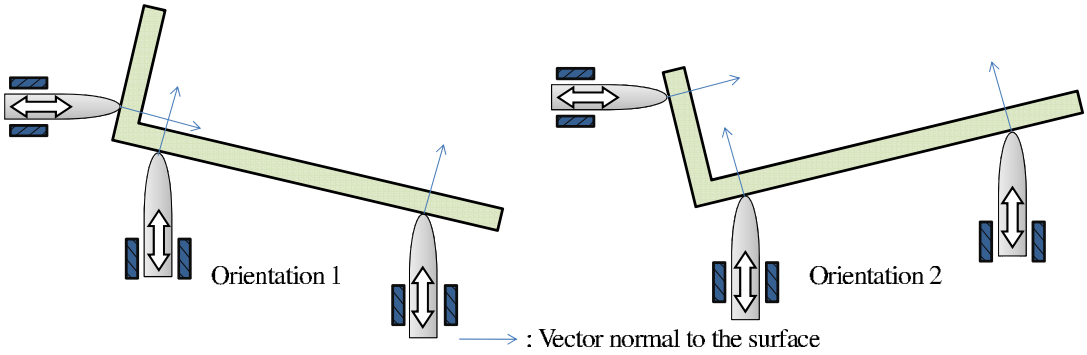

Figure 3.4: Normals are parallel for plane surface

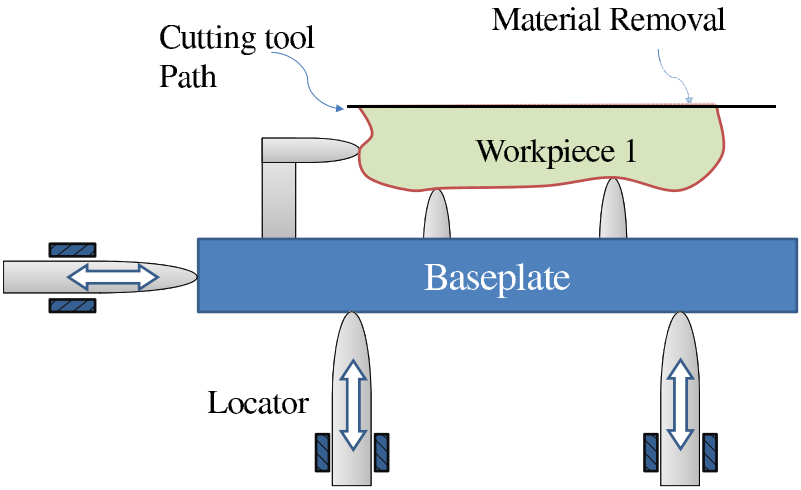

Figure 3.5: Workpiece placed on the baseplate

Considering that the next workpiece have dimensional errors, the same workpiece as in figure 3.2 is placed on the baseplate as shown in figure 3.6(a), where the locators are fixed at the same location as for the last workpiece. This workpiece is then relocated by moving the baseplate by the axial motion of locators (fig. 3.6(b)).

It can be seen from the figures 3.3 and 3.4 that the plane surfaces are practical for precise repositioning because of its uniform behavior on each of the locator's contact. The exact solution of the figure 3.2 is almost impossible because the motion of any locator causes all the normals to change their orientation with

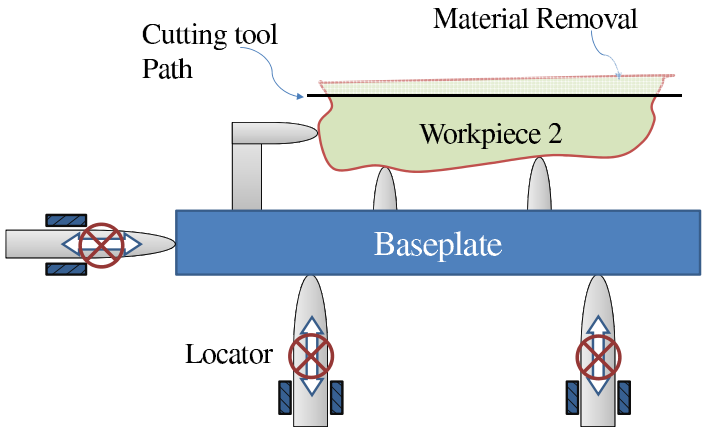

(a) Workpiece with error

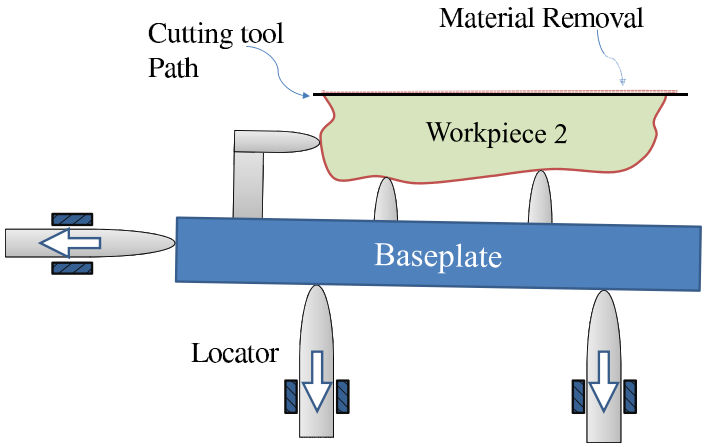

(b) Error compensation by locators' advancements

Figure 3.6: Relocation of workpiece-baseplate assembly

respect to each other, from one part to another, and the contact of locators form random normals which are not normal to the plane joining the contacting points. On the contrary, for the plane surface, if one normal is known (calculated in later sections), all the other normals can be calculated and the results are obtainable.

3.2 Proposed fixturing system

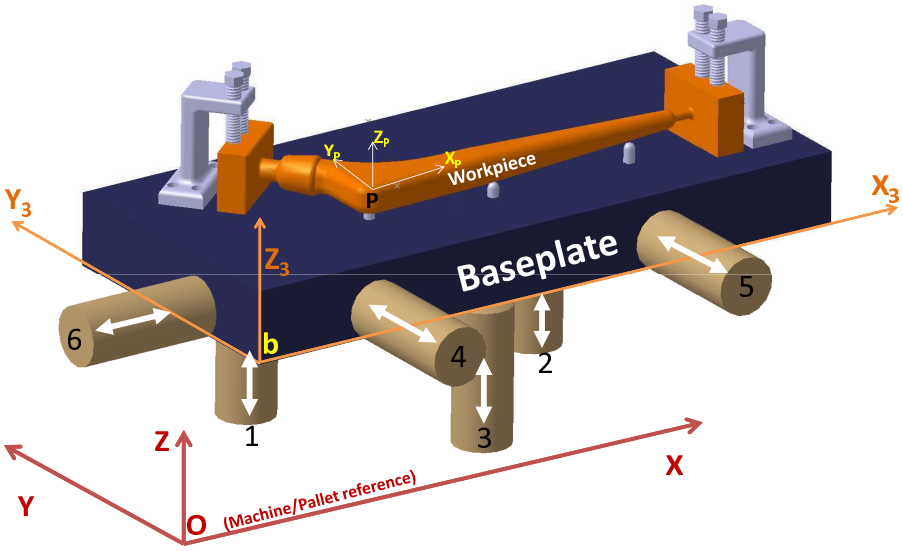

Figure 3.7: Fixturing system principle

The proposed fixturing system consists of a set of six locators whose positions and orientations are defined through locating holes of the machine table/pallet, a cuboid baseplate, and a workpiece (hip prosthesis) fixed on the baseplate as shown in fig 3.7. The locators are assumed to be in a 3-2-1r configuration and possess only one axial DOF. The lateral position of each locator is chosen by considering the constraints of accessibility, stability of the workpiece and manufacturing knowledge. It is also assumed that the workpiece is mounted rigidly on the baseplate and no additional deformation occurs between workpiece and baseplate except those caused during clamping the workpiece.

Assuming that unknown initial position could imply large displacements (LD) of workpiece during correction phase, the kinematic model is built using homogeneous transformation matrices (HTM) and LD formulation. Using the geometrical properties of the baseplate, exact position of the baseplate can be calculated from the six positioning locators. The exact position of the workpiece is obtained as per the hypothesis of the rigid workpiece-baseplate contact. This allows the kinematic model to be more efficient and repeatable. In addition, it would be easier to maneuver the workpiece-baseplate assembly through the locators. The pro-

posed fixturing system configuration is shown in figure 3.7, where the workpiece is located and clamped on the baseplate and both form a single rigid assembly.

3.3 Formalization

For repositioning the workpiece through the proposed fixturing system, initial position of the fixed workpiece can be measured through CMM as demonstrated in Appendix A and the whole workpiece-baseplate assembly can then be placed on the fabrication machine. It is assumed that the positioning error of the baseplate is negligible as compared to the positioning error of the workpiece. The initial position of the workpiece is then compared with the required position of the workpiece. Repositioning is necessary if the difference of initial and final position is beyond limits. There is a need of proper mathematical formulation to position the workpiece from initial to final position with the help of six locators which are able to move only in axial direction. To obtain this correction of the workpiece position, the formulation is explained in this section.

In this section, workpiece and baseplate positions are defined with reference to machine coordinates. The difference of the initial and final positions of the workpiece-baseplate assembly will be the correction required to attain through the advancements of locators. The relative correction required for the baseplate is converted to absolute position of each locator. At the end, the uncertainty of the position of the workpiece in terms of position uncertainty of each locator is demonstrated for the proposed fixturing system.

3.3.1 Baseplate coordinate definition

For the transformation from machine (O) to baseplate (b) coordinate system, vector method is used as the position of the spherical centers of locators tips (1 to 6) are known parameters. In this method, three surface normals of the baseplate are defined (fig. 3.8(b)) followed by the coordinate definition. Points 1 to 6 are the centers of spherical tips of the locators. Being parallel surfaces, the normal to the surface passing through the centers of contacting spheres would

be same as the normal to the surface of the baseplate as shown for the primary surface in figure 3.8(a).

3.3.1.1 Vectors normal to baseplate surfaces

For a cuboid with 3-2-1r configuration, the normals of all three planes can be found from the points' locations (Asante, 2009; Bourdet, 1999). Starting from the plane with three locators on the primary plane, the vectors from point 1 to 2 ($\vec{V}_{12}$) and point 1 to 3 ($\vec{V}_{13}$) give a normal vector ($\vec{N}_1$) to the primary plane.

$$\vec{V}_{12} = (u_2 - u_1)\vec{x} + (v_2 - v_1)\vec{y} + (w_2 - w_1)\vec{z} \tag{3.1}$$

$$\vec{V}_{13} = (u_3 - u_1)\vec{x} + (v_3 - v_1)\vec{y} + (w_3 - w_1)\vec{z} \tag{3.2}$$

$$\vec{N}_1 = \vec{V}_{13} \times \vec{V}_{12} \tag{3.3}$$

$$\vec{N}_1 = \begin{Bmatrix} u_3 - u_1 \\ v_3 - v_1 \\ w_3 - w_1 \end{Bmatrix} \times \begin{Bmatrix} u_2 - u_1 \\ v_2 - v_1 \\ w_2 - w_1 \end{Bmatrix} = \begin{Bmatrix} A_1 \\ B_1 \\ C_1 \end{Bmatrix} \tag{3.4}$$

$$\vec{N}_1 = \begin{Bmatrix} (v_3 - v_1)(w_2 - w_1) - (w_3 - w_1)(v_2 - v_1) \\ (w_3 - w_1)(u_2 - u_1) - (u_3 - u_1)(w_2 - w_1) \\ (u_3 - u_1)(v_2 - v_1) - (v_2 - v_1)(u_2 - u_1) \end{Bmatrix} = \begin{Bmatrix} A_1 \\ B_1 \\ C_1 \end{Bmatrix} \tag{3.5}$$

Similarly, points 4 and 5 give a vector $\vec{V}_{45}$ which is normal to the vector $\vec{N}_1$. The cross product of these two vectors would give a vector $\vec{N}_2$ normal to the secondary plane passing through points 4 and 5.

$$\vec{V}_{45} = (u_5 - u_4)\vec{x} + (v_5 - v_4)\vec{y} + (w_5 - w_4)\vec{z} \tag{3.6}$$

$$\vec{N}_2 = \begin{Bmatrix} u_5 - u_4 \\ v_5 - v_4 \\ w_5 - w_4 \end{Bmatrix} \times \begin{Bmatrix} A_1 \\ B_1 \\ C_1 \end{Bmatrix} = \begin{Bmatrix} A_2 \\ B_2 \\ C_2 \end{Bmatrix} \tag{3.7}$$

$$\vec{N}_2 = \begin{Bmatrix} (w_5 - w_4)B_1 - (v_5 - v_4)C_1 \\ (u_5 - u_4)C_1 - (w_5 - w_4)A_1 \\ (v_5 - v_4)A_1 - (u_5 - u_4)B_1 \end{Bmatrix} = \begin{Bmatrix} A_2 \\ B_2 \\ C_2 \end{Bmatrix} \tag{3.8}$$

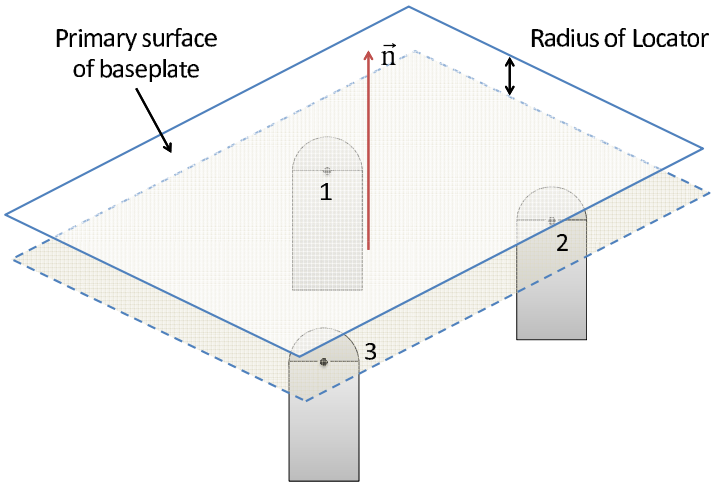

(a) Definition of baseplate surface from locators' points

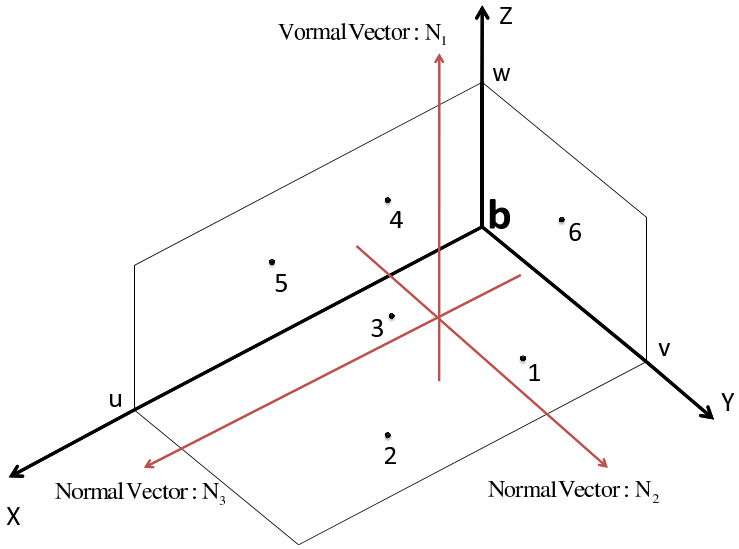

(b) Three normals to the baseplate surfaces in contact with the locators

Figure 3.8: Defining surface normals from the position of the six locators

In the same way, third surface is perpendicular to $\vec{N_1}$ and $\vec{N_2}$, and the position of point 6 does not have any effect on the surface normal which is,

$$\vec{N}_3 = \vec{N}_2 \times \vec{N}_1 \tag{3.9}$$

$$\vec{N}_3 = \left\{ \begin{array}{c} A_2 \\ B_2 \\ C_2 \end{array} \right\} \times \left\{ \begin{array}{c} A_1 \\ B_1 \\ C_1 \end{array} \right\} \tag{3.10}$$

$$\vec{N}_3 = \left\{ \begin{array}{c} B_2C_1 - B_1C_2 \\ A_1C_2 - C_1A_2 \\ B_1A_2 - A_1B_2 \end{array} \right\} = \left\{ \begin{array}{c} A_3 \\ B_3 \\ C_3 \end{array} \right\} \tag{3.11}$$

3.3.1.2 Unit Vectors

Unit vectors are required in order to obtain the elements of HTM from machine coordinate to baseplate coordinate. Unit vectors are calculated for each normal vector. According to the definition of unit vector;

$$\vec{n}_i = \frac{\vec{N}_i}{|N_i|} \tag{3.12}$$

where, $|N_i| = \sqrt{A_i^2 + B_i^2 + C_i^2}$, the transformation matrix then changes from machine coordinate to baseplate coordinate P_{Ob} which can be given as (Cazin, 1973):

$$[P_{Ob}] = \begin{bmatrix} a_3 & a_2 & a_1 & x_b \\ b_3 & b_2 & b_1 & y_b \\ c_3 & c_2 & c_1 & z_b \\ 0 & 0 & 0 & 1 \end{bmatrix} \tag{3.13}$$

where, $a_1, ...c_3$ are the unit vector components of $A_1, ...C_3$ ($a_1 = \frac{A_1}{\sqrt{A_1^2+B_1^2+C_1^2}}$) and x_b, y_b and z_b are the x, y and z co-ordinates of origin of reference b. Here a_i, b_i, c_i are the x, y, z components of normal unit vector $\vec{n_i}$, where,

$$\vec{n_1}.\vec{n_2} = 0$$

$$\vec{n_2}.\vec{n_3} = 0$$

$$\vec{n_3} = \vec{n_2} \times \vec{n_1}$$

3.3.2 Workpiece coordinate definition

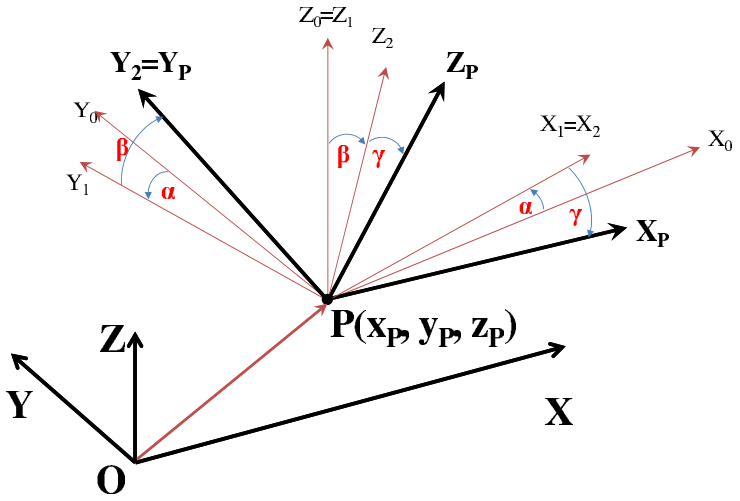

Figure 3.9: Rotation and translation of the workpiece (P) with respect to machine axis

In order to define the workpiece coordinate system with respect to machine coordinate system, the HTM of YPR [1] transformation of a workpiece at a point "P" in machine coordinate "O" $[P_{OP}]$ can be represented by;

$$[P_{OP}] = \begin{bmatrix} \cos\alpha & -\sin\alpha & 0 & x_P \\ \sin\alpha & \cos\alpha & 0 & y_P \\ 0 & 0 & 1 & z_P \\ 0 & 0 & 0 & 1 \end{bmatrix} \begin{bmatrix} 1 & 0 & 0 & 0 \\ 0 & \cos\beta & -\sin\beta & 0 \\ 0 & \sin\beta & \cos\beta & 0 \\ 0 & 0 & 0 & 1 \end{bmatrix} \begin{bmatrix} \cos\gamma & 0 & \sin\gamma & 0 \\ 0 & 1 & 0 & 0 \\ -\sin\gamma & 0 & \cos\gamma & 0 \\ 0 & 0 & 0 & 1 \end{bmatrix} \tag{3.14}$$

$$[P_{OP}] = \begin{bmatrix} \cos\alpha\cos\gamma - \sin\alpha\sin\beta\sin\gamma & -\sin\alpha\cos\beta & \cos\alpha\sin\gamma + \sin\alpha\sin\beta\cos\gamma & x_P \\ \sin\alpha\cos\gamma + \cos\alpha\sin\beta\sin\gamma & \cos\alpha\cos\beta & \sin\alpha\sin\gamma - \cos\alpha\sin\beta\cos\gamma & y_P \\ -\cos\beta\sin\gamma & \sin\beta & \cos\beta\cos\gamma & z_P \\ 0 & 0 & 0 & 1 \end{bmatrix} \tag{3.15}$$

where, α, β and γ are the rotations along z, x and y axes respectively. The classical result of equation 3.15 can also be found in Cazin (1973).

[1] YPR: Yaw (α), Pitch (β), Roll (γ)

3.3.3 Positioning error and correction calculation

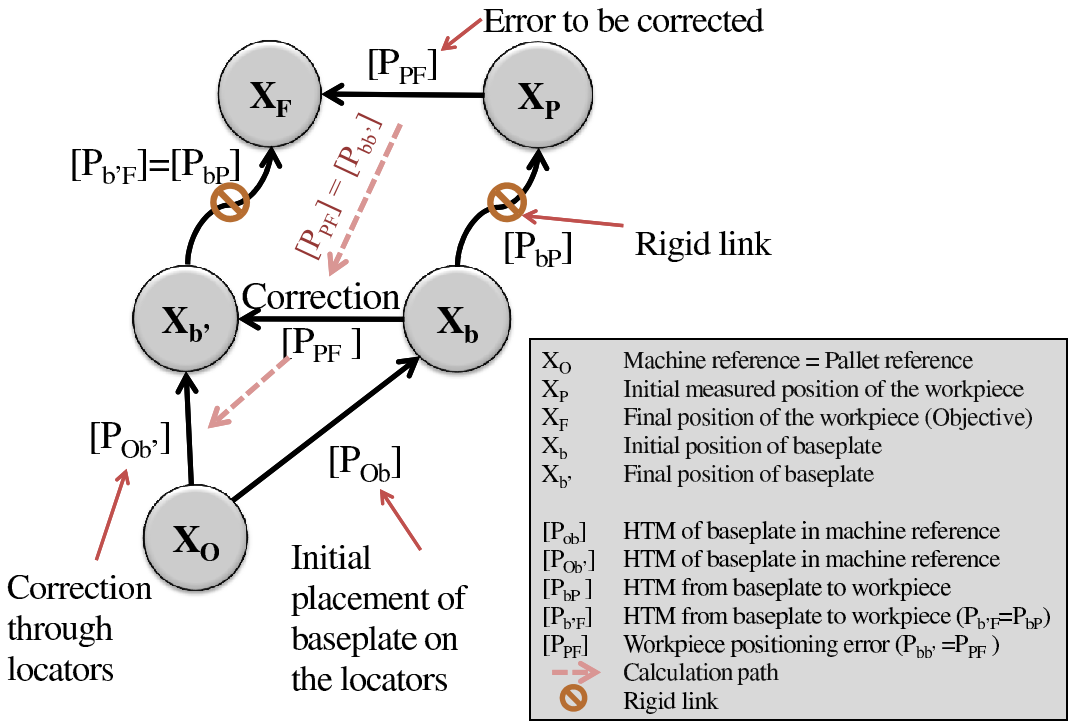

Figure 3.10: Transformation of reference axes for kinematic model transformation

Positioning transformation scheme of proposed fixturing system is shown in figure 3.10. Here X_i represents the position vector of reference i while $[P_{ij}]$ represents the transformation matrix from position i to j. Previously, the HTM of the baseplate with respect to machine reference ($[P_{Ob}]$) had been calculated. The transformation of the workpiece with respect to the machine ($[P_{OP}]$) can be measured through CMM as demonstrated in Appendix A which allows us to calculate the transformation of workpiece with respect to baseplate ($[P_{bP}]$).

$$[P_{bP}] = [P_{Ob}]^{-1}[P_{OP}] \tag{3.16}$$

The final position of the workpiece with respect to machine coordinate (X_F) is the required position of the workpiece and is known through part program. The reorientation of the baseplate ($[P_{bb'}]$) enables us to reorient the workpiece

($[P_{PF}]$) as the contact between the baseplate and workpiece ($[P_{bP}]$) is supposed to be unchanged by the load modifications ($[P_{bP}] \equiv [P_{b'F}]$) that could be implied by baseplate motion e.g. gravity. As the initial and final positions (X_P and X_F) of the workpiece are known, we get the HTM equations as,

$$\begin{aligned} [P_{OF}] &= [P_{Ob'}][P_{b'F}] \\ [P_{OF}] &= [P_{Ob'}][P_{bP}] \\ [P_{Ob'}] &= [P_{OF}][P_{bP}^{-1}] \end{aligned} \tag{3.17}$$

From equations 3.16 and 3.17, we can get the final HTM of the baseplate in machine coordinate system which can be written in terms of locators' positions in HTM form as given below.

$$[P_{Ob'}] = \begin{bmatrix} a'_3 & a'_2 & a'_1 & x'_b \\ b'_3 & b'_2 & b'_1 & y'_b \\ c'_3 & c'_2 & c'_1 & z'_b \\ 0 & 0 & 0 & 1 \end{bmatrix} = [P_{OF}]([P_{Ob}]^{-1}[P_{OP}])^{-1} \tag{3.18}$$

where, $[P_{Ob'}]$ is the absolute HTM of the baseplate with respect to machine coordinate system required to attain in order to reorient the workpiece at the position required by the part program. The resolution of the above equations does not give unique positions of locators because the contacting points of locators on the baseplate change as a result of baseplate motion on locators. To overcome this problem, a procedure is carried out to find a unique value of each locator's advancement.

3.3.4 Calculating the advancement of locators

It is assumed that there is no friction between locators and baseplate and at any instant the baseplate is in contact with all six locators. If the workpiece requires repositioning to attain final required position, the baseplate has to be relocated through six locators. If the calculated new position of the locators is not in line with the locator axis, the position is not attainable due to the constraint that the locators can only move in their axial directions.

To overcome this mathematical issue, the new position and advancement of each locator is calculated by the plane having an offset of the radius of locator's tip from the plane of the baseplate and finding the point on that plane which is on the axis of each locator. This can be explained by a two dimensional example of figure 3.11, where a surface is shown which is initially located by two locators on primary plane. The center points of contacting circles are 1 (x_1, z_1) and 2 (x_2, z_2). If the surface has to be relocated to attain the required position, the motion of the surface on the locators causes the reference contacting points to move with the surface. We suppose that the new positions of the centers of the locators' spherical tips are 1^* (x_1^*, z_1^*) and 2^* (x_2^*, z_2^*). As per our assumption, the locators can only move axially therefore the contacting points have to be aligned with the locators' axes.

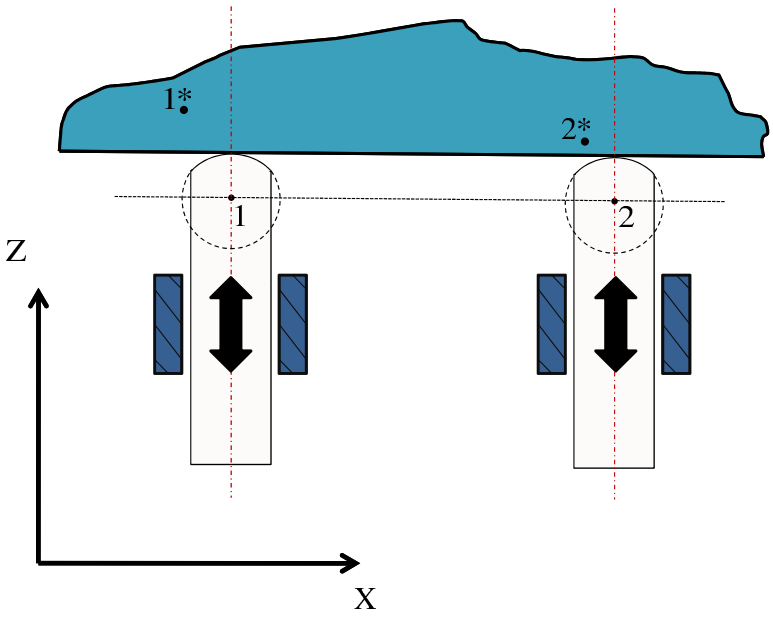

Figure 3.11: Repositioning of the workpiece from 1,2 to 1*,2*

For the resolution of this issue, a line is passed through the center of two contacting circles of locators. This gives an initial reference line. After the calculation, a final reference line is passed through final contacting points 1^* and 2^* (fig. 3.12). The locators' center points should lie on the line joining points 1^*

and 2^* and should have a fixed x position. So final positions of the locators should be the points $1'$ and $2'$ as shown in figure 3.12. Mathematically, it becomes,

$$\begin{aligned} ax_1^* + cz_1^* &= D \\ ax_1' + cz_1' &= D \\ z_1' &= \frac{D - ax_1}{c} \end{aligned} \tag{3.19}$$

where z_1' is the new position of the circle's center in axial direction of locator 1. Here x position is fixed i.e. $x_1^* = x_1$ also D is the same line passing through points 1^* and $1'$. The advancement of locator 2 can be calculated in the same way as equation 3.19.

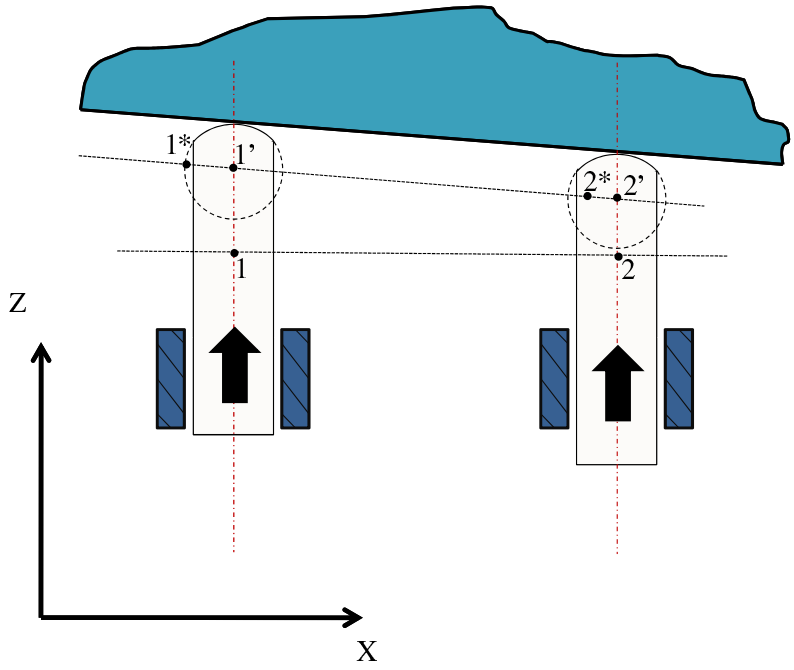

Figure 3.12: Workpiece after relocation from 1,2 to 1',2'

In our case (fig. 3.7 & fig. 3.8) , three locators on one side give a plane (line in the figure 3.11 and 3.12) which has to be reoriented to obtain the final required position of the baseplate-workpiece assembly. For the relocation, the plane passing through the point $1'$ (x_1', y_1', z_1') can be expressed as:

$$a'_1 x'_1 + b'_1 y'_1 + c'_1 z'_1 = D_1 \tag{3.20}$$

Then, the z-coordinate of the same plane can be calculated with the fixed positions of x_1 and y_1 and the perpendicular distance equal to D_1.

$$z_1{}' = \frac{D_1 - a'_1 x_1 - b'_1 y_1}{c'_1} \tag{3.21}$$

This point z'_1 would be the new position of z_1. As the same plane is passing through points $2'$ and $3'$, the new advancements z'_2 and z'_3 can be calculated by;

$$z_2{}' = \frac{D_1 - a'_1 x_2 - b'_1 y_2}{c'_1} \tag{3.22}$$

$$z_3{}' = \frac{D_1 - a'_1 x_3 - b'_1 y_3}{c'_1} \tag{3.23}$$

Similarly the same procedure can be followed for the other two planes. Here locators 4 and 5 are in contact with the secondary plane. The equation of the new plane passing through points $4'$ and $5'$ can be expressed as;

$$a'_2 x'_4 + b'_2 y'_4 + c'_2 z'_4 = D_2 \tag{3.24}$$

From the equation of the plane, the final advancements y'_4 and y'_5 can be calculated as:

$$y_4{}' = \frac{D_2 - a'_2 x_4 - c'_2 z_4}{b'_2} \tag{3.25}$$

$$y_5{}' = \frac{D_2 - a'_2 x_5 - c'_2 z_5}{b'_2} \tag{3.26}$$

At the end, the equation of the advancement of last locator in contact at the tertiary plane is calculated as,

$$a'_3 x'_6 + b'_3 y'_6 + c'_3 z'_6 = D_3 \tag{3.27}$$

$$x_6{}' = \frac{D_3 - b'_3 y_6 - c'_3 z_6}{b'_3} \tag{3.28}$$

The equations 3.21, 3.22, 3.23, 3.25, 3.26 and 3.28 give unique positions of all the six locators. These positions are the functions of unit vector coordinates of three baseplate normals calculated at final position of the baseplate. These coordinates of normal vectors are shown in the final transformation matrix $[P_{Ob'}]$ in equation 3.18. This procedure will be illustrated in the case study for validation.

3.3.5 Uncertainty of the workpiece position

In order to calculate the effect of the small locating errors (about 10 μm) on the global precision of the workpiece, assuming considering small displacement hypothesis to be valid, plucker matrix for the fixturing system is required as detailed in section 2.2.6. In this section, we are concentrating on the calculation of Plucker coordinates for the proposed fixturing system. Plucker coordinates are calculated separately for each locator and then they are placed in a matrix called Plucker matrix.

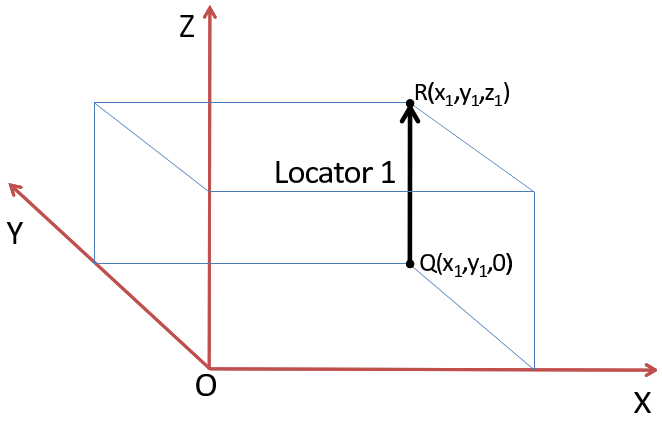

Figure 3.13: Plucker coordinates calculation for locator 1 of proposed fixture

Locator 1 of the proposed fixturing system of figure 3.8 is taken parallel to z-axis in figure 3.13 for the calculation of Plucker coordinates. Two points,

$Q(x_1, y_1, 0)$ and $R(x_1, y_1, z_1)$, are taken on the line of action with reference to machine origin O. It as assumed to the center axis of the locator 1. In order to calculate the plucker coordinates for locator 1, the line equation is drawn in the direction of R from Q, and hence we get,

$$\vec{L_1} = (x_1\hat{i} + y_1\hat{j} + z_1\hat{k}) - (x_1)\hat{i} + y_1)\hat{j} + 0\hat{k}) = z_1\hat{k} \tag{3.29}$$

and its unit vector becomes

$$n_1 = \begin{Bmatrix} 0 \\ 0 \\ 1 \end{Bmatrix}. \tag{3.30}$$

The projection of the displacement on the normal direction can be calculated using equation 2.8 as;

$$\xi_1 = \begin{Bmatrix} \delta x_P \\ \delta y_P \\ \delta z_P \end{Bmatrix} . \begin{Bmatrix} 0 \\ 0 \\ 1 \end{Bmatrix} + \left[\begin{Bmatrix} x_1 \\ y_1 \\ z_1 \end{Bmatrix} \times \begin{Bmatrix} 0 \\ 0 \\ 1 \end{Bmatrix} \right] . \begin{Bmatrix} \delta\beta \\ \delta\gamma \\ \delta\alpha \end{Bmatrix} \tag{3.31}$$

where, $\{\delta x_P, \delta y_P, \delta z_P\}^T$ and $\{\delta\beta_P, \delta\gamma_P, \delta\alpha_P\}^T$ are the translational and rotational vectors of the workpiece. The above equation can be written as;

$$\xi_1 = \delta z_P + y_1\delta\beta - x_1\delta\gamma \tag{3.32}$$

Same calculations are carried out for all the six locators and a final result is obtained using figure 2.11 and equation 2.9 as shown in equation 3.33 and the Plucker matrix for the proposed configuration is shown in equation 3.34.

$$\begin{Bmatrix} \xi_1 \\ \xi_2 \\ \xi_3 \\ \xi_4 \\ \xi_5 \\ \xi_6 \end{Bmatrix} = \begin{bmatrix} 0 & 0 & 1 & y_1 & -x_1 & 0 \\ 0 & 0 & 1 & y_2 & -x_2 & 0 \\ 0 & 0 & 1 & y_3 & -x_3 & 0 \\ 0 & 1 & 0 & -z_4 & 0 & x_4 \\ 0 & 1 & 0 & -z_5 & 0 & x_5 \\ 1 & 0 & 0 & 0 & z_6 & -y_6 \end{bmatrix} \begin{Bmatrix} \delta x_P \\ \delta y_P \\ \delta z_P \\ \delta\beta \\ \delta\gamma \\ \delta\alpha \end{Bmatrix} \tag{3.33}$$

$$[Plu] = \begin{bmatrix} 0 & 0 & 1 & y_1 & -x_1 & 0 \\ 0 & 0 & 1 & y_2 & -x_2 & 0 \\ 0 & 0 & 1 & y_3 & -x_3 & 0 \\ 0 & 1 & 0 & -z_4 & 0 & x_4 \\ 0 & 1 & 0 & -z_5 & 0 & x_5 \\ 1 & 0 & 0 & 0 & z_6 & -y_6 \end{bmatrix} \tag{3.34}$$

According to the definition of Plucker matrix, the precision of workpiece positioning defined as the function of locator precision, can be found using equation 2.11. We can write:

$$\{\delta\} = [Plu]^{-1}\{\xi_i\} \tag{3.35}$$

where, $\{\xi\} = \{\xi_1, \xi_2, \xi_3, \xi_4, \xi_5, \xi_6\}^T$ is vector with uncertainties for all the six locators and $\{\delta\} = \{\delta x_P, \delta y_P, \delta z_P, \delta\beta, \delta\gamma, \delta\alpha\}^T$ is the small displacement vector of the workpiece as the result of locators' uncertainties. The quality and positioning precision of locators can be chosen as the function of required precision of the workpiece.

3.4 Case Study

A case study is performed on a hip prosthesis repositioning through CATIA® simulation to validate the kinematic model. As explained in section 2.6, a CPT® 12/14 Hip Prosthesis by Zimmer (zimmer, 2011) is chosen as a demonstrative workpiece. In this section, the creation of hip prosthesis in CATIA ® is demonstrated followed by repositioning and machining of both sides through simulation.

3.4.1 Creating CATIA model

The workpiece (fig. 3.14(a)) is created in CATIA® using the specifications given in table 2.7. After the CATIA® model is created, original dimensions of the hip prosthesis are slightly increased and supports are added to obtain a rough workpiece before machining as shown in figure 3.14(b). It is supposed that this workpiece is clamped rigidly on the baseplate which is further located through

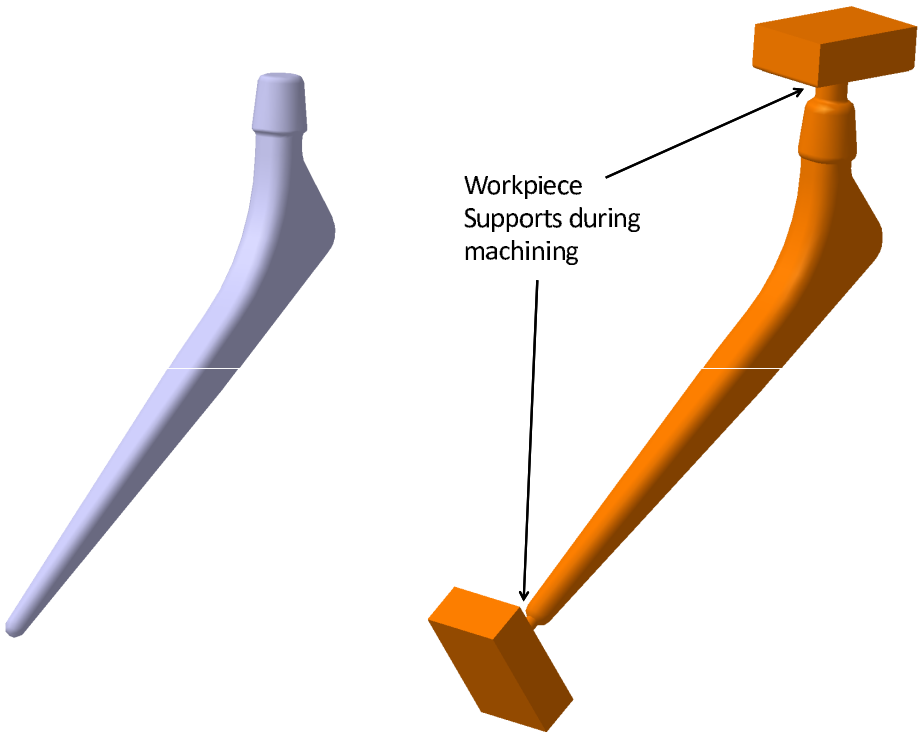

(a) Original hip prosthesis model (b) Hip prosthesis before machining

Figure 3.14: CATIA Model of CPT® 12/14 Hip Prosthesis

six rigid locators. If correct repositioning is performed on the rough workpiece, the final workpiece obtained after repositioning and machining should have been same as the original hip prosthesis model (fig. 3.14(a)).

Once the workpiece is repositioned, the validation of repositioning is to be performed by simulating machining operation. To simulate the machining operation, an inverse impression of the workpiece (like a half die) is created with the original hip prosthesis dimensions and is placed on a fixed position with reference to the machine origin. This position represents the tool path on the machine as the tool moves with reference to machine and not with reference to workpiece. This half machining simulation is shown in figure 3.15, containing slots for workpiece support and positioning. The two positioning slots will simulate the material removal from the supports of the rough workpiece during machining of the first

half. They will also help to place the workpiece on two well positioned blocks for positioning the second side of the workpiece. These two blocks will help to measure the precise position and orientation of the workpiece for the second side repositioning, with reference to first side and eliminate the errors.

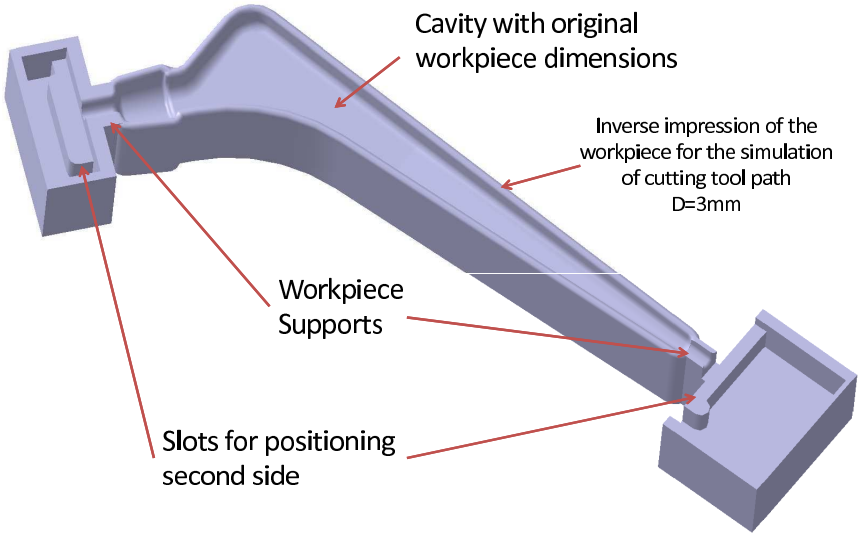

Figure 3.15: Inverse workpiece impression for simulation through boolean operation

The initial rough workpiece is placed and clamped rigidly on the baseplate with the help of locators and clamps, as shown in figure 3.16. To visualize, an unknown positioning error is induced intentionally while placing the workpiece. The baseplate is located on the fixture with 6 locators having 3-2-1r locating configuration. The six locators are just represented by cylinders with spherical heads. It is assumed that baseplate always remains in contact with all the locators and all the parts are perfectly rigid and no deformation takes place during machining operation.

3.4.2 Validation by simulation

Once the workpiece is positioned on the baseplate, the machine operation is performed. Boolean operation of CATIA ® is used to remove the material (fig. 3.15) from the workpiece of figure 3.14(b) which is placed at a specified place with

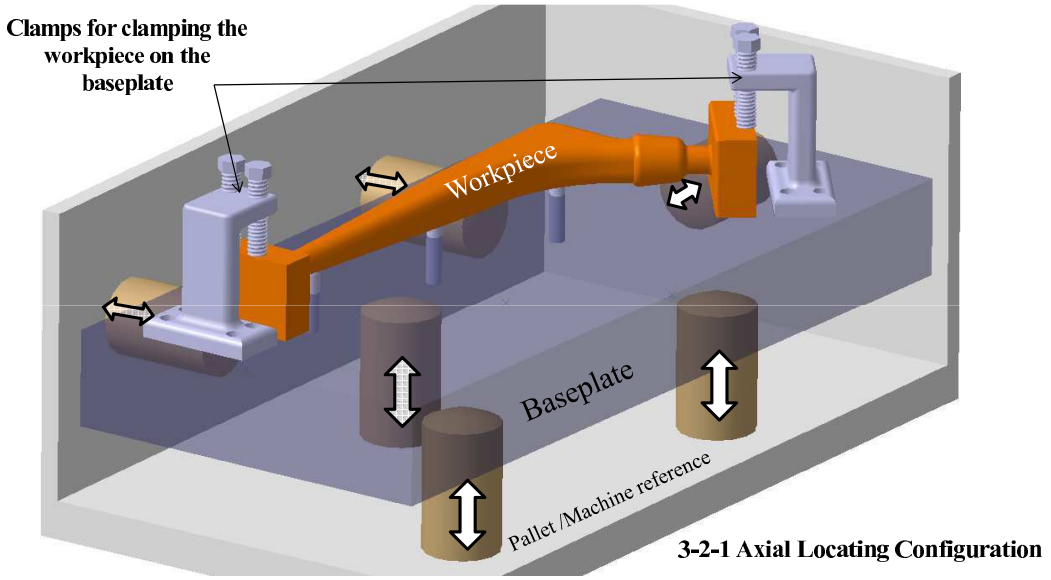

Figure 3.16: Rough workpiece is placed on the proposed fixturing system

reference to machine coordinate system to simulate machining operation. Initial placement error causes the part not to be machined accurately as shown in figure 3.17. In order to perform the repositioning of the workpiece-baseplate assembly through 3-2-1r configuration of locators and machining through simulation, a simplified procedure is explained in the following subsections.

3.4.2.1 Data input

For this case study, the analytical model is implemented in a worksheet directly linked to the CATIA® model. CATIA® furnishes the simulated initial position of workpiece ($[P_{OP}]$ of equation 3.18), which should be obtained by CMM (Appendix A) in real environment as presented in table 3.1. Point "P" is chosen as the point of intersection of centerline of two ends of the prosthesis while the angles are the angles of workpiece coordinate planes with respect to machine coordinate at the point P, defined while modeling. The initial position of the baseplate ($[P_{Ob}]$) is the function of locators' positions which are shown in table 3.2. The precision of the locators is assumed to be 0.01mm, therefore in all the tables, the data is rounded off to a value of 0.01mm.

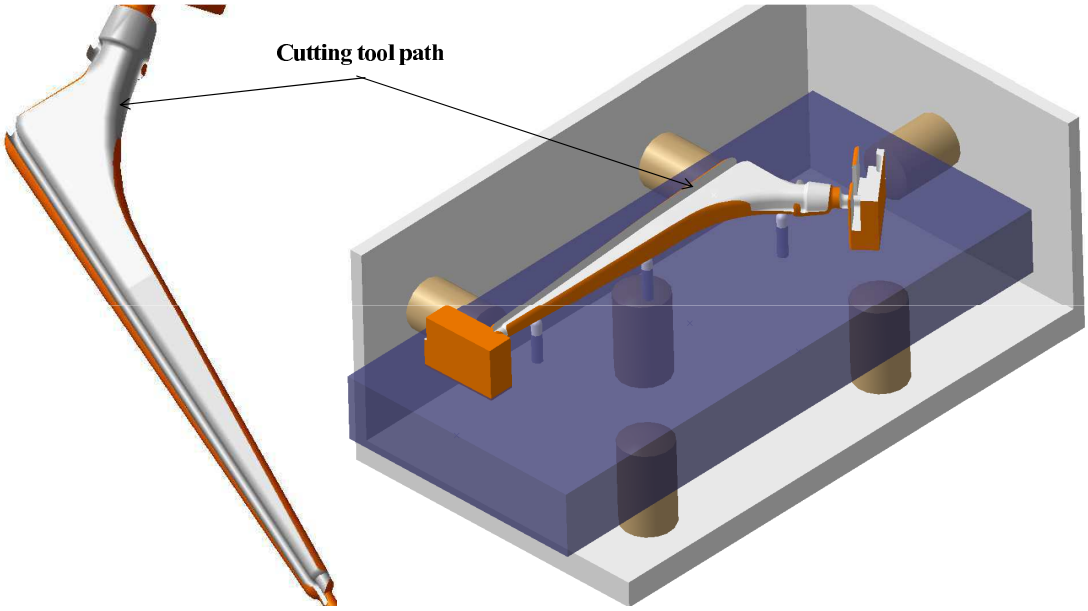

Figure 3.17: Material removal simulation of the workpiece without repositioning

Table 3.1: Initial position of the workpiece in machine coordinate system

Plane Angle	Degree	Point P	mm
α_i	0.75	x_P	102.62
β_i	-0.06	y_P	57.23
γ_i	0.45	z_P	70.19

Table 3.2: Initial positions of all six locators

Locator no	**x (mm)**	**y (mm)**	**z (mm)**
1	70	100	**15.00**
2	180	100	**15.00**
3	120	40	**15.00**
4	70	**10.00**	40
5	180	**10.00**	40
6	**8.00**	60	40

The final position of the workpiece ($[P_{OF}]$ of equation 3.18) is the required final position of the workpiece defined for the machining in the machine tool's program and is shown in the table 3.3.

All the input data is entered in the proposed algorithm and the algorithm

Table 3.3: Chosen final position of the workpiece in machine coordinate system

Plane Angle	Degree	Point P	mm
α_f	0	x_F	100
β_f	0	y_F	60
γ_f	0	z_F	70

calculates the locators' final positions ($[P_{Ob'}]$) to reorient the workpiece at required position.

Table 3.4: Calculated final positions of all the six locators

Locator no	**x (mm)**	**y (mm)**	**z (mm)**
1	70	100	**14.62**
2	180	100	**15.48**
3	120	40	**14.95**
4	70	**13.20**	40
5	180	**11.75**	40
6	**5.61**	60	40

3.4.2.2 Results

The algorithm calculates the advancements of all the six locators to reposition the workpiece in the machine reference, the final positions of all the six locators are shown in table 3.4. The new axial positions of locators (z_1, z_2, z_3, y_4, y_5, x_6) are again introduced to the CATIA® for validation. After changing the axial positions of locators, the workpiece was well positioned in the machine which is shown in figure 3.18 after performing the material removing boolean operation.

From the figure 3.18, it can be visualized that the workpiece was precisely centered at the required position in machine coordinate system, but the position of the workpiece is not perfect as required. This limitation in the precision is due to the assumed limited precision (0.01mm max) of locators. The part position is again extracted through CATIA® for rechecking and the final position error of the workpiece in machine coordinate system is shown in table 3.5. The calculation process to find the precision will be shown at the end of this case study.

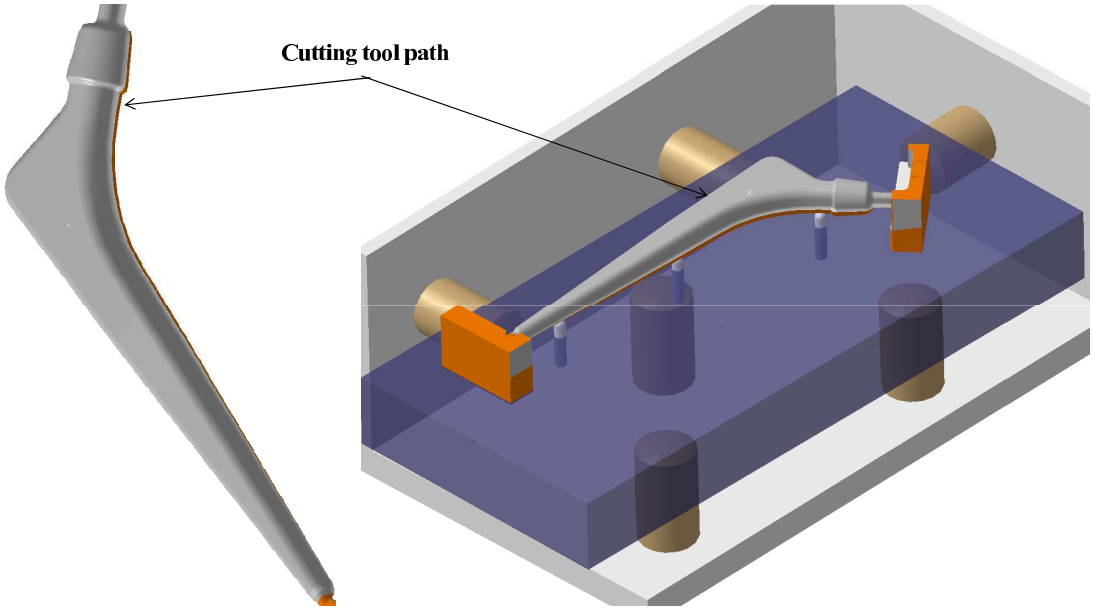

Figure 3.18: Material removal simulation of the workpiece after repositioning of side 1

Table 3.5: Workpiece positioning error due to locator's precision on the first side

Plane Angle	Degree	Point P	mm
α	0.002	x_P	0.006
β	0.008	y_P	-0.004
γ	-0.002	z_P	0.001

After the first side is relocated and machined, the prosthesis workpiece is then inverted and clamped on the baseplate. The two slots, created during the machining of the first side, are placed on two blocks fixed on the precise locations on the baseplate. This will help to reorient the workpiece with respect to the first machined surface. Now other part is created to simulate machining which can be said to be the mirrored part of the first one in figure 3.15. When the workpiece is placed and clamped on the baseplate, there would again be some error in positioning.

Same procedure is performed for the repositioning of the second side of the prosthesis on the baseplate. The final assembly and product after the repositioning of the prosthesis and machining simulation on the second face of the prosthesis is shown in figure 3.19, and the error with respect to required position

of the prosthesis is shown in table 3.6.

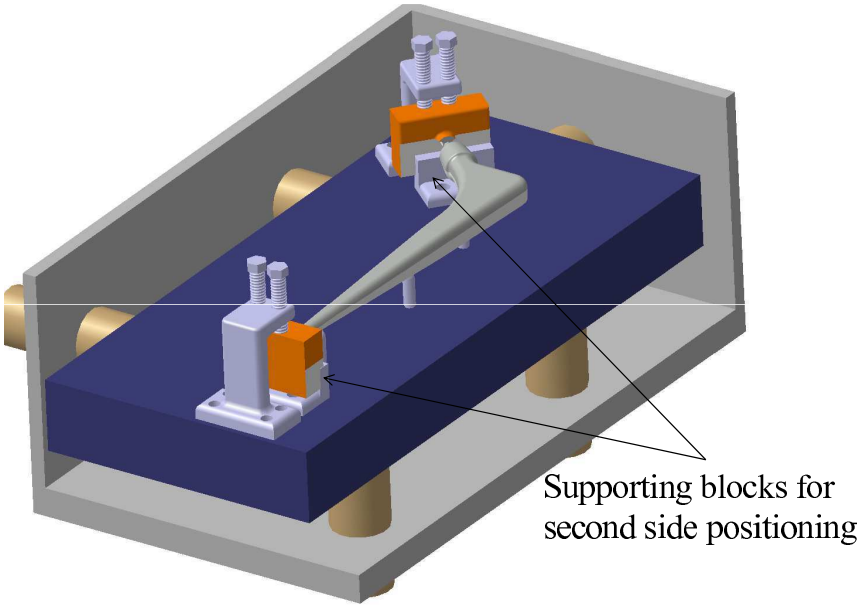

Figure 3.19: Material removal simulation of the workpiece after repositioning of side 2

Table 3.6: Workpiece positioning error due to locator's precision on the first side

Plane Angle	Degree	Point P	mm
α	0.00	x_P	0.002
β	0.00	y_P	0.00
γ	0.00	z_P	0.00

Figure 3.20 shows the final workpiece obtained after machining both sides. The above example validates the algorithm. For the second face repositioning, angular error is almost zero because of input data being the output of the first correction, which was in the precision range. Here, it is to be noted that the repositioning procedure does not change with the complexity of the workpiece. Therefore, the same repositioning procedure can be used for more complex workpieces.

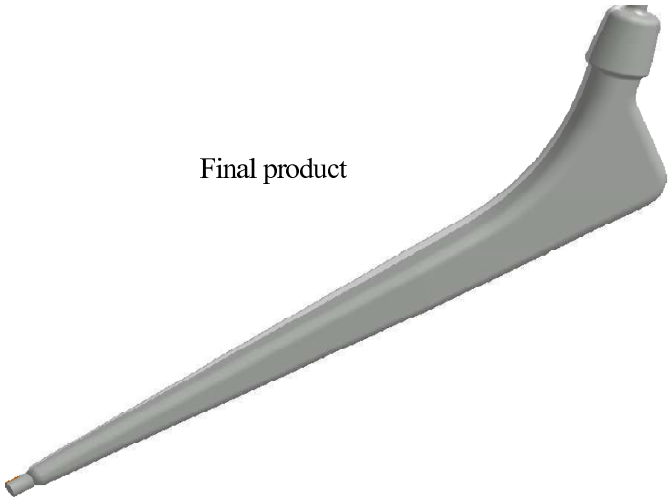

Figure 3.20: Final workpiece obtained after material removal from both sides of the workpiece

3.4.2.3 Robustness of the model

The uncertainty of position of the workpiece can be calculated from the Plucker coordinates as a function of locators' positions which was explained in section 2.2.6. In our case, using the lateral positions of locators (tab. 3.2), the uncertainty of orientation of the workpiece and the position of reference point P (table 3.3) is calculated as a function of six advancements as shown in equation 3.36,

$$\begin{Bmatrix} \delta x_P \\ \delta y_P \\ \delta z_P \\ \delta\alpha \\ \delta\beta \\ \delta\gamma \end{Bmatrix} = \begin{Bmatrix} dx_6 - \frac{6dy_4}{11} + \frac{6dy_5}{11} - \frac{4dz_1}{11} + \frac{4dz_2}{11} \\ \frac{18dy_4}{11} - \frac{7dy_5}{11} + \frac{4dz_1}{11} + \frac{10dz_2}{33} - \frac{2dz_3}{3} \\ \frac{8dz_1}{11} - \frac{46dz_2}{33} + \frac{5dz_3}{3} \\ \frac{dz_1}{110} + \frac{dz_2}{132} - \frac{dz_3}{60} \\ \frac{dz_1}{110} - \frac{dz_2}{110} \\ -\frac{dy_4}{110} + \frac{dy_5}{110} \end{Bmatrix} \tag{3.36}$$

where, dz_1, dz_2, dz_3, dy_4, dy_5 and dx_6 are uncertainties of the locators' advancements. Taking the worst case of the uncertainty, where all the values are added with each other, the equation 3.36 becomes,

$$\begin{Bmatrix} \delta x_P \\ \delta y_P \\ \delta z_P \\ \delta\alpha \\ \delta\beta \\ \delta\gamma \end{Bmatrix} = \begin{Bmatrix} 31/11 \\ 128/33 \\ 125/33 \\ 1/30 \\ 1/55 \\ 1/55 \end{Bmatrix} * \xi \tag{3.37}$$

where, ξ is the uncertainty of the locators' axial positions. Now the worst case of workpiece positioning uncertainty/precision can be calculated by replacing ξ with the positioning uncertainty of the locators. The precision/uncertainty of the workpiece position is shown in table 3.7 for the locator's axial uncertainty of 10μm and 10μm.

Table 3.7: Possible locators' positions as the result of locators' precision constraints

Parameter	Locators precision	
	10 μm	20 μm
$\delta x_P(\mu m)$	14.09	28.18
$\delta y_P(\mu m)$	19.39	38.79
$\delta z_P(\mu m)$	18.94	37.88
$\delta\beta(\mu rad)$	0.17	0.33
$\delta\gamma(\mu rad)$	0.09	0.18
$\delta\alpha(\mu rad)$	0.09	0.18

From table 3.7, it is clear that the overall uncertainty of the workpiece position decreases with the increase in locators' precision and the translational parameters are more sensitive for the specific configuration of locators in the case study.

3.5 Conclusion and discussion

This chapter presents an analytical kinematic model for repositioning of the workpiece in machine coordinates using six locators having a 3-2-1r locating configuration. In the proposed fixturing system, a baseplate is introduced in between the rough workpiece and the locators in order to precisely relocate the workpiece

by the axial movements of the locators and to avoid local errors that can be produced due to variations at workpiece-locator contacts. The baseplate is realized in such a way that its surfaces are plane and orthogonal to each other. All the elements of the system are considered rigid with the forces having no effect in the position. The friction at the contacts are also considered negligible.

For the repositioning algorithm, HTM are used for coordinate transformation from machine to workpiece and machine to baseplate. The former position can be measured through the CMM while the latter transformation is calculated through the positions of the locators in contact with the baseplate. The HTM from machine coordinate to the baseplate coordinate gives a matrix whose elements are the components of the three normal unit vectors of the baseplate surfaces.

Unique final positions of the locators cannot be calculated directly through the final calculated position of the baseplate due to the fact that zero friction causes the displacement of the contacting surface on the positioning locators. But as all the locators remain in contact with the baseplate at any instant for 6-DOF statically determinate case, the displacement of the baseplate is transformed to the displacement of the planes in contact with the locators. This method gives a unique axial position of each locator in machine coordinate system in terms of the normal unit vectors components.

The kinematic model is validated through the simulation in CATIA® performed on a chosen workpiece CPT® 12/14 Hip Prosthesis by Zimmer (zimmer, 2011). The workpiece is placed and clamped on the baseplate which is located on the six locators. The positioning error of the workpiece is measured and compensated through the advancements of the six locators calculated through the proposed algorithm. After the repositioning and machining simulation of one face, the workpiece is inverted and the same repositioning simulation is performed on the second face. The precision of the workpiece placement depends upon the precision of the locators. The uncertainty/precision of the workpiece is calculated for the configuration of locators in the case study.

This kinematic model helps to relocate the workpiece through the axial advancements of the six locators. The workpiece can have large variation, therefore this chapter deals with the large errors present in the positioning of the workpiece considering all elements to be rigid. In the next chapter, the locators and clamps

would be considered as elastic elements. Additionally, clamping and machining forces will be introduced which will add a small displacement to the workpiece due to deformation of the locators. For the purpose of simplifying the problem, after the displacement induced by the machining and clamping forces is calculated, the compensation will be performed through repositioning of locators using the kinematic model developed in this chapter. After repositioning the workpiece, the deformation of the locators at the new positions will be calculated which are again compensated.

Chapter 4

Positioning error due to deformation of elastic elements

In the previous chapter, a kinematic model is presented which is capable of correcting the positioning error if the initial and required positions of the workpiece are known with the hypothesis of all the elements being rigid. In reality, the locators can deform under the weight of the baseplate, as well as static (weight and clamping forces) and dynamic (machining) forces acting on the workpiece-baseplate assembly. The baseplate, repositioned by kinematic model, should be clamped to remain on the earlier corrected position and should support the clamping and machining forces etc.. In fact, these mechanical actions will imply displacements on the baseplate-workpiece assembly. In order to retain the previously corrected position more closer to the desired position, it is necessary to know the deformation caused by these forces. This deformation is then taken in to account for the repositioning of the workpiece.

In this chapter, an analytical model is presented to calculate the deformation of elastic elements and as a result the rigid body displacement of the workpiece-baseplate assembly under clamping and machining load. We called this analytical model as "mechanical model". The mechanical model calculates the stiffness and mass of the whole fixturing system considering the locators being the elastic elements with negligible masses and the workpiece-baseplate assembly being the rigid mass element. The FEA[1] approach requires lengthy initial modelling of the

[1]Finite Element Analysis

elements whenever the configuration or conditions change. Therefore, we used the analytical formulation for the problem solution. The analytical formulation allows obtaining the mass and stiffness matrices quickly for any configuration and position of locators as well as for any orientation of the baseplate on the locators just by changing the initial input parameters in the spreadsheet linked with the Mathematica®.

The stiffness matrix of the system is obtained by the Lagrange formalization resolved in Mathematica®. This stiffness depends on all the mechanical parameters e.g. position and orientation of locators, dimensions, material, etc.. Small displacement hypothesis may be applied as the deformation must remain small for the system reliability and precision.

This chapter is divided as follows: Initially, the mechanical model of the proposed fixturing system is constructed by the hypothesis of workpiece-baseplate assembly being rigid and locators being elastic elements. Then the overall energy of the system is calculated which consists of the potential energy contained in all the locators and clamps, kinetic energy of inertial elements and work done by the external applied load. Lagrangian formulation allows to calculate the stiffness and mass matrices of the fixturing system for a chosen configuration.

The displacement of the workpiece-baseplate assembly under load as well as the deformation of each locator can be calculated with the hypothesis of the contacts being rigid. The friction at the locator-baseplate contacts is neglected. Then, the contact deformation for Hertzian as well as rough contact is calculated for each locator with the modified formalization and overall deformation of each locator and overall displacement of workpiece-baseplate assembly is obtained. The chapter concludes with the discussion on the scope and application of this mechanical model.

4.1 Mechanical model representation

The basic mechanical model representation of the locators and workpiece-baseplaet assembly of the proposed fixturing system without clamps and external forces (fig. 3.7) is shown in figure 4.1. Clamping force, load of the workpiece-baseplate assembly and machining forces will be included during formalization. Initially for

the mechanical model, the locators are assumed to be elastic elements with negligible masses, each of them can be represented by proper stiffness matrix ($[K_1]$ to $[K_6]$). The workpiece-baseplate assembly is assumed to be rigid mass with no deformation possible under load. At this stage, the contact deformations between the baseplate and spherical locator are neglected.

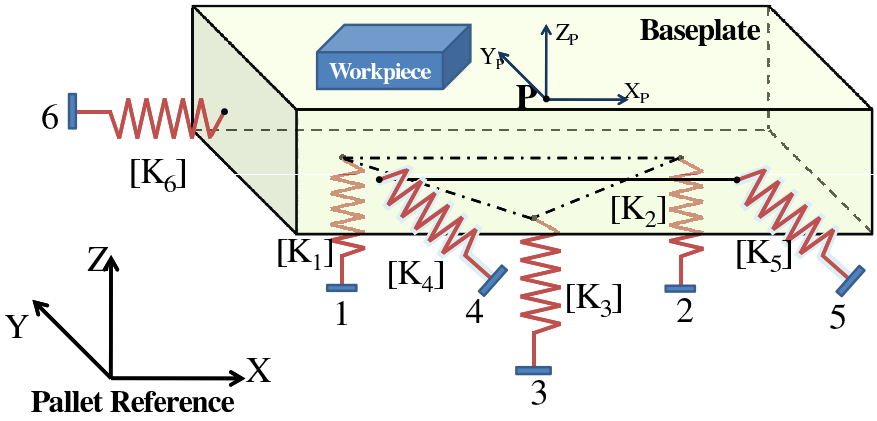

Figure 4.1: mechanical model representation of proposed fixturing system

4.2 Mechanical behavior formalization

In this section, the mechanical behavior of the fixturing system is formalized using Lagrangian formalization and small displacement. The generalized Lagrangian equation can be written as;

$$\frac{\partial}{\partial t}\left(\frac{\partial(T-U)}{\partial \dot{q}_i}\right) - \frac{\partial(T-U)}{\partial q_i} = \frac{\partial W}{\partial q_i} \tag{4.1}$$

where, U is the sum of potential energies contained in all of the elastic elements of the system, T is the kinetic energy of the system, W is the external work-done on the system as the result of all applied forces, q_i are the generalized coordinates. In our case these generalized coordinates are 6-DOF of the workpiece $q_i = \Delta X_P, \Delta Y_P, \Delta Z_P, \Delta\beta, \Delta\gamma, \Delta\alpha$ and $\dot{q}_i$ are 6 generalized velocities of the workpiece i.e. $\dot{q}_i = \partial q_i/\partial t$. In figure 4.2, position X_F and X_b' are the final corrected

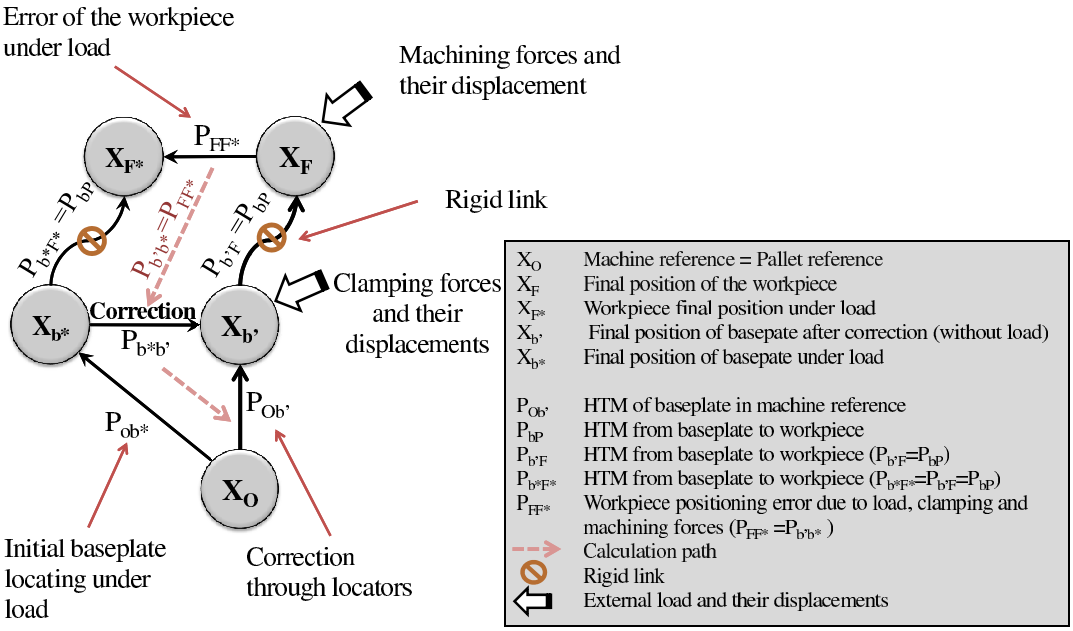

Figure 4.2: Positioning error for mechanical model

positions (kinematic repositioning) of the workpiece and baseplate respectively. The load of the baseplate and workpiece have already been taken into account while measuring the position of the workpiece through CMM and correcting it through the kinematic model. Once the correction is performed, the baseplate is clamped on the machine through clamps which displace the baseplate from its initial position. The machining forces also displace the workpiece. It has again been assumed that the contact of the workpiece and baseplate is rigid and no deformation is taking place between the baseplate and workpiece under load. Both the clamping forces and machining forces cause the workpiece to displace on the elastic locators and to move to the position X_F^*. Having rigid workpiece-baseplate contact, the baseplate will experience the same amount of displacement i.e. $P_{FF^*} = P_{b'b^*}$.

In this section, the aim is to calculate the displacement of the workpiece under load which will be the relative position of the baseplate to the one without load. That displacement enables us to calculate the positioning error of the workpiece. The repositioning can be performed by the modification of locators' advancements to move the baseplate from the initial (under load) position X_b^* to the required

one X_b' through the kinematic model.

The information regarding the system configuration is gathered which includes; initial positions ans orientations of locators, clamps, their stiffness matrices, mass matrix of workpiece-baseplate assembly and for the case of external load; placement and magnitude of the external applied forces and moments. The stiffness and mass calculation of the mechanical model of the fixturing system is performed by using small displacements and Lagrange formalization.

For the computation, the mechanical model needs initial values as input data, like the positions and orientations of the locators and clamps, their stiffness matrices, mass matrix of the baseplate, magnitudes and location of external forces and moments etc..

4.2.1 Potential energy of locators

For the fixturing system in figure 4.1, overall potential energy of the system is the sum of the potential energies of all the locators as the locators are the only elastic elements besides the workpiece-baseplate assembly being rigid. The total potential energy of the locators can be written as;

$$U = \frac{1}{2}\sum \{\Delta X\}_i^T [K]_i \{\Delta X\}_i \tag{4.2}$$

where, $[K]_i$ is the stiffness matrix of i^{th} locator and ΔX_i is the relative displacement vector of the contact point of that locator according to its other extremity, they can be defined as:

$$[K] = \begin{bmatrix} K_{xx} & K_{xy} & K_{xz} \\ K_{xy} & K_{yy} & K_{yz} \\ K_{xz} & K_{yz} & K_{zz} \end{bmatrix}, \qquad \{\Delta X\}_i = \begin{Bmatrix} \Delta X_i \\ \Delta Y_i \\ \Delta Z_i \end{Bmatrix}$$

Where, ΔX_i, ΔY_i and ΔZ_i are the x, y and z components of the displacement vector of the i^{th} locator's point of contact with the baseplate. The displacement vector of i^{th} locator is calculated with reference to point P of the baseplate which is assumed to be the center of gravity of the baseplate. If α, β and γ are the rotation angles of the baseplate along z, x and y axes, the position of i^{th} point on the baseplate, with respect to point P, can be written as;

$$\begin{Bmatrix} x_{fi} \\ y_{fi} \\ z_{fi} \\ 1 \end{Bmatrix} = \begin{bmatrix} \cos\alpha\cos\gamma - \sin\alpha\sin\beta\sin\gamma & -\sin\alpha\cos\beta & \cos\alpha\sin\gamma + \sin\alpha\sin\beta\cos\gamma & X_P \\ \sin\alpha\cos\gamma + \cos\alpha\sin\beta\sin\gamma & \cos\alpha\cos\beta & \sin\alpha\sin\gamma - \cos\alpha\sin\beta\cos\gamma & Y_P \\ -\cos\beta\sin\gamma & \sin\beta & \cos\beta\cos\gamma & Z_P \\ 0 & 0 & 0 & 1 \end{bmatrix} \begin{Bmatrix} x_i - x_P \\ y_i - y_P \\ z_i - z_P \\ 1 \end{Bmatrix} \tag{4.3}$$

Where, x_i, y_i and z_i are the coordinates of initial position of point i, x_{fi}, y_{fi} and z_{fi} are the coordinates of final position of point i, x_P, y_P and z_P are the initial coordinates of point P of the baseplate, and X_P, Y_P and Z_P are the displacements of point P of the baseplate under load. As small displacements are assumed, using small angles assumptions:

$$\sin\alpha \approx \alpha, \quad \sin\beta \approx \beta, \quad \sin\gamma \approx \gamma$$

$$\cos\alpha \approx \cos\beta \approx \cos\gamma \approx 1$$

$$\sin\beta\sin\gamma \approx \sin\alpha\sin\gamma \approx \sin\alpha\sin\beta \approx \sin\alpha\sin\beta\sin\gamma \approx 0$$

Using the small angles assumption, the final position of point i from equation 4.3, can be written as;

$$\begin{Bmatrix} x_{fi} \\ y_{fi} \\ z_{fi} \\ 1 \end{Bmatrix} = \begin{bmatrix} 1 & -\Delta\alpha & \Delta\gamma & \Delta X_P \\ \Delta\alpha & 1 & -\Delta\beta & \Delta Y_P \\ -\Delta\gamma & \Delta\beta & 1 & \Delta Z_P \\ 0 & 0 & 0 & 1 \end{bmatrix} \begin{Bmatrix} x_i - x_P \\ y_i - y_P \\ z_i - z_P \\ 1 \end{Bmatrix} \tag{4.4}$$

The final displacement of i^{th} point with respect to point P would be the final position minus the initial position with respect the the point P of the baseplate. The final displacement of i^{th} point can be written as;

$$\begin{Bmatrix} \Delta X_i \\ \Delta Y_i \\ \Delta Z_i \\ 1 \end{Bmatrix} = \begin{bmatrix} 0 & -\Delta\alpha & \Delta\gamma & \Delta X_P \\ \Delta\alpha & 0 & -\Delta\beta & \Delta Y_P \\ -\Delta\gamma & \Delta\beta & 0 & \Delta Z_P \\ 0 & 0 & 0 & 1 \end{bmatrix} \begin{Bmatrix} x_i - x_P \\ y_i - y_P \\ z_i - z_P \\ 1 \end{Bmatrix} \tag{4.5}$$

Equation 4.5 enables us to find the displacement of each locator's point of contact and hence the potential energy of each locator (eq. 4.2) as the function of linear and angular displacement of the baseplate $\{\Delta X_P, \Delta Y_P, \Delta Z_P, \Delta\beta, \Delta\gamma, \Delta\alpha\}^T$.

4.2.2 Kinetic energy of the assembly

As the workpiece-baseplate assembly is the only mass element, so they will experience kinetic energy as the result of external forces. Kinetic energy will have two components; linear and angular. The linear kinetic energy (T_V) of the workpiece-baseplate assembly can be calculated by the general kinetic energy equation;

$$T_V = \frac{1}{2}\{\vec{V}\}^T[M]\{\vec{V}\} \tag{4.6}$$

where [M] is the mass matrix and $\{\vec{V}\} = \{\vec{v_x} \;\; \vec{v_y} \;\; \vec{v_z}\}^T$ is the velocity vector. The components of the velocity vector can be defined as;

$$\vec{v_x} = \frac{\partial \vec{X_P}}{\partial t}, \quad \vec{v_y} = \frac{\partial \vec{Y_P}}{\partial t}, \quad \vec{v_z} = \frac{\partial \vec{Z_P}}{\partial t} \tag{4.7}$$

where X_P, Y_P and Y_P is the displacement of point P as in equation 4.5. The above equation 4.7 gives the linear velocities as the function of baseplate displacement. Now the angular part of the kinetic energy will be calculated. The general equation of the angular kinetic energy of the system in vectorial form can be written as,

$$T_\Omega = \frac{1}{2}\{\vec{\Omega}\}^T[I]\{\vec{\Omega}\} \tag{4.8}$$

where [I] is the inertia matrix and $\{\vec{\Omega}\} = \{\vec{\omega_x} \;\; \vec{\omega_y} \;\; \vec{\omega_z}\}^T$ is the angular velocity vector. The angular velocities of the workpiece-baseplate assembly is calculated by Lalanne *et al.* (1986) using figure 4.3, where the workpiece experiences three

rotations α, β and γ along z, x and y directions respectively. Lalanne *et al.* (1986) calculated the three angular velocities as a function of three angular displacements as,

$$\begin{aligned} \vec{\omega}_x &= -\frac{\partial \alpha}{\partial t}\cos\beta\sin\gamma + \frac{\partial \beta}{\partial t}\cos\gamma \\ \vec{\omega}_y &= \frac{\partial \gamma}{\partial t} + \frac{\partial \alpha}{\partial t}\sin\beta \\ \vec{\omega}_z &= \frac{\partial \alpha}{\partial t}\cos\beta\cos\gamma + \frac{\partial \beta}{\partial t}\sin\gamma \end{aligned} \tag{4.9}$$

Using the hypothesis of small displacement ($\cos\theta \approx 1, \sin\theta \approx \theta$), equation 4.9 can be simplified to equation 4.10.

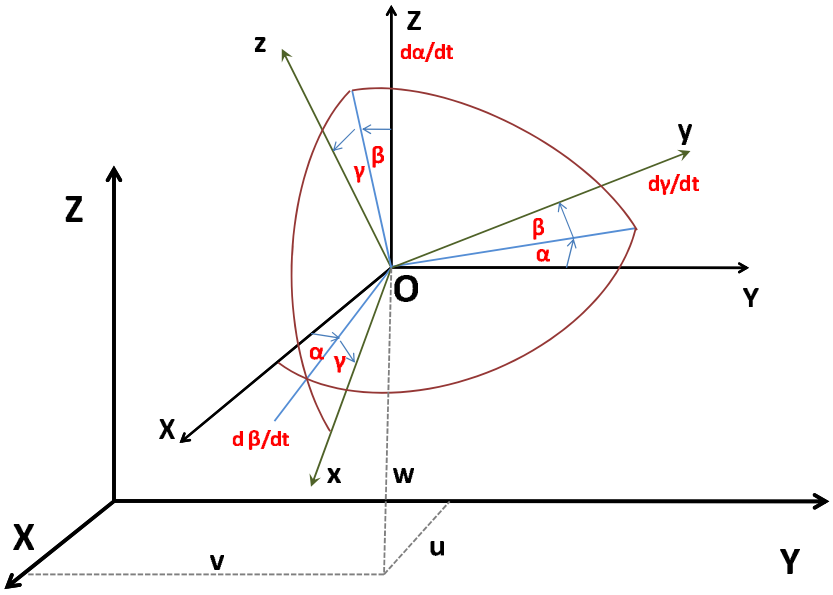

Figure 4.3: Rotations along the axes Lalanne *et al.* (1986)

$$\begin{aligned}\vec{\omega}_x &= -\frac{\partial\alpha}{\partial t}\gamma + \frac{\partial\beta}{\partial t} \\ \vec{\omega}_y &= \frac{\partial\gamma}{\partial t} + \frac{\partial\alpha}{\partial t}\beta \\ \vec{\omega}_z &= \frac{\partial\alpha}{\partial t} + \frac{\partial\beta}{\partial t}\gamma\end{aligned} \tag{4.10}$$

Equation 4.7 and 4.10 give linear and angular velocities of the workpiece-baseplate as a function of their displacement vector $\{\Delta X_P, \Delta Y_P, \Delta Z_P, \Delta\beta, \Delta\gamma, \Delta\alpha\}^T$. Thus, like potential energy, Linear and angular kinetic energies can also be calculated as a function of displacement of the baseplate. The total kinetic energy is the sum of linear and angular kinetic energies:

$$T = \frac{1}{2}\{\vec{V}\}^T[M]\{\vec{V}\} + \frac{1}{2}\{\vec{\Omega}\}^T[I]\{\vec{\Omega}\} \tag{4.11}$$

In our case, the kinetic energy is negligible but it has a great impact in case of turning process.

4.2.3 Work done due to external forces

Machining forces and weight of the body are considered as the external applied forces in Lagrangian formalization. In this section, generalized equation for work done by the external applied force and moment will be calculated. Here we take the workpiece-baseplate assembly without locators and clamps as shown in figure 4.4. As shown in the figure, the workpiece-baseplate assembly is experiencing a static external force $F = \{F_x, F_y, F_z\}^T$ and an external moment $\mathbb{T} = \{\mathbb{T}_x, \mathbb{T}_y, \mathbb{T}_z\}^T$.

Generally, the work done by the external applied load and moment can be written as

$$W = \{F\}.\{\Delta X_P\} + \{\mathbb{T}\}.\{\Delta\Theta\} \tag{4.12}$$

where, $\{F\}$ is the force vector, $\{\Delta X_P\}$ is the displacement vector of point P under force F, $\{\mathbb{T}\}$ is the external torque vector and $\{\Delta\Theta\}$ is the angular displacement

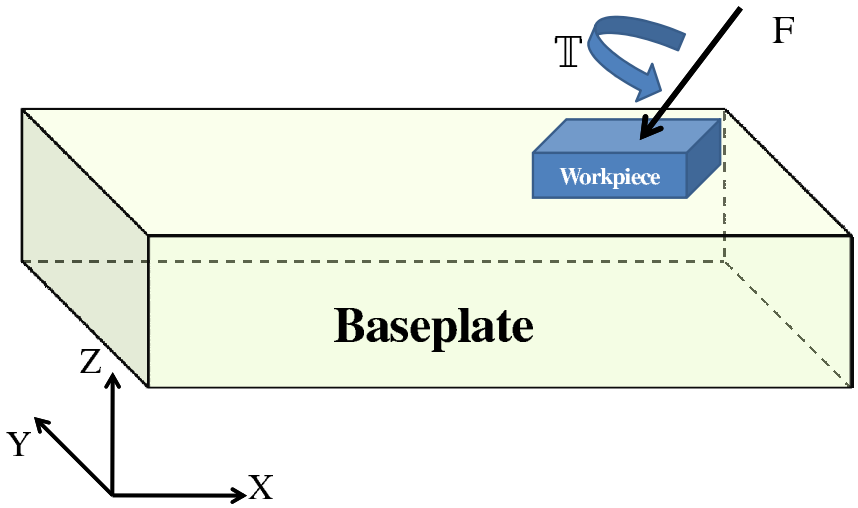

Figure 4.4: Workpiece-baseplate assembly under load

vector due to external torque. Isometric view of the baseplate of figure 4.4 is shown in figure 4.5, with three forces and three moment components.

If an external force is acting away from the center of gravity, it will cause linear displacement as well as angular displacement of the workpiece. The displacement caused by the external force, at the point of action of force, can be written in HTM form using small displacement hypothesis as;

$$\begin{Bmatrix} \Delta X_{Pf} \\ \Delta Y_{Pf} \\ \Delta Z_{Pf} \\ 1 \end{Bmatrix} = \begin{bmatrix} 0 & -\Delta\alpha & \Delta\gamma & \Delta X_P \\ \Delta\alpha & 0 & -\Delta\beta & \Delta Y_P \\ -\Delta\gamma & \Delta\beta & 0 & \Delta Z_P \\ 0 & 0 & 0 & 1 \end{bmatrix} \begin{Bmatrix} x_f - x_P \\ y_f - y_P \\ z_f - z_P \\ 1 \end{Bmatrix} \tag{4.13}$$

where, $\{x_f - x_P, \quad y_f - y_P, \quad z_f - z_P\}^T$ is the initial distance of point of action of force from the point P, while $\{\Delta X_{Pf}\} = \{\Delta X_{Pf}, \Delta Y_{Pf}, \Delta Z_{Pf}\}^T$ is the displacement of point of action of force (f) as the function of the displacement vector $\{\Delta X_P, \Delta Y_P, \Delta Z_P, \Delta\beta, \Delta\gamma, \Delta\alpha\}^T$ of the workpiece.

Equation 4.12 can be written in vector form for i external forces and j external torques as;

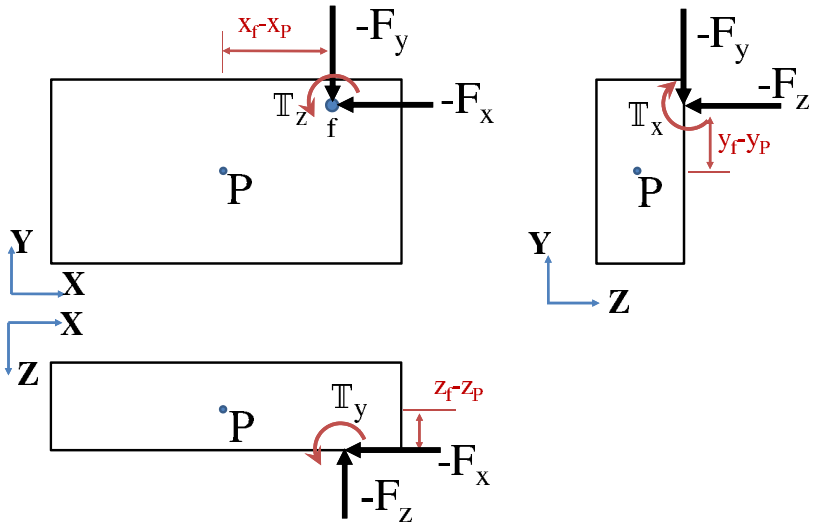

Figure 4.5: Isometric views of workpiece-baseplate assembly under load

$$W = \sum \begin{Bmatrix} F_x \\ F_y \\ F_z \end{Bmatrix}_i . \begin{Bmatrix} \Delta X_{Pf} \\ \Delta Y_{Pf} \\ \Delta Z_{Pf} \end{Bmatrix}_i + \sum \begin{Bmatrix} \mathbb{T}_x \\ \mathbb{T}_y \\ \mathbb{T}_z \end{Bmatrix}_j . \begin{Bmatrix} \Delta\beta \\ \Delta\gamma \\ \Delta\alpha \end{Bmatrix} \tag{4.14}$$

where, $\{\Delta X_{Pf}, \Delta Y_{Pf}, \Delta Z_{Pf}\}^T$ is the linear displacement vector of point of action of force while $\{\Delta\beta, \Delta\gamma, \Delta\alpha\}^T$ is the angular displacement vectors of the workpiece-baseplate assembly.

4.2.4 Clamping forces

Clamp is the mean of tightening the workpiece in the fixture, once it is located through the locators. As the locators are assumed to be elastic, the clamping force causes the locators to compress. Here, it is to note that, as the initial position of the workpiece is measured by CMM, the deformation of the locators due to the load of the baseplate-workpiece assembly is already taken into account, so only the external forces will cause further deformation. Normally, the clamp is brought in contact with the baseplate and then it is tightened. The clamps can be considered in two ways;

- Clamps can be replaced by constant static point forces acting on the baseplate at the contacting points of clamps. In this case, the clamping forces will be considered as the external applied forces at the known positions and the total work will become the sum of the work done by the external applied forces and clamping forces. The work done by the clamping forces will be calculated using equation 4.14.

- Clamps can also be considered as elastic elements with one end in contact with the baseplate while the other end is externally displaced by an unknown force as shown in figure 4.6. The external displacement (X_{E1}, X_{E2}) is assumed to be known and constant. In this case, the potential energy contained within each locator will be calculated and will be added to the overall potential energy of the system.

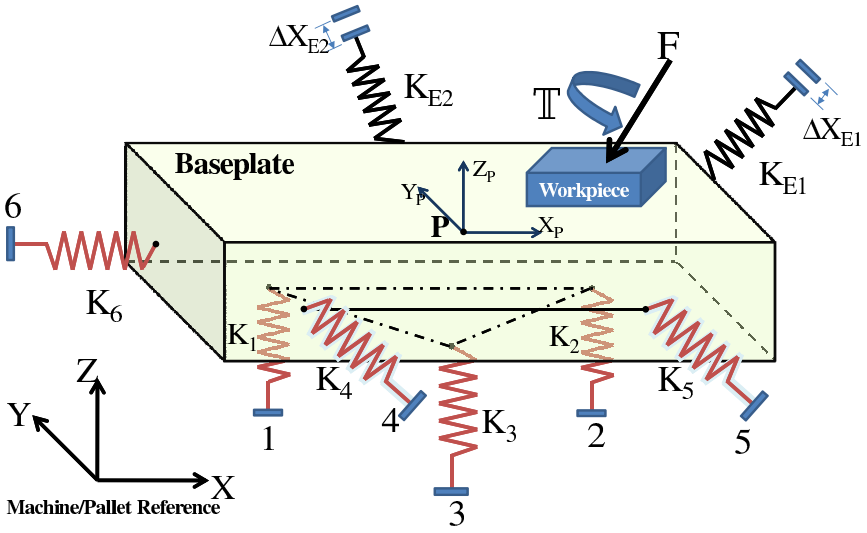

Figure 4.6: Modeling of clamps, XYZ: Pallet reference

Instead of measuring the clamping force exerted by each clamp, the amount of external displacement given to each clamp can easily be measured. So in this work, the clamps are considered as being elastic elements. Two externally displaced elastic clamps (C1 & C2) are shown in figure 4.6. A portion of the external displacement will be transferred to the other end of the clamp (baseplate-clamp contact) while the rest will induce potential energy in the clamp.

External applied displacement of each clamp is assumed to be known while the displacement of the end of j^{th} clamp in contact with the baseplate $\{\Delta X_{ij}, \Delta Y_{ij}, \Delta Z_{ij}\}^T$, as the result of YPR rotation, can be calculated using equation 4.15 which is same as displacement of locators' ends in equation 4.5.

$$\begin{Bmatrix} \Delta X_{ij} \\ \Delta Y_{ij} \\ \Delta Z_{ij} \\ 1 \end{Bmatrix} = \begin{bmatrix} 0 & -\Delta\alpha & \Delta\gamma & \Delta X_P \\ \Delta\alpha & 0 & -\Delta\beta & \Delta Y_P \\ -\Delta\gamma & \Delta\beta & 0 & \Delta Z_P \\ 0 & 0 & 0 & 1 \end{bmatrix} \begin{Bmatrix} x_{cj} - x_P \\ y_{cj} - y_P \\ z_{cj} - z_P \\ 1 \end{Bmatrix} \tag{4.15}$$

where $\{x_{cj} - x_P,\ y_{cj} - y_P,\ z_{cj} - z_P\}^T$ is the distance of point of contact of clamp j from point P. The final relative displacement between the two ends of the j^{th} clamp can be written as;

$$\begin{Bmatrix} \Delta X_{Cj} \\ \Delta Y_{Cj} \\ \Delta Z_{Cj} \end{Bmatrix} = \begin{Bmatrix} \Delta X_{Ej} \\ \Delta Y_{Ej} \\ \Delta Z_{Ej} \end{Bmatrix} - \begin{Bmatrix} \Delta X_{ij} \\ \Delta Y_{ij} \\ \Delta Z_{ij} \end{Bmatrix} \tag{4.16}$$

where $\{\Delta X_E\}_j = \{\Delta X_{Ej}, \Delta Y_{Ej}, \Delta Z_{Ej}\}^T$ is the external applied displacement vector of j^{th} clamp (preload). The negative sign of $\{X_{ij}\}$ is due to the fact that positive direction of inner end of the clamp will cause compression while negative displacement will cause tension in the clamp as the clamps are always placed in the direction opposite to the locators. Final potential energy of all the clamps can be written as;

$$U_C = \frac{1}{2} \sum \{\Delta X_C\}_j^T [K_E]_j \{\Delta X_C\}_j \tag{4.17}$$

where, $\{\Delta X_C\}_j = \{\Delta X_{Cj}, \Delta Y_{Cj}, \Delta Z_{Cj}\}^T$ is the relative displacement of the two ends of j^{th} clamp which can be calculated using equation 4.16, while $[K_E]_j$ is an isometric stiffness matrix of j^{th} clamp and it is also assumed to be known.

After calculating the potential energies of all the elastic elements, kinetic energies of all the inertial elements and work done by all the external forces and moments, the Lagrangian formulation (eq. 4.1) can be used to calculate the stiffness and mass matrices, linear and angular displacements of the workpiece under load and natural frequencies of the fixturing system.

4.2.5 Displacement of workpiece under load

The basic aim of this chapter is to calculate the positioning error of the workpiece due to the external force and moment acting on the workpiece-baseplate assembly which are located and clamped by the elastic locators and clamps. In the previous sections, potential energies of all the elastic elements, kinetic energies of all the inertial elements and work done by all the external forces and moments have been calculated. All of them are calculated in terms of displacement vector of the workpiece $\{\Delta X_P, \Delta Y_P, \Delta Z_P, \Delta\beta, \Delta\gamma, \Delta\alpha\}^T$. All the calculated energy terms are substituted in Lagrangian equation (eq. 4.1) to calculate the displacement vector of the workpiece. The six locators form six linear equations. This statically determinate problem can easily be solved for 6 unknown displacements. The solution is obtained using Mathematica® using small displacement hypothesis, i.e.

$$\ddot{q}_i \approx 0, \quad \dot{q}_i \approx 0, \quad q_i q_j \approx 0$$

where, q_i represents the 6 DOF parameters $(\Delta X_P, \Delta Y_P, \Delta Z_P, \Delta\beta, \Delta\gamma, \Delta\alpha)$ of the workpiece, $\dot{q}_i$ represents the velocity parameters with $\dot{q}_i = \partial q_i/\partial t$ and $\ddot{q}_i$ represents the acceleration parameters with $\ddot{q}_i = \partial^2 q_i/\partial t^2$ of the fixturing system. The displacement of the workpiece-baseplate, calculated in this section, can be compensated through the modification of advancement of six locators as demonstrated in the previous chapter. After calculating the displacement of the workpiece, the mechanical behavior of the fixturing system can also be calculated with already calculated potential and kinetic energies of the system.

Kinetic energy of the fixturing system gives mass matrix of the system and the sum of all the potential energies of the fixturing system gives the overall stiffness of the fixturing system acting at point P as shown in figure 4.7. From equation 4.2 and equation 4.6, the components of $i \times j$ mass and stiffness matrices are calculated using equation 4.18.

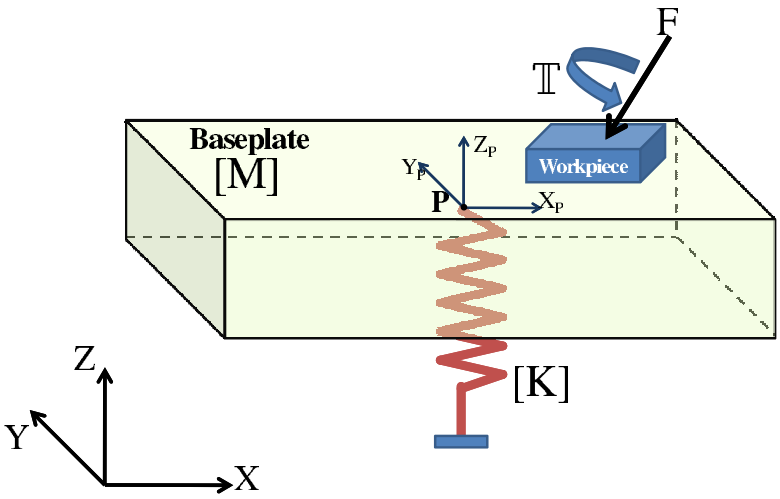

Figure 4.7: Overall stiffness and mass matrix representation

$$[K_{ij}] = \frac{\partial U}{\partial q_i \partial q_j} \tag{4.18}$$
$$[M_{ij}] = \frac{\partial T}{\partial \dot{q}_i \partial \dot{q}_j}$$

With the help of stiffness and mass matrices, the vibrational modes are calculated by solving the equation 4.19 which can be found in (Kelly, 1996).

$$[M]^{-1}[K] - \omega^2[I] = 0 \tag{4.19}$$

The natural frequency helps to determine the safe operating frequency of the machine tool. In order to be safe, the frequency of the machine tool has to be away from the natural frequency of the fixturing system. This will be illustrated at the end of this chapter.

4.3 Deformation of locators with zero friction

Once the displacement of the workpiece-baseplate assembly is calculated, the next step is to calculate the deformation of each locator caused under clamping

and machining forces which can be seen in the flow chart in figure 4.8. As the proposed mechanical model is built on the assumption of small displacement (SD), the Plucker matrix (section 2.2.6) can be used to calculate the deformation of each locator as a function of the displacement of the workpiece-baseplate assembly as shown in equation 3.33. The Plucker matrix for the proposed fixturing system is calculated in section 3.3.5 and it will change with the change in the configuration of locators. The deformation of a locator under load is shown in figure 4.9 where the plane of the baseplate, in contact with the locator, is moved from initial to final position under load. The normal to the plane forms an angle Φ with the locator axis. This angle Φ can be calculated through the normals of the contacting surfaces calculated in section 3.3.1.2. Plucker deformation of the locator gives the deformation of the contacting sphere normal to the contact surface which is shown by δ_{sph} where, $\delta_{sph} = \delta_{Plu} - \delta_C$. The contact deformation δ_C will be introduced in following sections. If the locator deforms following Plucker deformation, it should move at position 2. For a rigid contact, δ_{sph} in figure 4.9 will be same as the deformation of the center of the contacting sphere of the locator, which helps in building the vector diagram of the deformation in figure 4.9 for the calculation.

Since zero contact friction is assumed during the mechanical model development, the final position of the locator will be different from position 2 depending upon the stiffness of the locator. If the locator is rigid in radial direction, it will move only axially and it will deform radially if it is assumed axially rigid. Axial (k_{aL}) and radial (k_{tL}) stiffness of the locator is calculated using the equation 4.20.

$$k_{aL} = \frac{EA}{L} \qquad (4.20)$$
$$k_{tL} = \frac{k_f k_s}{k_f + k_s}$$

where, $k_s = GA/h$ is the shear stiffness, $k_f = 3EI/h^3$ is the flexural stiffness, E is the modulus of elasticity, G is shear modulus of elasticity, L is the total length of locator, h is the length of locator which is out of the support and A is the cross sectional area of the locator. The stiffness matrix of a locator having axis along Z-axis will be,

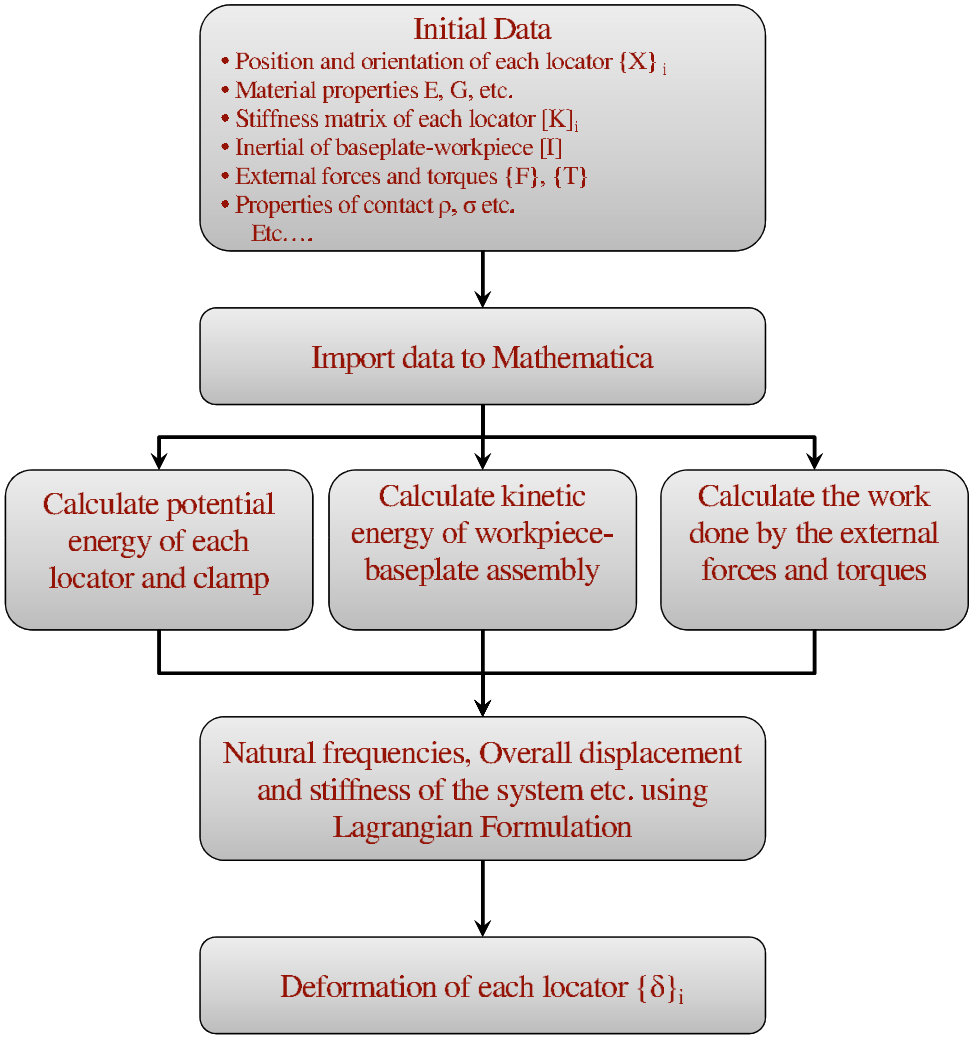

Figure 4.8: Flow chart of the algorithm to calculate the deformation of each locator

$$[K_L]_i = \begin{bmatrix} k_{tL} & 0 & 0 \\ 0 & k_{tL} & 0 \\ 0 & 0 & k_{aL} \end{bmatrix} \tag{4.21}$$

To calculate the effect of radial and axial stiffness on the final position of the locator, in figure 4.9, the locator having both axial and radial stiffness is moved to point 3 after deformation. The final deformation of the locator's tip is the

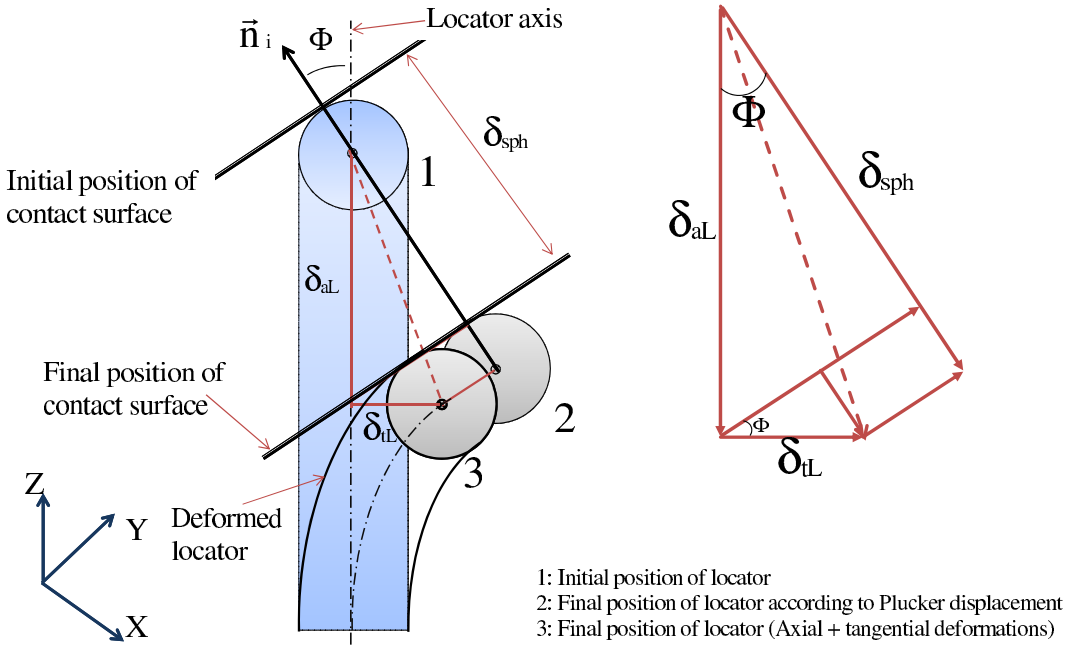

Figure 4.9: Relation of the locator deformation with calculated Plucker deformation

projection of δ_{sph} having components δ_{aL} and δ_{tL} so that,

$$\delta_{aL} \cos \Phi + \delta_{tL} \sin \Phi = \delta_{sph} \tag{4.22}$$

The potential energy of the locator as the function of its radial and axial stiffness and deformation is calculated using figure 4.9, which is

$$U = \frac{1}{2} k_{aL} \delta_{aL}^2 + \frac{1}{2} k_{tL} \delta_{tL}^2 = \frac{1}{2} k_{aL} \left(\frac{\delta_{sph} - \delta_{tL} \sin \Phi}{\cos \Phi} \right)^2 + \frac{1}{2} k_{tL} \delta_{tL}^2 \tag{4.23}$$

According to the principle of minimum potential energy, the locator should deform to a position that minimizes the total potential energy of the locator. Therefore, the total potential energy is differentiated with respect to the radial deformation δ_{tL} and is equated to zero to find the deformation following minimum potential energy principle

$$\frac{\partial U}{\partial \delta_{tL}} = k_{aL}\left(\frac{\delta_{sph} - \delta_{tL}\sin\Phi}{\cos\Phi}\right)\left(-\frac{\sin\Phi}{\cos\Phi}\right) + k_{tL}\delta_{tL} = 0 \tag{4.24}$$

The final radial deformation of the locator is calculated by

$$\delta_{tL} = Abs\left[\frac{k_{aL}\delta_{sph}\sin\Phi}{k_{aL}\sin^2\Phi + k_{tL}\cos^2\Phi}\right] \tag{4.25}$$

Here, absolute magnitudes of δ_{tL} is written as it is evident from figure 4.9 that δ_{tL} and the projection of δ_{sph} on XY plane will be in same direction but different in magnitude. Therefore it can be concluded that the sign of δ_{tL} depends upon the sign of the radial component of δ_{sph}. The calculated δ_{tL} will be alloted the same sign as the radial component of δ_{sph} during calculation.

4.4 Potential energy of locators with no friction

The potential energy equations of locators calculated in section 4.2.1 assume the locators to be elastic elements fixed with the baseplate which is against the zero friction assumption of the proposed fixturing system. The earlier equations of locators' potential energies are replaced here by the equations calculated in the section 4.3, using the zero friction assumption, where δ_{tL} and δ_{aL} being the radial and axial components of the locators' deformations. The stiffness matrix of the locator, parallel to z-axis, is defined in the equation 4.21. This stiffness matrix will be transformed using a transformation matrix constructed through the orientation of each locator with reference to the orientation of the locator 1. Similarly the displacement vector of locator 1 (axis parallel to z-axis) is defined to be

$$\{X\}_1 = \{\delta_{tLx}, \delta_{tLy}, \delta_{aL}\}^T \tag{4.26}$$

where, $\delta_{tLx} = \delta_{tL}a_1/\sqrt{a_1^2 + b_1^2}$ and $\delta_{tLy} = \delta_{tL}b_1/\sqrt{a_1^2 + b_1^2}$ with a_1 and b_1 are the x and y components of first normal vector n_1. The transformation of $\{X\}_i$ is performed for each locator to obtain a displacement vector as a function of workpiece displacement parameters $\{\Delta X_P, \Delta Y_P, \Delta Z_P, \Delta\beta, \Delta\gamma, \Delta\alpha\}^T$. Similarly the plucker displacement is also a function of these six parameters. That give us

the potential energy of each of the locator using the equation 4.2 with only six unknowns.

In contrast, the clamps are assumed to be fixed at the baseplate with no slippage, so the equation 4.17 is valid for the potential energy calculation for the clamps. The rest of the calculation is same as detailed in section 4.2.5 to calculate the displacement of the workpiece.

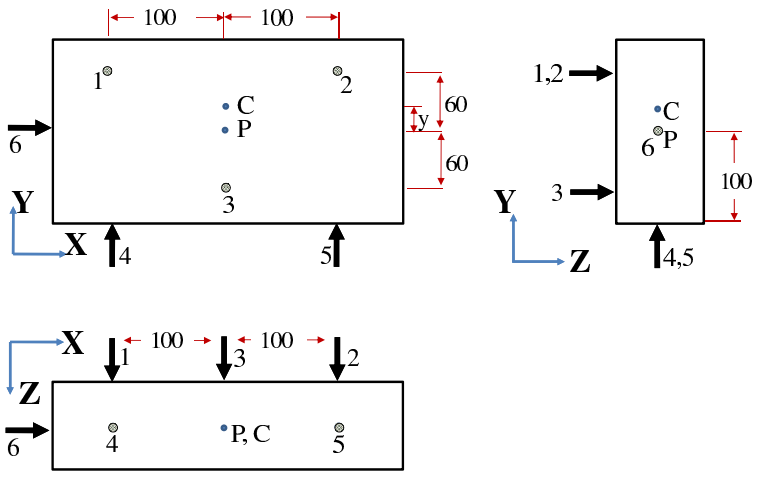

Figure 4.10: Positions of the locators on the baseplate

A simple example is demonstrated for the validation of the proposed mechanical model. A baseplate with six locators is shown in figure 4.10 with point P being the center of mass of the baseplate. For simplicity, no clamp is used and only a 50N vertical downward force is applied at the centroid (C) of the triangle formed by three locators on the primary plane. Locators are assumed to be having three dimensional stiffness. With no friction hypothesis and the centroid being the point of action of vertical force, all the three locators should deform at an equal amount and the only possible displacement of the baseplate would be in z-direction and the remaining 5 displacements (x, y , β, γ, α) should be zero. The coordinates of the point C(x_C, y_C) are calculated by

$$x_C = \frac{-100 + 100 + 0}{3} = 0$$
$$y_C = \frac{60 + 60 - 60}{3} = 20mm$$

The point C(0, 20) is chosen as the point of action of force and the displacement of the baseplate is calculated.

Table 4.1: Displacements of baseplate under static load at point C

Parameter	Point of action of force		
	C(0, 19)	C(0, 20)	C(0, 21)
Δx_P	0	0	0
Δy_P	0	0	0
Δz_p μm	$-1.9E^{-2}$	$-1.8E^{-2}$	$-1.8E^{-2}$
$\Delta\beta$ μrad	$-5.6E^{-3}$	0	$5.6E^{-3}$
$\Delta\gamma$	0	0	0
$\Delta\alpha$	0	0	0

For demonstration, two points are chosen at 1mm on both sides of the point C. It is clear from the table 4.1 that at point C(0, 20) the baseplate is experiencing only vertical displacement while displacement of angle β is negligible. At both points on each side of centroid, displacement of β is same but opposite in direction, this result validates the mechanical model. It can also be concluded that besides calculating the displacement of the baseplate, this mechanical model can also help the user to place the locators according to the position of the applied load.

4.5 Elastic contacts

In the previous sections, the deformation of the locators is calculated under load considering the workpiece-baseplate assembly to be rigid and the locators being elastic with no deformation at the contact between the locators and the baseplate surface. All of the deformation of the locators, calculated in the previous section, is due to locator body stiffness only. But the locator-baseplate contact is not rigid in reality, it will experience local deformation under load and the effect of contact

deformation, on total displacement, is significant when the locator is shorter in length or more rigid.

In this section, the baseplate is considered non-rigid at the contacting points. This can cause small displacements at the baseplate-locators contacts. The remaining baseplate is still considered rigid. The overall deformation of each locator will be the deformation of locator (calculated earlier) and the deformation of its contact with the baseplate. Applying Hertz contact theory, the contact of two elastic bodies is considered as the contact of a rigid plane and a sphere having an equivalent elasticity as shown in figure 4.11.

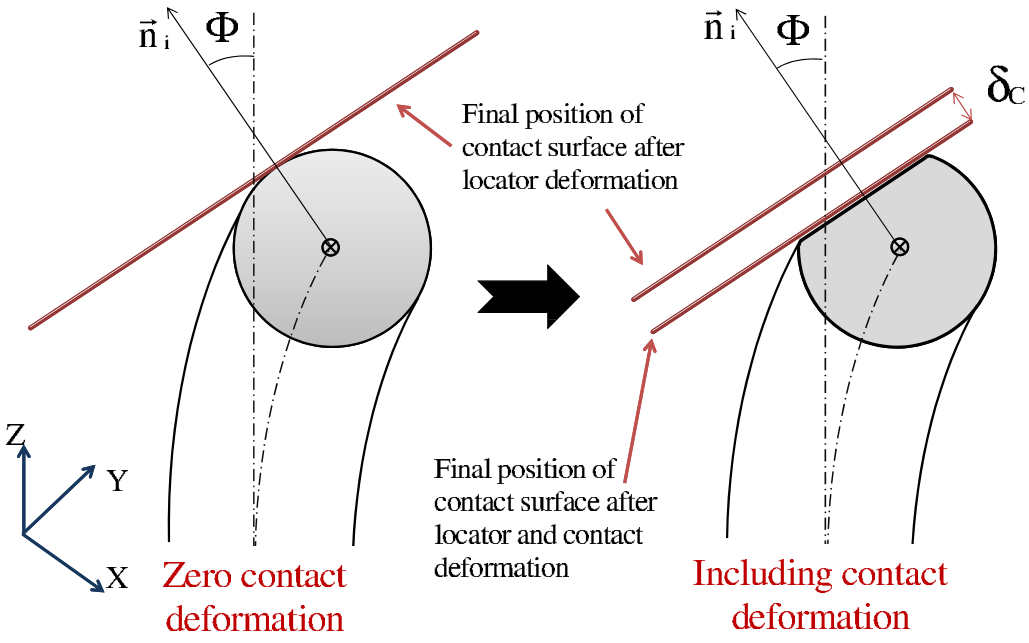

Figure 4.11: Contact deformation of locator

In figure 4.11, contact deformation is added with earlier deformation of the locator of figure 4.9, where the contact deformation δ_C is parallel to the surface normal with $\delta_{aC} = \delta_C \cos\Phi$ and $\delta_{tC} = \delta_C \sin\Phi$ being axial and radial components of contact deformation respectively. For the contact between a plane baseplate and a spherical locator, the maximum deformation will be at the center of the contact area which is given by Hertz contact theory.

4.5.1 Contact deformation

A systematic procedure is explained here to calculate the contact deformation of each locator for ideal Hertzian contact. The deformation of rough contacts will be explained in the next section with roughness to be defined at the start of the algorithm. The convergence of displacement error enables us get a final uniform result. Here, zero friction is assumed between the locator and the baseplate contact.

According to Hertz contact theory, the contact stiffness behaves non-linearly as shown in equation 2.37. The potential energy of a locator, including its contact deformation, can be written as,

$$U = \frac{1}{2}k_{aL}\delta_{aL}^2 + \frac{1}{2}k_{tL}\delta_{tL}^2 + \frac{2}{5}\kappa\delta_C^{5/2} \tag{4.27}$$

where, $\delta_{Plu} = \delta_{sph} + \delta_C$, $\kappa = \sqrt{\frac{16RE'^2}{9}}$, k_{tL} and k_{aL} can be calculated from equation 4.20 while δ_{tL} and δ_{aL} can be found from equations 4.25 and 4.22 respectively as the function of δ_{sph}, Φ, δ_{tL} and δ_{aL}. Following the principle of minimum potential energy, the locator's potential energy (eq. 4.27) is differentiated with respect to δ_C to find the contact deformation following the minimum potential energy principle. By solving the equation for δ_C, we obtain

$$\delta_C = \frac{\delta_{Plu}(k_{aL}k_{tL}(k_{tL}\cos^2\Phi + k_{aL}\sin^2\Phi))}{k_{aL}k_{tL}\cos^2\Phi + \sqrt{\delta_C}\kappa k_{tL}^2\cos^4\Phi + k_{aL}^2k_{tL}\sin^2\Phi + 2\sqrt{\delta_C}\kappa k_{aL}k_{tL}\cos^2\Phi\sin^2\Phi + \sqrt{\delta_C}\kappa k_{aL}^2\sin^4\Phi} \tag{4.28}$$

This equation is solved iteratively to obtain the contact deformation of each locator for their respective δ_{Plu}. To calculate the linearized stiffness of each contact, the force vector acting on each of the locator is calculated. For the contact and the body stiffness being in series, same amount of force will be acting on the contact as on the locator. The force causing the overall deformation $\{\delta\}$ in i^{th} locator having a stiffness matrix of $[K]$, is calculated using equation 4.29. Equation 4.28 calculates the non-linear Hertz contact deformation which enables us to calculate the equivalent linearized contact stiffness for each locator using equation 4.30. Deformation of each locator's body $\{\delta_L\}$ is the function of contact

deformation ($\delta_{Sph} = \delta_{Plu} - \delta_C$), Therefore equation 4.31 can be used to calculate the new body stiffness of each locator.

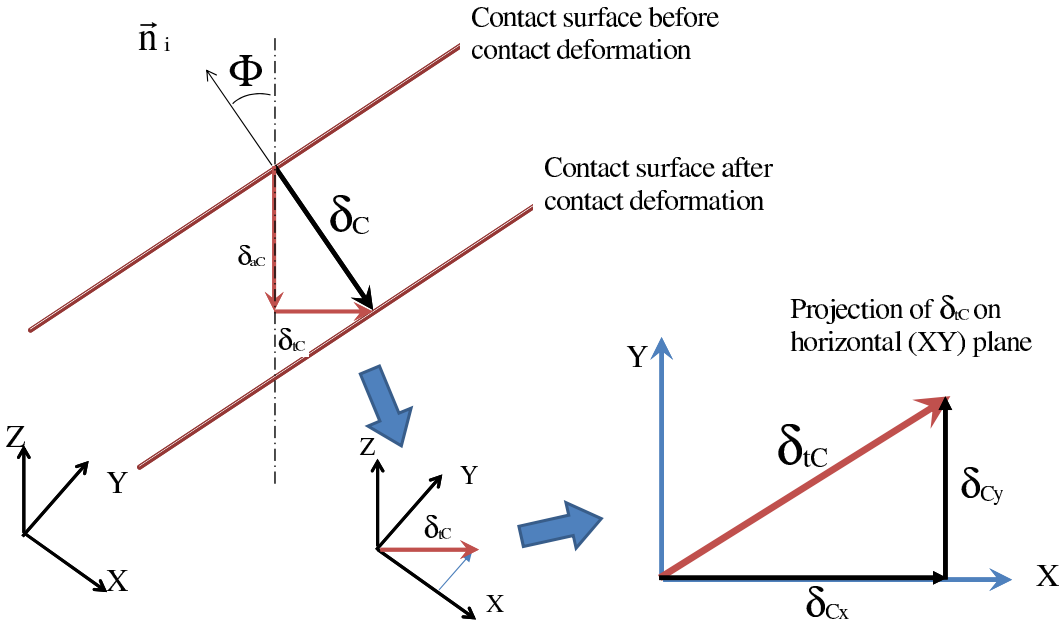

Figure 4.12: Projection of contact deformation on X, Y and Z plane for a Z-axis locator

$$\{F\}_i = [K]_i\{\delta\}_i \tag{4.29}$$

$$\kappa\{\delta_C\}_i^{3/2} = \{F_n\}_i \Longrightarrow [K_C]_i = \frac{\{F_n\}_i}{\{\delta_C\}_i^T} \tag{4.30}$$

$$[K_L]_i = \frac{\{F\}_i}{\{\delta_L\}_i^T} \tag{4.31}$$

where, $\{F_n\}_i = (\{F\}_i.\vec{n_i})\times\vec{n_i}$ is the force vector acting on the i^{th} locator normal to the contacting surface. The deformation δ_C is a scalar value calculated normal to the contact surface. It has to be transformed in to vector form in order to continue the calculation process. The projection of calculated contact deformation on X, Y and Z plane is shown in figure 4.12. The final contact deformation vector can be written as;

$$\{\delta_C\}_i = -\delta_C * \vec{n_i} = -\delta_C * \{a_i, b_i, c_i\}^T \tag{4.32}$$

where, $\vec{n_i}$ is the surface normal vector. The negative sign is for the fact that the contact deformation will be opposite to the surface normal.

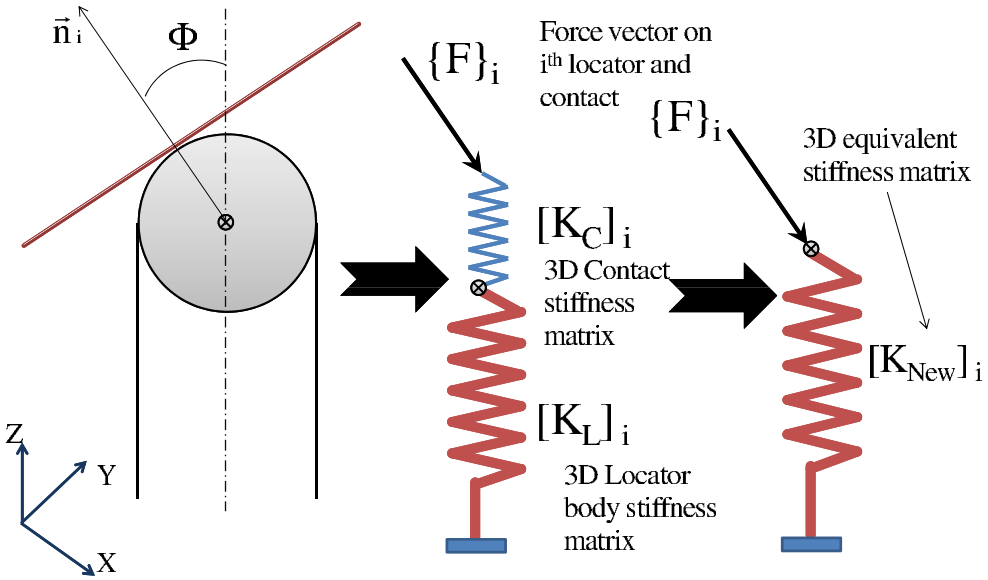

Figure 4.13: Equivalent stiffness matrix $[K_{New}]_i$ representation of locator

4.5.2 Converging overall deformation of each locator

The contact deformation is the function of the force acting on the contact surface and changes non-linearly with the change in force. Therefore, contact deformation cannot be calculated directly without linearizing. In order to linearize the non-linear behavior of the contact deformation, a closed loop calculation is performed. Once the deformation vector $\{\delta_C\}_i$ and contact stiffness matrix $[K_C]_i$ are calculated for each locator, they are added with the locator's body deformation vector $\{\delta_L\}_i$ and stiffness matrix $[K_L]_i$ by taking $[K_C]_i$ and $[K_L]_i$ in series. Thus the overall deformation vector $\{\delta_{New}\}_i$ and overall stiffness matrix $[K_{New}]_i$ for each locator is obtained as shown in figure 4.13. $\{\delta_{New}\}_i$ is compared with the overall deformation vector $\{\delta\}_i$ for each locator calculated in the preceding iteration. If the difference in the deformation is more than the predefined limit, the

calculation is re-performed by substituting the newly calculated stiffness matrix $[K_{New}]_i$ as the base stiffness matrix for each locator. For the next calculation loop, the resultant contact deformation will be closer to the former one and the error will reduce. The loop is continued till the error comes within the allowed error limit. This maximum error limit should be defined in the global data definition of our algorithm. The flow diagram for linearizing the contact deformation, till the required precision is attained, is shown in the flow chart in figure 4.14, where the kinetic energy and work done remain unchanged and can be calculated from figure 4.8.

4.5.3 Convergence gain

As mentioned earlier, the convergence error is obtained while comparing the displacement vector $\{\Delta X\}$ calculated through the Lagrangian equation with the displacement vector $\{\Delta X_{New}\}$ calculated at the end of each iteration.The algorithm shows the oscillation while converging quickly. Therefore, a convergence gain is introduced in flow chart of figure 4.14 on the displacement vector. The displacement vector, after the introduction of gain, can be written as;

$$\{\Delta X\} = \{\Delta X_{New}\} + gain * [\{\Delta X\} - \{\Delta X_{New}\}] \tag{4.33}$$

where, $\{\Delta X\} = \{\Delta X_P, \Delta Y_P, \Delta Z_P, \Delta\beta, \Delta\gamma, \Delta\alpha\}^T$ is the displacement vector of the workpiece-baseplate assembly. The above equation gives $\{\Delta X\} = \{\Delta X\}$ for the gain value of 1. The convergence speed can be controlled by adjusting the gain value. The gain can be applied separately to each element of the displacement vector $\{\Delta X\}$, but here for simplicity, a single gain value is used for all the elements. The effect of gain on the convergence will be discussed at the end of case study.

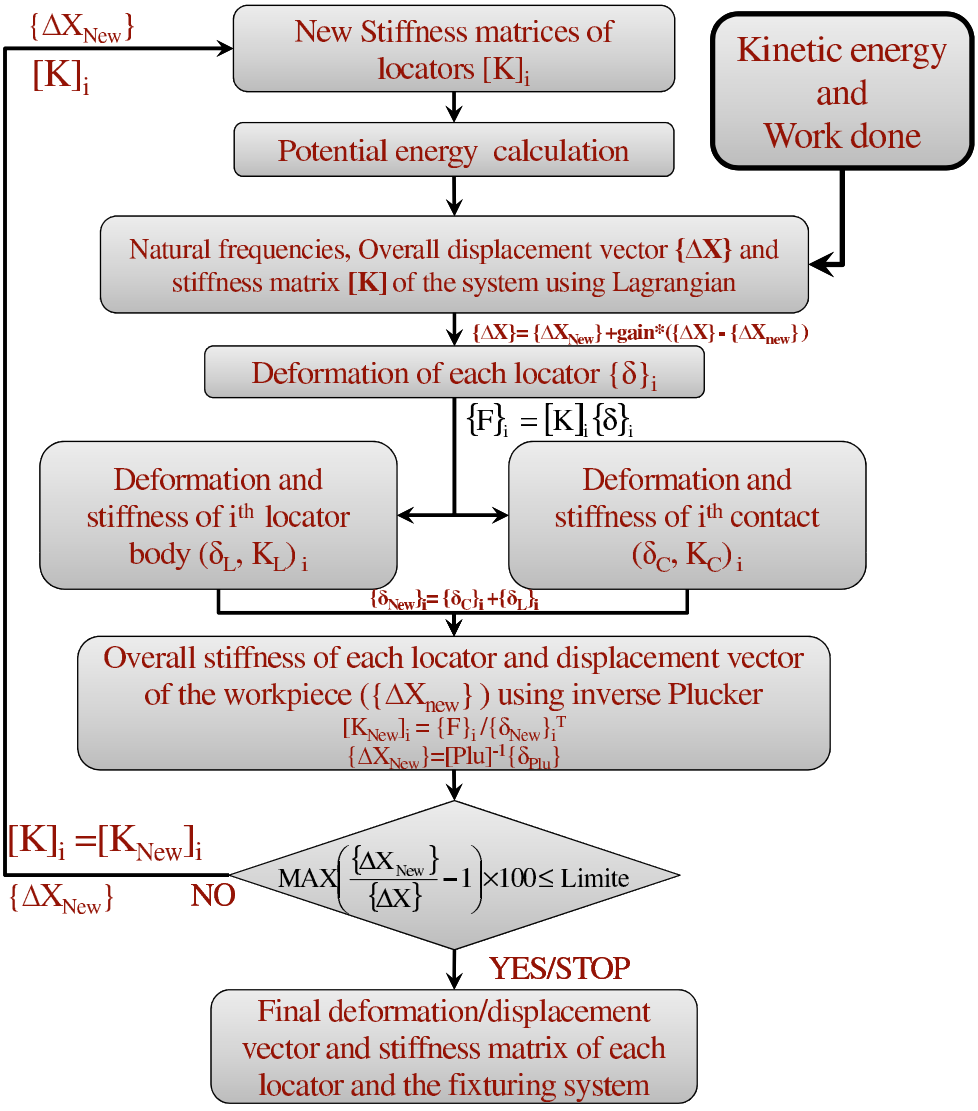

Figure 4.14: Deformation convergence flow chart

4.6 Rough elastic contacts

In the previous section, the stiffness and deformation of ideal elastic contacts and their effect on the overall stiffness of the system and the deformation of the workpiece is detailed. This section deals with the deformation and stiffness of the rough contacts between the locators and the baseplate. The maximum contact deformation will be at the center of the contact which is formalized by

Bahrami *et al.* (2005) for rough contacts as detailed in section 2.5.3.

The model of Bahrami involves testing of P_0' (eq. 2.34) for calculating non-dimensional contact area from pressure distribution which is time consuming. Therefore, a single analytical equation for the non dimensional contact area (eq. C.1) as well as beta function approximation (for the calculation of the contact deformation dedicated for very small values of γ) are proposed in appendix C.

4.6.1 Effect of roughness on contact stiffness and deformation

Contact stiffness is detailed in section 2.5.4 with $k_C = \frac{3}{2}\kappa\sqrt{\delta_C}$, where δ_C is the function of applied force and the roughness (σ) of the contact surface while Hertz deformation is independent of surface roughness. To visualize the effect of roughness on surface stiffness and contact deformation, the graphs of theoretical stiffness of rough surface to Hertz stiffness and rough surface deformation to Hertz deformation are plotted against roughness (σ) of contact for different values of forces acting on the contact as shown in figures 4.15 and 4.16 respectively. For realistic values, the range of roughness [1] $0.4\mu m \leq \sigma \leq 150\mu m$ is used for each value of force 10^j N, where j=-2,-1,...5.

Real to Hertz contact stiffness ratio can be written as the real to Hertz deformation ratio from equation 2.38 as

$$\frac{k_C}{k_H} = \sqrt{\frac{\delta_C}{\delta_H}}$$

Therefore, contact stiffness and deformation show similar trend with respect to Hertz stiffness and deformation under same applied load as shown in figures 4.15 and 4.16 where the stiffness and deformation being reduced as compared to the values obtained by Hertz with the increase in the contact roughness. For the same surface roughness, relative contact stiffness and deformation are directly related to applied load. The quality of the contacting surface has to be chosen according to the operating conditions as the contact deformation causes the geometrical deviation of the workpiece. After a value, unnecessarily extra finished surface will

[1] σ: Average roughness of the contacting surface, R_a

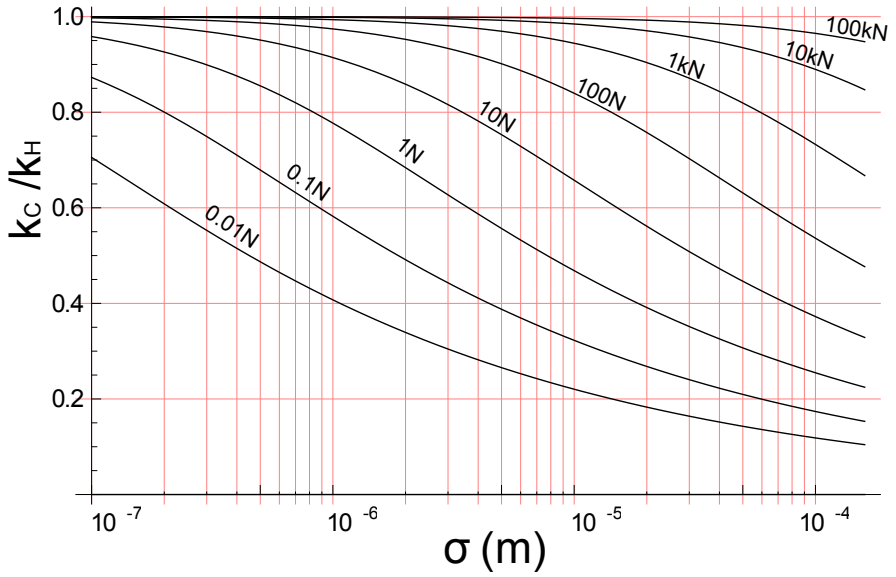

Figure 4.15: Effect of contact's roughness on its relative stiffness for different applied loads

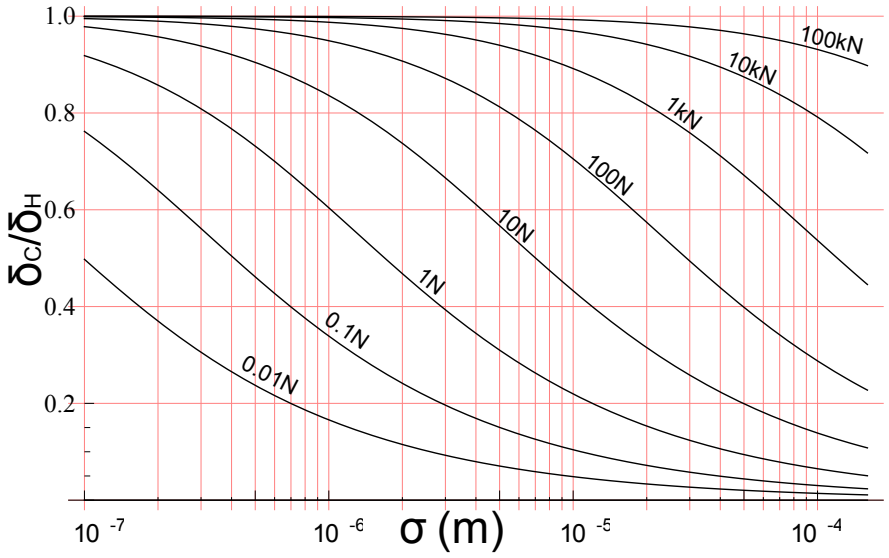

Figure 4.16: Effect of contact's roughness on its relative deformation for different applied loads

not have any necessary influence on the geometrical deviation. If the stiffness, that the part should exhibit to allow acceptable deformation under machining forces, is known then an "economic roughness" can be defined in order to avoid machining of unnecessary superfine surface.

4.6.2 Deformation of rough contacts

The contact deformation, calculated section 4.5.1, is valid for the ideal Hertzian contact only and not for the rough contact between the workpiece/baseplate and the locator. Therefore, the formalization of contact mechanics is used here to calculate the contact deformation for the ideal Hertzian contact as well as for rough contact. Contact mechanics theory for rough contacts is detailed in section 2.5 while an analytical solution to calculate the deformation at the center of rough contacts is proposed in Appendix C.

To calculate the contact deformation, the force normal to the contacting surface ($F = \{F\}_i.\vec{n}_i$) is used. There are two possibilities while calculating the contact deformation. In case of ideal contact with no roughness, Hertzian contact theory may be applied. Contact deformation can be calculated using equation set of table 4.2.

Table 4.2: Equation set for calculating the deformation of Hertzian ideal contact

Calculation Step	Equation
1 Hertz contact area	$a_H = \left(\frac{3F\rho}{4E'}\right)^{1/3}$
2 Contact deformation at r=0	$\delta_H = \frac{{a_H}^2}{\rho} = \left(\frac{9F^2}{16\rho E'^2}\right)^{1/3}$

Once the contact deformations for all the locators are known, the stiffness matrices of that contact and locator are calculated using equations 4.30 and 4.31, which should give the same result as in section 4.5.1. This is due to the fact that both the calculations are performed for the ideal contacts. The advantage of developing the later method is that the similar approach is used to calculate the deformation for the rough locator-baseplate contact, therefore the algorithm becomes uniform and flexible.

In case when the surface roughness is also taken into account, the Hertzian contact theory will no longer be valid. Therefore, the contact deformation has to be calculated using the equations developed in Appendix C for the contact between a rigid sphere of equivalent radius having zero roughness and a rough elastic plane having equivalent modulus of elasticity and equivalent roughness as

explained in section 2.5. The deformation of the contact between rough surfaces can be calculated by using the equation set shown in table 4.3. The contact deformation vector can be deduced from equation 4.32 as explained earlier.

Table 4.3: Equation set for calculating the deformation of rough contact

	Calculation Step	Equation
1	Roughness parameter	$\alpha = \sigma\rho/a_H^2$
2	First non-dimensional parameter	$\tau = \frac{E'}{H_{mic}}\sqrt{\frac{\rho}{\sigma}}$
3	Non-dimensional pressure distribution	$P_0' = \frac{1}{1+1.22\ \alpha\ \tau^{-0.16}}$
4	Non-dimensional contact radius	$a_L' = 1.631\ {P_0'}^{-0.496} - 0.631\ {P_0'}^{3.358}$
5	General pr. distribution exponent	$\gamma = 1.5 P_0' {a_L'}^2 - 1$
6	Area of rough contact	$a_L = a_L' a_H$
7	Max contact pressure	$P_0 = (1+\gamma)F/(\pi a_L^2)$
8	Estimated Gamma function	$\Gamma(b+1) = a_1(b+a_2)^{b+a_2}\left(1+\frac{a_3}{a_4+b^{a_5}}+\frac{a_6}{b^{a_7}+a_8}\right)e^{-b^{a_9}}\sqrt{2\pi}$
9	Estimation of beta function	$B(0.5,\gamma+1) = \frac{\Gamma(1/2)\Gamma(\gamma+1)}{\Gamma(\gamma+1.5)}$
10	Contact deformation at r=0	$\delta_C = \frac{P_0 a_L}{E'} B(0.5,\gamma+1)$

This mechanical model is capable of calculating the contact deformation for the ideal case of Hertzian contact as well as for the rough surface contacts. The total deformation of locator will be the sum of locator body deformation and its contact deformation. The proposed algorithm calculates the overall displacement vector of the workpiece-baseplate assembly, stiffness and mass matrices of the fixturing system and its vibrations modes.

4.7 Case Study

In this section, a case study is performed on a fixturing system to explain the working and findings of the proposed mechanical model. A fixturing system, having six locators and two clamps, considered as three dimensional springs, is shown

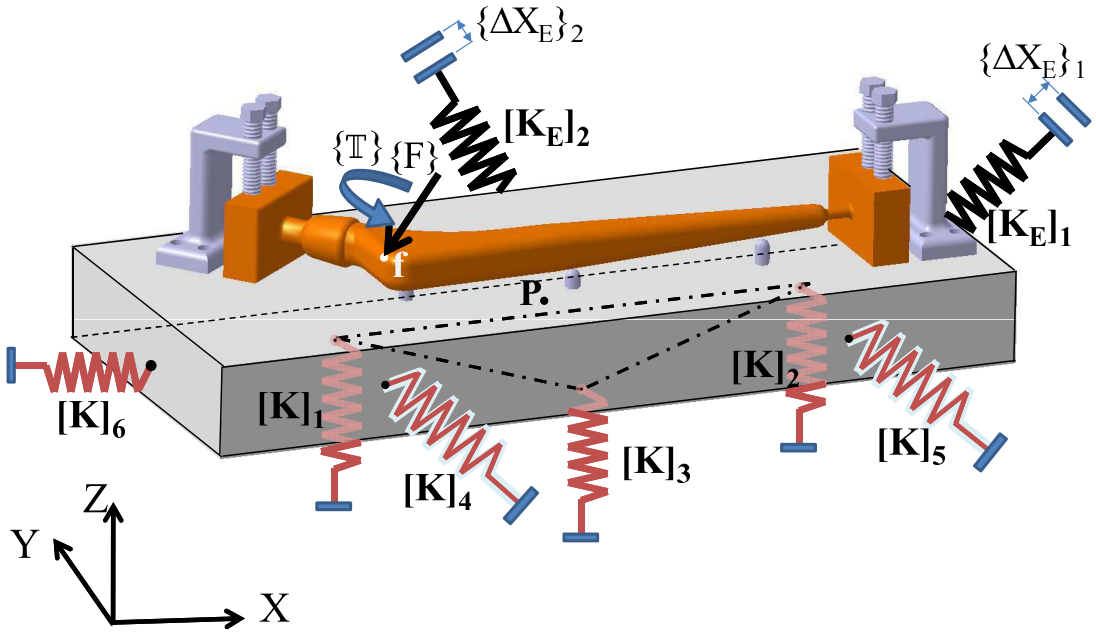

Figure 4.17: Representation of the fixturing system as spring mass system

in figure 4.17. $\{F\}$ is taken as machining force at any point on the workpiece, $\{\mathbb{T}\}$ is the moment of cutting tool, $[K_E]_1$ and $[K_E]_2$ are the stiffness matrices of clamps, $\{\Delta X_E\}_1$ and $\{\Delta X_E\}_2$ are the external displacements of clamps and $[K]_1, [K]_2, ...[K]_6$ are the stiffness matrices of the locators.

4.7.1 Data input

The baseplate is considered to be inclined initially at small angles α_B, β_B and γ_B which can be calculated through the initial positions of the locators. The locators are placed at fixed lateral positions on the machine and can only move axially. Initial advancement of each locator is taken randomly so that the baseplate remains inclined. The initial positions of the center of the contacting sphere of each locator is shown in figure 4.18 and are written in table 4.4.

Three planes of the baseplate can be obtained by the position of each locator as explained in section 3.3.1, where the position of each locator is measured at the center of contacting arc of each of the locator. The position of each locator allows us to calculate the three surface normals which can be expressed in a matrix form

Table 4.4: Initial positions of the center of contacting sphere of all six locators

Locator no	x (mm)	y (mm)	z (mm)
1	70	100	23
2	180	100	22
3	120	40	21
4	70	8	60
5	180	10	60
6	14	60	60

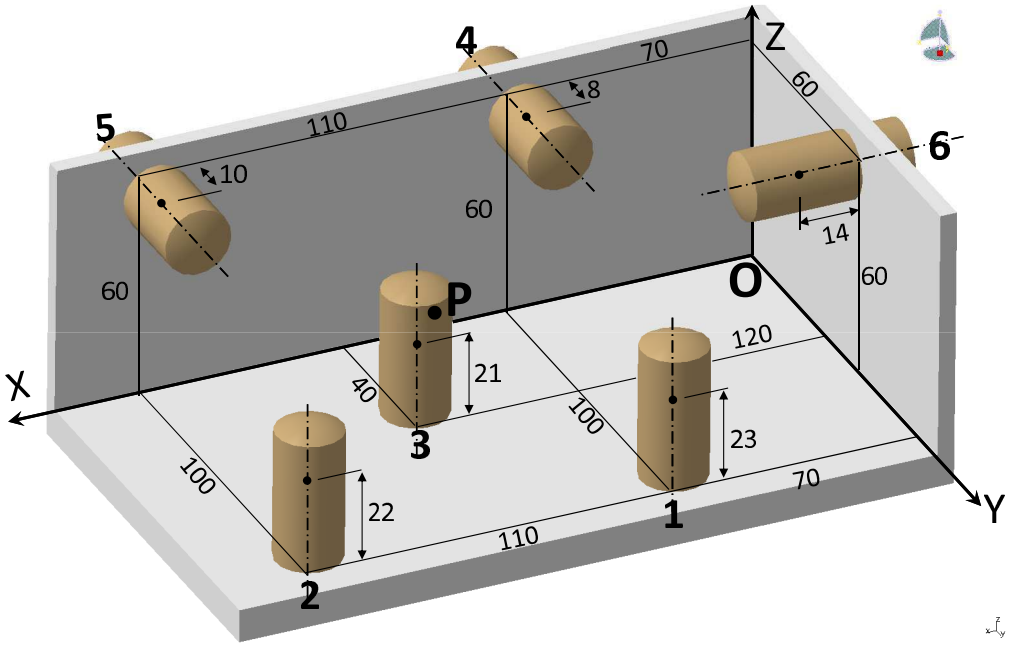

Figure 4.18: Position of all the locators in machine coordinate system

and is equal to the YPR [1] transformation matrix of the baseplate with respect to machine coordinate "O" as written in equation 4.34.

[1]YPR: Yaw (α_B), Pitch (β_B), Roll (γ_B)

$$\begin{bmatrix} \cos\alpha_B\cos\gamma_B - \sin\alpha_B\sin\beta_B\sin\gamma_B & -\sin\alpha_B\cos\beta_B & \cos\alpha_B\sin\gamma_B + \sin\alpha_B\sin\beta_B\cos\gamma_B \\ \sin\alpha_B\cos\gamma_B + \cos\alpha_B\sin\beta_B\sin\gamma_B & \cos\alpha_B\cos\beta_B & \sin\alpha_B\sin\gamma_B - \cos\alpha_B\sin\beta_B\cos\gamma_B \\ -\cos\beta_B\sin\gamma_B & \sin\beta_B & \cos\beta_B\cos\gamma_B \end{bmatrix} = \\ = \begin{bmatrix} a_3 & a_2 & a_1 \\ b_3 & b_2 & b_1 \\ c_3 & c_2 & c_1 \end{bmatrix} \tag{4.34}$$

where subscript B with the angles shows the baseplate rotation angles while $\{n_1\} = \{a_1, b_1, c_1\}^T$, $\{n_2\} = \{a_2, b_2, c_2\}^T$ and $\{n_3\} = \{a_3, b_3, c_3\}^T$ are the unit vectors of the primary, secondary and tertiary plane of the baseplate respectively. These normals can be calculated by the position of the locators as explained in section 3.3.1. Equation 4.34 gives three initial rotation angles α_B, β_B and γ_B of the baseplate which are shown in table 4.5.

Table 4.5: Baseplate angles calculated from the locators' positions

Angle	degree
α_B	1.039
β_B	1.485
γ_B	0.494

Here, the locators are assumed to be having arc radius of 20mm, therefore the actual surfaces will be at an offset of 20mm from the measured planes in the direction of surface normal. The final contacting point of each locator will change at an amount $20 * a_i$, $20 * b_i$ and $20 * c_i$ in x, y and z direction respectively. Therefore, the position of each contacting point obtained from table 4.4 and normals of equation 4.34 is written in table 4.6.

Table 4.6: Contacting points of all the locators

Locator no	x (mm)	y (mm)	z (mm)
1	70.18	99.49	42.99
2	180.18	99.49	41.99
3	120.18	39.49	40.99
4	69.64	27.99	60.52
5	179.64	29.99	60.52
6	34	60.37	59.83

All of the calculation is performed according to center of mass of the baseplate therefore, the position of the center of mass of the baseplate is measured in CATIA® which is found to be P(143.619, 79.521, 54.315)mm. This position is shown as point P in figure 4.18. The distance of contacting point of each locator from the center of mass of the baseplate is calculated by subtracting the position of contacting point of each locator (tab. 4.6) from the position of point P, and is written in table 4.7.

Table 4.7: Positions of each locator with respect to the center point P

Locator	$X_p - X_i$(mm)	$Y_p - Y_i$(mm)	$Z_p - Z_i$(mm)
1	73.44	-19.96	11.32
2	-36.56	-19.96	12.32
3	23.44	40.04	13.32
4	73.98	51.53	-6.20
5	-36.02	49.53	-6.20
6	109.62	19.15	-5.51

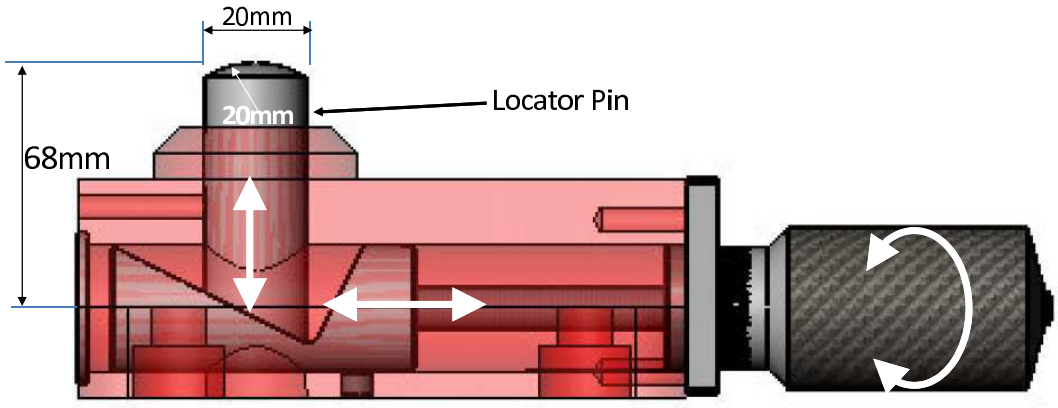

Figure 4.19: Screw-nut controlled wedge-slope locator

A model of a locator has been developed as shown in figure 4.19 having the locator diameter of 20mm, the radius of contacting arc as 20mm and axial length of 68mm. Stiffness matrix of a locator 1 is taken as,

$$[K]_i = \begin{bmatrix} k_{tL} & 0 & 0 \\ 0 & k_{tL} & 0 \\ 0 & 0 & k_{aL} \end{bmatrix} \tag{4.35}$$

where, radial (k_{tL}) and axial (k_{aL}) locator stiffness can be calculated using equation 4.20. k_{aL} will remain the same while k_{tL} varies with the advancement of locator pin. All the locators are similar, so the stiffness matrix will be same but only the components of the stiffness matrices will interchange for each locator according to the orientation of that locator with reference to locator 1. The orientation of each locator with reference to locator 1 is shown in table 4.8. New stiffness matrix for each locator is calculated within the algorithm from these orientations and the original stiffness matrix of locator 1. These new stiffness matrices are used for the calculation of the potential energy of each locator.

Table 4.8: Orientation of each locator with reference to locator 1

Locator no.	α_L (deg)	β_L (deg)	γ_L (deg)
1	0	0	0
2	0	0	0
3	0	0	0
4	0	-90	0
5	0	-90	0
6	0	0	90

For the mass and inertia matrices of the system, CATIA® model is used. The mass elements of the fixturing system include baseplate, workpiece, locators between the baseplate and workpiece and workpiece clamps as shown in figure 4.17. All of these elements are chosen to be made of steel with a density of 7850kg/m^3 and, their mass and inertia matrices of the workpiece-baseplate assembly are obtained through CATIA® model which are written in equation 4.36.

$$[M] = \begin{bmatrix} 4.318 & 0 & 0 \\ 0 & 4.318 & 0 \\ 0 & 0 & 4.318 \end{bmatrix} kg \tag{4.36}$$

$$[I] = \begin{bmatrix} 0.004 & -2.55E^{-4} & 1.50E^{-4} \\ -2.55E^{-4} & 0.018 & -8.46E^{-5} \\ 1.50E^{-4} & -8.46E^{-5} & 0.021 \end{bmatrix} kg - m^2$$

The obtained inertia matrix is the inertia of all the mass elements at point P of the baseplate along the global machine coordinates. The clamps have to be

placed on the baseplate so that they oppose the locators. The position of each clamp is measured in CATIA®, and their position with reference to the center of mass of the baseplate is calculated as shown in table 4.9.

Table 4.9: Positions of each clamp with respect to the center of mass P of the baseplate

Clamp no.	$X_p - X_C$ (mm)	$Y_p - Y_C$(mm)	$Z_p - Z_C$(mm)
1	0.80	-49.65	-13.80
2	-110.09	-1.7	-11.55

In this case study, clamps are assumed to be springs having unidirectional axial stiffness ($k_{E1} = k_{E2} = 9 * 10^8\ N/m$) and the external displacement of both of the clamps are taken as $\Delta X_{E1} = \Delta X_{E2} = -0.25mm$. Both the clamps are supposed to be inclined at 14.6 degree angles with horizontal. The external displacement vectors for clamps become,

$$\{\Delta X_E\}_1 = \begin{Bmatrix} 0 \\ -2.42 \\ -0.63 \end{Bmatrix} * 10^{-4}m, \quad \{\Delta X_E\}_2 = \begin{Bmatrix} -2.42 \\ 0 \\ -0.63 \end{Bmatrix} * 10^{-4}m$$

The algorithm calculates the energy contained by clamps from the stiffness, external displacement and the position of each clamp. In this study, end milling operation is chosen as the machining operation to be performed on the prosthesis. A common material used for the fabrication of the hip prosthesis is X4CrNiMoN21-9-4 with the common name of M30NW. The closest material found in Sandviken (2011) is M3.2.C.AQ having σ = 880MPa, $k_{c1} = 2200N/mm^2$ and $m_c = .25$, while the machining parameters are:

Tool : CoroMill 216 ball nose endmill of 3mm diameter
a_p : 0.5 mm
f_z : 0.03 mm
n : 8000 RPM
σ_{Max} : 88 dN/mm^2
Ψ_r : 15 degree

The forces vector $\{F\} = \{-89.75, -60, -24\}^T$N and torque vector $\mathbb{T} = \{0, 0, -0.09\}^T$Nm are calculated using the formalization from section 2.4 for the

tool angle of 0 degree. A point f(89.9, 59.19, 80.32)mm is chosen on the workpiece (from CATIA model) as the point of action of force and torque at time t. The position of force with reference to the center of mass of the baseplate is shown in table 4.10.

Table 4.10: Point of action of force with respect to the center of mass P of the baseplate

Force no.	$X_P - X_F$ (mm)	$Y_P - Y_F$(mm)	$Z_P - Z_F$(mm)
1	53.72	20.33	-26.01

4.7.2 Data output

The mass and stiffness matrices of the system are obtained from calculation carried out in Mathematica®. The baseplate rotates due to compliance of the spring, so the terms with angles appear in mass matrix calculation. These terms can be neglected as the displacements are assumed to be small. Total potential energy is the sum of potential energies of all the locators and clamps, and it gives the overall stiffness matrix of the fixturing system. The final stiffness matrix of the fixturing system is given in equation 4.37. The algorithm also calculates the work done by the external applied force and gives the six degree displacement of the workpiece-baseplate assembly, using Lagrangian formulation, as shown in table 4.11.

$$[K] = \begin{bmatrix} 272.13 & -1.7 & 1.68 & 0.03 & 2.75 & -2.98 \\ -1.7 & 363.96 & -2.31 & -3.66 & -0.06 & 6.2 \\ 1.68 & -2.31 & 453.93 & 4.48 & -4.37 & 0.03 \\ 0.03 & -3.66 & 4.48 & 0.48 & -0.03 & -0.09 \\ 2.75 & -0.06 & -4.37 & -0.03 & 1.78 & -0.05 \\ -2.98 & 6.2 & 0.03 & -0.09 & -0.05 & 1.97 \end{bmatrix} * 10^7 \qquad (4.37)$$

The above calculation is carried out considering only locators' body stiffness and it gives large stiffness and small displacement values. In fact, total stiffness of any locator is the combination of locator's body stiffness and its non-linear contact stiffness. Both stiffness are in series which causes the total stiffness of

Table 4.11: Displacements under static mean load without taking contact deformation into account

Parameter	Displacement
Δx_P	-81.98 μm
Δy_P	-64.50 μm
Δz_p	-19.99 μm
$\Delta\beta$	-241.96 μrad
$\Delta\gamma$	280.47 μrad
$\Delta\alpha$	104.05 μrad

the locator to decrease. The iterative calculation process (sec. 4.5.2) is carried out to calculate the overall stiffness of each locator by linearizing the non-linear locator contact behavior. The overall stiffness of the system, calculated as the result of locators' body and contact stiffness, is shown in equation 4.38 and the workpiece-baseplate displacements are shown in table 4.12.

$$[K] = \begin{bmatrix} 194.95 & -0.43 & 0.18 & 0.01 & 2.35 & -4.35 \\ -0.43 & 218.29 & 0.09 & -2.57 & 0.01 & 8.88 \\ 0.18 & 0.09 & 214.93 & 4.65 & -9.24 & -0.01 \\ 0.01 & -2.57 & 4.65 & 0.28 & -0.02 & -0.11 \\ 2.35 & 0.01 & -9.24 & -0.02 & 1.2 & -0.06 \\ -4.35 & 8.88 & -0.01 & -0.11 & -0.06 & 1.46 \end{bmatrix} * 10^7 \tag{4.38}$$

Table 4.12: Displacements under static mean load taking contact deformation into account

Parameter	Displacement
Δx_P	-100.19 μm
Δy_P	-160.70 μm
Δz_p	-50.14 μm
$\Delta\beta$	-154.41 μrad
$\Delta\gamma$	142.29 μrad
$\Delta\alpha$	840.32 μrad

Three dimensional stiffness matrices are defined for each locator and also the baseplate was inclined therefore,all locators will experience three dimensional

deformation. The deformation of each locator, calculated for the workpiece-baseplate displacement of table 4.12, is written in table 4.13.

Table 4.13: Deformation of each locator

Locator	X(μm)	Y(μm)	Z(μm)
1	-1.09	2.96	-38.02
2	-1.62	4.43	-56.01
3	-0.86	2.35	-36.48
4	7.29	-221.31	-10.54
5	4.82	-129.4	-6.97
6	-87.54	-3.73	1.84

The vibrational modes can be found by solving the equation 4.19 as in Kelly (1996). The calculated pulsation of this example, taking contact stiffness into account, are shown in equation 4.39.

$$\omega = \{34098.7,\ 31139.4,\ 24484.7\ ,21546.7,\ 15649.2,\ 8987.47\}\ rad/sec \quad (4.39)$$

The kinematic model (chapter 3) can be used to relocate the workpiece by eliminating the errors calculated in table 4.12. The advancement of each locator, required to reorient the workpiece-baseplate assembly and having precision of 1μm, is shown in table 4.14. Here it is to note that, the kinematic advancement is calculated with the hypothesis of all the elements to be rigid. So, the mechanical model deformation can be recalculated to see if the error is within the acceptable limit.

Table 4.14: Advancement of each locator to compensate the positioning error

Locator	**Advancement μm**
1	-17
2	75
3	33
4	148
5	168
6	101

From the above results of tables 4.11 and 4.12, it can be observed that the system is more rigid in Z-direction, and least rigid in x-direction if the contact stiffness is not considered. But, while contact stiffness and contact deformation are taken into account, the system became least rigid in y-direction.

By comparing equation 4.37 and equation 4.38, a clear decrease in the overall stiffness (53% for K_{33} which is the stiffness in z-direction) of the fixturing system can be noticed. This decrease in the stiffness causes a significant increase in the rigid body displacement of the workpiece-baseplate assembly. For example in this case study, α is 8 times larger than the one calculated without contact while the displacements in y and z directions are increased by 2.5 times. Therefore the effect of contact stiffness on the precision of the workpiece cannot be neglected.

4.7.3 Effect of gain on convergence

The convergence of each parameter of the workpiece displacement and their convergence errors, with respect to the previous iteration values, are shown in the figure 4.20 and figure 4.21 respectively for the gain of 1. In figure 4.20, the 6 displacement parameters at iteration no 1 correspond to the values without the contact deformation while these parameters at iteration 2 correspond to the values when the contact stiffness is introduced for the first time. At point 2, the deformation of each contact is calculated from the initial force on that locator which causes large contact initial deformation and hence the overall displacement vector increases significantly causing large displacement values and huge initial errors. In figure 4.21, the 1 at x-axis corresponds to the error between iteration 1 and 2 of figure 4.20. In this example, the convergence is attained after 48 iterations. $\Delta\alpha$ is quickest while $\Delta\beta$ is the last parameter to converge to the predefined error limit of 0.01%.

To see the effect of the gain, the convergence and errors of each parameter are plotted for different values of gain. The convergence curves smoothen while reducing the convergence gain and on the other hand the oscillation increase by increasing the convergence gain. After a point, if the gain is further increased, the high oscillation does not allow the system to attain convergence and the system tends toward divergence.

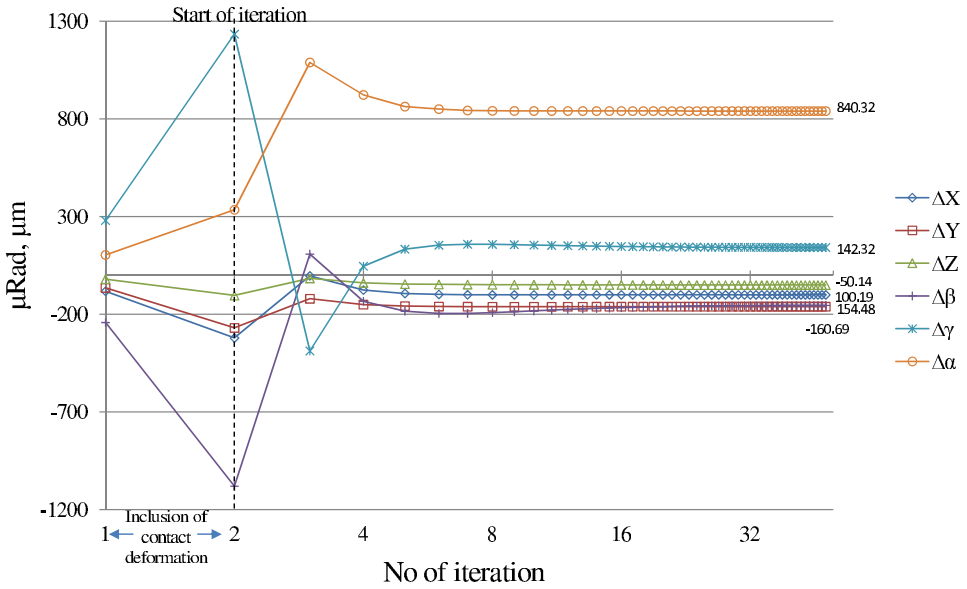

Figure 4.20: Convergence of the six displacement parameters for gain=1

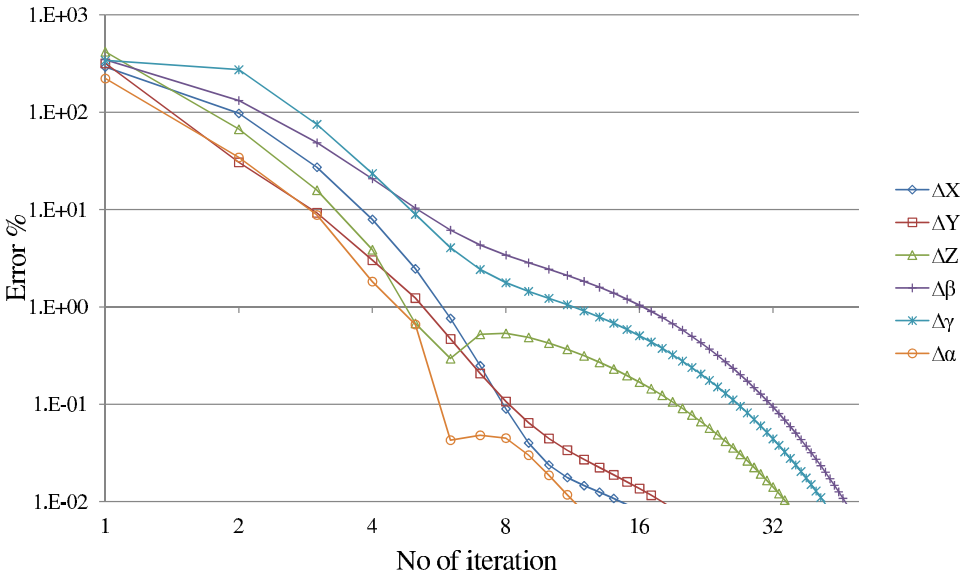

Figure 4.21: Convergence error of the six displacement parameters with respect to the previous iteration for gain=1

Since $\Delta\beta$ is the slowest convergence parameter therefore, it is chosen here for illustration purpose. The convergence of $\Delta\beta$ and its error of convergence, with respect to the previous iteration values are shown in figures 4.22 and 4.23,

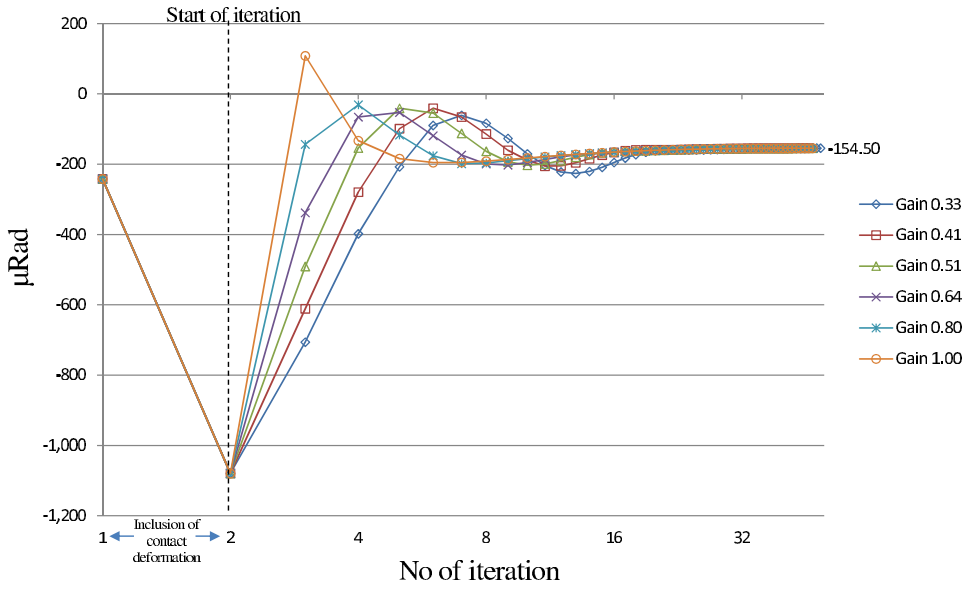

Figure 4.22: Convergence of $\Delta\beta$ for different gains

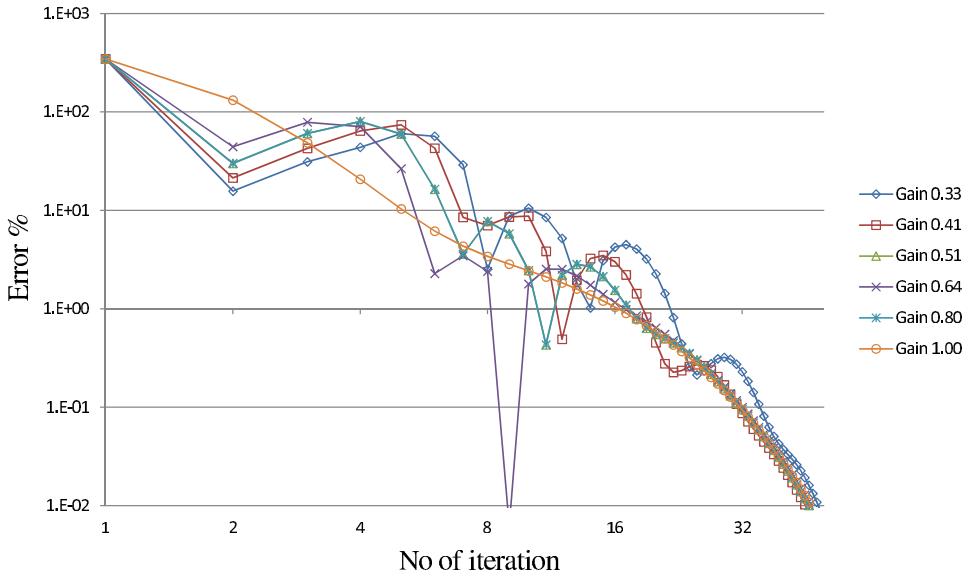

Figure 4.23: Convergence error of $\Delta\beta$ with respect to the previous iteration for different gains

respectively for different values of gain . The absolute convergence error for $\Delta\beta$ is shown in figure 4.24, which is the error of each iteration value with respect to the final value (154.50 μrad). The fastest convergence is attained for gain

of 0.41. The convergence is not smooth due to the coupling among all the six displacement parameters. Moreover, an increase in gain value causes the increase in oscillation. After the gain value of 1.4, the algorithm does not converge due to high oscillations.

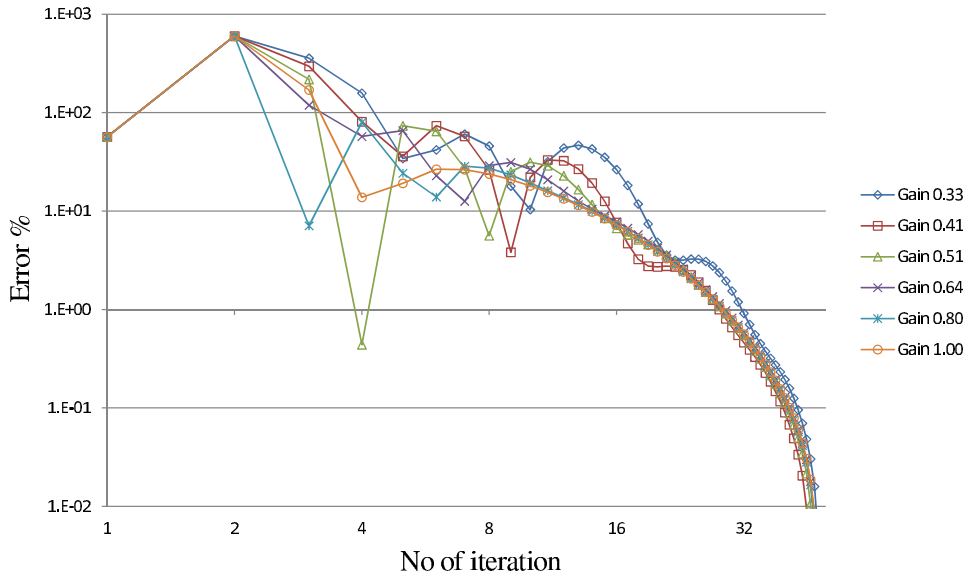

Figure 4.24: Convergence error of $\Delta\beta$ with respect to the final value for different gains

For the comparison with the gain 1, the convergence graphs for the gain=0.51 are shown in figures 4.25. The convergence of the gain=0.51 can be noticed to be smoother than the one with the gain of 1, but it took only two iterations less than the gain=1.

4.7.4 Effect of external displacement of clamps

The effect of gain on the convergence is illustrated with another example here. For this second example, all of the parameters of the case study are kept the same, only the external displacements of the clamps are changed to 0.025mm from 0.25mm (10% of the value). The convergence graph for all of the parameters is shown in figure 4.26 while their convergence errors, with respect to the previous iteration values, are shown in figure 4.27. In this case, $\Delta\gamma$ is the last parameter to

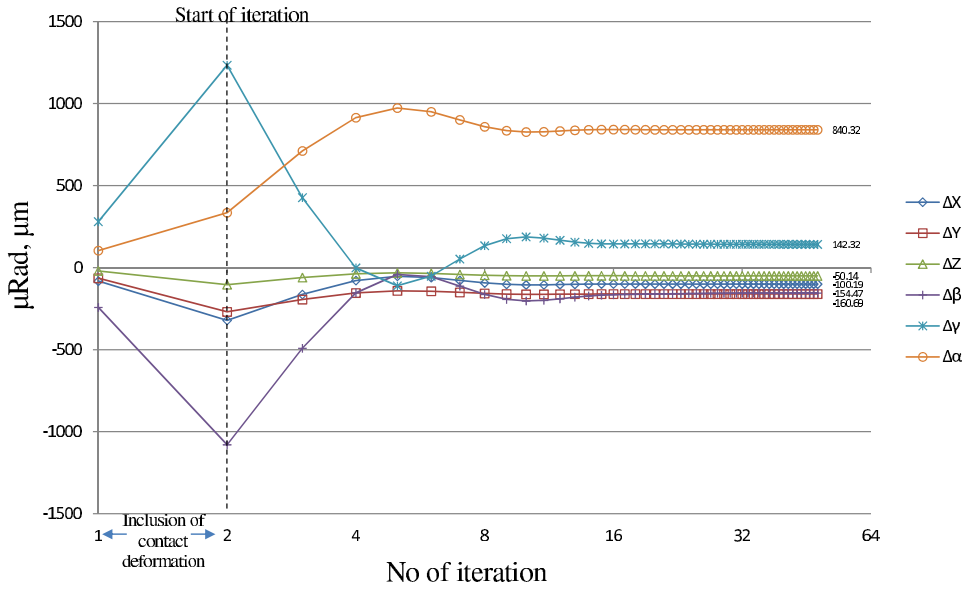

Figure 4.25: Convergence of the six displacement parameters for gain = 0.51

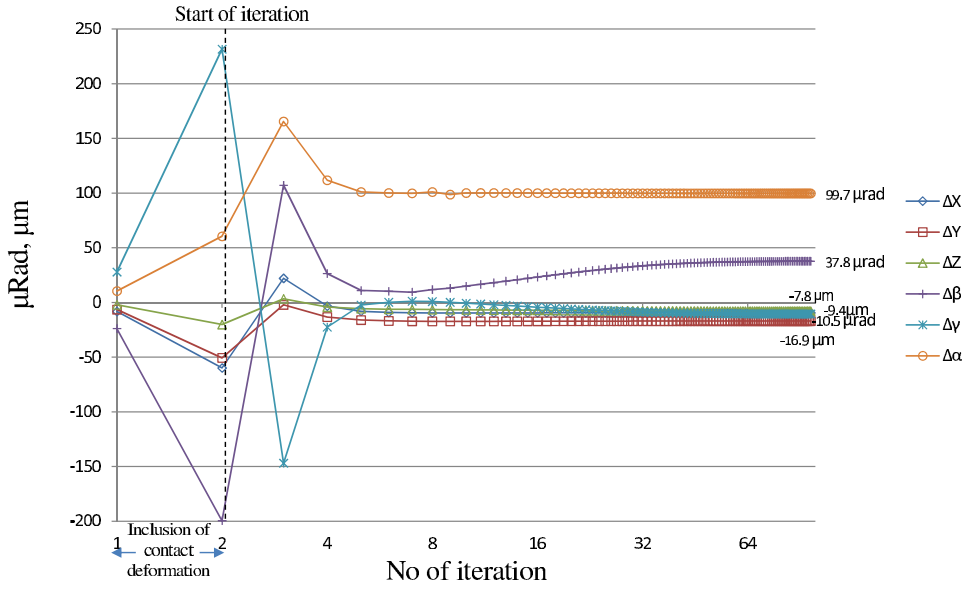

Figure 4.26: Convergence of the six displacement parameters for gain=1 and external displacement=0.025mm

converge whose convergence is shown in figure 4.28 for different gain values. The effect of the gain is noticed in this second example. The algorithm converged in 98 iterations for gain=1. The value reduced to 86 iterations for the gain of 0.64

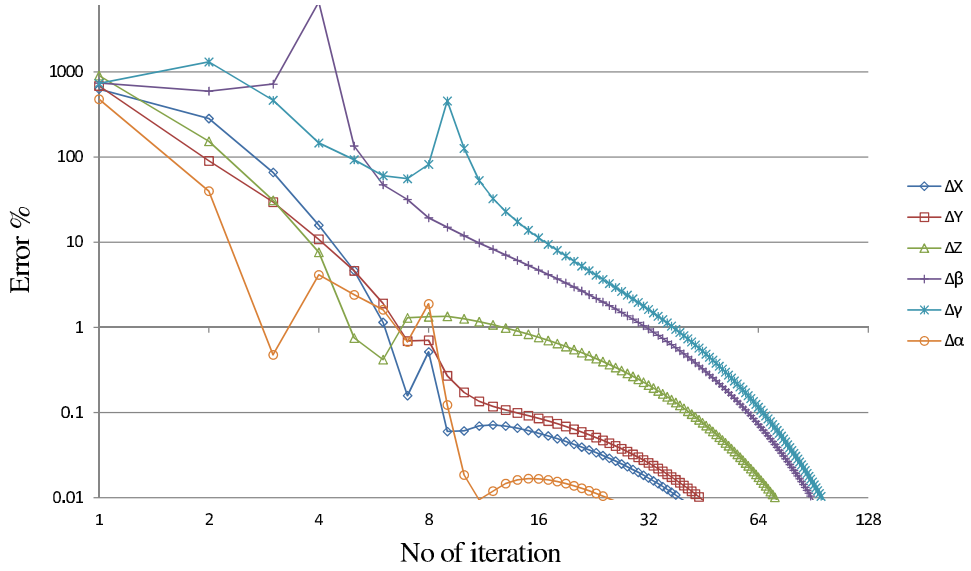

Figure 4.27: Convergence error of the six displacement parameters with respect to the previous iteration for gain=1 and external displacement=0.025mm

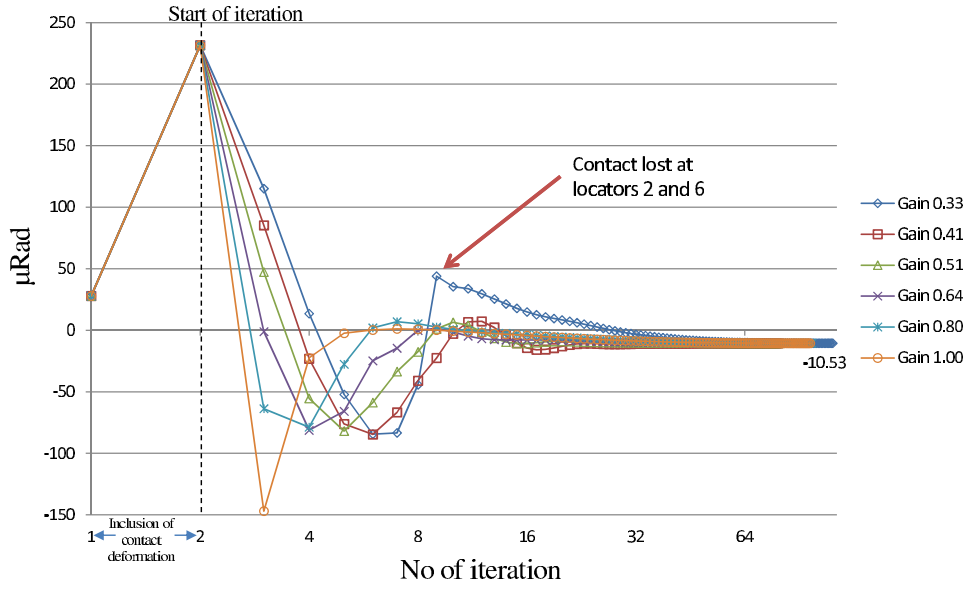

Figure 4.28: Convergence of $\Delta\beta$ for different, external displacement=0.025mm

and 79 iterations for the gain of 0.41. Further reduction of the gain caused the number of iterations to increase. For example, for the gain of 0.33, the algorithm converged to the final result in 112 iterations. A sudden shoot of the curve can be

seen for the gain of 0.33 at 8th iteration. Here, the algorithm showed a message of loss of contact at locators 2 and 6 at the iterations 6, 7 and 8. Generally, the contact loss causes in-equilibrium of the system but, in this case, the system again returned to the equilibrium state after the 8^{th} iteration. The final result was same for all the gain values.

For the comparison with the external clamps displacements of 0.25mm, the overall stiffness matrix of the fixturing system is shown in equation 4.40 where a decrease of the stiffness in all directions, as compared to the previous example, can be noticed.

$$[K] = \begin{bmatrix} 185.42 & -0.19 & 0.1 & 0 & 2.31 & -4.52 \\ -0.19 & 195.81 & -0.03 & -2.4 & 0 & 9.42 \\ 0.1 & -0.03 & 196.9 & 4.59 & -9.47 & 0 \\ 0 & -2.4 & 4.59 & 0.27 & -0.01 & -0.11 \\ 2.31 & 0 & -9.47 & -0.01 & 1.16 & -0.06 \\ -4.52 & 9.42 & 0 & -0.11 & -0.06 & 1.37 \end{bmatrix} * 10^7 N/m \quad (4.40)$$

Due to the reduction in stiffness in all the direction, the pulsation modes will be decreased. The change in the pulsation with the tightening/loosening of the clamps is shown in table 4.15 and the its effect on the workpiece displacement parameters is shown in table 4.16. A huge decrease can be seen in each of the parameter, this is due to the fact that the external displacement is reduces to 10% of its original value (from 0.25mm to 0.025mm).

Table 4.15: Effect of external clamps displacements on systems' pulsation modes

Pulsation	X_E**=0.25mm**	X_E**=0.025mm**	**Decrease**
	(rad/sec)		**(%age)**
ω_1	34098.7	33530.8	1.7
ω_1	31139.4	30769.1	1.2
ω_1	24484.7	23893.8	2.4
ω_1	21546.7	20853.8	3.2
ω_1	15649.2	13663.1	12.7
ω_1	8987.47	6605.06	26.5

Table 4.16: Effect of external clamps displacements on the displacement vector of the workpiece

Parameter	Displacement		Decrease	
	X_E=0.25mm	X_E=0.025mm	μm/μrad	%age
Δx_P	-100.19 μm	-9.944 μm	90.246 μm	90.1
Δy_P	-160.7 μm	-16.95 μm	143.75 μm	89.5
Δz_p	-50.14 μm	-7.83 μm	42.31 μm	84.4
$\Delta\beta$	-154.41 μrad	37.76 μrad	192.17 μrad	124.5
$\Delta\gamma$	142.29 μrad	-10.53 μrad	152.82 μrad	107.4
$\Delta\alpha$	840.32 μrad	99.75 μrad	740.57 μrad	88.1

4.7.5 Effect of rough contacts on the fixturing system

The effect of roughness of the contacting surface on the contact stiffness is studied in section 4.6.1, where the stiffness of the rough contact decrease with the increase of the surface roughness or decrease of the force normal to the contact. The decrease in the stiffness of the contact causes the decrease in the overall stiffness of the system. Here, the baseplate is considered rough having the roughness $\sigma = 0.8\mu m$ as shown in figure 4.29.

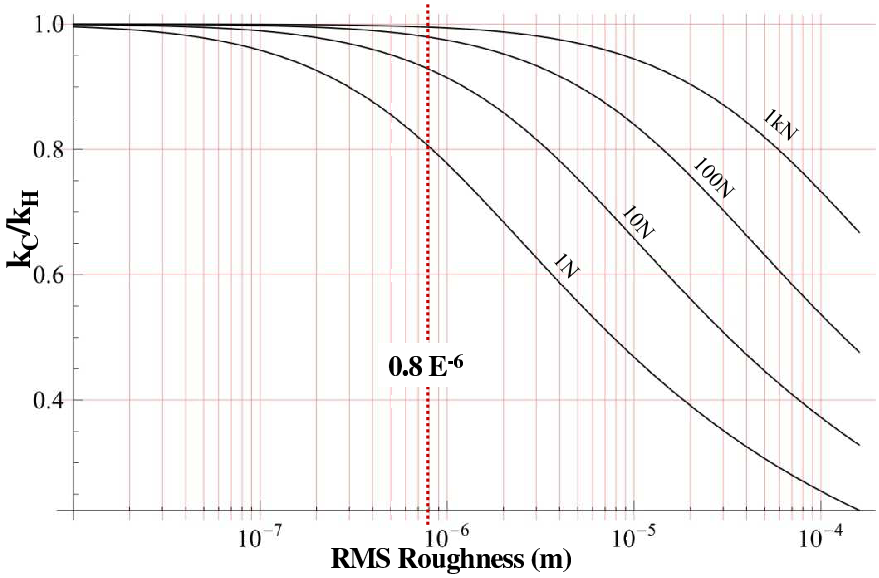

Figure 4.29: The rough locator-baseplate contacts cause a decrease in the contact stiffness

The mechanical model calculates the stiffness of each contact considering its normal. After the convergence of the system displacement, the model calculates the properties of the mechanical system. For this specific example, the algorithm converged after 17 iterations for the gain of 1. The stiffness matrix of the system with rough baseplate is shown in equation 4.42 while the comparison of the pulsation modes and the displacement parameters of the rough baseplate with the ideal baseplate is shown in tables 4.17 and 4.18 respectively.

$$[K] = \begin{bmatrix} 188.28 & -0.15 & 0.16 & 0 & 2.32 & -4.47 \\ -0.15 & 196.56 & -0.24 & -2.41 & -0.01 & 9.51 \\ 0.16 & -0.24 & 205.84 & 4.62 & -9.32 & 0 \\ 0 & -2.41 & 4.62 & 0.27 & -0.01 & -0.11 \\ 2.32 & -0.01 & -9.32 & -0.01 & 1.18 & -0.06 \\ -4.47 & 9.51 & 0 & -0.11 & -0.06 & 1.37 \end{bmatrix} * 10^7 N/m \quad (4.41)$$

Table 4.17: Effect of surface roughness on systems' pulsation modes

Pulsation	**Ideal contacts**	**Rough contacts**	**Increase**
	(rad/sec)		**(%age)**
ω_1	34098.7	33733.4	1.1
ω_1	31139.4	30870.8	0.9
ω_1	24484.7	24140.9	1.4
ω_1	21546.7	21003.7	2.5
ω_1	15649.2	13674.4	12.6
ω_1	8987.47	7922.84	11.8

4.7.6 Analytical mechanical model flexibility

One of the biggest interests of the analytical modelling is its flexibility to adopt to the system changes and resolve the problem. The 3-2-1r configuration of the locating elements is changed with the 4-2-2 locating configuration as shown in figure 4.30. The placements of the newly added locators are changed but their stiffness matrices remain the same. Also they are placed in a manner that the initial baseplate surface remain at the same position.

Table 4.18: Effect of surface roughness on the displacement vector of the work-piece

Parameter	Displacement		Change	
	Hertz contact	Rough Contact	μm/μrad	%age
Δx_P	-100.19 μm	-97.87 μm	2.32 μm	2.3
Δy_P	-160.7 μm	-180.94 μm	20.24 μm	12.6
Δz_p	-50.14 μm	-36.47 μm	13.67 μm	27.3
$\Delta\beta$	-154.41 μrad	-468.71 μrad	314.3 μrad	203.5
$\Delta\gamma$	142.29 μrad	261.17 μrad	118.88 μrad	83.5
$\Delta\alpha$	840.32 μrad	1017.71 μrad	177.39 μrad	21.1

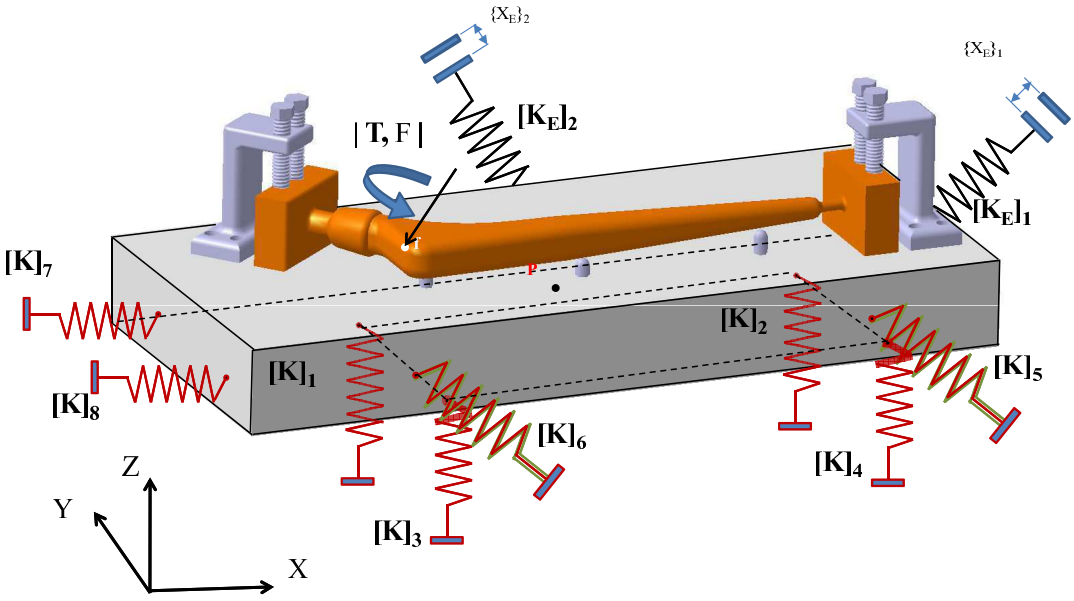

Figure 4.30: Fixturing system with 4-2-2 locating configuration

The mechanical model calculates the properties of the mechanical system. The stiffness matrix of the system is shown in equation 4.42 while the comparison of the pulsation modes and the displacement parameters of the 4-2-2 configuration with the 3-2-1r configuration of the fixturing system is shown in tables 4.19 and 4.20 respectively.

$$[K] = \begin{bmatrix} 210.11 & -0.25 & 0.16 & 0.01 & 2.11 & -4.08 \\ -0.25 & 223.72 & -0.1 & -2.55 & 0.01 & 8.5 \\ 0.16 & -0.1 & 227.76 & 4.17 & -9.11 & -0.02 \\ 0.01 & -2.55 & 4.17 & 0.3 & -0.02 & -0.11 \\ 2.11 & 0.01 & -9.11 & -0.02 & 1.3 & -0.07 \\ -4.08 & 8.5 & -0.02 & -0.11 & -0.07 & 1.49 \end{bmatrix} * 10^7 N/m \quad (4.42)$$

Table 4.19: Effect of locators configurations on systems' pulsation modes

pulsation	**3-2-1r**	**4-2-2**	**Increase**
	(rad/sec)		**(%age)**
ω_1	34098.7	34229.8	0.38
ω_1	31139.4	31493.4	1.14
ω_1	24484.7	25190.5	2.88
ω_1	21546.7	22218.9	3.12
ω_1	15649.2	16693.3	6.67
ω_1	8987.47	12174	35.46

Table 4.20: Effect of locators configurations on the displacement vector of the workpiece

Parameter	**Displacement**		**Decrease**	
	3-2-1r	**4-2-2**	**μm/μrad**	**%age**
Δx_P	-100.19 μm	-99.95 μm	0.24 μm	0.2
Δy_P	-160.7 μm	-155.03 μm	5.67 μm	3.5
Δz_p	-50.14 μm	-53.01 μm	-2.87 μm	-5.7
$\Delta\beta$	-154.41 μrad	-87.61 μrad	66.8 μrad	43.3
$\Delta\gamma$	142.29 μrad	111.18 μrad	31.11 μrad	21.9
$\Delta\alpha$	840.32 μrad	786.64 μrad	53.68 μrad	6.4

It can be seen that stiffness of the fixturing system in increased causing an decrease in overall displacement vector of the workpiece. The parameter Δz_p is increased because all the parameters are coupled with each other. The displacement of Δz_p is compensated by the reduction of $\Delta\beta$ and $\Delta\gamma$. Similarly, the increase in the system stiffness caused the increase in the pulsation of the fixturing system.

The proposed mechanical model gives a quick result for the workpiece displacement and system behavior under load by taking into account the stiffness of the locators and locator-baseplate contacts. The stability of the system for different positions and the displacements of the clamps can also be verified e.g. the system in unstable or indeterminate if the workpiece loses contact with any of the locator either due to less or extra load. A quick correction can be performed to overcome the workpiece displacement by relocating the workpiece through the advancement of locators. Also the pulsation of the system can be modified by increasing or decreasing the clamping forces. To see the dynamic behavior of the system under dynamic forces, a dynamic analysis is detailed in Appendix D.

The mechanical model is demonstrated on a simple mechanical problem but it can be applied to more complex problems with multiple loads and different orientations of locators and clamps. This model solves the problem using work done and energy method which is more flexible as compared to widely used static equilibrium conditions.

4.8 Conclusion and discussion

In this chapter, a mechanical model of the fixturing system is established to calculate the small displacement of the workpiece and system behavior under load. This is done by calculating the stiffness and mass of the whole fixturing system considering the locators being the elastic elements with negligible masses while the workpiece-baseplate assembly is taken as rigid mass element and the contacts as elastic. The analytical formulation is used because it allows obtaining the mass and stiffness matrices quickly for any configuration and position of locators as well as for any orientation of the baseplate on the locators. The mechanical model is solved in Mathematica®. As the deformation must remain small for the system reliability, the small displacement theory is applied.

Initially, the mechanical model of the proposed fixturing system is demonstrated by the hypothesis of workpiece-baseplate assembly being rigid and locators being elastic elements. Overall energy of the system is calculated which consists of the potential energy contained in all the locators, kinetic energy of inertial elements and work done by the external applied load. Clamps could be used as

the external static force but instead, they are preferred to be used as externally displaced elastic elements (known external displacement) with one end in contact with the baseplate. Lagrangian formulation is used to calculate the stiffness matrix, mass matrix and vibrational behavior of the fixturing system; displacement of the workpiece-baseplate assembly under load; as well as the deformation of each locator depending upon their stiffness matrix. This whole calculation is performed considering the contact between the locators and baseplate being rigid.

Later, the problem is extended to the contacts of the baseplate and the locators being elastic. The non-linear behavior of the contact deformation under load is linearized by converging the locators' deformations until the predefined precision is attained for all the parameters of the displacement vector. In our case, the precision is kept as 0.01% of the precedent value for each parameter. A case study is also performed on two similar examples with only changing the external displacements of the clamps. The convergence gain does not show a great advantage on the number of iteration in the first example. But in the example, a notable change in the number of iteration can be seen by changing the gain parameter.

The proposed algorithm is capable of calculating the deformation of the Hertzian contact as well as the rough contact for which the contact roughness has to be defined initially. During iterations, the algorithm continuously calculates the stiffness of the system, displacement of the baseplate, and deformation vector of each locator etc. under load. The kinematic model again compensates these positioning errors by relocating the workpiece at the required position through the advancement of locators. A complete schematic diagram of both kinematic and mechanical models can be expressed as in figure 4.31, where $[P_{PF}]$ is the initial correction of the workpiece while $[P_{F^*F}]$ is the compensation of error calculated through the mechanical model.

The proposed mechanical model can be applied to more complex problems with multiple loads and different orientations of locators and clamps. This model solves the problem using work done and energy method which is more flexible as compared to widely used static equilibrium conditions. Furthermore, the model reports if the baseplate loses contact with any of the locator, either due to less or

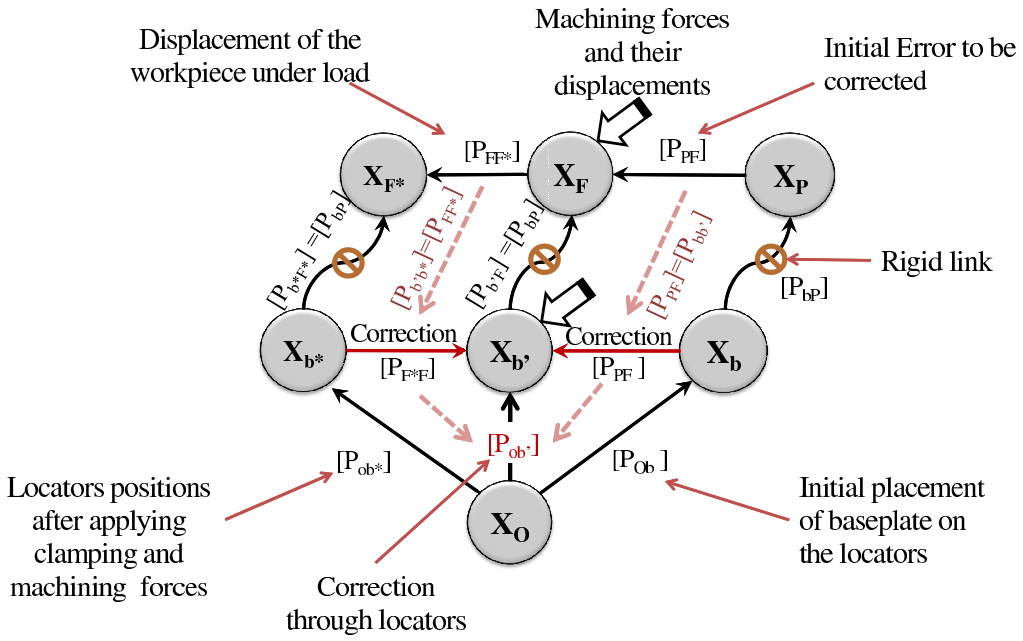

Figure 4.31: Representation of kinematic and mechanical model of the fixturing system

extra load, which causes the system to become indeterminate indicating instability of the fixturing system.

Chapter 5

Conclusion and Perspectives

5.1 Conclusion

This thesis is positioned in the domain of design and modeling of reconfigurable fixture. The work consists of establishing a geometrical model which allows a precise positioning of the workpiece from its geometry, its dimensional quality, and the configuration chosen for assembling. A mechanical model is then proposed which allows the correction of this initial position by taking into account the externally applied clamping and machining forces. Both geometrical and mechanical models allow a precise placement of the part with an expected precision of 10μm.

The position of the workpiece is measured with respect to the machine reference or reference of the transporting pallet. A 6-DOF offset of the workpiece, with reference to the position required by the fabrication process, is calculated and then the unidirectional translational adjustment of 6-locators is deducted in order to perform this 6-DOF offset compensation. Following the clamping protocol and the external applied forces being known, the deformation of the fixturing elements is then predicted using the mechanical model. This prediction allows calculating the additional unidirectional advancements of the locators so that, as the result of clamping, the workpiece remains at a position during machining or assembling operation which is compatible to the fabrication needs and under allowed precision.

5. CONCLUSION AND PERSPECTIVES

To achieve the objective of the repositioning system modeling, the thesis is decomposed as follows:

- **Literature review:** A bibliographic study on the positioning errors, and their origins, encountered during the fixture design is performed. Main causes of the positioning errors are: the errors caused by the geometrical deviation of rough part with respect to its nominal geometry, the locators placement errors, fixture positioning errors due to the deformation of the locators under load and machine tool or kinematic errors. The study is focused on the positioning errors of the workpiece due to geometrical variations as well as the deformation of elastic elements caused by external applied forces. Hertz contact theory is used for the modeling of the non-linear behavior of the contacts between locators and the baseplate.

- **Kinematic model:** An analytical kinematic model is proposed for the repositioning of the workpiece in machine coordinates. The kinematic model is capable of reorienting the workpiece at the desired position by the axial movement of the locators which are placed at 3-2-1 locating configuration. In this pure kinematic study, all the mechanical elements of the system are considered to be rigid and also the friction at the contacts is neglected. The relation between the displacements of six locators and associated geometrical transformation is given. The necessary transformation for the repositioning of the workpiece is calculated from the initial and required final positions of the workpiece. Initial position of the workpiece on the pallet is measured through a scanning machine like coordinate measuring machine while the required final position is defined by the part program of the machine tool. From this transformation, the necessary advancements of the locators are obtained by considering the adjustment precision.

- **Mechanical model:** In order to calculate the small displacements due to applied forces, an analytical mechanical model is proposed considering the workpiece-baseplate assembly being rigid. The locators are the elastic elements and the small displacement hypothesis is applied. Local deformations are present at the contacts between the locators and the baseplate so

the Hertz contact theory is applied to calculate the contact behavior. The analytical calculation is performed using the Lagrangian formalization, in order to obtain the movement equations taking the dimensional variations and changes in system configurations into account. The iterative calculation is necessary due to the non-linear behavior of the workpiece-baseplate contacts. The calculated position of the baseplate, with the contacts being rigid, is taken as the initialization value for the algorithm. The stiffness matrix, as the result of the modification of contact stiffness, is calculated in each iteration. Again, new displacements are calculated for the next calculation cycle. Considering the coupling and non-linearity, the convergence towards the final result is attained with oscillations. To limit the oscillation amplitude, a convergence gain is used. The obtained results are satisfactory and are validated on a couple of examples.

To avoid the positioning uncertainty due to geometrical/form defects a high quality baseplate is added in between the workpiece and the locators. The rough workpiece is placed and clamped rigidly on the baseplate instead of locators and it is assumed that no deformation is possible between the workpiece and the baseplate. The workpiece repositioning is performed through baseplate mobilization using 6-locators. Because the baseplate surfaces are considered to be perfectly plane, the positioning uncertainty is eliminated and the workpiece can precisely be positioned on the machine.

The positioning error of the workpiece due to the deformation of elastic elements under load is calculated in this thesis using Analytical formulation. Analytical formulations is lengthy at the start, but once established, it provides quick results to the given problem as compared to classical numerical/FEA approach. These calculated positioning errors can be compensated through the proposed kinematic model.

The proposed mechanical model does not calculate the optimal positions of the locators and clamps to hold the workpiece during machining. Instead, if we know a few possible locating configurations and the placements of locators and clamps, the proposed mechanical model enables us to choose the best possible configuration by calculating the displacement of the workpiece under machining

and clamping forces. The configuration having minimum displacement will be more stable and will be the suitable locating choice.

Similarly, our model does not calculate the kinematic, thermal, NC system errors or the error due to tool wear. But if these errors are known, our system is capable of performing the compensating of these errors as well.

Briefly, the final required compensation of the workpiece-baseplate assembly is determined by the sum of all the errors i.e. errors due to geometrical/form defects, due to deformation of elastic elements, machine tool errors, thermal errors and error due to tool wear. The one placement configuration giving the minimum workpiece displacement or maximum stability will be chosen. A complete schematic diagram of the fixture, including both kinematic and mechanical models, is shown in figure 4.31.

The proposed fixturing system also allows precise positioning of the workpiece even on special manufacturing machine-tool without the need of supplementary machine axis, or production line without the use of multi axis machines. The workpiece, to be machined or assembled, can individually be positioned on special dedicated pallets, equipped with the proposed 6-DOF positioning system, insuring precise workpiece positioning on the machine. Either on-line or off-line adjustment of the workpiece can be performed.

The proposed system allows the reduction of machining allowances through the optimal balancing of the workpiece. The limited dimensional errors of the rough part result a decrease in the material removal. The system contributes to tool wear reduction and machining time sparing. It is very important aspect when the workpiece material is expensive and/or difficult to machine. The positioning of the workpiece becomes repeatable, cost effective and more reliable.

Another application of the system is the optimal positioning of large, complex or flexible parts during assembling operation, where the positioning precision of a part with respect to the other is crucial (adjustments, deformability, fragile or brittle parts). These parts can be reoriented or repositioned at an optimized position for an automatic assembling operation.

The proposed mechanical model can be applied to more complex problems with multiple loads and different orientations of locators and clamps. The same mechanical model can be used to calculate the displacement of workpiece and

stiffness and mass matrices of the system for "bed of nails" type fixture without any modifications to the algorithm. The contact of rough surfaces is also studied which enables the algorithm to calculate the workpiece displacement in case of ideal as well as the rough baseplate in contact with the locators.

This mechanical model solves the problem using energy methods which is more flexible as compared to the widely used static equilibrium conditions because it is insensitive to the modifications of system configuration (locators added or displaced). Furthermore, the algorithm is programmed in a manner that it predicts the loss of contact of any locator due to force unbalance. This continuous loss of contact does not allow the model to converge.

5.2 Limitations and future work

There is a limitation of the proposed model while kinematic model is used to compensate the errors calculated through the mechanical model. The positioning errors of the workpiece under load is calculated through the mechanical model. While compensating these errors, the kinematic model assumes all the fixturing elements to be rigid. The locators advancements cause the workpiece displacement to change from one calculated through the mechanical model. Therefore, the mechanical model should again be tested with the new positions of the locators. The process can be repeated a few times until the workpiece displacement of the workpiece becomes equal to the compensated displacement.

CMM measuring process often needs a prepositioning to place the measuring part at a convenient place on measuring marble before the touch-probe data acquisition. The proposed system allows the positioning of the workpiece, increasing the measuring precision by using the Abbe principle or obtaining a best orientation of the workpiece to insure the accessibility of measuring sensors.

We had started the fabrication of the experimental setup for the validation of the mechanical model. We could not complete the fabrication of the experimental setup for due to the time required and the cost associated with the production of precise locators. In future, a manual actuation mechanical system should be constructed for the validation. Then, an automated reconfiguration process

of the system could be developed to perform the workpiece repositioning after CMM measurement and error calculation.

A dynamic compensation of vibrations which occurs during machining process could be performed by using fast actuators, like piezoelectric-actuators, and additional position sensors. This compensation would be dedicated to super finishing operations with less varied cutting conditions, limited cutting forces and low cutting volumes where the prediction of vibration modes is not greatly influenced by the form modification of the machined workpiece.

References

Abramowitz, M. & Stegun, I.A. (1972). *Handbook of Mathematical Functions with Formulas, Graphs, and Mathematical Tables.*. Dover, New York. 30, 226

Ahn, K.G. & Cho, D.W. (2000). An analysis of the volumetric error uncertainty of a three-axis machine tool by beta distribution. *International Journal of Machine Tools and Manufacture*, **40**, 2235–2248. 89

Antoine, J., Visa, C., Sauvey, C. & Abba, G. (2006). Approximate analytical model for hertzian elliptical contact problems. *Journal of Tribology*, **128**, 660–664. 102

Aoyama, T. & Kakinuma, Y. (2005). Development of fixture devices for thin and compliant workpieces. *CIRP Annals - Manufacturing Technology*, **54**, 325 – 328. 78

Araujo, A. & Silveria, J.L. (1999). Models for the prediction of instantaneous cutting forces in end milling. *15th Brazillian congress of mechanical engineering*. 14, 96

Asante, J. (2009). A small displacement torsor model for tolerance analysis in a workpiece-fixture assembly. *Proceedings of the Institution of Mechanical Engineers, Part B: Journal of Engineering Manufacture*, **223**, 1005–1020. viii, 12, 79, 80, 121

Asante, J.N. (2010). Effect of fixture compliance and cutting conditions on workpiece stability. *The International Journal of Advanced Manufacturing Technology*, **48**, 33–43. viii, 12, 81, 85, 95

Bahrami, M. (2004). *Modeling of Thermal Joint Resistance for Sphere-Flat Contacts in a Vacuum*. Ph.D. thesis, University of Waterloo, Canada. 105

Bahrami, M., M.Yovanovich, M. & Culham, J. (2005). A compact model for spherical rough contacts. *Journal of Tribology*, **127**, 884–889. viii, xi, 16, 30, 103, 104, 105, 172, 223, 224, 225, 226

Ber, A., Rotberg, J. & Zombach, S. (1988). A method for cutting force evaluation of end mills. *CIRP Annals - Manufacturing Technology*, **37**, 37–40. 14, 96, 100

Black, S., Chiles, V., Lissaman, A. & Martin, S. (1996). *Principles of engineering manufacture*. Arnold, Bristol, 3rd edn. 96, 97

Bourdet, P. (1999). Logiciels des machines à mesurer tridimensionnelles. *Techniques de l'ingénieur. Mesures et contrôle*, R1316–1. xiii, 54, 55, 78, 121

Bourdet, P. & Mathieu, L. (1998). *Tolérancement et métrologie dimensionnelle: qualité des produits dans les entreprises*. CETIM. xiii, 7, 52, 56, 57

Bourdet, P. & Schneider, F. (2007). *Spécification géométrique des produits: cotation & tolérancement ISO (Coll. Technique & ingénierie)*. DUNOD, Paris. vii, xiii, 8, 56, 57, 58, 60, 61

Boyle, I., Rong, Y. & Brown, D. (2011). A review and analysis of current computer-aided fixture design approaches. *Robotics and Computer-Integrated Manufacturing*, **27**, 1–12. vii, xiii, 9, 41, 69, 70, 71

Brewe, D.E. & Hamrock, B.J. (1977). Simplified solution for elliptical-contact deformation between two elastic solids. *ASME, Transactions, Series F-Journal of Lubrication Technology*, **99**, 485–487. 102

Brewster, K. (2006). ActiveJoints total hip replacement manufacturers. http://www.activejoints.com/manuf.html. 16, 109

Cazin, M. (1973). *Cours de mécanique générale et industrielle 2*. Bordas Paris. 123, 124

Cecil, J. (2001). Computer-Aided fixture design - a review and future trends. *The International Journal of Advanced Manufacturing Technology*, **18**, 790–793. 72

Choi, J.P., Min, B.K. & Lee, S.J. (2004). Reduction of machining errors of a three-axis machine tool by on-machine measurement and error compensation system. *Journal of Materials processing technology*, **155**, 2056–2064. 13, 89

Clement, A. & Bourdet, P. (1988). A study of Optimal-Criteria identification based on the Small-Displacement screw model. *CIRP Annals - Manufacturing Technology*, **37**, 503–506. 78

Clément, A., Rivière, A. & Temmerman, M. (1994). *Cotation tridimensionnelle des systèmes mécaniques: théorie et pratique*. Pyc. xiii, 8, 56, 57

Coorevits, T. & David, J. (1991). *Le contrôle tridimensionnel sur machine à mesurer et machine-outil*. Renishaw/Nathan. xiii, 54, 55

Deng, H. & Melkote, S.N. (2006). Determination of minimum clamping forces for dynamically stable fixturing. *International Journal of Machine Tools and Manufacture*, **46**, 847–857. viii, 13, 85, 86, 95

Dietrich, M. & Skalski, K.R. (2004). Designing and manufac turing of customized human bone endoprostheses. In *The Eleventh World Congress in Mechanism and Machine Science*, 92–95. viii, 106, 107, 108

Dursapt, M. (2009). *Aide-mémoire métrologie dimensionnelle*. Dunod. vii, 53, 54, 61, 62, 63

Faux, I.D. & Pratt, M.J. (1979). *Computational geometry for design and manufacture*. Halsted Press New York, NY, USA, Paris. 80

Greenwood, J. & Tripp, J. (1967). The elastic contact of rough spheres. *J. Appl. Mech*, **89**, 153. 15, 102, 105

Greenwood, J.A. (1985). Formulas for moderately elliptical hertzian contacts. *Journal of tribology*, **107**, 501. 102

Greenwood, J.A. (1997). Analysis of elliptical hertzian contacts. *Tribology International*, **30**, 235–237. 102

Greenwood, J.A. & Wu, J.J. (2001). Surface roughness and contact: an apology. *Meccanica*, **36**, 617–630. 103

Greenwood, J.A., Johnson, K.L. & Matsubara, E. (1984). A surface roughness parameter in hertz contact. *Wear*, **100**, 47–57. 16, 103, 104

Halevi, G. & Weill, R. (1995). *Principles of Process Planning: a Logical approach*. Chapman and Hall, London. vii, xiii, 9, 50, 51, 64

Hamrock, B. & Brewe, D. (1981). Simplified solution for stresses and deformations. In *American Society of Mechanical Engineers and American Society of Lubrication Engineers, Joint Lubrication Conference, New Orleans, LA*, 1981. 102

Houpert, L. (2001). An engineering approach to hertzian contact elasticity: Part i. *Journal of tribology*, **123**, 582–588. 102

Hsu, Y. & Wang, S. (2007). A new compensation method for geometry errors of five-axis machine tools. *International Journal of Machine Tools and Manufacture*, **47**, 352–360. 13, 88, 89

Hurtado, J.F. & Melkote, S.N. (2001). Improved algorithm for Tolerance-Based stiffness optimization of machining fixtures. *Journal of Manufacturing Science and Engineering*, **123**, 720–730. viii, 12, 81, 83, 84, 95

Jayaram, S., El-Khasawneh, B., Beutel, D. & Merchant, M. (2000). A fast analytical method to compute optimum stiffness of fixturing locators. *CIRP Annals - Manufacturing Technology*, **49**, 317 – 320. 12, 80, 95

Jha, B.K. & Kumar, A. (2003). Analysis of geometric errors associated with five-axis machining centre in improving the quality of cam profile. *International Journal of Machine Tools and Manufacture*, **43**, 629–636. 13, 89

Johnson, K.L. (1987). *Contact mechanics*. Cambridge Univ Pr. 15, 101, 102, 103

Kagami, J., Yamada, K. & Hatazawa, T. (1983). Contact between a sphere and rough plates. *Wear*, **87**, 93–105. 16, 103

Kang, X. & Peng, Q. (2008). Computer-Aided fixture planning: A review. In *ASME 2008 International Design Engineering Technical Conference*, New York. 78

Kang, Y., Rong, Y. & Yang, J.A. (2003). Geometric and kinetic model based Computer-Aided fixture design verification. *Journal of Computing and Information Science in Engineering*, **3**, 187–199. 9, 69

Kelly, S.G. (1996). *Schaum's outline of Theory and Problems of Mechanical Vibrations*. McGraw Hills. 159, 184

Kim, G.M. & Chu, C.N. (2004). Mean cutting force prediction in ball-end milling using force map method. *Journal of Materials Processing Technology*, **146**, 303–310. 14, 96

Kreyszig, E. (2007). *Advanced engineering mathematics*. Wiley-India. 226

Lahousse, L., David, J., Leleu, S., Vailleau, G. & Ducourtieux, S. (2005). Application d'une nouvelle conception d'architecture à une machine de mesure de résolution nanométrique. *Revue française de métrologie*, 35–43. 114

Lalanne, M., Berthier, P. & Der Hagopian, J. (1986). *Mécanique des vibrations linéaires (avec exercices corrigés et programmes de calcul)*. Masson, Paris. ix, 27, 151, 152

Legoff, O., Tichadou, S. & Hascoët, J. (2004). Manufacturing errors modelling: Two three-dimensional approaches. *Proceedings of the Institution of Mechanical Engineers, Part B: Journal of Engineering Manufacture*, **218**, 1869 –1873. 12, 79

Lesage, D. (2002). *Un modèle dynamique de spécifications d'ingénierie basé sur une approche de géoméetrie variationnelle*. Ph.D. thesis, INP, Grenoble. 8, 55

Li, B. & Melkote, S.N. (1999). Improved workpiece location accuracy through fixture layout optimization. *International Journal of Machine Tools and Manufacture*, **39**, 871 – 883. vii, 11, 15, 73, 100

Li, B. & Melkote, S.N. (2001). Fixture clamping force optimisation and its impact on workpiece location accuracy. *The International Journal of Advanced Manufacturing Technology*, **17**, 104–113. 12, 13, 81, 84, 95

Li, B., Melkote, S.N. & Liang, S.Y. (2000). Analysis of reactions and minimum clamping force for machining fixtures with large contact areas. *The International Journal of Advanced Manufacturing Technology*, **16**, 79–84. 13, 84

Liao, Y. & Hu, S. (2001). An integrated model of a Fixture-Workpiece system for surface quality prediction. *The International Journal of Advanced Manufacturing Technology*, **17**, 810–818. viii, 13, 86, 88, 95

Lin, Y. & Shen, Y. (2000). *A Generic Kinematic Error Model for Machine Tools*. Citeseer. 13, 89

Marin, R.A. & Ferreira, P.M. (2001). Kinematic analysis and synthesis of deterministic 3-2-1 locator schemes for machining fixtures. *Journal of Manufacturing Science and Engineering*, **123**, 708–719. 10, 72

Marin, R.A. & Ferreira, P.M. (2003). Analysis of the influence of fixture locator errors on the compliance of work part features to geometric tolerance specifications. *Journal of Manufacturing Science and Engineering*, **125**, 609–616. 84

Martin, P., Dantan, J. & D'Acunto, A. (2011). Virtual manufacturing: prediction of work piece geometric quality by considering machine and set-up accuracy. *International Journal of Computer Integrated Manufacturing*, **24**, 610–626. viii, 14, 92, 93, 94

Mativenga, P.T. & Hon, K.K.B. (2005). An experimental study of cutting forces in High-Speed end milling and implications for dynamic force modeling. *Journal of Manufacturing Science and Engineering*, **127**, 251–261. 14, 96

Menassa, R.J. & Devries, W.R. (1991). Optimization methods applied to selecting support positions in fixture design. *Journal of engineering for industry*, **113**. 11, 75

Méry, B. (1997). Machines à commande numérique. *Hermès, Paris*. vii, 65, 66, 67

Mikic, B.B. & Roca, R.T. (1974). A solution to the contact of two rough spherical surfaces. *Journal of Applied Mechanics*, **41**, 801. 16, 103

Nee, A.Y.C., Tao, Z.J. & kumar, A.S. (2004). *An advanced treatise on fixture design and planning*. World Scientific. 52

Nemes, G. (2008). New asymptotic expansion for the gamma function. *Archiv der Mathematik*, 1–9. 30, 226

News, O.N. (1992). How an orthopedic implant is made. Tech. rep., Mendenhall Associates Inc. 109

Okafor, A. & Ertekin, Y.M. (2000). Derivation of machine tool error models and error compensation procedure for three axes vertical machining center using rigid body kinematics. *International Journal of Machine Tools and Manufacture*, **40**, 1199–1213. 88

Paris, H. (1995). *Contribution à la conception automatique des gammes d'usinage: le probléme du posage et du bridge des pièces*. Ph.D. thesis, Université Joseph Fourier Grenoble. vii, 50, 51, 52, 78

Pruvot, F. (1993). *Conception et calcul des machines-outils: études cinématique et statique. Les broches*, vol. 2. PPUR presses polytechniques. viii, 15, 96, 99, 221

Pruvot, F. (1995). *Conception et calcul des machines outils: Les broches, études dynamiques*, vol. 3. Presses Polytechniques et universitaires Romandes. 99

Raghu, A. & Melkote, S. (2005). Modeling of workpiece location error due to fixture geometric error and fixture-workpiece compliance. *Journal of manufacturing science and engineering*, **127**, 75. viii, 12, 81, 82, 95

Raghu, A. & Melkote, S.N. (2004). Analysis of the effects of fixture clamping sequence on part location errors. *International Journal of Machine Tools and Manufacture*, **44**, 373–382. viii, 11, 12, 75, 77, 81, 82

Raksiri, C. & Parnichkun, M. (2004). Geometric and force errors compensation in a 3-axis CNC milling machine. *International Journal of Machine Tools and Manufacture*, **44**, 1283–1291. 14, 93

Ramesh, R., Mannan, M.A. & Poo, A.N. (2000). Error compensation in machine tools – a review: Part i: geometric, cutting-force induced and fixture-dependent errors. *International Journal of Machine Tools and Manufacture*, **40**, 1235–1256. 13, 88, 91

Rosenberg, O., Vozny, V., Sokhan, C., Gawlik, J., Mamalis, A.G. & Kim, D.J. (2006). Trends and developments in the manufacturing of hip joints: an overview. *The International Journal of Advanced Manufacturing Technology*, **27**, 537–542. xiii, 106, 107

Roy, U. & Liao, J. (2002). Fixturing analysis for stability consideration in an automated fixture design system. *Journal of Manufacturing Science and Engineering*, **124**, 98–104. 11, 74

Ryll, M., Papastathis, T.N. & Ratchev, S. (2008). Towards an intelligent fixturing system with rapid reconfiguration and part positioning. *Journal of Materials Processing Technology*, **201**, 198 – 203, 10th International Conference on Advances in Materials and Processing Technologies - AMPT 2007. 4, 42, 68

Sandviken (2011). Sandvik coromant, technical guide. http://www2.coromant.sandvik.com/coromant/downloads/tech_-guide/FRE/MTG.zip. viii, 15, 97, 98, 99, 181

Sandviken, A.S.C. (1997). *Techniques modernes d'usinage: guide pratique*. Sandviken Coromant. 15, 97

Siebenaler, S.P. & Melkote, S.N. (2006). Prediction of workpiece deformation in a fixture system using the finite element method. *International Journal of Machine Tools and Manufacture*, **46**, 51–58. 86, 95

Somashekar R., S. (2002). Fixturing features selection in feature-based systems. *Computers in Industry*, **48**, 99–108. vii, 11, 73, 74

Trappey, J. & Liu, C. (1990). A literature survey of fixturedesign automation. *The International Journal of Advanced Manufacturing Technology*, **5**, 240–255. vii, 50

Trotignon, J., Coorevits, T., David, J., Dietrich, R., Facy, G., Hugonnaud, E. & Pompidou, M. (1996). *Précis Construction Mécanique; projects-méthods, production, normalisation*, vol. 2. Nathan, AFNOR, Paris. 50

Tsukada, T. & Anno, Y. (1979). On the approach between a sphere and a rough surface (1st. report-analysis of contact radius and interface pressure. *J. Jpn. Soc. Precis. Eng*, **45**, 473–479. 16, 103

Villeneuve, F., Legoff, O. & Landon, Y. (2001). Tolerancing for manufacturing: a three-dimensional model. *International Journal of Production Research*, **39**, 1625–1648. 12, 78

Wan, X., Xiong, C., Zhao, C. & Wang, X. (2008). A unified framework of error evaluation and adjustment in machining. *International Journal of Machine Tools and Manufacture*, **48**, 1198–1210. viii, 71, 91, 92

Wang, H., Rong, Y.K., Li, H. & Shaun, P. (2010). Computer aided fixture design: Recent research and trends. *Computer-Aided Design*, **42**, 1085–1094. 9, 69

Wang, M. (2002). Tolerance analysis for fixture layout design. *Assembly Automation*, **22**, 153–162. viii, 77, 78

Werner, A., Lechniak, Z., Skalski, K. & Kedzior, K. (2000). Design and manufacture of anatomical hip joint endoprostheses using CAD/CAM systems. *Journal of Materials Processing Technology*, **107**, 181–186. ix, 107, 108

Yeh, J. & Liou, F. (1999). Contact condition modelling for machining fixture setup processes. *International Journal of Machine Tools and Manufacture*, **39**, 787–803. 105

Zhang, W. (2001). Flexible fixture design and automation: review, issues and future directions. *International Journal of Production Research*, **39**, 2867–2894. 42, 50

Zheng, Y., Rong, Y. & Hou, Z. (2007). The study of fixture stiffness part i: a finite element analysis for stiffness of fixture units. *The International Journal of Advanced Manufacturing Technology*, **36**, 865–876. viii, 13, 85, 87, 95

Zhu, S., Ding, G., Qin, S., Lei, J., Zhuang, L. & Yan, K. (2012). Integrated geometric error modeling, identification and compensation of CNC machine tools. *International Journal of Machine Tools and Manufacture*, **52**, 24–29. viii, 12, 13, 79, 89, 91

zimmer (2011). zimmer hip prosthesis, CPT 12/14 cemented stems. http://www.zimmer.co.uk/web/enUS/pdf/product_brochures/ CPT_-12_14_Hip_System_97-8114-01_rev_1.pdf. ix, xiii, 17, 110, 111, 132, 142

Zirmi, S., Paris, H. & Belaidi, I. (2009). Conception de montage d'usinage: placement des éléments technologiques en contact avec la pièce. *19ème Congrès Français de Mécanique*. vii, 11, 74, 75, 76

Appendix A

Measurement of Hip Prosthesis through CMM

The hip prosthesis measurement, through CMM, is explained here with a simple two dimensional example in a plane. The hip prosthesis, having the original dimensions, is shown in figure A.1. The hip prosthesis consists of a conical neck and a rounded rectangular prismatic stem. A rough part is shown in figure A.2. The CMM measures points on the surfaces of the rough workpiece using touch-prob. These measured points form an extracted surfaces and help to define an associated theoretical surfaces through any optimization criteria detailed in section 2.2.5.

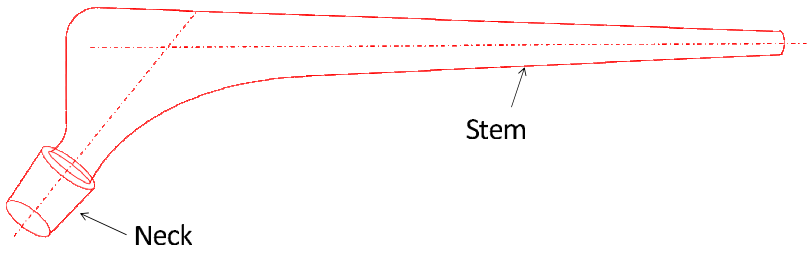

Figure A.1: The product required after machining operation

Two optimization criteria are explained here; root mean square criterion and Chebyshev (minimum material) criterion. In case of RMS criterion, a line (surface

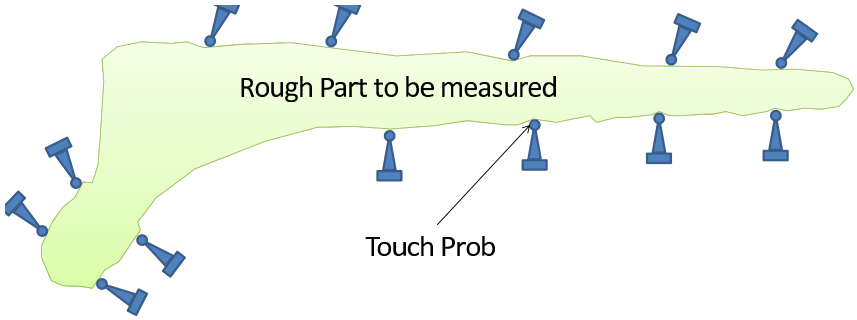

Figure A.2: Touch-probe measurement of the rough part before machining

in case of 3D) is defined which minimizes the squares of errors of each measured point. Two associated surfaces (two cones in this case) are constructed for both stem and the neck of the part and their centerlines are defined as shown in figure A.3. The intersection point of both centerlines (in plane) is the reference point used for the part positioning in the machine while its orientation is defined by the stem axis in the plane. In two dimensional problem, the plane can easily be defined. But in 3D case, the plane can be defines by the surface passeing through the stem centerline and the center point of the neck. Similarly, the point P can be defined by the projection of the neck axis on the stem axis perpendicular to the plane. The final part can be defined within the measured part by centering the measured axis to the real product as shown in figure A.4 where the final part position is defined in the rough part. The extra material between the associated surface and the required surface is the machining allowance.

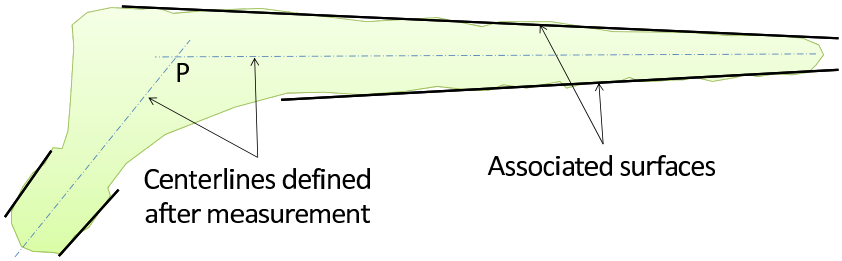

Figure A.3: Optimization through Root Mean Square criterion

In figure A.5, the optimization of the surface through the measured points is performed using the method of minimum material which finds a surface which

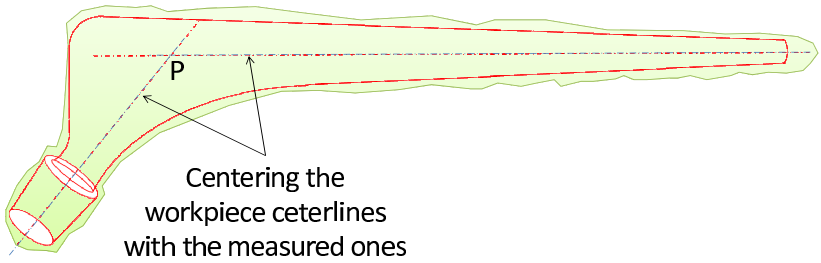

Figure A.4: Final workpiece defined with in the measured part optimized through RMS

passes through the lowest points of the surface profile to make sure that the defined associated surfaces are completely inside the physical material. This method is more practical to avoid the material waste. Two centerlines are also defined for rectangular prismatic stem and conical neck. In figure A.6, it can be seen that the final part is uniformly defined within the measured part as compared to RMS criterion. The difference is more clear if the part variation is increased. A small reorientation is performed to center the final product within the measured parts in figures A.4 and A.6. This compensation should be performed by reorientating the part, machine tool or by modifying the part program.

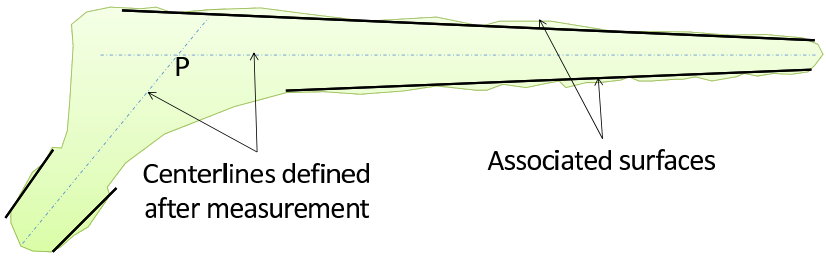

Figure A.5: CMM optimization through Minimum Material criterion

The same example can be explained mathematically. The lines defining the hip prosthesis are defined in excel with some allowances. Random points are generated, along this defined part, representing the points measured through CMM as shown in figures A.7 and A.8. RMS criterion in used to define the lines from the measured points in figure A.7 while Chebyshev (min. material) criterion

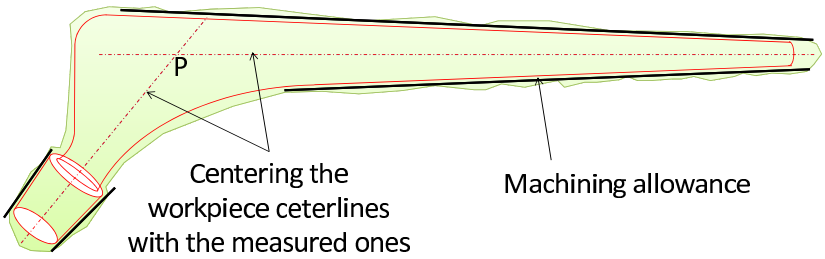

Figure A.6: Final workpiece defined with in the measured part optimized through Mim. Material criterion

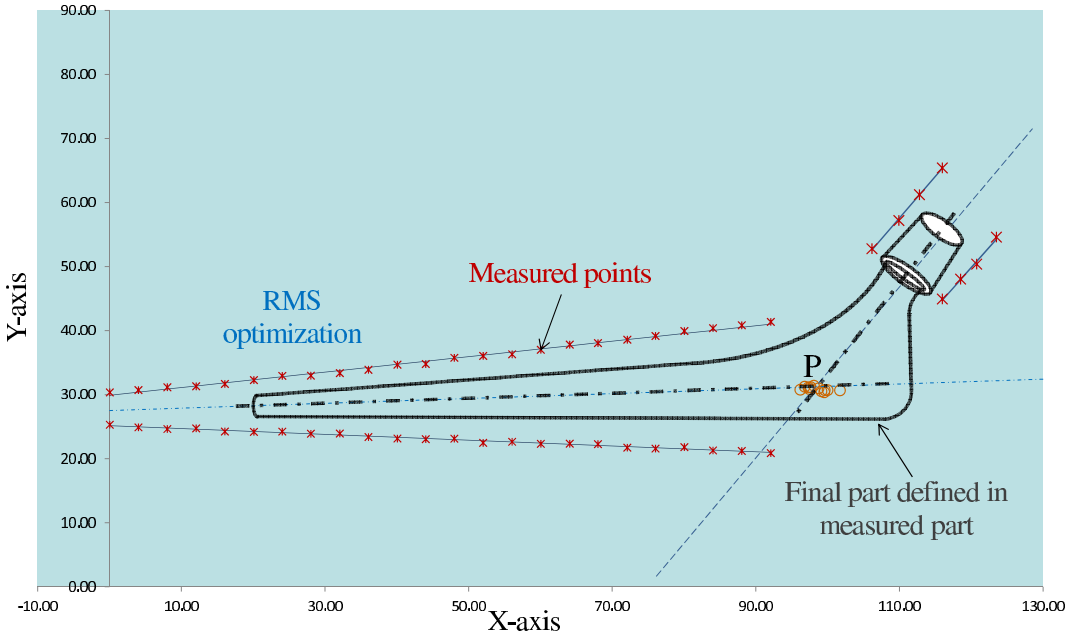

Figure A.7: Associating measured points using RMS criterion

is used to define the lines in figure A.8. In both the figures, the actual part is shown by centering its centerlines with the centerlines of associated surfaces.

If the same part is measured multiple times, there will be some uncertainty of the measurement. Random variables are generated multiple times causing random generated surfaces. The centerlines of these randomly generated measured points will cause uncertainty of point P on the part. The round marks shows the possible positions of point P for different measured points on the same part.

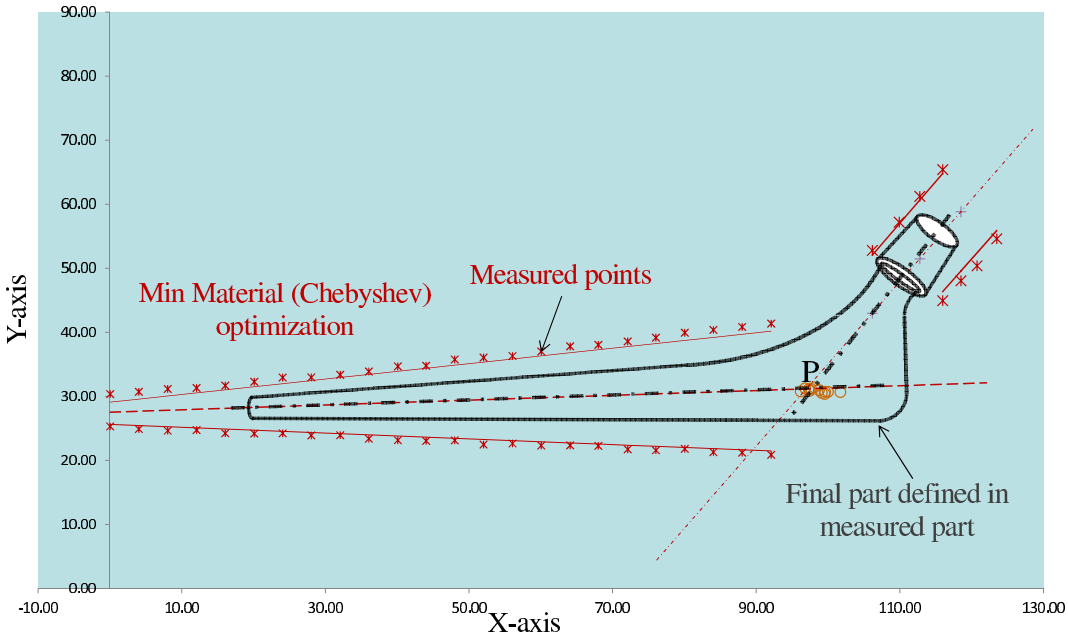

Figure A.8: Associating measured points using Chebyshev criterion

A three dimensional view of the hip prosthesis is shown in figure A.9. While measuring it through CMM, two centerlines for stem and neck can be defined in the machine reference through CMM as detailed. The complete part position can be defined by:

- The position of the point P which is the point of intersection of two centerlines. The definition of point P blocks 3 translational DOFs (X,Y & Z) of the measured part. If the lines do not intersect, the point P can be defined by the projection of centerline of the neck axis on the stem centerline along plane normal.

- The orientation of the plane formed by two centerlines. The definition of the plane blocks two additional rotational DOFs (β & γ) of the measured part. If the centerlines do not intersect, the plane can be defined to be one passing trough the stem centerline and the center point of the external neck surface.

- The orientation of stem axis along $z-$axis (α). This definition blocks the remaining DOF of the measured part.

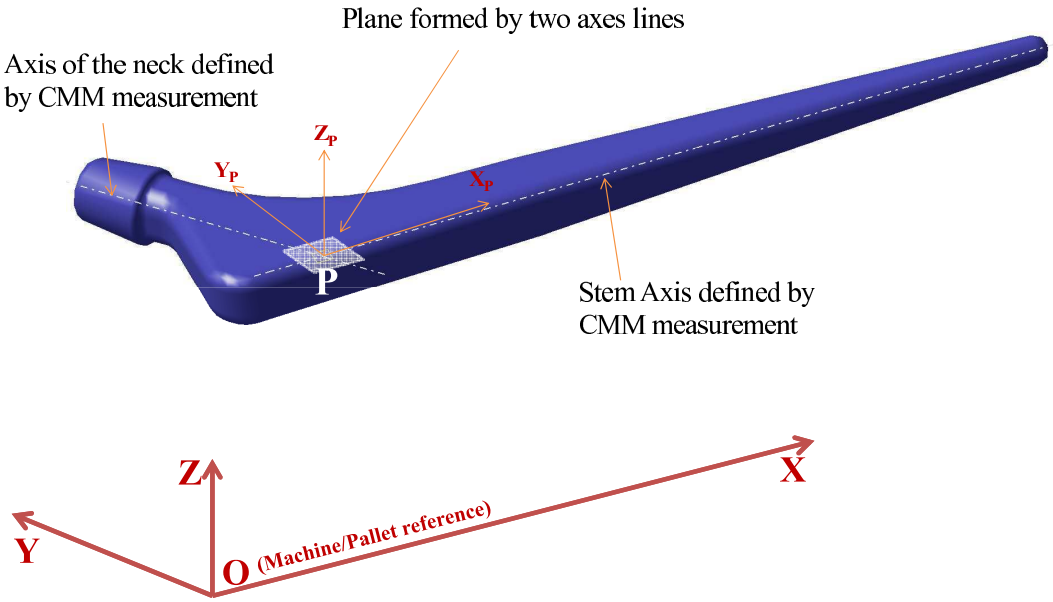

Figure A.9: Defining the part in machine reference

Appendix B

Calculation of specific force coefficients

Our aim is to calculate the cutting force on the workpiece along x, y and z directions. This cutting force is used in the mechanical model simulation to calculate the deformation caused on each locator under load. Research teams from USA, France and Germany have experimentally developed tables for a wide range of materials and possible cutting conditions containing the cutting force, speed, type of cutting tool etc. These tables are widely used by the professionals (Pruvot, 1993). Pruvot (1993) used an analytical approach to calculate the tangential and repulsion specific force coefficients (fig. 2.34). This approach can only be used to calculate the machining force for simulation. It gives the values of the cutting force which are probable and near to the real values and change with different parameters. These equations do not have any physics base and they are constructed experimentally and these equations are valid for the material having maximum stress from 40 to 180 daN/mm^2.

B.1 Coefficient of tangential cutting force

Coefficient of cutting (k_{T_V}) speed and coefficient of chip rack angle (k_{T_γ})are calculated by,

$$k_{T_V} = \frac{11.7}{V_C - 10} + 0.89 \tag{B.1}$$

$$k_{T_\gamma} = 1.1 - \frac{\gamma_0}{100} \tag{B.2}$$

where γ_0 (the chip rack angle) is in degree. The variable a can be calculated by using,

$$a = \left[\frac{180 - \sigma_{max}}{95}\right]^2 * 0.4914 + 1.075 \tag{B.3}$$

with σ_{max} is the ultimate strength of the material under traction in daN/mm^2. The specific tangential force coefficient K_T is found to be,

$$K_T = \left[\frac{27.5}{f_z^{0.65}} + a * \sigma_{max}\right] * k_{T_V} * k_{T_\gamma} \tag{B.4}$$

with f_z is the chip thickness.

B.2 Coefficient of Repulsive force

Coefficient of cutting (k_{R_V}) speed, coefficient of cutting angle (k_{R_γ}) and b can be calculated by,

$$k_{R_V} = \frac{32}{V_C - 10} + 0.7 \tag{B.5}$$

$$k_{R_\gamma} = -0.0375\gamma_0 + 1.45 \tag{B.6}$$

$$b = 0.5743 * \sigma_{max} - 3.93 \tag{B.7}$$

which gives the specific repulsive force coefficient K_R,

$$K_R = \left[\frac{b}{f_z^{0.6}} + 0.4 * \sigma_{max}\right] * k_{R_V} * k_{R_\gamma} \tag{B.8}$$

Appendix C

Deformation of rough contacts

The numerical results of Bahrami model are valid over full range of rough contacts but this thesis involved the deformation at the rough contact between the cuboid baseplate and the spherical locator. In this case, maximum deformation occurs at the center of the contact. The deformation at the center of the rough contacts, proposed by Bahrami *et al.* (2005), is in terms of a numerical (beta) function . Also the calculation of a'_L involves testing of P'_0 (eq. 2.34) for calculating non-dimensional contact area from pressure distribution which is time consuming. Here, a single analytical equation for the non dimensional contact area is proposed followed by a beta function approximation for the calculation of the contact deformation dedicated for very small values of γ.

C.1 Non-dimensional Contact Area Estimation

The curve fitted non-dimensional contact area (eq. 2.34) is compared with the estimated contact area by Bahrami *et al.* (2005) (eq. 2.35) and the error is evaluated for different values of α and τ. An error of up to 30% has been revealed for some values of τ and α in figure C.2(b). This highlights the need of more precise estimated value of contact. For this purpose, a more precise equation is proposed for the estimation of a'_L for all values of P'_0 which is further a function of τ and α. Estimation is performed by plotting equation 2.34 for all values of a'_L, and then by fitting the power equation curve with minimal least square error. New proposed value of non-dimensional contact area is shown in equation C.1.

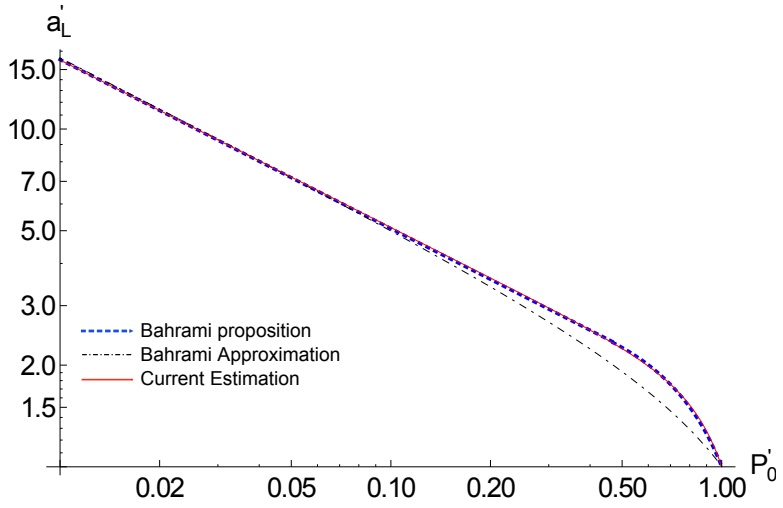

(a) $\tau = 1$

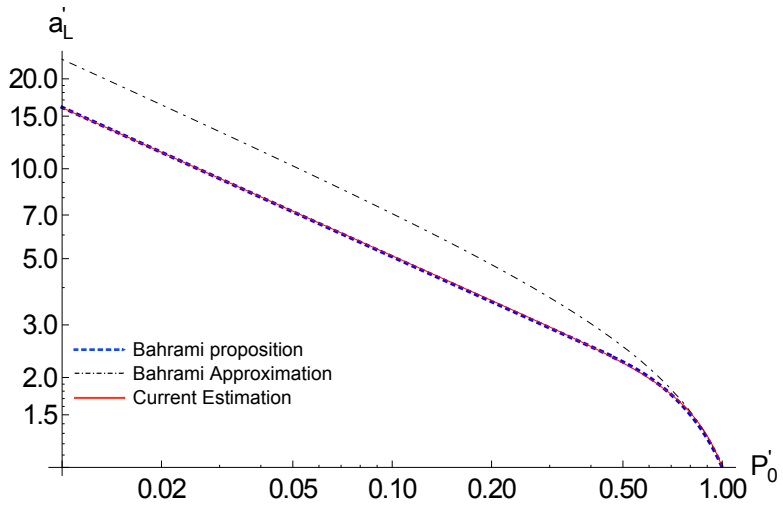

(b) $\tau = 1000$

Figure C.1: Comparison of proposed a'_L estimation with Bahrami et al. Bahrami *et al.* (2005) estimation

$$a'_{L,new} = 1.631\ P_0'^{-0.496} - 0.631\ P_0'^{3.358} \tag{C.1}$$

where, P'_0 can be calculated using equation 2.33. In equation C.1, power values -0.496 and 3.358 are obtained through the power function optimization by curve fitting while proportional coefficients 1.631 and 0.631 have been chosen to keep the border condition $a'_L(P'_0 = 1) = 1$ valid. This proposed estimated contact area

(eq. C.1) is compared with the estimated contact area proposed by Bahrami *et al.* (2005) (eq. 2.35) for two different values of τ (1 and 1000) in figure C.1 and their relative error is compared in figure C.2. Curves in figure C.2 are discontinuous, it is only because the actual function of equation 2.34 is discontinuous at $P'_O = 0.47$.

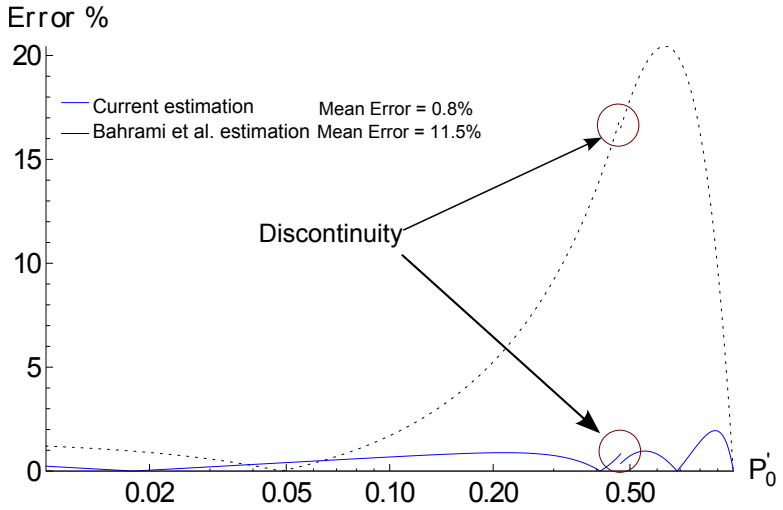

(a) $\tau = 1$

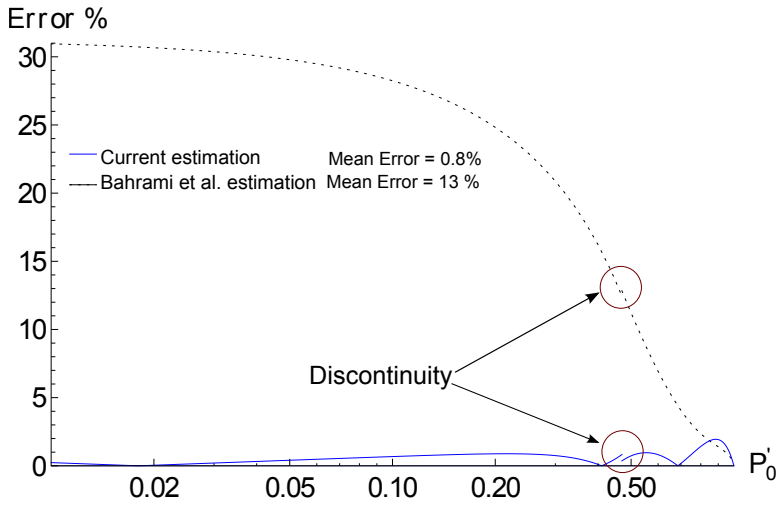

(b) $\tau = 1000$

Figure C.2: Comparison of error of current model with Bahrami et al. Bahrami *et al.* (2005)

Assuming that equation 2.34 is a valid formulation, from figure C.2, it can be seen that the current equation describes the equation of non-dimensional contact

area with least error for all values of α and τ and it is convenient to replace both previous equations with a single formula in equation C.1. The next step is to estimate the deformation at the center of contact which is given in terms of beta function (eq. 2.36) by Bahrami *et al.* (2005).

C.2 Beta Function Estimation

In case of baseplate-locator contact, the deformation at the center of contacting surfaces is the required parameter to calculate the accuracy of the workpiece in machine's frame of reference. Bahrami *et al.* (2005) proposed the deformation at the center of the contact (eq. 2.36) in terms of beta function which is a numerical function. An analytical solution to the problem is necessary to obtain quick results. For this purpose, an analytical solution is proposed which satisfies the results from the numerical solution proposed by Bahrami *et al.* (2005) with the minimum error. By investigating the numerical result, it is observed that the beta function is further a function of "Gamma Function(Γ)"(eq. C.2) which is again a numerical value. These numerical functions slow down the iterative calculations therefore, threr is the need of finding out the explicit approximations of these functions.

$$B(x,y) = \frac{\Gamma(x)\Gamma(y)}{\Gamma(x+y)} \tag{C.2}$$

C.3 Gamma Function

In Kreyszig (2007) and Abramowitz & Stegun (1972) the complete gamma function $\Gamma(z)$ is defined by the improper integral $\int_0^\infty e^{-t}t^{z-1}dt$ for $z > 0$. It is also defined to be an extension of factorial to complex and real number arguments presented by L. Euler (in 1729). It is related to the factorial by the relation $\Gamma(z) = (z-1)! : z \in N$, where N is positive integer.

Estimation models like Stirling Approximation (Abramowitz & Stegun, 1972) and Gergö Approximation (Nemes, 2008) for gamma functions are available in literature. Gergö approximation is similar to Stirling approximation but easier to use. Our work focuses on the contact of locators with baseplate, i.e. very small

Table C.1: Optimized parameters in Gamma Function Approximation (eq. C.3)

a_1	0.5641886354	a_2	0.5000070960	a_3	0.1091637999
a_4	1.621840565	a_5	-0.9929252979	a_6	0.01158345729
a_7	-1.271839956	a_8	1.505508639	a_9	1

values of parameter γ, but Stirling and Gergö approximations give large errors for very small values of parameter γ. An analytical estimation needs to be formalized which describes the beta function for small values of the parameter γ as well. For this purpose, an analytical expression for gamma function estimation (eq. C.3) has been obtained by adjusting the function over a large range of numerical values for the parameter γ. Beta function can further be obtained using equation C.2 as given above.

$$\Gamma(b+1) = a_1(b+a_2)^{b+a_2}\left(1+\frac{a_3}{a_4+b^{a_5}}+\frac{a_6}{b^{a_7}+a_8}\right)e^{-b^{a_9}}\sqrt{2\pi} \tag{C.3}$$

where, $a_1, ...a_9$ are the parameters and their optimal values are shown in table C.1. A comparison of errors in gamma and beta function using equation C.3 is presented in figure C.3 where Absolute values of errors in Beta and Gamma functions are plotted to compare the results in logarithmic scale. Higher values of paremeter γ cause the cumulative error to often return infinity which can be seen in figure C.3(a).

The proposed expression for Gamma function gives better results for small γ values which is of great interest in the scope of this work. Other asymptotic models are more efficient for large values of γ, but their calculation produces noise for very large values of γ. The proposed model shows a homogeneous absolute error for all values of γ. It can be concluded that the proposed model gives better accuracy for the surfaces having small γ values.

Once the analytical equations for contact area are obtained and beta function estimations are performed, the contact center deformation can be calculated as a function of σ from equation 2.36, C.1 & C.3 without testing pressure distribution in equation 2.34.

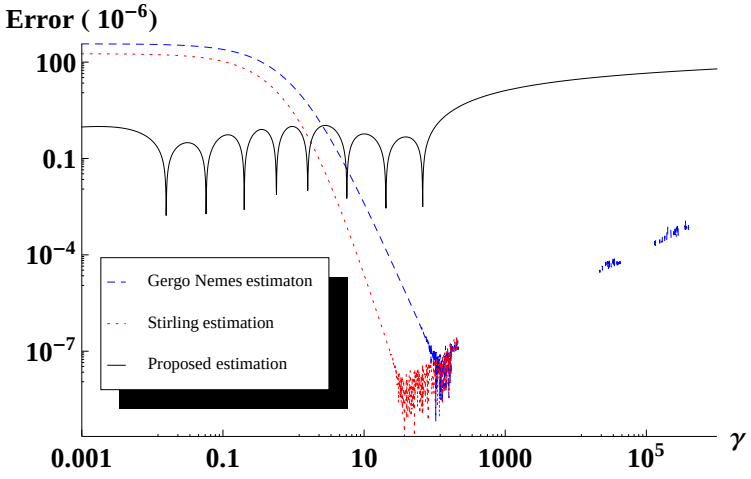

(a) Gamma error (absolute) for $\Gamma(\gamma + 1)$

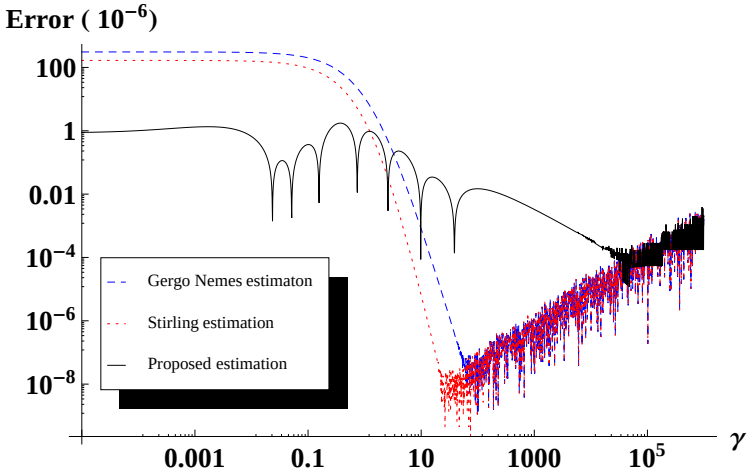

(b) Beta error(absolute) for B(0.5,$\gamma + 1$)

Figure C.3: Comparison of proposed and existing approximations

Appendix D

Dynamic loading effect on the displacement

The displacement of the workpiece and the deformation of each locator is calculated in the case study of chapter 4 for the static maximum load. This appendix details the study carried out to see the effect of dynamic loading on the workpiece positioning. In our case, the total force vector is written as;

$$\{F\}_T(t) = \{F\}_0 + \{F\}\cos(\omega t) \tag{D.1}$$

where, vector $\{F\} = \sum\{F_X, F_Y, F_Z, \mathbb{T}_X, \mathbb{T}_Y, \mathbb{T}_Z\}^T$ is the sum of all external forces and torques, $\{F\}\cos(\omega t)$ is the dynamic force vector, $\{F\}_0$ is the force vector at zero frequency, ω is the frequency, while t is the time. The force changes within zero and maximum value so for uniformity, using the same force vector as the force amplitude vectors. the equation D.1 becomes;

$$\{F\}_T(t) = \frac{\{F\}_{Max}}{2} + \frac{\{F\}_{Max}}{2}\cos(\omega t) \tag{D.2}$$

Equation D.2 gives $\{F\}_T = \{F\}_{Max}$ for $\omega = 0$ or t=0. The static displacement of the system is calculated from;

$$\{X\}_{Stat} = [K]^{-1}\{F\}_{Stat} \tag{D.3}$$

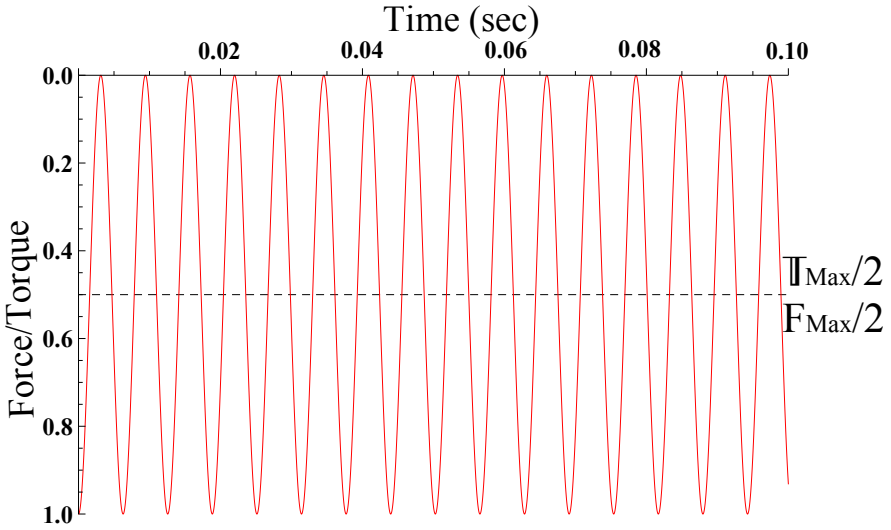

Figure D.1: Total cutting force and moment for $\omega = 1000\ rad/sec$

Where, $\{F\}_{Stat} = \{F\}_{Max}/2$. In case of dynamic force, the differential equation of motion can be written as:

$$[M]\{\ddot{x}\} + [K]\{x\} = \{F\}_{Dyn}\cos(\omega t) \tag{D.4}$$

where, $\{F\}_{Dyn} = \frac{\{F\}_{Max}}{2}$ is the dynamic part of the force vector. Assuming $\{x\} = \{X\}_{Dyn}\cos(\omega t)$, the equation D.4 can be solved for the amplitude $\{X\}_{Dyn}$, which is

$$\{X\}_{Dyn} = [-\omega^2[M] + [K]]^{-1}\{F\}_{Dyn} \tag{D.5}$$

$\{X\}_{Dyn}$ is the function of ω therefore $\{X\}_{\omega} = \{X\}_{Dyn}/\{X\}_{Stat}$ is plotted against ω to see the effect of ω on the amplitude of displacement, but vector $\{X\}_{\omega} = \{\Delta x_{p,\omega},\ \Delta y_{p,\omega},\ \Delta z_{p,\omega},\ \Delta\beta_{\omega},\ \Delta\gamma_{\omega},\ \Delta\alpha_{\omega}\}$ contains both linear and angular displacements. Instead of plotting all the six parameters, the magnitude of linear ($\Delta X_{\omega,L} = |\sqrt{\Delta x_{p,\omega}^2 + \Delta y_{p,\omega}^2 + \Delta z_{p,\omega}^2}|$) and angular elements ($\Delta X_{\omega,A} = |\sqrt{\Delta\alpha_{\omega}^2 + \Delta\beta_{\omega}^2 + \Delta\gamma_{\omega}^2}|$) of $\{X_{\omega}\}$) are plotted against ω. The linear term signifies the magnitude while the angular terms does not have a physical signification, it is used for visualization of the results. The rotational speed of spindle has to be away from the resonance frequencies of the system for safe machining operation.

D.1 Effect of dynamic loading on studied example

Dynamic loading is applied on the workpiece of the case study performed in section 4.7 to see its impact and dynamic behavior of the system. In this case study, the maximum external force vector is $\{F\}_{Max} = \{-89.75, -60, -24, 0, 0, -0.09\}^T$. Total force vector can be written as,

$$\{F\}_T(t) = \frac{\{F\}_{Max}}{2} + \frac{\{F\}_{Max}}{2}\cos(\omega t) \tag{D.6}$$

Displacements under static and dynamic loads are calculated using,

$$\begin{aligned} \{X\}_{Stat} &= [K]^{-1}\{F\}_{Stat} \\ \{X\}_{Dyn} &= [-\omega^2[M] + [K]]^{-1}\{F\}_{Dyn} \end{aligned} \tag{D.7}$$

where $[K]$ is written in equation 4.38, ω is the frequency of the spindle, $\{F\}_{Stat} = \{F\}_{Dyn} = \{F\}_{Max}/2$, while [M] is the inertial matrix containing [M] and [I] diagonally.

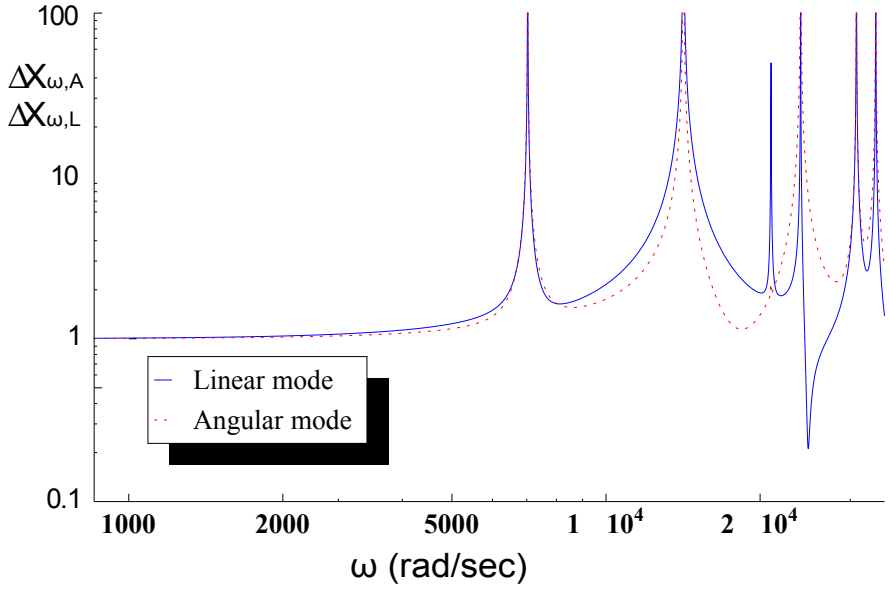

Figure D.2: Effect of ω on the amplitude of displacement for clamps' external displacement of 0.25mm

A Bode diagram is plotted for $\Delta X_{\omega,L}$ and $\Delta X_{\omega,A}$

against the frequency of spindle as shown in figure D.2. Peeks can be seen at the natural frequencies of the fixturing system which are written in equation 4.39. The spindle speed has to be away from these peeks for a safe machining operation. In our case study, a spindle speed of 8000 RPM is used which is equal to 838 rad/sec, so our system is well within the safe limit. The peeks in bode diagram can be shifted towards right or left side by tightening or loosening the clamps. If in this case, we think that the fixture is very stiff, external displacement of clamps can be reduced from 0.25mm to 0.05mm which causes the peeks to shift towards left side as shown in figure D.3 where, the first peek is moved from 8988 rad/sec to 7030 rad/sec. If the external displacement is further reduced to 0.025mm, the baseplate loses its contact with the locator 6 and the system becomes statically indeterminate or unstable.

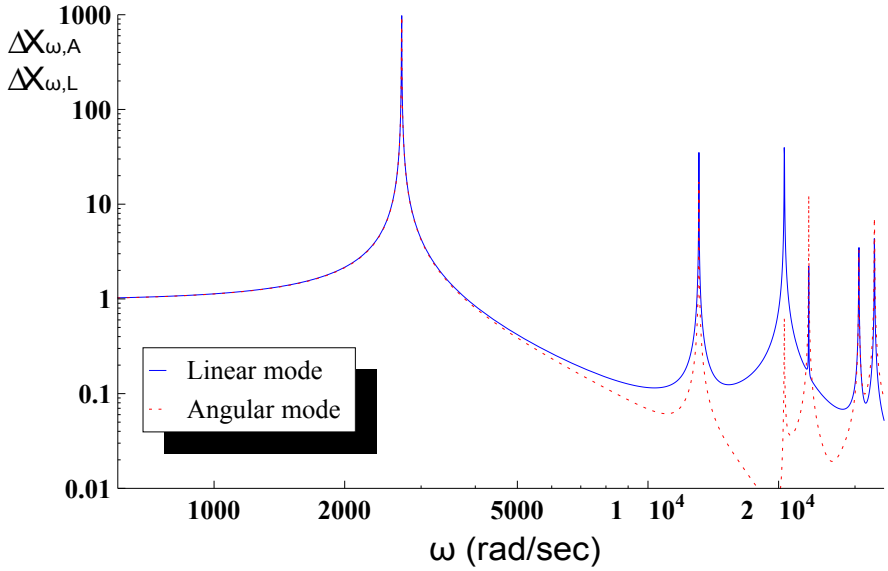

Figure D.3: Effect of ω on the amplitude of displacement for clamps' external displacement of 0.05 mm

CONCEPTION ET MODELISATION D'UN MONTAGE DE FABRICATION POUR LE BALANÇAGE OPTIMISE D'UNE FAMILLE DE PIECES

RESUME: Les erreurs dimensionnelles des pièces d'une famille de pièces provoquent un mauvais placement initial de la pièce sur le montage affectant la qualité du produit final. Même si la pièce est positionnée correctement, la pièce s'écarte de cette position initiale à cause des forces externe d'usinage et de bridage et de la rigidité du montage. Dans cette thèse, un modèle analytique complet, composé d'un modèle cinématique et un modèle mécanique, ayant une configuration de type 3-2-1 des appuis est proposé. Le modèle cinématique remet la pièce, initialement mal placée dans la référence machine, sur la bonne position par les avancements axiales des six appuis en tenant compte de tout les éléments du montage considérés rigides. Cette pièce repositionnée se déplace à nouveau à partir de la position corrigée sous les forces de bridage et d'usinage. Le modèle mécanique calcule ce déplacement de la pièce en considérant les appuis et des brides élastiques. Le plateau cuboïde rigide, utilisé pour repositionner la pièce précisément, est également considéré élastique au niveau des contacts avec les appuis. Le comportement non-linéaire de la déformation des contacts est linéarisé en convergeant la déformation des appuis jusqu'à ce que la précision requise est atteinte. En utilisant l'hypothèse des petits déplacements et en considérant le frottement nul au niveau des contacts, On calcule le déplacement de la pièce, la déformation de chaque appui suivant l'énergie minimale, la matrice de rigidité et le comportement mécanique du système du montage grâce à la formalisation Lagrangienne. Le déplacement de la pièce est à nouveau compensé par l'avancement axial des six appuis calculés par le modèle cinématique.

Mots clés : montage de fabrication, conception du montage, modélisation mécanique, balançage optimale, erreur de positionnement, formalisation Lagrangien.

DESIGN AND MODELING OF A FIXTURING SYSTEM FOR THE OPTIMIZED BALANCING OF A PART FAMILY

ABSTRACT: Dimensional errors of the parts of a part family cause the initial misplacing of the workpiece on the fixture affecting the final product quality. Even if the part is positioned correctly, the external machining forces and clamping load cause the part to deviate from this initial position depending upon that external load and the stiffness of the fixture. In this thesis, a comprehensive analytical model, consist of a kinematic and a mechanical model, of a 3-2-1 fixturing system is proposed. The kinematic model relocates the initially misplaced workpiece in the machine reference by the axial advancements of the six locators considering all the fixturing elements to be rigid. This repositioned part again displaces from the corrected position under the clamping and machining forces. The mechanical model calculates this displacement of the part considering the locators and clamps to be elastic. The rigid cuboid baseplate, used to precisely relocate the workpiece, is also considered elastic at the contacts with the locators. The non-linear behavior of the contact deformation is linearized by the converging the deformation of locators till the required precision is attained. Using small displacement hypothesis with zero friction at contacts, Lagrangian formulation enables us to calculate the rigid body displacement of the workpiece, deformation of each locator following minimum energy, and stiffness matrix and mechanical behavior of the fixturing system. This displacement of the workpiece is again compensated by the advancement of the six axial locators calculated through the kinematic model.

Keywords : fixturing system, fixture design, mechanical modeling, optimal balancing, positioning error, Lagrangian formulation.

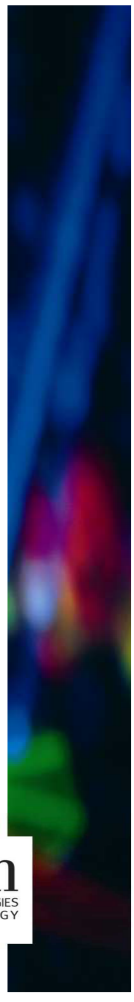

ARTS ET MÉTIERS ParisTech

ParisTech INSTITUT DES SCIENCES ET TECHNOLOGIES PARIS INSTITUTE OF TECHNOLOGY